UNIVERSITAT DE BARCELONA

Polyene sphingolipids with latent fluorescence: new tools to study the biophysical properties of cellular membranes

Ingrid Nieves Calatrava

UNIVERSITAT DE BARCELONA

FACULTAT DE FARMÀCIA
PROGRAMA DE DOCTORAT DE QUÍMICA ORGÀNICA

POLYENE SPHINGOLIPIDS WITH LATENT FLUORESCENCE: NEW TOOLS TO STUDY THE BIOPHYSICAL PROPERTIES OF CELLULAR MEMBRANES

Memòria presentada per **Ingrid Nieves Calatrava**
per optar al Grau de Doctora per la Universitat de Barcelona

Tesi realitzada al Departament de Química Biomèdica
de l'Institut de Química Avançada de Catalunya (iQAC-CSIC)

Director:

Dr. José Luís Abad Saiz
Departament de Química Biomèdica (iQAC-CSIC).

Tutor:

Prof. Antonio Delgado Cirilo
Departament de Química Farmacèutica, Facultat de Farmàcia (UB)

Doctorand:

Ingrid Nieves Calatrava

“In short, it takes all kinds to make alkenes,
just as it takes all kinds to make the world”

(By Ei-ichi Negishi)

This work was supported in full by the “Fundación Biofísica Bizkaia” and, in part, by the Spanish Ministry of Economy and Competitiveness (Project CTQ2014-54743). I am also grateful to “Fundación Biofísica Bizkaia” for personal financial support and to the CSIC predoctoral research training support within JAE-predoc fellowship.

Abbreviations

ΔH	Phase transition enthalpy
$\Delta T_{1/2}$	Phase transition width
ε	Molar extinction coefficient
Φ_F	Fluorescence quantum yield
τ_C	Rotational correlation time
A	Absorbance
ACN	Acetonitrile
AKT	Protein kinase B
a_N	Isotropic coupling constant
Atm	Atmospheric pressure
Boc	*tert*-Butoxycarbonyl
BODIPY	4,4-Difluoro-4-bora-3a,4a-diaza-*s*-indacene
BOP	(Benzotriazol-1-yloxy)tris(dimethylamino)phosphonium hexafluorophosphate
BuLi	Butyllithium
CDase	Ceramidase
Cer	Ceramide
CerS	Ceramide synthase
CERT	Ceramide transfer protein
Chl	Cholesterol
CM	Cross-metathesis
C_p	Heat capacity
Cp	Cyclopentadienyl ligand
C1P	Ceramide 1-phosphate
CPTP	C1P specific transfer protein
DCM	Dichloromethane
DCS	Differential scanning calorimetry
dhCer	Dihydroceramide
DIBAL-H	Diisobutylaluminium hydride
DiO	3,3'-Dioctadecyloxacarbocyanine perchlorate
DIPEA	*N,N*-Diisopropylethylamine
DMAP	*N,N*-Dimethylpyridin-4-amine
DMF	*N,N*-Dimethylformamide
DMSO	Dimethyl sulfoxide
DOPC	1,2-Dioleoyl-*sn*-glycero-3-phosphocholine
5-DOXYL-staric acid, free radical	2-(3-Carboxypropyl)-4,4-dimethyl-2-tridecyl-3-oxazolidinyloxy
16-DOXYL-stearic acid, free radical	2-(14-Carboxytetradecyl)-2-ethyl-4,4-dimethyl-3-oxazolidinyloxy
9,10-DPA	9,10-Diphenylanthraceneç
DPH	Diphenylhexatrienyl
DPPC	1,2-Dipalmitoyl-*sn*-glycero-3-phosphocholine

DSC	Differential scanning calorimetry
DSPC	1,2-Distearoyl-*sn*-glycero-3-phos-phocholine
EDC	*N*-(3-Dimethylaminopropyl)-*N*′-ethylcarbodiimide hydrochloride
ePC	egg Phosphatidylcholine
EPR	Electron paramagnetic resonance
eq	Equivalents
ER	Endoplasmatic reticulum
ESI-MS	Electrospray ionization-mass spectrometry
eSM	Egg sphingomyelin
Et_3N	Triethylamine
Et_2O	Diethyl ether
EtOAc	Ethyl acetate
EtOH	Ethanol
EWG	Electron-withdrawing group
FCS	Fluorescence correlation spectroscopy
FG	Functional group
Fmoc	Fluorenylmethyloxycarbonyl
FRAP	Fluorescence recovery after photobleaching
FRET	Förster/Fluorescence resonance energy transfer
FTIR	Fourier transform infrared spectroscopy
g	Landé factor, splitting factor
GABA	γ-Aminobutyric acid
GalCer	Galactosylceramide
GCase	Glycosidase
GC-MS	Gas chromatography- mass spectrometry coupling
GluCer	Glucosylceramide
GSLs	Glycosphingolipids
GUV	Giant unilamellar vesicle
HMPA	Hexamethylphosphoramide
HMPT	Hexamethylphosphorous triamide
HOBt	1-Hydroxybenzotriazole
HPLC	High pressure liquid chromatography
HWE	Horner-Wadsworth-Emmons
I	Nuclear spin
IBX	2-Iodoxybenzoic acid
KHMDS	Potassium bis(trimethylsilyl)amide
LDA	Lithium diisopropylamide
LiHMDS	Lithium bis(trimethylsilyl)amide
LR	Lissamine-rhodamine
LUV	Large unilamellar vesicle
Me_3Al	Trimethylaluminium
MeOH	Methanol
m_i	Spin quantum number
MLV	Multilamellar vesicle
MOM	Methoxy-methyl ether

MPA	α-Methoxyphenylacetic acid
m_S	Magnetic spin quantum number
NBD	Nitrobenzo-2-oxa-1,3-diazole
nCDase	Neutral ceramidase
NMM	*N*-Methylmorpholine
NMR	Nuclear magnetic resonance
NR	Nile Red
pCer	Palmitoyl ceramide
PE	Phosphatidylethanolamine
PG	Protecting group
PKC	Protein kinase C
PP1	Protein phosphatase 1
PP2A	Protein phosphatase 2A
Red-Al	Sodium bis(2-methoxyethoxy)aluminum hydride
ref	Reference
Rf	Retention factor
Rt	Retention time
RT	Room temperature
S	Empirical order parameter
SK-1	Sphingosine kinase-1
SK-2	Sphingosine kinase-2
SLs	Sphingolipids
SM	Sphingomyelin
SMase	Sphingomyelinase
S1P	Sphingosine 1-phosphate
Sph	Sphingosine
SphK	Sphingosine kinase
SPL	Sphingosine 1-phosphate lyase
SPT	Serine palmitoyltransferase
S-PT	Single-particle tracking
STORM	Stochastic optical reconstruction microscopy
SUV	Small unilamellar vesicle
T	Temperature
TBAF	Tetra-*n*-butylammonium fluoride
TBS	*tert*-Butyldimethylsilyl
TBSCl	*tert*-Butyldimethylsilyl chloride
t-BuOK	Potassium *tert*-butoxide
TEM	Transmission electron microscopy
THF	Tetrahydrofuran
TLC	Thin-layer chromatography
Tm	Gel-liquid phase transition temperature
ULV	Unilamellar vesicle

Table of contents

1. GENERAL INTRODUCTION

1.1 Sphingolipids

Sphingolipids (SLs) are important constituents of eukaryotic cells and are also found in the bacterial genus *Sphingomonas*[1]. SLs are a large family of naturally occurring lipids containing the common (*E*,2*S*,3*R*)-2-aminooctadec-4-ene-1,3-diol *D-erythro*-sphingoid backbone[2]. Since 1884, SLs have been considered as inert structural components of cell plasma membranes. However, in the second half of the past century, diverse studies revealed their major role as bioactive molecules taking part in signalling events that regulate various cellular activities[3–5].

Ceramide (Cer), sphingosine (Sph), and their related phosphate analogues ceramide 1-phosphate (C1P) and sphingosine 1-phosphate (S1P) are the main bioactive sphingolipids (Figure 1.1):

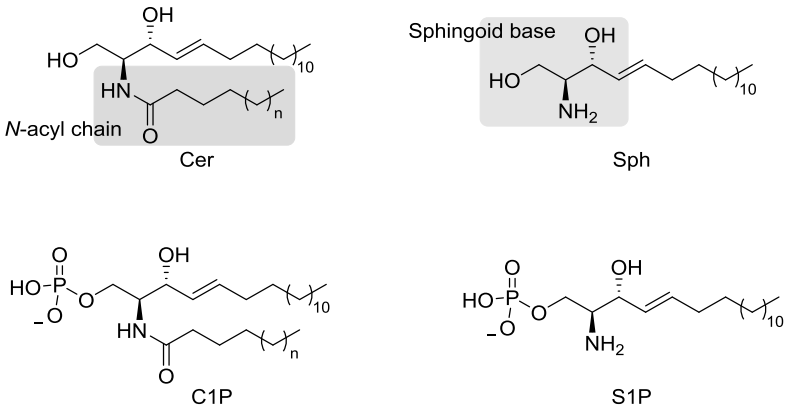

Figure 1.1 Structure of the main bioactive SLs (n represents diverse acyl chain lengths).

1.1.1 Sphingolipid metabolism and compartmentalization

Sphingolipid metabolism includes a series of biosynthetic and catabolic reactions in which Cer plays a central role. Cer may be found in different subcellular compartments, in biological fluids, or in different metabolic contexts in the cell[6]. Basically, Cer can be generated by two major mechanisms (Figure 1.2).

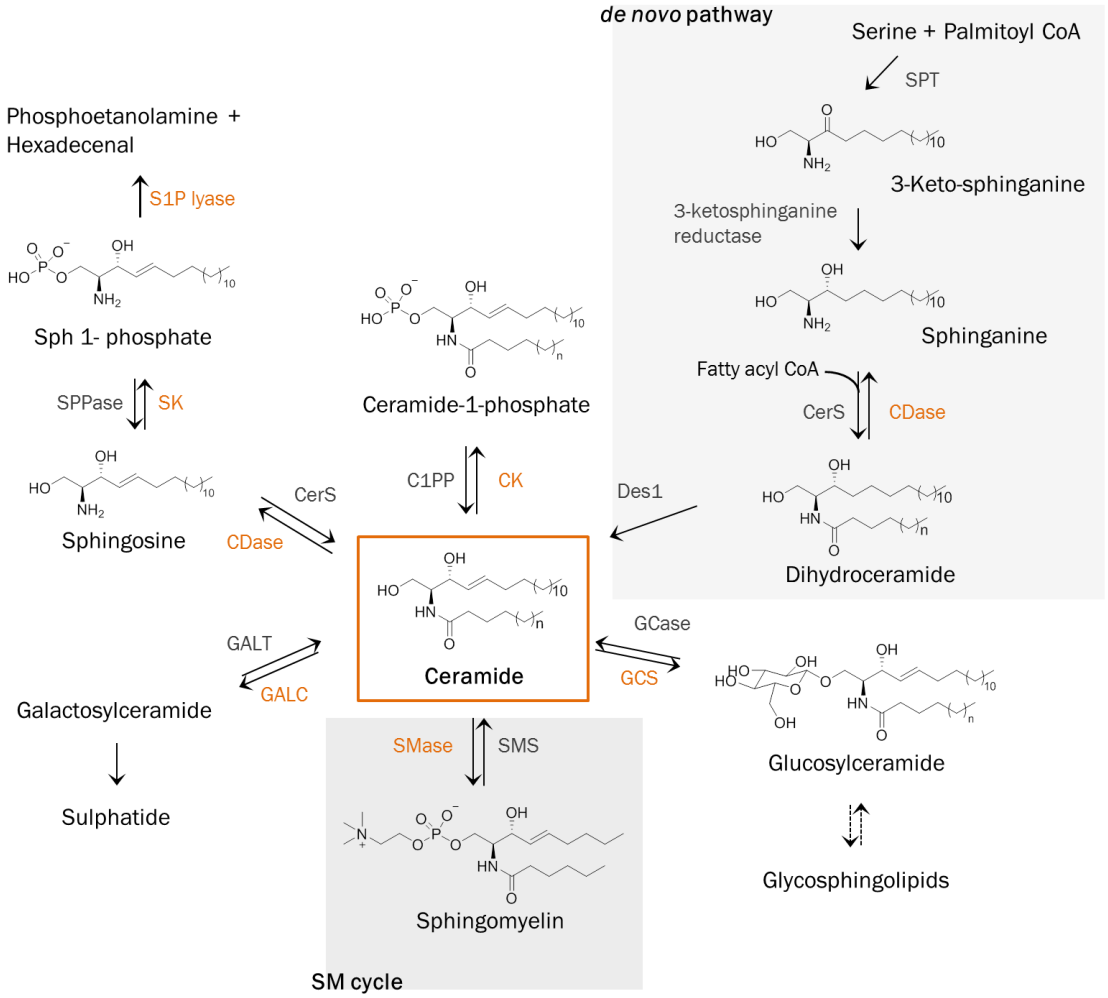

Figure 1.2 The SL metabolic pathway.

The first one is the ***de novo* pathway**, an anabolic pathway that takes place on the cytosolic surface of the endoplasmic reticulum (ER) (Figure 1.3). In this pathway, Cer is firstly synthesised from serine and palmitoyl-CoA to form 3-keto-dihydrosphingosine through the rate limiting action of serine palmitoyltransferase (SPT). Subsequent steps involve the conversion of 3-keto-dihydrosphingosine to dihydrosphingosine (sphinganine), which is then *N*-acylated to dihydroceramide (dhCer) by specific synthases[7]. Different ceramide synthases (CerS) genes are responsible for the synthesis of dhCer with different acyl chain lengths. These dhCer are then desaturated by dhCer desaturase, to generate Cer in the last step of *de novo* synthesis pathway[8]. Cer is delivered by ceramide transfer protein (CERT)[9] or vesicular transport to the Golgi (Figure 1.3) for synthesis of C1P (by ceramide kinase (CK)), sphingomyelin (SM) and glucosylceramide (GluCer). Four-phosphate adaptor protein 2 (FAPP2) then transports GluCer to the *trans*-Golgi for biosynthesis of complex glycosphingolipids

(GSLs). SM and GSLs are delivered to the plasma membrane by vesicular transport and C1P by a C1P-specific transfer protein (CPTP).

Another mechanism known as the **"SM cycle"** is responsible for the production of Cer and involves the hydrolysis of plasma membrane SM to Cer and phosphorylcholine through the action of the enzyme sphingomyelinase (SMase)[10] (Figure 1.2 and 1.3). At the plasma membrane, SMase, ceramidase (CDase), and sphingosine kinase (SK) produce the bioactive metabolites Cer, Sph and S1P, respectively. S1P is then transported across the membrane to exert its autocrine or paracrine activities.

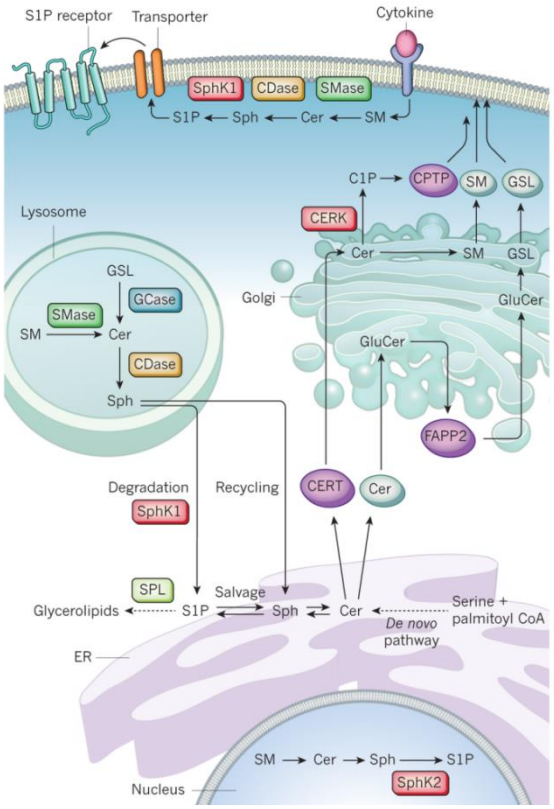

Figure 1.3 Subcellular compartmentalization of SL metabolism. Image taken from Maceyka *et al.*[11].

Membrane sphingolipids are internalized by the endocytic pathway to the lysosome, where they are degraded by acidic forms of SMase, glycosidase (GCase) and CDase[11]. The Sph formed can be metabolised to glycerolipids after phosphorylation by SK-1 in the cytosol or by SK-2 in the nucleus to produce S1P[12]. Sphingolipids, including Cer, Sph and S1P can be converted back to Sph by lipid phosphatases[13]. Additionally, S1P can be irreversibly cleaved by the enzyme S1P lyase (SPL) to generate ethanolamine phosphate and 2-hexadecenal[14]. This step is the only way out from the sphingolipid pathways[15,16]

Cer can also be generated by the breakdown of glycosphingolipids, a mechanism called the **"salvage pathway"** (Figure 1.3). In this mechanism, the terminal hydrophilic portions of GluCer and galactosylceramide (GalCer) are hydrolysed by specific β–glucosidases and galactosidases to produce Cer[17] at the lysosome. The Cer produced through the *de novo* pathway or sphingolipid recycling can be reversely metabolized into Sph by CDases[4].

1.1.2 Sphingolipids and diseases

Bioactive sphingolipids are involved in the regulation of important signalling pathways. Thus, alteration of sphingolipid metabolism may cause pathologic conditions and contribute to fatal diseases. Although many of the bioactive sphingolipids have essential roles in metabolic alterations[18,19], this section will focus on the roles of Cer and Sph in disease.

Ceramide

Diverse studies suggest that an increased production of Cer mediates cell growth arrest and/or apoptosis in response to stressful stimuli[4] (Figure 1.4). Cancer cells behave avoiding cell death due to alterations in the enzymes involved in Cer generation (SMase, CerS) or degradation (CDase)[20, 21]

Lysosomal storage disorders can promote cellular, tissue and organ failure. The lack of a CDase activity in the lysosome results in Farber disease. Moreover, Gaucher's disease presents accumulation of GluCer because of the absence of the enzyme that hydrolyses GluCer to Cer and glucose[22].

Sphingosine

Sph is a bioactive lipid that promotes apoptosis or inhibits cell proliferation, depending upon the cell type. Cancer cells are related to an overexpression of the enzymes involved in the biosynthesis of S1P. In that case, unlike Cer, increases of S1P levels induce cell proliferation, angiogenesis, cell invasion, and cell migration[23, 24] (Figure 1.4). However, Sph is also reported to have anti-tumour activity in certain animal models, suggesting that an increased generation of Sph inhibits the proliferation of tumour cells *in vivo*[25,26]

Furthermore, there are indications that Sph induces fragmentation of the Golgi complex during apoptosis, like in some neurodegenerative disorders, such as amyotrophic lateral sclerosis, Alzheimer's disease[27], and Parkinson's disease[28].

Niemann-Pick disease type C (NPC) is a rare lysosomal storage disorder, which is characterised by the accumulation of multiple lipid species, including Sph, cholesterol (Chl), GSLs and SM. However, little is known about Sph interaction with other lipids in biological membranes[29].

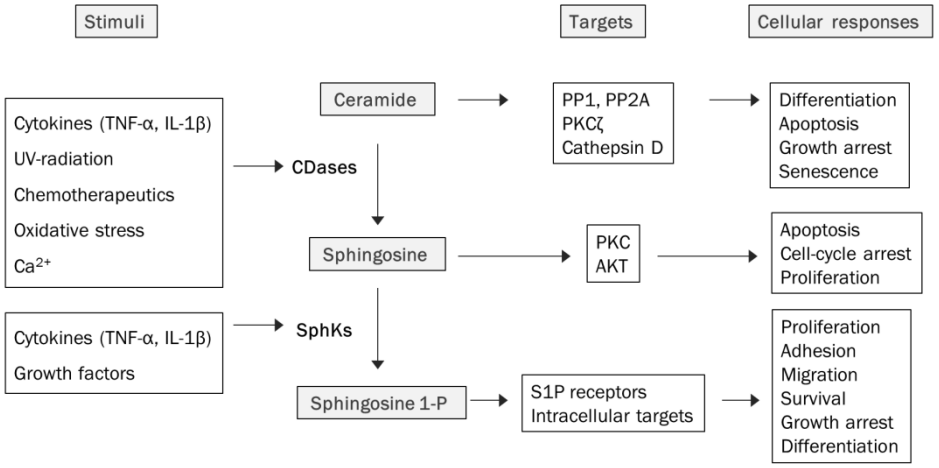

Figure 1.4 Role of SLs in cellular responses. PP1, protein phosphatase 1; PP2A, protein phos-phatase 2A; PKCζ, protein kinase C ζ; AKT, protein kinase B.

1.2 Biophysical properties of the cell membrane

Cell membranes are lipid bilayers, which delimit the boundaries of biological cells, as well as the perimeter of intracellular organelles. One of the vital roles of lipid membranes is to maintain and regulate cellular functions and communications.

The fundamental architecture of the cell membrane is a lipid bilayer, composed of amphipathic phospholipids that contain both polar (head group) and nonpolar (acyl chains) moieties. Moreover, the cell membrane is an enormously complex entity composed of phospholipids, sphingolipids, and sterols (e.g., cholesterol), together with membrane bound proteins, which can occupy 70% of the surface. Although SLs are minor components of the overall cell membranes, their local concentration can be high in the outer of the plasma membrane[30].

*Lamellar phases (*L*)*

Lipids from biological membranes present a lipid polymorphism. Due to the low water solubility of lipids, they tend to self-aggregate when dispersed in an aqueous solution and the structures adopted change depending on pH, temperature, pressure, ionic strength, hydration level and the geometry of the lipid[31]. These structures can be responsible for the processes that take place in the cell membranes. Under equilibrium conditions, lipid bilayers are in a lamellar configuration, where the most significant phases are:

Fluid or liquid-disordered ($\mathbf{L_d}$) or liquid-crystalline ($\mathbf{L_\alpha}$): lipids are free to diffuse laterally or rotationally, and display their acyl chains in a complete disordered state with high flexibility. In this phase, most of the acyl chains present carbon-carbon (C-C) conformers in a *gauche* conformation.

Gel or solid-ordered ($\mathbf{L_\beta}$): in this phase, the acyl chains of the lipids are highly ordered and display high proportions of *trans* C-C conformers, being almost immobile and not allowing lateral or rotational motion [32].

Liquid-ordered ($\mathbf{L_o}$): phase with intermediate properties between the gel and the fluid phases. It was recently named to denote lipid mixtures of sphingolipids or glycerolipids with sterols, in which lateral diffusion is allowed but there is a low level of *gauche* conformers.[33].

Although the lipid bilayer of a natural cell membrane resembles the structure of a lamellar phase, transient generation of non-lamellar structures appears to be important for several mechanisms, such as fusion or fission processes.

Lipid motion

Lipid bilayers under physiological conditions generally exist in a liquid-disordered phase characterized by high fluidity. Membrane fluidity enables lipids and proteins to move along the plane of the bilayer and in some cases between monolayers. That fluidity is strongly associated with lipid motion, which can be classified into four different groups: lateral diffusion[34], rotational movement, flexion and transversal diffusion or flip-flop[35] (Figure 1.5).

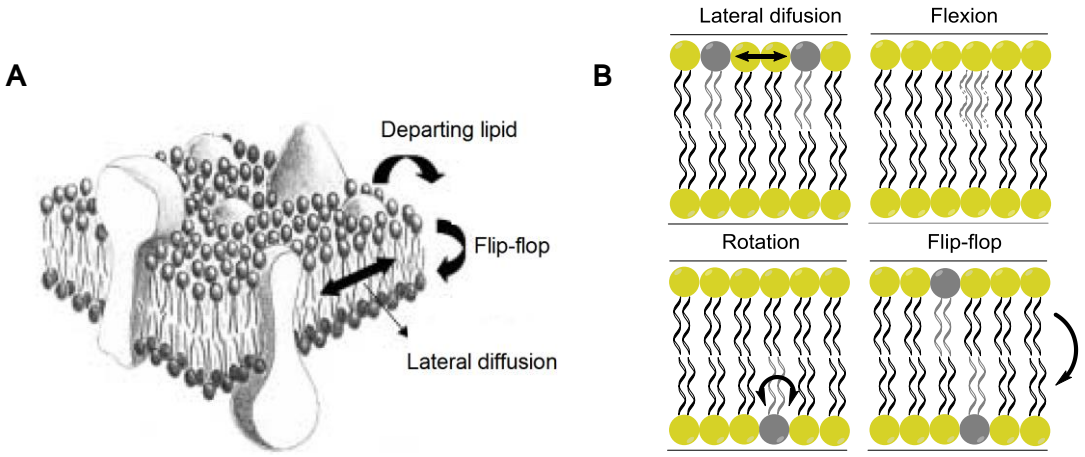

Figure 1.5 A: Lipid motion in membrane. Image taken from Binder *et al.*[36]; **B**: Lipid motion scheme.

1.2.1 Lipid domains

In 1972, Singer and Nicolson[37] proposed a model named the "*fluid mosaic model*" with the aim of defining and understanding the organization of the biomembranes. This model guarantees that both lipids and proteins can freely diffuse laterally within the membrane plane. Although this model became widely accepted, in 1997 Simons and Ikonen[38], proposed the so-called "*raft model*" introducing the concept of lipid domain to explain the structural heterogeneity of the membranes. These lipid domains, together with membrane proteins, are expected to be involved in controlling a large number of biological processes[39]. Some years later, in 2006, the membrane raft was commonly defined as small (10-200 nm), heterogeneous, highly dynamic, sterol and sphingolipid-enriched domains in L_o phase that compartmentalize cellular processes (Figure 1.6). Small rafts can sometimes be stabilized to form larger platforms through protein–protein and protein–lipid interactions [40].

However, the existence of rafts is still controversial and not completely accepted. There are a large number of unresolved questions with regard to the origin and real nature of membrane rafts *in vivo* and *in vitro* [41], basically due to a lack of direct visualization of rafts in biomembranes.

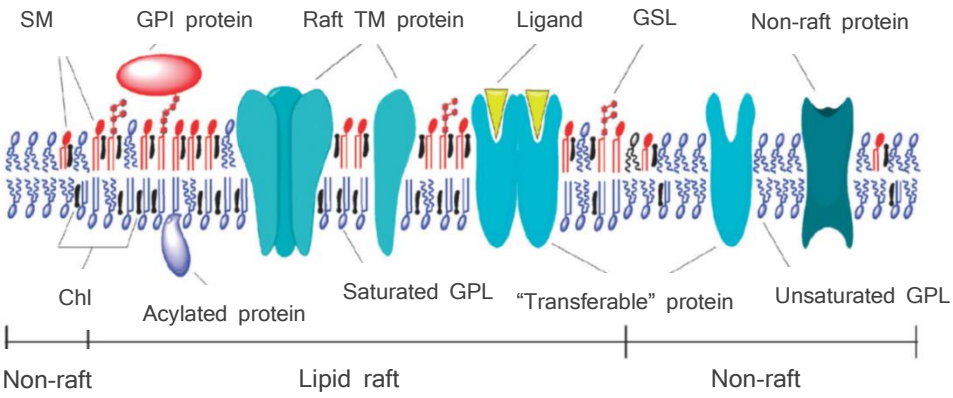

Figure 1.6 Schematic diagram of lipid raft-based heterogeneity. Glycosphingolipid (GSL), glycerophospholipid (GPL), sphingomyelin (SM), cholesterol (Chl), transmembrane (TM) protein, glycosylphosphatidylinositol-anchored protein (GPI protein). Image taken from Zhong, J.[42]

1.2.2 Ceramide

In general, Cers present very low polarity and are highly hydrophobic. They can exert their physiological effects either through changes in membrane properties or else through binding specific target proteins that dock more or less transiently the membrane bilayer[43].

Cers have a unique ability to induce a broad range of biophysical alterations in lipid membranes. The peculiar molecular structure of Cers, containing a diol and an amide linkage on the Sph backbone (Figure 1.1), let them form extensive hydrogen bonds. This characteristic contributes to increase their transition temperature (Tm), decreasing the miscibility with other membranes lipids, and to their in-plane phase separation into Cer-enriched domains[44]. Differences in the unsaturation number[45], or the acyl chain length[46–48], are crucial to determine the biophysical properties of the lipid bilayers.

Diverse studies with mixtures of Cers with phospholipids in monolayers or bilayers, show that Cers have two main effects: they increase the molecular order of phospholipids[49,50] and they give rise to lateral phase separation and domain formation[51,52].

Data also reveals that Cer increases the membrane permeability, probably due to particular structural features, namely its propensity to destabilize the bilayer by facilitating the formation of non-lamellar phases and its high tendency to segregate into

ordered domains that would be responsible for the creation of packing defects at the interface between Cer-enriched domains and the fluid bulk membrane[53,54]. An alternative mechanism by which Cer mediates membrane permeability consists of the formation of large, structured, stable and rigid Cer channels[55,56]. However, this last mechanism is still highly controversial in the field of ceramide biophysics[57].

The formation of Cer-rich domains on the plasma membrane after external *stimuli,* contributes to increase the signalling effectiveness in cell physiology. The Cer rapid trans-bilayer movement, flip-flop, may facilitate this process[58,59]. Furthermore, Cers are associated in the generation of large platforms from the coalescence of small rafts, which would be responsible for the spatial and temporal reorganization of receptors and signalling molecules at the cell surface, facilitating and stabilizing signal transmission and transduction[60].

Currently, the full understanding of the roles of Cer in cell membranes is far for complete, due to the complexity of the cellular environment. In addition, several of these studies require high amounts of Cer to observe the physical changes in membranes and they are also hampered by a lack of adequate experimental conditions able to mimic the physiological environment[61].

1.2.3 Sphingosine

Sph (Figure 1.1), as most bioactive lipids, may act directly through enzyme binding or indirectly through changes in cell membrane properties[62]. However, little is known about its effect on the lipid bilayer structure and the interaction with other lipids. Recent studies have revealed that Sph is able to change the permeability and rigidity of the membrane, which might have an impact in signalling, sorting of proteins and lipids, and membrane trafficking[62–65].

Under physiological conditions, Sph is positively charged, because its pK_a in the membrane environment is around 8.9-9.1[66]. However, the protonation state of this SL is depends largely on the cellular compartment[29,61]. When released into the lysosomal acidic environment, Sph is positively charged[66] and its ability to diffuse across membranes is reduced[29]. On the contrary, in negatively charged membranes, Sph can present a non-protonated form able to rapidly move across and between the biological membranes[65] (Figure 1.7).

Recently, the capacity of the Sph to permeabilize cell membranes to small solutes has been related to its ability to form non bilayer (cubic phase) intermediates in negatively charged membranes, where the contents are released in a graded way[65]. This data agrees with previous studies that interpreted the Sph-induced efflux of aqueous solutes as a result of bilayer-rigidification. This rigidification would stabilize gel domains in membranes, raising their melting temperatures and increasing the transition cooperativity. Thus, the presence of coexisting gel and fluid domains in the plasma membrane would result in permeabilization[62]. However, this mechanism differs from previous hypothesis where the efflux was due to the capacity of Sph to form channels[64]. A channel would give rise to a rapid and complete release of contents and not in a graded manner.

Experiments to observe the role of Sph in cell or model membranes are currently hampered by a lack of adequate experimental conditions able to mimic the physiological environment. As in the case of Cer, it is necessary to employ high molar concentrations of Sph to analyse its influence in lipid bilayers.

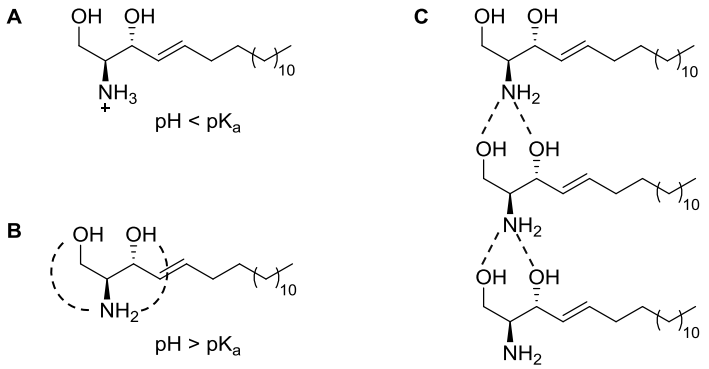

Figure 1.7 Protonation state of Sph depending on pH environment. (*broken lines*) Intermolecular hydrogen bonds. **A:** Protonation state of Sph at pH lower than pKa; **B:** Protonation state of Sph at pH higher than pKa; **C:** Intermolecular H bonds in Sph. Hydrogen bonds are formed only when molecules exist in close proximity. Image taken from Sasaki, *et al.*[67]

1.3 Biophysical tools

One of the ultimate goals in biology is to understand the relationship between structure, function, and dynamics of biomolecules in their natural environment, namely the living cell. Although the combination of work on model membranes with living cells has made enormous progress in identifying and characterizing the heterogeneities both inside and at the cell membrane, direct visualization of molecular interactions at physiological conditions remains as a major challenge[68–70].

Since the first isolation of sphingolipids from SL-containing biomaterial by extractions and subsequent thin layer chromatographic separation (TLC)[71], a wide array of biophysical tools has been developed to gain more insight into metabolism, trafficking and interaction of the sphingolipids.

Model membranes have been useful to enforce some biophysical methodologies that cannot be carried out in living cells. Techniques such as differential scanning calorimetry (DSC), together with monolayer studies, describe lipid domain formation[48,72,73], and the molecular parameters of the bioactive sphingolipids[74] in model systems.

Proton or phosphorous nuclear magnetic resonance (^{2}H-NMR, ^{31}P-NMR) spectroscopies[51,65,75] or solid-state magic angle spinning (MAS)-NMR[76] , offer unique insights into membrane assembly and changes in the membrane structure and dynamics. The use of a combination of NMR with other spectroscopic techniques, such as X-Ray scattering[65,73], provides information on the overall membrane structure from positional correlations of the bilayers and hydrocarbon chains[77]. However, because of the difficulties associated to sample preparation, these techniques have so far only been used in model-membrane studies[69].

Other spectroscopic techniques are, for instance, electron paramagnetic resonance (EPR), a technique able to monitor the molecular dynamics of lipids in a model membrane (see section 3.1.3.5), Fourier transform infrared spectroscopy (FTIR), which provides information on the level of local lipid ordering and on intermolecular interactions with inherent timescale[77–79], and mass spectrometry[39,80] or MALDI imaging mass spectrometry (MALDI-IMS)[81].

Alternative methods in cells rely on the use of fluorescently labelled antibodies or protein-tagging. These techniques are able to localize lipid domains and the associations of their components and are observed by immunodetection[82], antibody patching and immunofluorescence microscopy[83], also combined with transmission electron microscopy (TEM)[52,84].

Most of the membrane heterogeneities are however highly dynamic, since the cellular plasma membrane is not in thermodynamic equilibrium and a lot of structural characteristics change over space and time. Therefore, a complete picture of membrane organization and dynamics requires experiments on the living cell. Optical microscopy has proven valuable for live cell studies, since light is minimally invasive. However, in order to be able to image heterogeneous distributions of the sphingolipids, some requirements have to be fulfilled. For instance, the image acquisition time has to be faster than the dynamics or diffusion. Moreover, the spatial resolution of the image has to be larger than the size of the heterogeneity, and finally, the image will only show a contrast if the labelled molecule distributes differently between different heterogeneities[85].

Different kinds of fluorescence-based microscopy techniques exist, such as confocal laser microscopy, which can be single-photon[29] or two-photon. In cellular applications, the two-photon technique has the added advantage of minimizing both the bleaching and the damaging effects associated to ultra-violet excitation, as only the dye molecules in the optical section are excited[49,86,87] (see Section 3.1.3.4).

Advanced fluorescence correlation spectroscopy characterizes domains that are not visible by ordinary fluorescence microscopy, but can be detected using other specialized tools (Table 1.1). Thus, single-particle tracking (S-PT), is based on the direct observation of the hindered diffusion of labelled molecules instead of acquiring an instantaneous image[85]. On the other hand, this method demands for extremely bright and photostable fluorescent labels. Further techniques, which require much shorter measurement times and small labels to simultaneously observe the diffusion characteristics of a multitude of single molecules, are fluorescence correlation spectroscopy (FCS)[85,88,89]and fluorescence recovery after photobleaching (FRAP)[70,85].

Table 1.1. Some advanced fluorescence correlation spectroscopy methods for detecting membrane domains in living cells

Method	Primary observables	Spatial/temporal resolution	References
FCS	Fluorophore translational mobility & dynamics of lateral heterogeneity	~250 nm/~1 μs	[85, 90]
FRET	Donor-acceptor proximity	~5-10 nm separation detected (no size)/<1 s	[91–93]
S-PT	Translational trajectory of particle (40 nm gold particle or quantum dots)	~250 nm /25 μs	[30,94]
FRAP	Translational mobility of a fluorophore	~ 50 nm /13 s	[95, 96]
STED-FCS	Time traces of single molecule diffusion of a fluorescence-labelled probe	<50 nm/0.5-3 ms	[85,97,98]

Atomic force microscopy (AFM) is one of the families of scanning probe microscopes, which provides a three-dimensional surface profile of the biological sample. Samples do not require any specific treatment. However, high quality AFM profiles are taken at low time resolution (min), making dynamic processes less tractable[42,99].

Förster resonance energy transfer (FRET), is a photophysical process highly dependent on interchromophore distance between a donor and acceptor fluorophores. Such experiments demand a too large concentration of the dye incorporated into the membrane, which may induce changes in the membrane morphology[85,100,101].

At present, new super-resolution fluorescence techniques offer several possibilities for detecting subcellular structures at higher resolution than conventional microscopy. Fluorescence or not photo-activated localization microscopy (fPALM or PALM) and stochastic optical reconstruction microscopy (STORM) are some of these new biophysical tools. STED microscopy, stimulated emission depletion microscopy, allows reconstruction of an image by selectively deactivating fluorophores, thus enhancing the resolution in an area of a sample. The combination of STED and FCS is currently a sensitive tool for studying nanoscale membrane organization, interaction, metabolism and trafficking[68,85,88,102].

Although the above emerging techniques are already providing highly detailed information at the nanometre scale, their time scale is still slow and applications in living cells are scarce[68].

1.4 Labelled sphingolipids as probes

Mostly biophysical techniques from the previous section require the use of radioactive, spin-labelled or fluorescent lipid analogues, in order to study and visualise the sphingolipid interactions, trafficking and metabolisms in membranes.

A suitable sphingolipid analogue must fulfil two main criteria: Its structure needs to be very similar to that of the natural counterpart and it has to be traceable. Moreover, labelled analogues have to be easy to use, present high sensitivity and versatility of detection, as well as strong biological acceptance, applicability to many biological systems and low risk potential[103].

1.4.1 Radioactive labelled sphingolipids

Isotope-labelled lipids have represented a valuable tool to describe the biosynthesis of the sphingolipids in living cells[104]. The structure of these lipid analogues is optimal for very sensitive detection. However, their use in combination with modern analytical techniques, such as microscopy, is impracticable or inconvenient.

Tritium and carbon-14 are the main isotopes used for labelling sphingolipids (Figure 1.8). When radioisotope-labelled lipids are used for metabolic studies in living cells, the resulting lipid pattern reflects not only anabolic but also catabolic processes and their interpretation becomes confusing. Towards this end, non-degradable substrates have been used, offering more specificity about the metabolic processes of single sphingolipids and the possibility of gaining information on their intracellular trafficking[105].

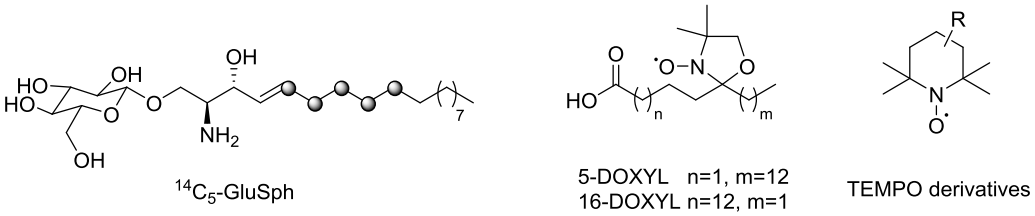

Figure 1.8 Structure of ^{14}C-labelled glucosylsphingosine ($^{14}C_5$-GluSph) and some of the commercial free radical *n*-DOXYL stearic acid and TEMPO derivatives. ●=carbon-14.

1.4.2 Spin-labelled sphingolipids

Spin-labelled lipids provide useful information about the membrane environment using EPR spectroscopy. These lipid analogues have been especially helpful for the study of lipid-lipid or lipid-protein interactions[106], their distribution and trafficking, and the difussion[107] and asymmetry of the lipid bilayers[108].

The most employed free radicals groups to label sphingolipids are the commercial free radical *n*-DOXYL-stearic acid and TEMPO derivatives, because of their stability and affordable price (Figure 1.8). Spin-labelled probes are commonly used as fluorescence quenchers in studies of membrane penetration of dye-labelled sphingolipids[109], proteins and peptides[110] using depth-dependent quenching, and also to provide information on the fluidity of the membrane (see Section 1.4.4).

1.4.3 Fluorescent sphingolipid analogues

The ideal fluorescent sphingolipid analogue should present a high fluorescence quantum yield and the possibility of being followed at low concentration for a long time using high illumination intensity without photobleaching and without affecting the natural behaviour of the native molecules. However, the majority of fluorescent labels are rigid structures of considerable size and bulkiness and are used above physiological concentrations. Since lipids are relatively small molecules, often with complex physicochemical and biological properties, the use of bulky fluorescent probes can result in altered lipid metabolism, localization, or trafficking[103,111,112].

The most representative synthetic chromophores used to label sphingolipids are summarized next.

Bulky chromophores

Classical studies in sphingolipid trafficking involve the fluorophores nitrobenzo-2-oxa-1,3-diazole (NBD) and 4,4-difluoro-4-bora-3a,4a-diaza-*s*-indacene (BODIPY) (Figure 1.9). In the eighties, the short six carbon Cer analogue C6-NBD-Cer[113] was tested in living cells, allowing a detailed characterization of their intracellular transport and metabolism using a combination of biochemistry and fluorescence microscopy. A decade later, BODIPY-lipid probes enabled the extension of the detection range in sphingolipid metabolism[114]. Although both of them have high fluorescence quantum yield and a relatively long excited-state lifetime, they dramatically change the physical properties of the lipid to which they are attached. Thus, NBD derivatives are more polar than natural lipids and, when used at high concentrations, they undergo self-quenching[112]. On the other hand, the BODIPY-modified sphingolipids are more hydrophobic and present an electrically neutral chromophore, thus being more similar to their natural counterpart. However, neither NBD– nor BODIPY–lipids can accurately mimic the preference of natural lipids for liquid-ordered and liquid-disordered lamellar phases[115].

Pyrene is another common fluorophore used in lipid studies (Figure 1.9). It is hydrophobic and presents high quantum yield and lifetime. Nonetheless, its fluorescence pattern is complex because the monomer emits at 380 nm and only high concentrations can be visualized through the formation of excimers that emit at 470 nm[116]. Although pyrene labels are better mimics[117], the four-aromatic rings also disfigure the structure of the natural SLs (Figure 1.10).

Diphenylhexatrienyl (DPH) was also used as chromophore to label Sph and Cer, in order to study their distribution and metabolism in human cells, showing similar behaviour to NBD[118,119].

An alternative chromophore to label sphingolipids is Nile Red (NR) (Figure 1.9). NR is a hydrophobic dye[120] whose fluorescence is strongly enhanced when inserted into a lipid environment. The excitation profile of NR-probes has been useful to design diverse FRET experiments[121].

Additional bulky fluorophores are, for instance, lissamine-rhodamine (LR)[122] and Alexa dyes[123]. Although they are readily visualized by fluorescence microscopy, their geometry cause disruptions to the lipid bilayer and, as such, they would not be suitable molecules to use in cell membranes.

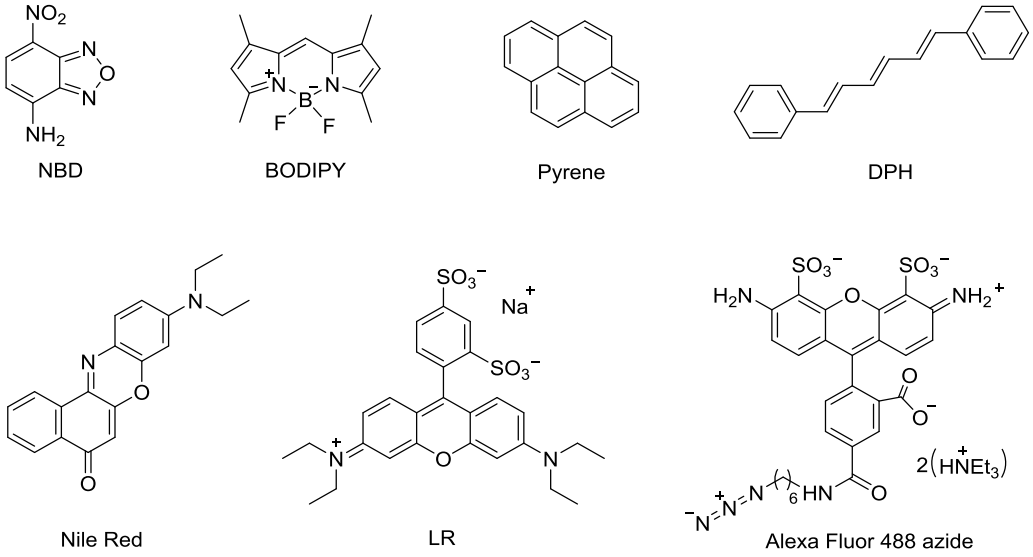

Figure 1.9 Chemical structures of some common fluorophores.

Polyene structures

In order to diminish the impact of the bulky chromophore on the chemical structure and packaging of the resulting lipid on the cell membrane, a conjugated double bond system was designed. This optically active π-electron system, importantly minimizes structural alterations[124]. Several naturally occurring polyene systems are known[125], such as organic pigments[126] and antibiotics[127].

Initially, parinaric acid (Figure 1.10), a natural tetraene-fatty acid, was introduced to serve as membrane probe[128]. However, because of its short-wavelength UV excitation and emission was not visualized by confocal microscopy, being only useful for physicochemical studies[129]. Indeed, parinaric acid is lacking of acceptance by cellular enzymes as it is only poorly metabolized[130].

These drawbacks were circumvented by the introduction of a fifth conjugated double bond[131], which was suitable for fluorescence studies in membranes. The pentaene-moiety is characterized by an excitation maximum above 340 nm and displays a maximal emission between 440 and 475 nm[132]. Due to the five conjugated double bonds, the pentaene-analogues are slightly shorter (1 Å) than the respective saturated acids or sphingolipids (Figure 1.10). Nevertheless, these type of intrinsically-fluorescent probes behave like their endogenous counterparts in vivo, with respect to uptake, metabolism, transport and localization in membrane microdomains[109,132,133].

Several synthetic probes incorporating a pentaene structure as a part of a fatty acid[109,132,134,135], a fatty diacid[136,137], or by derivatization of natural lipids [109,124,138,139] have been designed as model membranes and also for its incorporation in living cells (Figure 1.10). Since these labelled lipids are usually part of the *N*-acyl or the *O*-acyl chains, the fluorophore can be released by hydrolysis of the amide or the ester bonds and the resulting sphingoid base is hampered by a lack of detection. Currently, there is still no direct method to observe the distribution of sphingoid bases, such as Sph labelled with a pentaene moiety that faithfully mimic the natural sphingolipid.

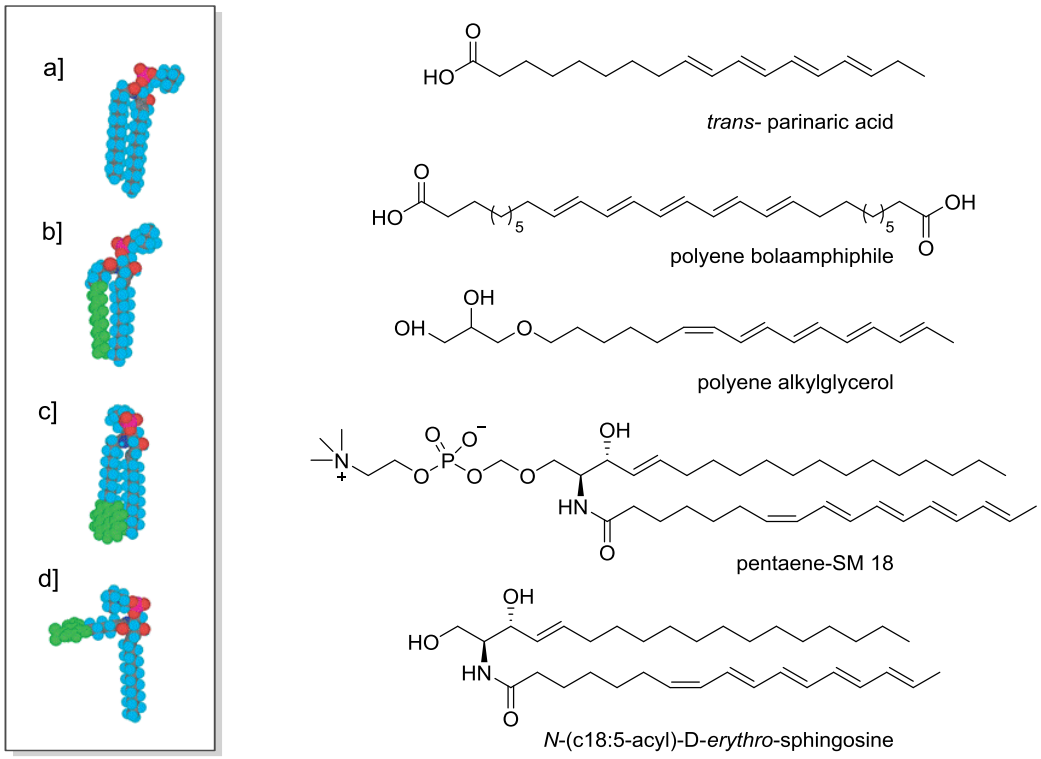

Figure 1.10 On the left: 3D models of fluorescent analogues of SM; a] natural lipid, b] pentaene tag, c] pyrene tag, d] NBD tag. Image taken from van Meer *et al.*[116]. On the right: chemical structures of selected polyene lipids. Image taken from Kuerschner *et al.*[109] and Quesada *et al.*[136]

Collectively, these characteristics make the pentaene lipids excellent tools to study lipid–lipid and lipid–protein interactions in the context of membranes at physiological conditions. However, the spectral range of five conjugated double bound is fixed and their photostability is limited. Although the introduction of extra conjugated double bonds lead to even more red-shifted spectra, for reasons of size and compound stability the pentaenes will be the polyene lipid of choice for many applications.

1.4.4 Dual Fluorophore-Quencher: profluorescent nitroxides

Nitroxides, widely recognized as stable and kinetically persistent free radicals, have been the subject of extensive research over the last 40 years. The unpaired electron of the nitroxide group appears coupled to the nitrogen atom, and the substituent groups at the alpha position of the free radical site, prevent from side disproportionation reactions[140,141].

Recently, nitroxide groups have been covalently bonded to fluorophores, providing dual-functional molecules which act as fluorometric probes. In this context, when the nitroxide and fluorophore are in a close proximity, the fluorescence yield diminishes, but, on removal of the radical quencher from the molecule, the fluorescence is completely returned (Figure 1.11). The ability of nitroxide–fluorophore couples to act as profluorescent probes arises owing to the nitroxide's ability to efficiently quench excited states, both inter- and intramolecularly. The mechanism by which nitroxides facilitate this phenomenon is based on electron-exchange interactions between the paramagnetic species and the excited-state of the fluorophore (see also 3.1.3.2)[142,143].

These dual compounds, keeping all properties of chromophore, fluorescence and nitroxide spin probe at the same time, have enabled the study of oxidative stress status in living cells[144–146], to prove the depth of fluorescent markers within lipid membranes[147], among other applications[142,148,149].

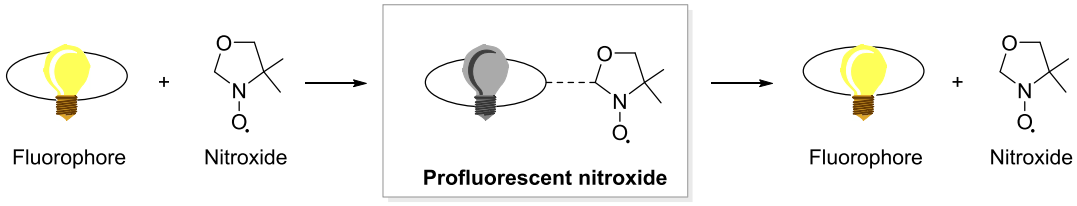

Figure 1.11 Representation of the tethering of a fluorophore to a nitroxide, which first leads to masked fluorescence followed by removal of spin to return fluorescence. Image adapted from Blinco *et al.*[143].

1.5 Context and perspectives

As evidenced in the following general objectives, the main idea and motivation behind the present doctoral thesis has been the development of suitable probes for their application in studies related to the biophysical and biochemical properties of SLs.

In this context, we wish to provide the reader a general overview of some of the most relevant roles played by polyene SLs, considered as potential probes to gain more insight into structure, function and dynamics of these SLs on model or cell membranes. Especially, we will focus on those concerning synthetic aspects and biophysical processes.

2. GENERAL OBJECTIVES

The full understanding of the roles of Cer and Sph in cell membranes is far for complete, due to the complexity of the cellular environment. The information retrieved from individual studies on model membranes, together with further research on the biophysical and physiological actions of these lipids, will assist the establishment of their mechanisms of action at molecular level.

Nevertheless, the experiments designed to observe these sphingolipids are currently hampered by a lack of adequate experimental conditions able to mimic the physiological environment. In this sense, fluorescent lipid analogues become useful biophysical tools. As described in Section 1.4.3, despite these amphipathic lipids can be labelled with bulky chromophores, such as BODIPY or NBD, the resulting probes give rise to substantial alterations of electron charge distribution, molecular size and conformation of the lipid bilayer. However, conjugated linear polyenes are strongly absorbing chromophores that may attain modest but useful fluorescence yields. Most important, they are reported to behave *in vivo* like their endogenous counterparts with respect to uptake, metabolism, transport and localization in membrane microdomains. However, when these labelled lipids are part of the *N*-acyl or the *O*-acyl chains of the SLs, the fluorophore can be released by hydrolysis of the amide or the ester bonds and the resulting sphingoid base is no longer traceable.

Taking into account the above considerations, the following main objective was pursued in the present thesis:

1. To synthesise a novel ceramide analogue, containing a conjugated pentaene moiety as fluorescent tag. Its fluorescence is expected to be modulated with total spatiotemporal control by the presence of a suitable radical quencher that can be removed by the action of a specific enzyme in the natural membrane (neutral ceramidase, nCDase) (Figure 2.1). Thus, when the fluorophore and the quencher are in close proximity, the fluorescence will be attenuated. Upon releasing of the quencher, the resulting pentaene sphingosine-like probe would recover its fluorescence, allowing its detection throughout the lipid bilayer or cell system. This type of fluorescent probes can be useful to study the formation and fate of microdomains at concentrations closer to those present in the cell

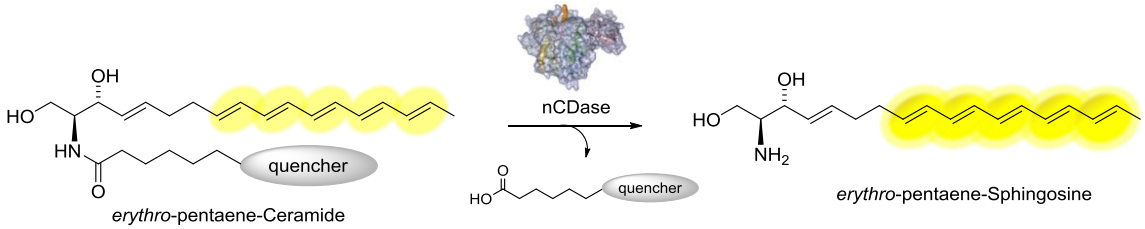

Figure 2.1 General overview of the present project.

The introduction of radical scavengers (*n*-DOXYL) as part of the *N*-acyl chain of the natural ceramide (*n*-DOXYL-Cer) was already studied in our research group (data not shown). Thus, *n*-DOXYL-Cer behaves similarly to Cer as nCDase substrate. Additionally, studies with differential scanning calorimetry and confocal/two-photon microscopy, confirmed that the *n*-DOXYL-Cer probes also behaved similarly to the natural Cer in lipid vesicles, exhibiting a cooperative profile and partitioning in ordered-domains. However, the introduction into lipid bilayers of a pentaene moiety containing a radical quencher in the same molecule had not been examined previously. In this sense, as a proof of concept, the following objective was considered:

2. To synthesize a simplified model, based on a conjugated pentaene system with a radical scavenger at different positions (Figure 2.2). This will allow us:

i. To evaluate the capacity of the radical quencher to modulate the fluorescence of the probe in model membranes.
ii. To verify if the radical quencher, after hydrolysis of the amide bond, would be able to quench intermolecularly the reporter polyene system.
iii. To confirm if the conjugated pentaene moiety is suitable to be analysed by fluorescence confocal microscopy.

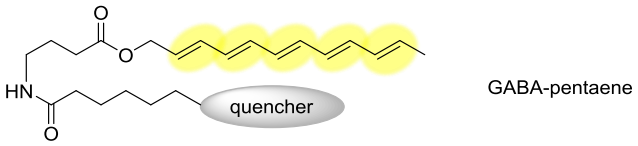

Figure 2.2 GABA-pentaene model probes. Simplify structure as a proof of concept.

3. RESULTS & DISCUSSION

3.1 GABA-pentaene analogues as membrane probes

The studies comprehended in Section 3.1 resulted in the following publication:

Nieves, I.; Artetxe, I.; Abad, J. L.; Alonso, A.; Busto, J. V.; Fajarí, L.; Montes, L. R.; Sot, J.; Delgado, A.; Goñi, F. M. *Langmuir* **2015**, *31*, 2484–2492.

3.1.1 Introduction

The studies of lateral phase separation in bilayers have benefited from the use of fluorescence techniques, both spectroscopic and microscopic[49,79,87,150,151], as reviewed in the General Introduction. Nevertheless, fluorescence studies of lipids suffer from the inherent limitation of requiring fluorescent probes. An important property of any membrane probe is its distribution among the various lamellar phases (gel, liquid-ordered, liquid-disordered), therefore a detailed understanding of the behaviour of fluorescent probes in defined lipid bilayer systems is essential before they can be used in physicochemical studies of lipid mixtures.

Fluorescence arising from natural polyene systems has been known for decades, and more recently, pentaene derivatives probes have been synthesised for biophysical studies (see also 1.4.3). In contrast to most bulky labelled lipids, such as BODIPY- or NBD-lipids, the pentaene system has been described to behave like their endogenous counterparts in model and cell membranes[109,131–133]. On the other hand, dual fluorophore-quencher systems have been reported as powerful analytical tools to detect changes in the lipid environment[142,143,152] (see 1.4.4).

Following this line of experimental research, the present chapter introduces the unreported GABA-pentaene probes, which combine a conjugated pentaene system (fluorophore) with a DOXYL group (profluorescent nitroxide), as fluorometric probes for the study of cell membranes (Figure 3.1.1).

Our GABA-pentaene probes have been designed as structural analogues of palmitoyl-Cer in order to mimic and behave as closely as possible to the natural Cer. However, the sphingoid base backbone of GABA-pentaene probes differ in the lack of the hydroxyl group at C1, and the presence of an ester group instead of the secondary hydroxyl functionality in C3. (Figure 3.1.1). The overall effect is a decrease of the head group polarity. Noteworthy, a group of natural 1-deoxy ceramides have recently been reported to exhibit interesting biophysical properties in mammalian cells [153]. Altogether, this structural modification enables to simplify their synthetic preparation, and then, to readily study their biophysical properties as a proof of concept.

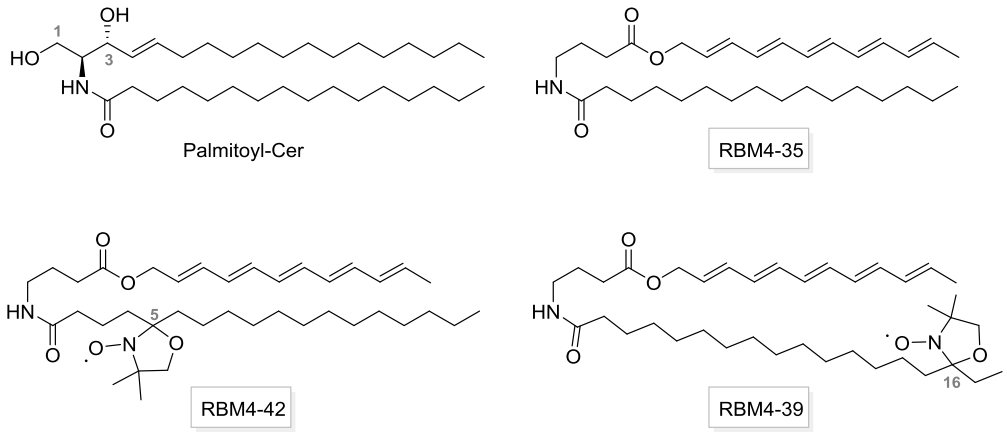

Figure 3.1.1 GABA-pentaene probes described in this chapter as structural analogues of palmitoyl-ceramide.

As depicted in Figure 3.1.1, the palmitoyl-RBM4-35 probe was designed as a reference of maximum fluorescence intensity, since it did not contain a radical quencher. On the other hand, the novel compounds RBM4-39 and RBM4-42, containing a DOXYL radical in the *N*-acyl chain at positions 16 and 5, respectively, represented suitable probes to monitor the decay of fluorescence intensity by DOXYL quenching. The nitroxide radical is likely to quench the fluorescence of the pentaene moiety when both the acyl and sphingosine-like chains are in close proximity. As a result, these GABA-pentaene probes can act as useful tools in the study of SLs in membranes.

This chapter is divided into two parts. In section 3.1.2, we present the synthetic approaches developed to prepare the GABA-pentaene probes, whereas in section 3.1.3, we summarise the biophysical studies carried out with these probes. According to the objectives of this doctoral thesis, the GABA-pentaene compounds were designed to gain valuable preliminary information about pentaene-nitroxide systems, in order to design further fluorescent tools containing the *erytho*-ceramide framework (see 2.General Objectives).

The fluorescence spectroscopy and microscopy studies, as well as the differential scanning calorimetry assays presented in section 3.1.3, were performed in collaboration with the Biophysics Unit of the University of the Basque Country, as part of a pre-doctoral stay. Besides, the EPR studies were developed in collaboration with the EPR Unit of the Institute of Advanced Chemistry of Catalonia of the Spanish Council for Scientific Research.

3.1.2 Synthesis of GABA-pentaene probes

3.1.2.1 Introduction and scope

Synthesis of polyenes

The synthesis of conjugated polyenes is a challenging task by their sensitivity to light, oxygen and some reagents, including protic and Lewis acids, as well as by the difficulties in controlling the double bond stereochemistry. In this sense, the success in the synthesis of these systems lies in producing alkenes in high geometric purity by a reliable olefination procedure, which, in turn, must be mild and functional group tolerant. In addition, the degree of substitution of the conjugated polyene chains, can determine the stability of the compound[154].

Common methods for the synthesis of polyenes include carbonyl olefination, transition metal couplings, alkenylations via alkyne addition, and elimination reactions (Figure 3.1.2).

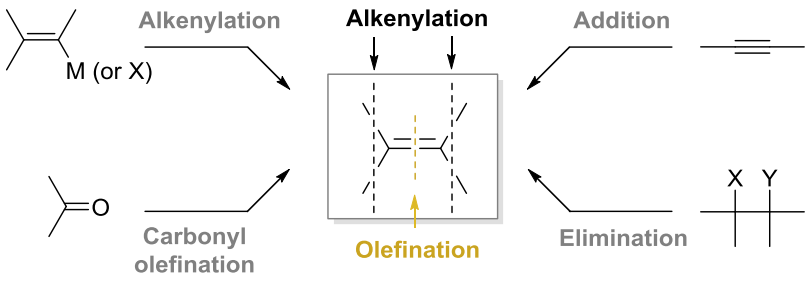

Figure 3.1.2 Principal strategies to prepare polyconjugated compounds. Image taken from Negishi *et al.*[155]

Over the last decades, the regio- and stereoselective synthesis of alkenes have been reinforced by the development of P-, S-[156], and Si-based[157] carbonyl olefinations. Representative P-based reactions are the Wittig olefination (see section 3.2.2.1) and its variant, the Horner-Wadsworth-Emmons reaction (HWE). However, the Wittig reaction often suffers from a lack of stereocontrol leading to a mixture of isomers, which can be avoided by the use of the HWE approach.

In recent years, a series of stereoselective and group tolerant organometallic alkenylation strategies have been developed using transition metals, for instance Pd, Zn, Sn, B, Al or Zr, affording new synthetic protocols, such as the Negishi cross-

coupling or the hydrozirconation reaction, as described in sections 3.2.4 and 3.2.5, respectively.

Although generally considered as competitive, the metal alkenylation and the carbonyl olefination to synthesise alkenes are also complementary routes. Recently, the combination of both strategies has gained relevance into the synthesis of conjugated polyene systems, highlighting their efficiency and selectivity[125,155,158–160].

Horner-Wadsworth-Emmons olefination

The modification of the Wittig olefination, involving the reaction of phosphonate-stabilized carbanions with aldehydes or ketones, is generally referred to as Horner-Wadsworth-Emmons olefination (Figure 3.1.3).

Despite this reaction was originally described by Horner *et al*., the advantages of using phosphonates in alkene synthesis were not demonstrated until Wadsworth and Emmons popularized this method among the organic synthetic community[161,162].

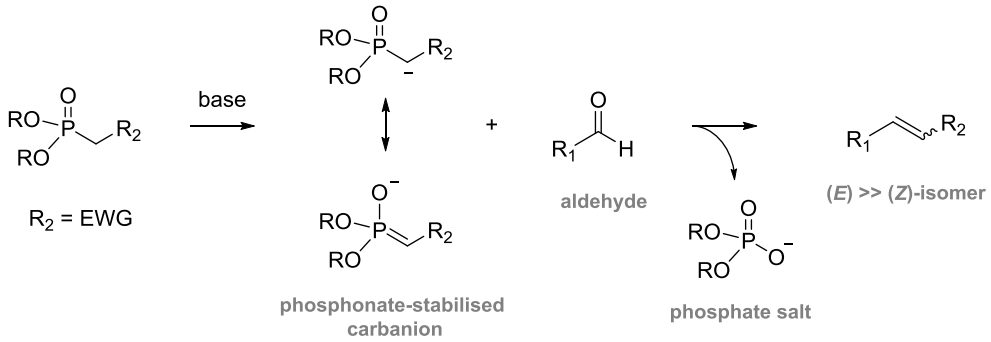

Figure 3.1.3 Example of a HWE reaction between a phosphonate-stabilised carbanion and an aldehyde. EWG: electron-withdrawing group.

Mechanistically (Figure 3.1.4), it is generally accepted that the HWE reaction occurs with the addition of a phosphonate-stabilised carbanion to an aldehyde or ketone, followed by formation of an oxaphosphetane, pseudo-rotation, and final P-C and O-C bond cleavage[163]. It should be pointed out that the decomposition of the oxaphosphetane intermediate requires an electron-withdrawing group (EWG) α to the phosphonate moiety.

The stereochemical outcome of the HWE reaction is a result of both kinetic and thermodynamic controls upon the reversible formation of *erythro* and *threo* aldehyde/phosphonate adducts and their decomposition to alkenes. Generally, the phosphonates containing alkyl substituents favour the formation of (*E*)-olefins[162,164].

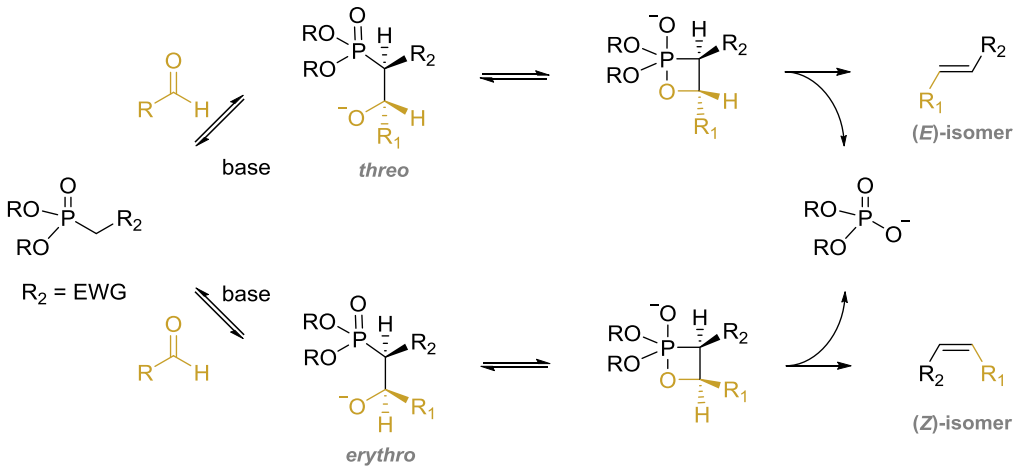

Figure 3.1.4 Mechanism of the HWE olefination. Image adapted from Gu *et al.*[162]

In contrast to the Wittig reaction (see section 3.2.2.1), the phosphonate-stabilised carbanions are more nucleophilic than the phosphonium ylides. In addition, the HWE reaction yields water-soluble phosphate salts as by-products, which can be readily removed from the desired alkenes by simple extraction.

Phosphorous ylide-based reactions have played a pivotal role in the construction of long polyene chains, whereas the HWE reaction has enabled the elongation of aldehydes by the sequential introduction of one double bond in each synthetic step.

3.1.2.2 Retrosynthetic analysis of GABA-pentaene probes

The assembly of GABA-pentaene probes was initially envisaged by an esterification between the pentaene alcohol RBM4-33 and a *N*-protected γ-aminobutyric acid (GABA), as depicted in Scheme 3.1.1. In light of the sensitivity of the conjugated polyene systems, we initially considered the one-pot deprotection-acylation of the amino group as the most suitable approach[165].

The key pentaene alcohol precursor RBM4-33 was planned by applying two cycles of chain elongation using the HWE olefination strategy[166] from the commercially available 2,4-hexadienal.

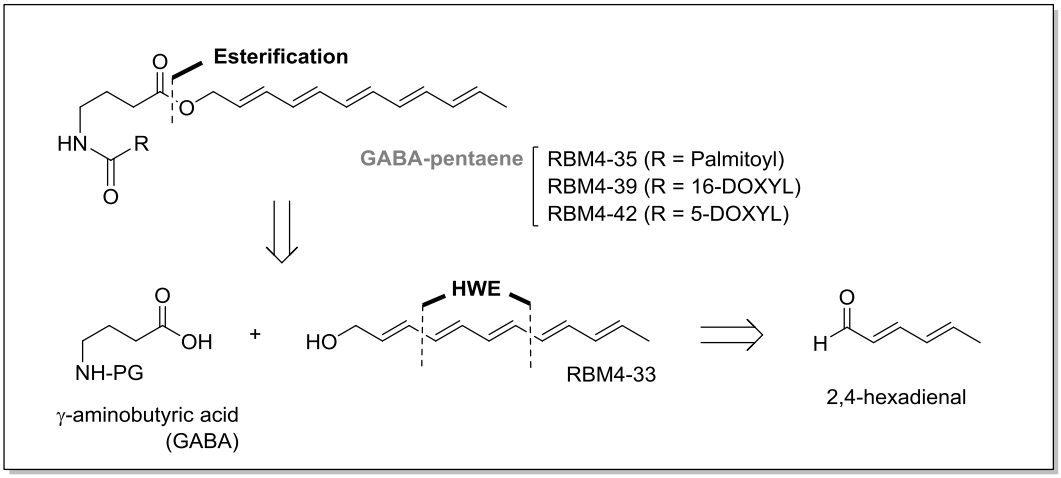

Scheme 3.1.1 Retrosynthetic analysis of GABA-pentaene probes.

3.1.2.3 Synthesis of pentaene alcohol RBM4-33

The diverse synthetic strategies reported for the construction of the pentaene alcohol RBM4-33 were based on the reduction of the corresponding pentaene aldehyde precursor[166–169]. Initially, the polyene aldehydes were obtained by the iterative aldol-type condensation of aldehydes with crotonaldehyde, using piperidinium acetate as catalyst[170,171]. However, in recent years, the use of Wittig[109,131,172] or HWE olefination reactions[166,168,173–175] have become the strategy of choice.

In the present section, two routes for the synthesis of RBM4-33 are described.

Route I

The elongation of the conjugated double bond system was first carried out by applying a series of iterative Wittig olefinations between a polyene aldehyde and the triphenylphosphonium salt **1**, as reported by Kuerschner *et al.*[109] following the procedure of Duhamel *et al.*[172] (Figure 3.1.5).

The required triphenylphosphonium salt **1** was obtained in excellent yield by heating commercial 2-bromomethyl-1,3-dioxolane with neat PPh_3. Subsequent Wittig reaction with commercial 2,4-hexadienal provided the corresponding conjugated dioxolane RBM4-1 (data not shown), which was next deprotected with aqueous HCl in THF, affording RBM4-2 in moderate yield (34%) However, the low yields (11%) obtained in the second elongation cycle to give RBM4-4, we disregarded this approach to the synthesis of alcohol RBM4-33.

Attempts to increase the reaction yield by generating the phosphorous ylide with KHMDS or by reducing the concentration of acid in the deprotection step, turned out to be fruitless, possibly due to the instability of the polyene system.

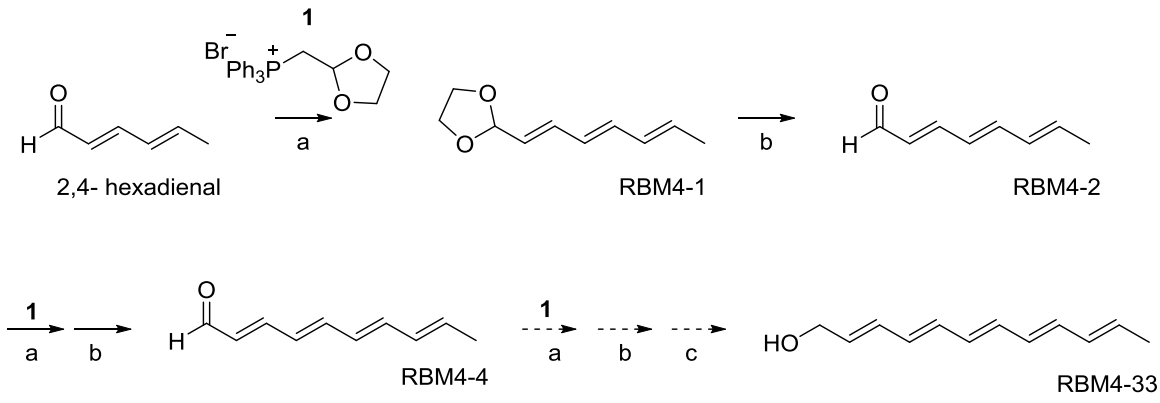

Figure 3.1.5 Initial route for the synthesis of RBM4-33. Reagents and conditions: (a) NaH, THF, 50 ºC, 2h; (b) HCl (12%), THF, RT, 16h. RBM4-2: 35% (over steps a-b); RBM4-4: 11% (over steps a-b).

Route II

In consideration of the above results, we were attracted by the simplicity of the iterative HWE approach, which had already been applied in several syntheses[173,174], including that of our target pentane alcohol RBM4-33[166]. Furthermore, in this work, 2-iodoxybenzoic acid (IBX) was used as a mild oxidant of the intermediate aldehyde, in contrast to other common oxidants reported in the literature, such as permanganate salts[174] or the Jones reagent[176].

Accordingly, the commercial 2,4-hexadienal was elongated with two double bonds in one step by means of the HWE reaction with triethyl 4-phosphonocrotonate ylide. The resulting ester RBM4-5 was reduced to the corresponding alcohol, and further oxidised with IBX to give the aldehyde RBM4-4 in excellent yield (Figure 3.1.6). It is worthy of mention that aldehyde RBM4-4 was also a versatile starting material for the different synthetic strategies that will be described in section 3.2. Finally, the aldehyde RBM4-4 was again elongated by HWE olefination to give a pentaene ester, which was reduced with DIBAL-H to the desired alcohol RBM4-33 in good yield. In consideration of the NMR spectral data, the pentaene RBM4-33 was mostly obtained as the (*all-E*)-isomer.

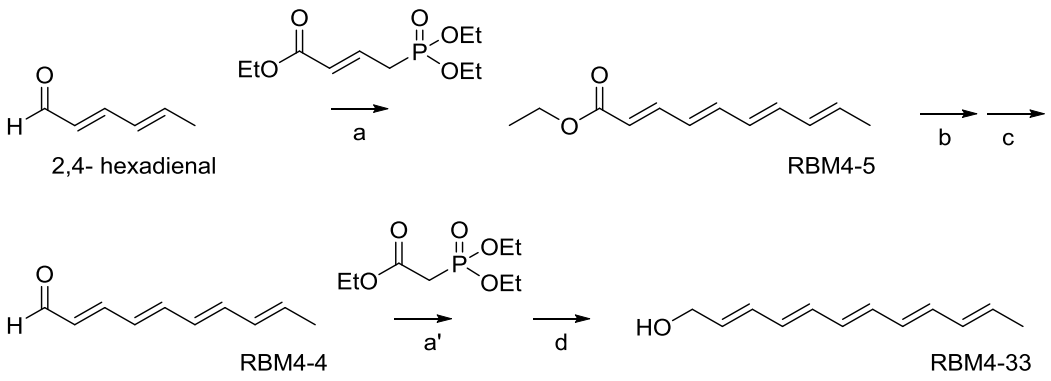

Figure 3.1.6 Route II for the synthesis of RBM4-33. Reagents and conditions: (a) NaH, THF, 0 ºC, 3h, RBM4-5: 40%; (b) DIBAL-H, hexane, -78ºC, 1h; (c) IBX, AcOEt, reflux, 16h, RBM4-4: 80% (over b-c steps); (a') RBM4-32: 75%; (d) DIBAL-H, DCM, -78ºC, 2h, RBM4-33: quantitative.

Due to the observed instability of polyene alcohol RBM4-33, its chromatographic purification must be avoided and the compound must be freshly prepared just before use.

3.1.2.4 Synthesis of the GABA-pentaene system

Route I

With the required polyenic alcohol RBM4-33 in hand, we next focused our attention on the assembly of the polyene moiety to the GABA framework. To address this need, we examined an esterification reaction between the commercially available *N*-Fmoc GABA and the alcohol RBM4-33 (Figure 3.1.7).

Initial attempts were based on the reported method of Fichna *et al.*[177], using *N*-methylmorpholine as base and HOBt as coupling reagent in DMF. However, these conditions afforded complex reaction mixtures and low yields of the required ester. Alternatively, the use of EDC/HOBt as coupling system in DCM afforded RBM4-34, albeit in low yield (<20%). (Figure 3.1.7).

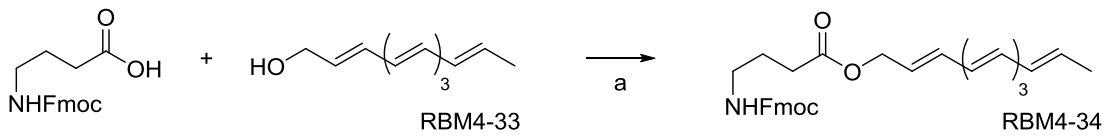

Figure 3.1.7 Esterification of GABA-Fmoc with RBM4-33. Reagents and conditions: (a) EDC, HOBt, Et_3N, DCM, RT, 16h, <20%.

In light of the sensitivity of the long conjugated polyene chains, and also to avoid a intramolecular *N*-acylation of the intermediate amino ester arising from RBM4-34 after the required Fmoc removal in the subsequent synthetic step, we focused on a sequential one-pot deprotection-acylation of RBM4-34, according to the method described by Li *et al*.[165] This method requires KF to remove the Fmoc group, followed by reaction of the transient amino ester with an activated carboxylic acid. Initial experiments with Fmoc-amino ester **2**, a saturated analogue of RBM4-34, and palmitic acid, in the presence of different coupling reagents, are shown in Table 3.1.1. While the use of HOBt as coupling partner was inefficient (entry 1), the pair EDC/HOBt afforded the saturated RBM4-36 in 40% yield (entry 2). However, these conditions were not suitable for the amidation of RBM4-34 (entry 3), whose polyene moiety appeared clearly deteriorated in the crude reaction mixture.

In order to find milder reaction conditions, compatible with the pentaene framework, the excess KF was reduced (entry 4), amine bases, such as piperidine or *N*-methylmorpholine were used to remove the Fmoc group (entries 5-7), and BOP was

used as coupling reagent[178] (entry 6). Nevertheless, any of the above conditions proved suitable for the amidation of RBM4-34.

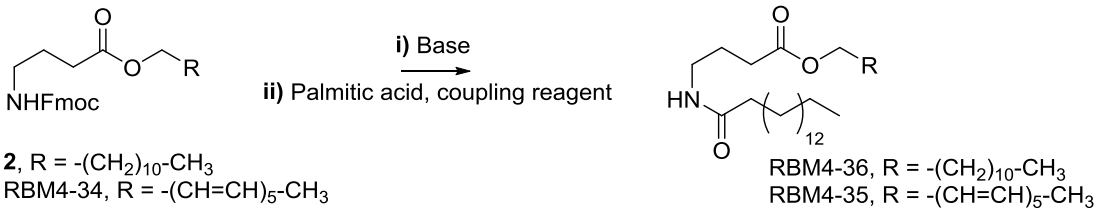

2, R = -$(CH_2)_{10}$-CH_3
RBM4-34, R = -$(CH=CH)_5$-CH_3

RBM4-36, R = -$(CH_2)_{10}$-CH_3
RBM4-35, R = -$(CH=CH)_5$-CH_3

Table 3.1.1 Attempts for the one-pot deprotection and *N*-acylation of RBM4-34

Entry	Substrate	Base (eq)	Coupling conditions	Solvent	Product yield (%)
1	2	KF (4)	A	DMF	-----
2	2	KF (4)	B	DMF	RBM4-36 (40%)
3	RBM4-34	KF (4)	B	DMF	----
4	RBM4-34	KF (2)	B	DMF	----
5	RBM4-34	Piperidine (0.05)	B	DMF	----
6	RBM4-34	Piperidine (0.05)	C	DCM	----
7	RBM4-34	NMM (0.5)	----	DCM	----

A: HOBt, Et_3N; **B:** EDC, HOBt, Et_3N; **C:** BOP, DIPEA.

Route II

In view of the above results, we considered to carry out the esterification of the polyene alcohol RBM4-33 with a suitably functionalized GABA derivative in the last step of the synthesis.

To address this need, the commercial GABA was quantitatively protected as the methyl ester **3**[179], which was then *N*-acylated with the required carboxylic acid. In this context, the *N*-acylation with palmitic acid under standard conditions proceeded smoothly, affording the intermediate **4** in 60% yield (Figure 3.1.8, a-b).

Initial attempts for the selective hydrolysis of the ester bond in **4** were carried out using potassium carbonate in MeOH or MeOH:H_2O. However, compound **5** was isolated along with fully deprotected GABA, as a result of the hydrolysis of the amide bond under these conditions. Alternatively, the hydrolysis of ester **4** with LiOH in THF:H_2O[180], afforded the corresponding acid **5** in excellent yield.

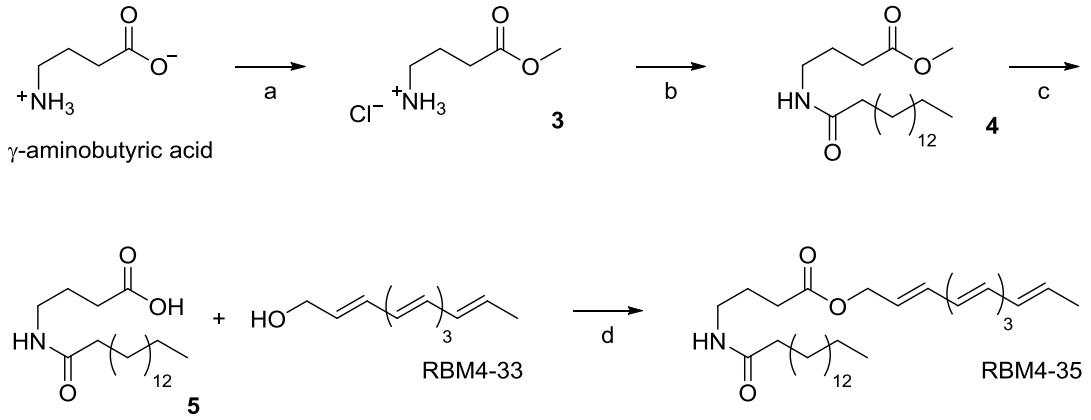

Figure 3.1.8 Synthesis of the GABA-pentaene-palmitoyl RBM4-35. Reagents and conditions: (a) acetyl chloride, MeOH, 0ºC to reflux, 16h, quantitative; (b) palmitic acid, EDC, HOBt, Et_3N, DCM, RT, 1.5h, 60%; (c) LiOH, THF:H_2O, RT, 1.5h, 80%; (d) EDC, DMAP, 0ºC to RT, 16h, 30%.

The carboxylic acid **5** was next esterified with the pentaene alcohol RBM4-33 (Figure 3.1.8, d) under Steglich conditions[181]. Thus, the carboxylic acid **5** was activated with EDC, in the presence of DMAP as an acyl transfer reagent, and coupled with the alcohol RBM4-33 to afford the desired pentaene GABA-palmitoyl RBM4-35 in 30% yield.

Aside from the palmitoyl derivative RBM4-35, we were also interested in the synthesis of the GABA-pentaene probes containing a nitroxide radical in the acyl chain (

Figure **3.1.9**). For this goal, the above synthetic route was slightly modified by *N*-acylation of the intermediate amino ester **3** with the free radicals 16-DOXYL- and 5-DOXYL-stearic acids, leading to probes RBM4-39 and RBM4-42, respectively.

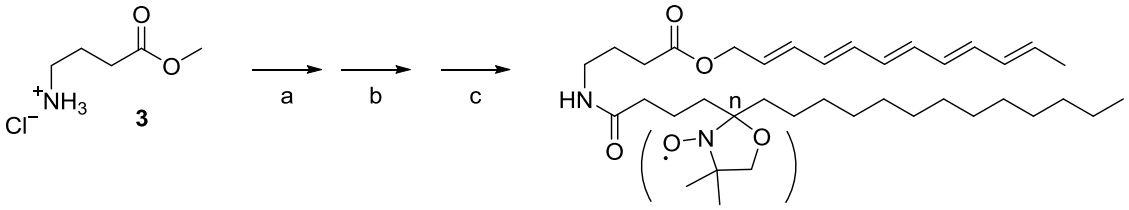

RBM4-39 **n** = DOXYL group at C16
RBM4-42 **n** = DOXYL group at C5

Figure 3.1.9 Synthesis of GABA-pentaene probes RBM4-39 and RBM4-42. Reagents and conditions: (a) free radical 16-DOXYL- or 5-DOXYL-stearic acid, EDC, HOBt, Et_3N, DCM, RT, 2h, quantitative; (b) LiOH, THF:H_2O, RT, 1.5h, 70-85%; (c) EDC, DMAP, RBM4-33, 0ºC to RT, 6h, 40%.

3.1.3 Biophysical studies with GABA-pentaene probes

3.1.3.1 Model membranes

Biological systems are characterised for their enormous complexity. Thus, biophysical studies generally aim at the reconstitution of cellular or molecular subsystems of reduced complexity in cell-free, well-controlled environments, in order to assess the properties and behaviour of the biological system. In this context, many cell membrane studies rely on model membranes[182].

Different model membranes have been developed through the years, such as lipid monolayers, supported planar bilayers and lipid vesicles or liposomes, each suitable for specific studies or techniques. Amongst these oversimplified versions of natural membranes, the present section will focus on liposomes.

Liposomes

Liposomes or lipid vesicles are microscopic structures consisting of one or more concentric lipid bilayers surrounding aqueous compartments. Liposomes are spontaneously generated upon hydration of cylindrically shaped lipids in aqueous solutions, thus organising their polar head groups and hydrophobic parts to form a closed bilayer, lamellar membrane-like structure (Figure 3.1.10, A-B). The amphipathic molecules more often used are the phospholipids, whose length and unsaturation of the acyl chains can determine the structural and physical state of the model membranes (see General Introduction 1.2). In practice, the most frequent components of liposomes are natural egg phosphatidylcholine (ePC) and synthetic analogues, such as 1,2-dioleoyl-*sn*-glycero-3-phosphocholine (DOPC), 1,2-dipalmitoyl-*sn*-glycero-3-phosphocholine (DPPC), 1,2-distearoyl-*sn*-glycero-3-phos-phocholine (DSPC), and phospholipid-sterol mixtures[183] (Figure 3.1.10, C).

Since Alec Bangham described in 1965 the first liposomes[184], their application has been extensively studied in different fields. For instance, for measuring fusion, fission, leakage processes, lipid flip-flop motion, protein–protein or protein–lipid interactions. Besides, liposomes have been used as carriers for drug delivery and combined with other nanomaterials to form multifunctional nanoparticles[185,186].

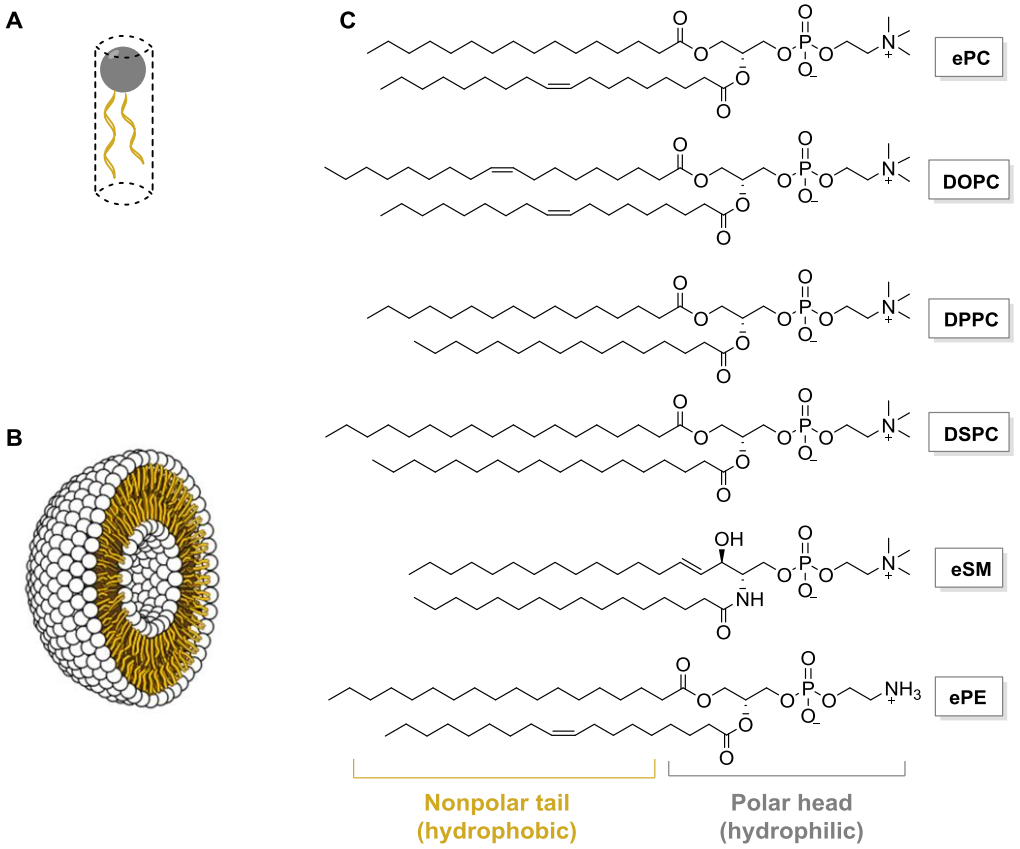

Figure 3.1.10 A: Cylindrical-shaped phospholipid; **B**: Cross section view of liposome**; C:** SLs and phospholipids used in this section.

Liposomes are structurally classified into multilamellar vesicles (MLVs) and unilamellar vesicles (ULVs). The latter can be further classified on the basis of their size and the method of preparation as large unilamellar vesicles (LUVs), small unilamellar vesicles (SUVs), and giant unilamellar vesicles (GUVs).

The MLVs are spontaneously generated after lipid hydration and sample shaking, leading to liposomes containing between 7 and 10 concentric bilayers, each of them separated by a thin layer of water. The hydration step is done at a temperature above the gel-liquid phase transition temperature (Tm) of the lipid or above the Tm of the highest melting component in the lipid mixture. Vesicles are heterogeneous in size, displaying an average diameter of around 700 nm, but ranging from 100 to 5000 nm (Figure 3.1.11). As MLVs are easy and fast to prepare, they are mostly used in the characterisation of lipid phases, either by differential scanning calorimetry (DSC, see Section 3.1.3.3), NMR or X-ray diffraction techniques. However, the data analysis and interpretation of some processes can be affected by the presence of multilamellar systems.

To overcome the above drawback, LUVs are mostly generated by mechanical extrusion of MLVs suspensions, through polycarbonate porous filters, resulting in homogenous small stable vesicles with low curvature stress (60-500 nm of average diameter). Thus, LUVs represent suitable model systems for many biophysical studies (Figure 3.1.11).

On the other hand, SUVs, with diameters below 60 nm, present a high curvature stress, differing from natural cell membranes. However, the curvature stress can be useful for the study of membrane fusion and/or fission processes. SUVs are generally formed by sonication of MLVs suspensions.

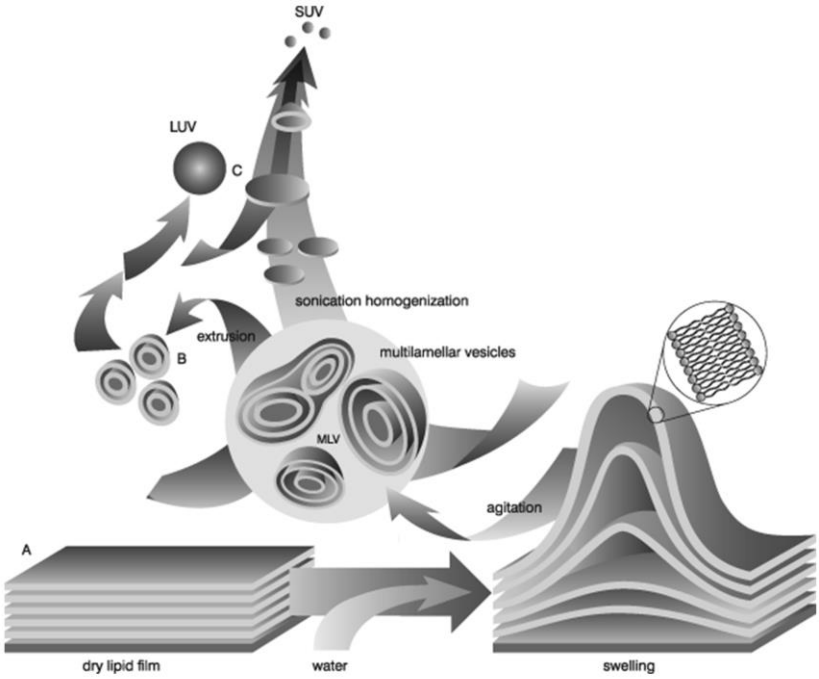

Figure 3.1.11 Liposomes: preparation and classification. A: dry lipid film; B: large multilamellar vesicles; C: large unilamellar vesicles. Image taken from Avanti Polar Lipids®.

As the diameters of GUVs vary from 5 to 100 μm, they are visible under the light microscope. Therein, the individual vesicle details can be directly observed and qualitative studies involving vesicle morphology shape and transformations can be carried out[187–190]. The generation of GUVs was first described by exposing dry lipid films to aqueous solutions, at temperature above that of the lipid main phase transition temperature. Thus, GUVs were spontaneously formed, but in very low total lipid yield and a with a very heterogeneous size distribution[191]. Some years later, Angelova and coworkers[192,193] developed a new method for GUVs preparation, based on the

exposure of dry lipid films to an aqueous solution under electric fields, leading to liposomes with a higher size homogeneity. In this context, two GUVs generation procedures have been reported; those prepared in solution, and those attached to a platinum wire for direct microscopy visualization (see Section 5.1.5).

In consideration of the liposomes described above, the present work was developed by using MLVs, LUVs and GUVs as suitable model systems for the study of fluorescent GABA-pentaene probes inside membrane environments.

3.1.3.2 Fluorescence spectroscopy

The absorption of ultraviolet and/ or visible radiation results in the excitation of electrons from the ground state to higher energy levels. The fluorescence process occurs when an excited electron in a S_2 state emits a photon from a lower energy S_1 state after an internal conversion process (Figure 3.1.12, left). In organic molecules, the electrons that contribute to the absorption/fluorescence processes are those that participate directly in bond formation, and those from nonbonding or unshared outer electrons of heteroatoms.

In conjugated polyene systems, the delocalised electrons from the π-orbitals enable the required transitions to the excited states, which bring the absorption peaks into an accessible spectral region (between 200 and 700 nm).

In symmetric, linear conjugated polyene systems the first excited singlet state (S_1) is of type ^1A_g, whereas the S_2 state is ^1B_u (Figure 3.1.12, left). In this case, the most intense absorption transition recorded experimentally corresponds to the $S_0 \rightarrow S_2$ excitation[194], because $S_0 \rightarrow S_1$ is symmetry-forbidden. However, the emission takes place exclusively from the S_1 state ($S_1 \rightarrow S_0$)[195]. Generally, the absorption and emission of (*all-E*) conjugated polyene systems follow this pattern[196].

The fluorescence quenching refers to any process that decreases the fluorescence intensity of a given substance[197]. When the fluorophore and the nitroxide (*n*-DOXYL) groups are combined in the same molecule, the quenching process arises through electron exchange, which modifies the electronic states of the fluorophore due to the unpaired electron spin of the nitroxide radical[142,152] (Figure 3.1.12, right). On removal of the radical quencher from the molecule, fluorescence is completely restored[142,143].

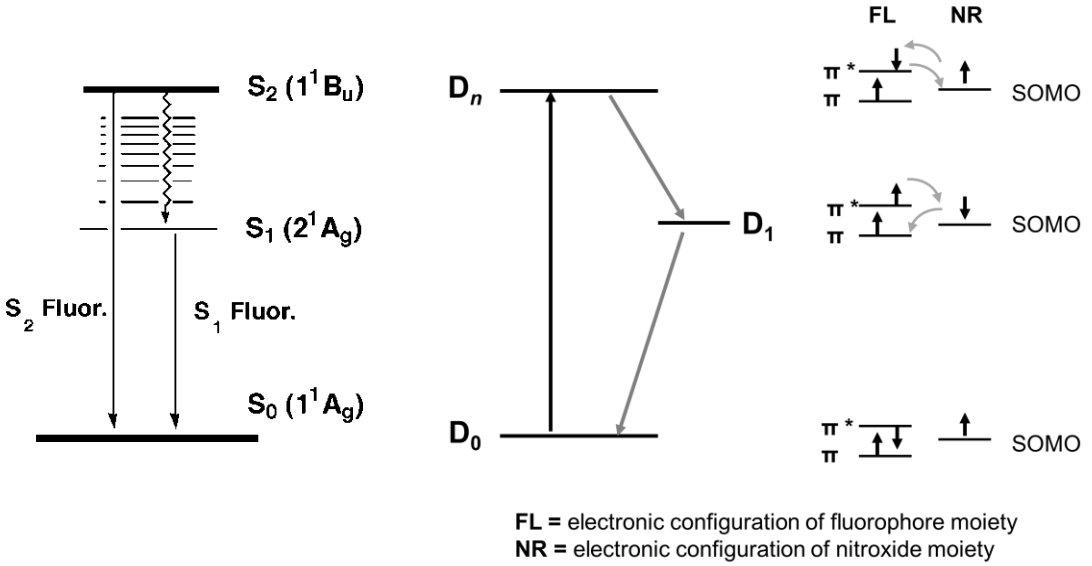

Figure 3.1.12 Left: General energy-level scheme and emitting states for (*all-E*)-polyenes. Image taken from Itoh[198]. **Right**: When the unpaired spin of a nitroxide radical interacts with the electrons in the conjugated system of a fluorophore, a change in the multiplicity of the electronic states results. The singlet ground state (S_0) and the lowest singlet excited state (S_1) become doublet states (D_0 and D_n respectively) owing to the antiparallel spin of the nitroxide radical. This results in a loss of fluorescence quantum yield due to an increase in the radiationless process of $D_n \rightarrow D_1 \rightarrow D_0$. SOMO: singly occupied molecular orbital. Image taken from Blinco *et al* [143].

Herein, the GABA-pentaene RBM4-35, containing a palmitoyl acyl chain, was taken as a reference for the maximum intensity of the absorbance and fluorescence processes possible for this type of structure. On the other hand, compounds RBM4-39 and RBM4-42, which were *N*-acylated with free radical DOXYL stearic acids, represented suitable probes to evaluate the fluorescence quenching (Figure 3.1.13).

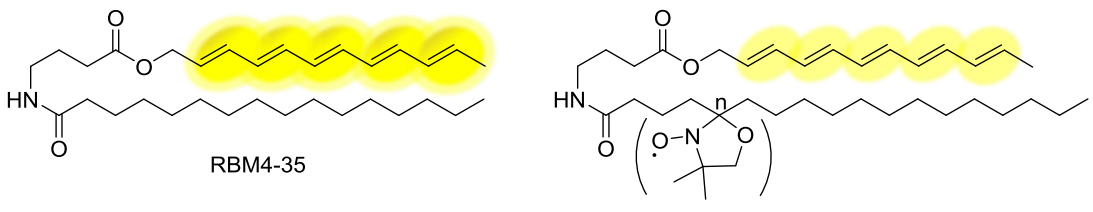

Figure 3.1.13 GABA-pentaene probes tested in this section.

Absorption and fluorescence properties of GABA-pentaene probes in solution

The first step in the characterization of the GABA-pentaene probes was the measurement of the excitation and emission spectra in various solvent systems, by using a QuantaMaster 40 spectrofluorometer (see Section 5.1.3.1). For this purpose, the pentaene probes were dissolved in different organic solvents, as 0.9 μM solutions, since this concentration was that required for further biophysical assays with liposomes.

As depicted in Figure 3.1.14, both excitation and emission spectra of the three probes varied depending on the solvent used. In all cases, the lowest absorption and emission intensities were observed in hexane and the highest ones in chloroform. The spectral properties of GABA-pentaene probes were similar to those of related conjugated pentaene compounds reported in the literature[132,136,154,196,199].

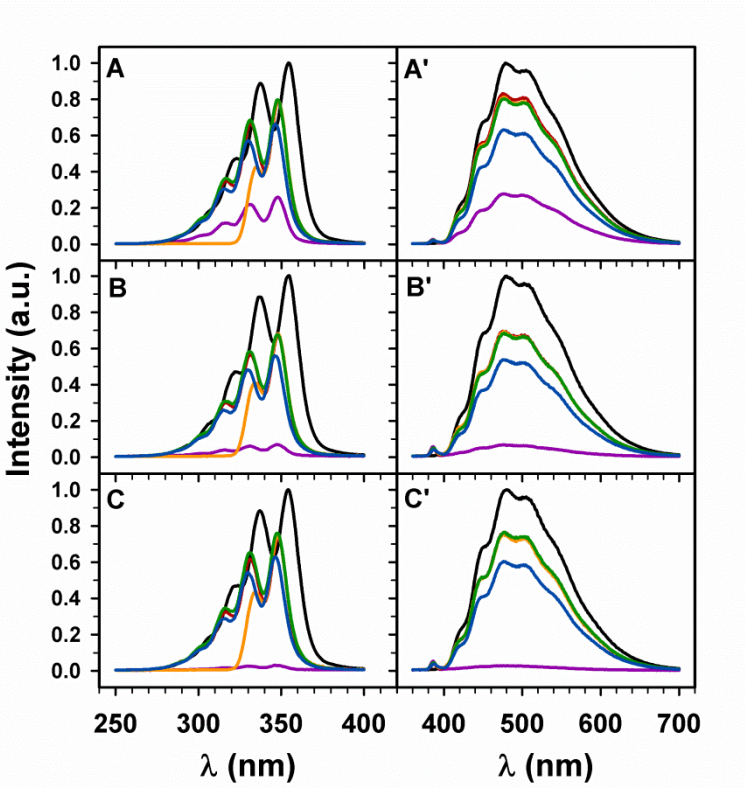

Figure 3.1.14 Fluorescence excitation (left panels) and emission (right panels) spectra for RBM4-35 (A and A'), RBM4-39 (B and B') and RBM4-42 (C and C') in different solvents. From less polar to more polar: hexane (purple), ethyl acetate (red), chloroform (black), acetone (orange), ethanol (green), methanol (blue).

Molar extinction coefficient and quantum yield measurements

The molar extinction coefficient (***ε***) and quantum yield (Φ_F) of GABA-pentaene probes were determined by using a SpectraMax M5 spectrophotometer (see Section 5.1.3.2).

Molar extinction coefficient (***ε***) is a parameter which defines the capacity of a substance to absorb light at a given wavelength per molar concentration. Polyenes are characterized by high molar extinction coefficients, despite their relatively simple and short π-system[200].

The ***ε*** calculated for pentaene probes applying Lambert-Beer's law, when excited at λ= 325 nm in ethanol, are outlined in Table 3.2.2. Regarding the molar extinction coefficients described for polyunsaturated systems (around 100,000 $M^{-1}cm^{-1}$ in ethanol)[196], GABA-pentaene probes presented lower values (around 16,000-24,000 $M^{-1}cm^{-1}$). Noteworthy, compound RBM4-42, which contained a nitroxide radical, exhibited major ***ε*** value towards RBM4-35, the probe of reference lacking a quencher.

Table 3.1.2 Molar extinction coefficient (ε) and fluorescence quantum yields ($\boldsymbol{\Phi_F}$) of GABA-pentaene probes.

Compound	Solvent	ε ($M^{-1}cm^{-1}$) λ_{ex}=325 nm	[conc.] (10^{-6} M)	Absorbance λ_{ex}=346 nm	Φ_F λ_{ex}=346 nm
9,10-DPA[201]	EtOH		5	0.043	0.95
RBM4-35	EtOH	16,028	2	0.041	0.060
RBM4-39	EtOH	14,972	2.25	0.045	0.048
RBM4-42	EtOH	23,659	1.5	0.044	0.031

The fluorescence quantum yield is defined as the ratio of the number of photons emitted to the number of photons absorbed, giving information of the efficiency of the fluorescence process. The maximum fluorescence quantum yield is 1.0 (100%), where each photon absorbed results in a photon emitted.

The fluorescence quantum yields were calculated by measuring the integrated emission area for the spectra of the pentaene compound, related to the area measured for 9,10-diphenylanthracene (9,10-DPA) in ethanol (η=1.361)[202] after excitation at 346 nm (Φ_F^{ref} = 0.95)[201]. Quantum yields for GABA-pentaene products were then calculated using the equation (**5**) described in the Experimental Section 5.1.3.3..

Thus, the fluorescence quantum yield obtained for all GABA-pentaene compounds, (Table 3.2.2), were consistent with those reported in the literature[196]. As expected, the Φ_F of the model probe RBM4-35 was higher those of RBM4-39 and RBM4-42, having a radical nitroxide in the acyl chain.

Absorption and fluorescence properties of GABA-pentaene probes in lipid bilayers

In order to monitor the absorption and fluorescence properties of the GABA-pentaene probes in relation to the nature of the environment, the fluorophores were incorporated into liposomes of different lipid composition.

To address this need, large unilamellar vesicles (LUVs) with different fluidities were generated. The unsaturations of the acyl chains from the glycerophospholipids DOPC and ePC conferred fluid bilayers ($\mathbf{L_d}$), whereas the long saturated acyl chains from DPPC and DSPC induced gel phase ($\mathbf{L_\beta}$) membranes (see Figure 3.1.10 and General Introduction 1.2).

Fluorescence measurements were performed in liposome suspensions (0.3 mM in lipid with 0.3 mol% of the polyene probes), by using a QuantaMaster 40 spectrofluorometer (see Section 5.1.3.4). Three independent experiments were done for each of the four lipid compositions used, and the fluorescence values of RBM4-39 and RBM4-42 were normalised to the maximum intensity of RBM4-35. The background signal was subtracted from a control liposome with no fluorophore.

The fluorescence excitation and emission spectra of the GABA-pentaene probes after their incorporation in pure lipid bilayers of different fluidities are outlined in Figure 3.1.15. The three polyenes showed a maximum excitation around 353 nm and a maximum emission at 478 nm, regardless of the environment. Additionally, the absolute intensity of the reference probe RBM4-35 remained fairly constant (±10%) in all four lipid compositions.

According to Figure 3.1.15, probes containing the nitroxide radical (RBM4-39 and RBM4-42) exhibited lower fluorescent emissions related to RBM4-35 when incorporated in gel-phase membranes (DSPC and DPPC). Nevertheless, in fluid bilayers (Figure 3.1.15, C-C' and D-D') the intensities of RBM4-39 and RBM4-42 were very similar to those of the reference. Thus, the fluorescence quenching by the presence of the DOXYL stearoyl radical evidenced a clear dependency on the membrane fluidity. This tendency is also illustrated in Figure 3.1.16.

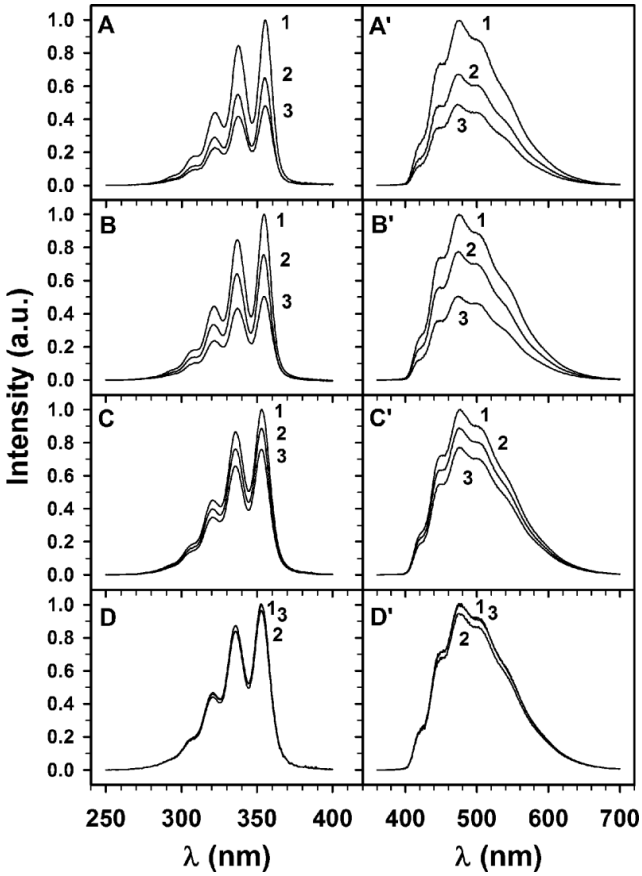

Figure 3.1.15 Fluorescence excitation (left panels) and emission (right panels) spectra for probes RBM4-42 (2) and RBM4-39 (3), normalized to RBM4-35 (1). Lipid bilayers were composed of DSPC (A-A'), DPPC (B-B'), ePC (C-C'), and DOPC (D-D').

The quenching efficiency was determined by comparison with the intensity of probe RBM4-35. In this regard, in RBM4-39 (DOXYL group at C16 position of the acyl chain), the fluorescence quenching showed a high dependency on the fluidity of the bilayer, reaching a 50% in gel liposomes, but only a 20% in fluid liposomes (Figure 3.1.16). In contrast, the quenching ability of RBM4-42 (DOXYL group at C5 position of the acyl chain), exhibited a more gradual sensitivity to the bilayer composition, from about 30−35% quenching in liposomes made of DSPC to <10% in ePC bilayers. These results were consistent with a tighter packing of the probes in the rigid bilayers, which reduces the conformational mobility of the DOXYL-stearoyl chain and favours the spatial proximity of the DOXYL radical to the polyene system.

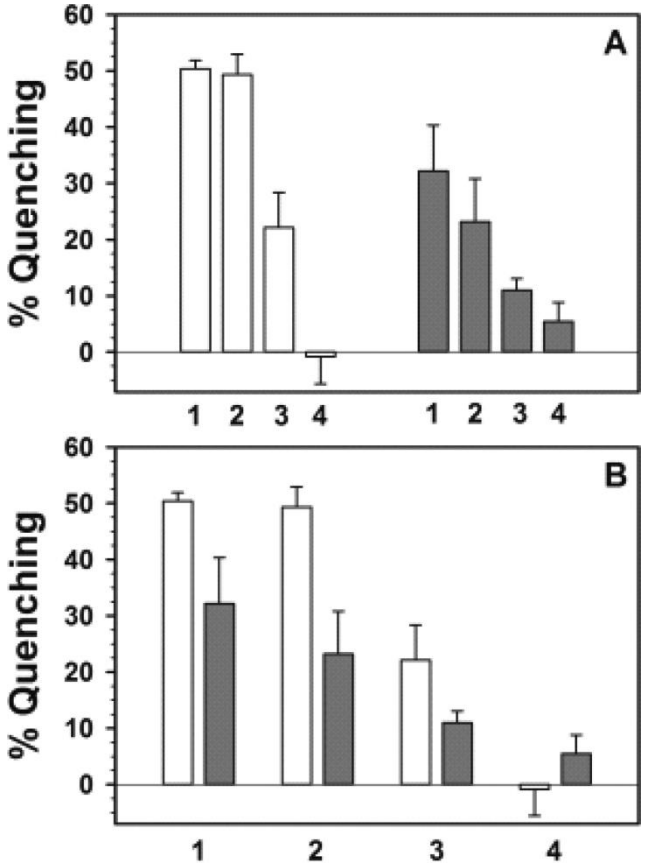

Figure 3.1.16 (A) Effect of lipid composition; (B) effect of the DOXYL position. Quenching of pentaene fluorescence emission in liposomes of varying compositions: DSPC (1), DPPC (2), ePC (3), and DOPC (4). RBM4-39 (empty bars) and RBM4-42 (full bars).

In consideration of the above results, we were prompted to evaluate if free *n*-DOXYL stearic acid, would be able to interact *intermolecularly* as a radical quencher with the polyene moiety, a situation that would take place if the amide bond of the target polyene-Cer were hydrolysed by nCDase in a natural membrane (see Figure 2.1). For this purpose, the model probe RBM4-35 was incorporated into LUVs of different lipid composition (0.3 mol % probe in 0.3 mM lipid), doped with increasing percentages of 5-DOXYL or 16-DOXYL stearic acids. As shown in Figure 3.1.17, it was necessary to reach a (1:70) ratio of (RBM4-35:*n*-DOXYL stearic acid) to observe a significant fluorescence quenching. The high DOXYL:polyene ratio required for an effective fluorescence quenching make us assume that *no intermolecular* quenching is expected to take place from the hypothetical hydrolysis of a Cer-polyene probe, which can only give rise to a DOXYL:polyene ratio of 1.1.

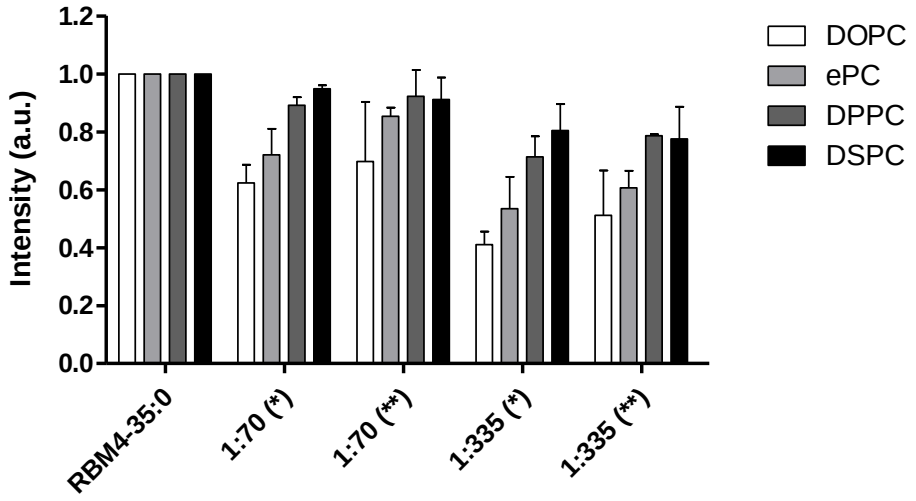

Figure 3.1.17 Fluorescence intensities of RBM4-35 in liposomes of different fluidities, after the external addition of increasing percentages of (∗) 5-DOXYL stearic acid and (∗∗) 16-DOXYL stearic acid. Ratio (RBM4-35: *n*-DOXYL stearic acid added).

3.1.3.3 Differential scanning calorimetry (DSC)

Differential scanning calorimetry (DSC) monitors heat effects associated with phase transitions or chemical processes. This technique is based on recording, as a function of temperature (T), the difference of the heat capacity (C_p) between a cell containing a sample (MLVs suspension) and a reference cell (pure buffer used to form the liposomes) at the same temperature. Both cells are in an adiabatic chamber[203].

The recent improvements in DSC instrumentation have generated new opportunities for the study of the effects of structure and the environment changes on the behaviour of proteins, nucleic acids, and lipids[204].

Focusing on the study of lipid phase transitions, DSC allows determining the thermodynamic parameters for the lipid phase transition induced by temperature changes. The resulting scan of a sample is called thermogram, where C_p is represented as a function of T. Lipid phase transitions typically display a peak on the thermogram, whose area corresponds to the enthalpic change, and the direction of the peak indicates whether the thermal event is exothermic or endothermic. In addition, pure lipids with measurable phase transitions commonly display symmetric peaks, whereas asymmetric peaks are obtained when measuring lipid mixtures. Three main parameters can be defined in lipid phase transitions, as depicted in Figure 3.1.18:

i. *Phase transition temperature* (Tm): it is given by the temperature associated to the maximum change of entropy.[205] It corresponds to the transition of lamellar gel phase to lamellar fluid phase.

ii. *Phase transition width* ($\Delta T_{1/2}$), is the increment in ºC at half the height of the transition temperature. It gives information on the transition´s cooperativity or molecular cooperation between lipid molecules. Lower values of $\Delta T_{1/2}$, indicates phase transitions with high cooperativity.

iii. *Phase transition enthalpy* (ΔH), measures the amount of heat required to complete the phase transition, and is obtained by integration of the phase transition curve.

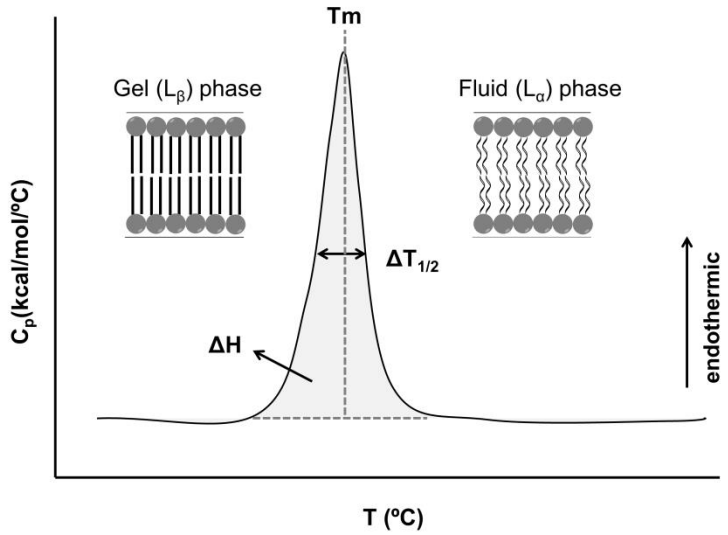

Figure 3.1.18 Thermodynamic parameters derived from a DSC thermogram. Image adapted from Goñi *et al.*[203]

DSC of RBM4-35 in aqueous dispersion and in DPPC lipid vesicles

GABA-pentaene probes can be regarded as structural analogues of natural palmitoyl-Cer. Nevertheless, the lack of the primary hydroxyl group at C1 and the ester group at C3, instead of the secondary hydroxyl group, leads to a decrease in the polarity of the head group. Since polar lipids spontaneously organize in bilayers, and strictly nonpolar lipids tend to occupy the bilayer hydrophobic matrix, we were prompted to examine the distribution of the partially polar palmitoyl-GABA-pentaene RBM4-35 into an artificial membrane.

For this purpose, DPPC bilayers were used as host for the polyene lipid. In this sense, MLVs were prepared to a final 1 mM concentration and all the measurements were performed in a VP-DSC high-sensitivity scanning microcalorimeter (see Section 5.1.4).

The DSC thermogram profile of the DPPC bilayer (

Figure **3.1.19**, top), showed a main endothermic gel-fluid transition (Tm =41.33191; $\Delta T_{1/2}$=0.69215) and a smaller pre-transition (Tm=35.4198; $\Delta T_{1/2}$=2.41147), which were characteristics of fully hydrated pure DPPC. However, incorporation of probe RBM4-35 into the liposome, gave rise to a single major endotherm, centred at 40.7 ºC (T_m =40.71355; $T_{1/2}$=1.79576), and the disappearance of the pre-transition endotherm. In addition, the main transition of the mixture was moderately widened (from 0.69 ºC for pure DPPC to 1.80 ºC in the mixture), while the main transition enthalpy hardly changed (13 000 cal/mol for DPPC versus 12 900 cal/mol for DPPC+RBM4-35). The profile of RBM4-35 in buffer solution, which, as expected for polyunsaturated lipids, did not exhibit any thermal signal in the temperature range under study (10−100 °C), is also shown In

Figure **3.1.19**.

The above results indicated that RBM4-35 behaved similarly as other amphipathic, unsaturated lipids, mixing well with phospholipids in a bilayer form[206,207]. Thus, palmitoyl-GABA-pentaene RBM4-35 seems to orient, mainly, their polar moieties at the lipid−water interface. Furthermore, the DSC data suggested that RBM4-35 partitioned preferentially in fluid over gel phases, since it causes a decrease in the gel−fluid transition temperature of DPPC[208].

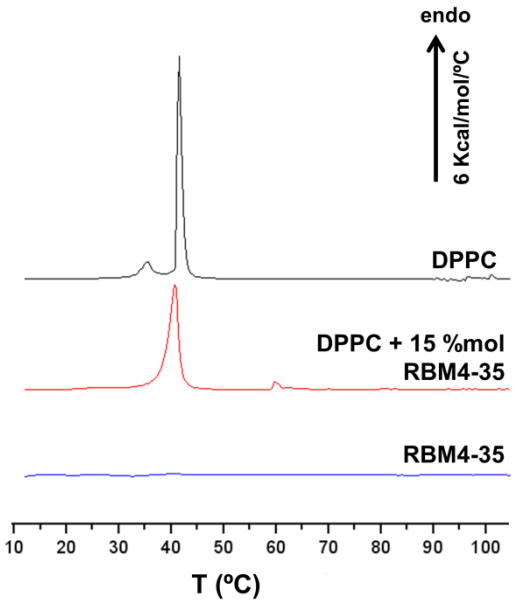

Figure 3.1.19 From the top to the bottom: DSC of aqueous dispersions of DPPC, DPPC + 15 mol % of RBM4-35, and RBM4-35.

3.1.3.4 Confocal fluorescence and multiphoton microscopy

Confocal microscopy is an advanced fluorescence microscopy technique that allows the direct visualization of the fluorescence coming from an individual thin in-focus plane of the sample, enabling the construction of real three-dimensional images. To discard fluorescence coming from out-of-focus planes, and in contrast to common epifluorescence microscopy, confocal imaging is achieved by introducing a pinhole next to the detector that allows only fluorescence coming from the in-focus plane to reach the detector[209,210].

A schematic representation of the central components of a fluorescence confocal microscope is depicted in Figure 3.1.20 (Left). Essentially, when an incident light source illuminates a single point on the focal plane of a specimen, fluorescent light is emitted, channelled back through the objective lens and through a dichroic mirror. It then impinges upon the confocal aperture (pinhole), which is located in the primary image plane of the objective. The confocal aperture allows all of the in-focus light from the region of interest on the sample to pass through to the detector.

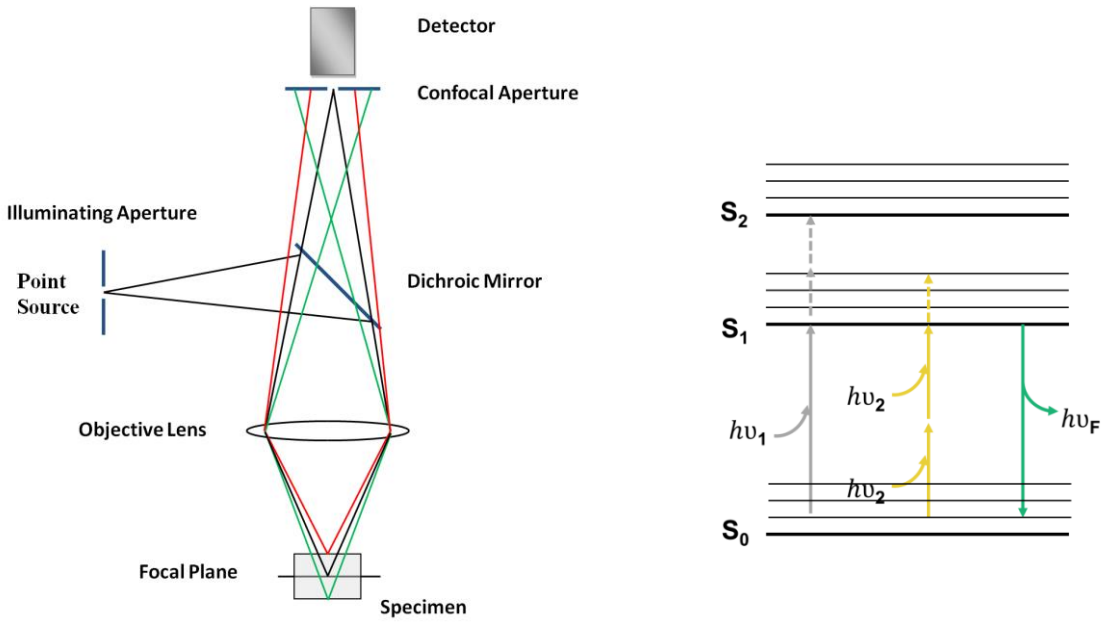

Figure 3.1.20 Left: Central components of a fluorescence confocal microscope. Only fluorescence from the in-focus plane (black) reaches the detector. Right: Jablonski diagram for one- (grey) and two-photon (ochre) excitation, with the same fluorescence emission (green). Image adapted from **Lakowicz[210].**

The conventional fluorescence microscopy (one-photon excitation) was modified by a multiphoton excitation mode[211]. This technique uses a pulse laser, such as titanium-sapphire laser, with femtosecond pulse widths to excite fluorophores by two-photon absorption. Despite the wavelength of the photons are twice of that of the absorption band of the fluorophore, their emission spectra and lifetimes are the same as if they were excited by one-photon absorption (Figure 3.1.20, right). In addition, since the two-photon absorption process only occurs at the focal point of the laser beam, the photobleaching of the fluorophore is minimized.

The confocal/two-photon excitation fluorescence microscopy represents a very powerful technique to visualise fluorophores that can be susceptible of photobleaching at UV wavelengths, such as the conjugated pentaene systems under study. Furthermore, the confocal fluorescence microscopy, in combination with the use of GUVs provides suitable systems to analyse the fluorophores in different lipid environments under thermodynamic equilibrium conditions[212].

GABA-pentaene RBM4-35 in microscopy studies

Microscopy studies with the model GABA-pentaene probe RBM4-35 were carried out in GUVs with different lipid compositions. The liposomes were prepared by electroformation[213], and were attached to platinum electrodes to directly visualise them under an inverted confocal/two-photon excitation fluorescence microscope (See Section 5.1.5). The lipid mixtures under study were prepared to a final concentration of 0.2 mM in chloroform/methanol (2:1 v/v), plus 0.3 mol % DiO and the desired mol % of RBM4-35.

The lipophilic oxacarbocyanine dye DiO (Figure 3.1.21) was incorporated into the lipid bilayer as a fluorescent tracer of disordered domains, enabling also the initial localisation of GUVs by epifluorescence. DiO was excited at 488 nm and its emission was collected in the 500-600 nm channel. In this sense, control GUVs of ePC with 0.3% DiO were used to confirm that the emission of the commercial tracer did not significantly contribute to the signal observed on the polyene channel, which was excited using the two-photon excitation mode at 706 nm (353 nm x 2), and their emission was collected in the 467−499 nm range (Figure 3.1.21, middle panel).

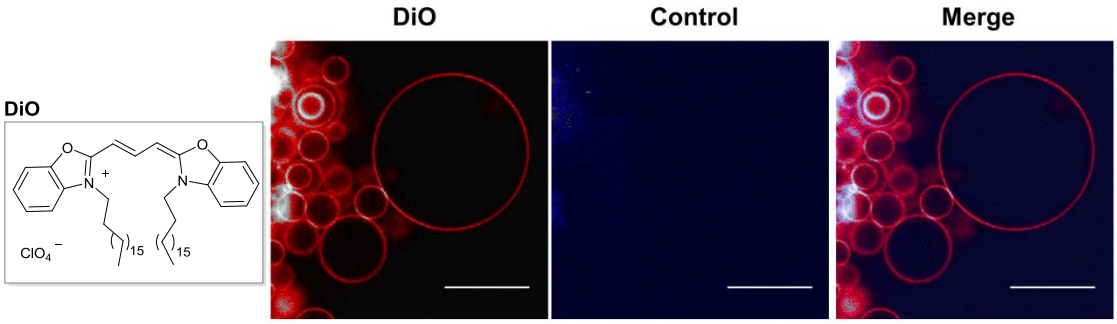

Figure 3.1.21 GUVs control of ePC containing 0.3% DiO. Left panel: 500-600nm channel. Middle panel: 467-499nm channel. Scale bar = 10 µm.

Initial attempts to examine the fluorescence of RBM4-35 by multiphoton/confocal microscopy were based on GUVs of ePC incorporating 15% of RBM4-35. However, the resulting sample exhibited low fluorescence intensities (Figure 3.1.22, center top). Due to the decrease of polarity of the GABA-pentaene head groups in comparison with natural Cer, their incorporation into the lipid bilayer might be hindered during the electroformation process. Thus, we increased the membrane permeability by adding a mixture of phosphatidylethanolamines (PE) and cholesterol (Chl). In this way, GUVs composed of ePC:PE:Chl (50:25:25) and RBM4-35 (15% molar ratio) were generated. As observed in Figure 3.1.22 (center bottom), they showed an increase of the fluorescence intensity in comparison with ePC GUVs (Figure 3.1.22, center top). According to the literature, a possible oxidation of the polyunsaturated lipids can occur during the electroformation process[214]. However, we observed that GABA-polyene compounds did not suffer from oxidation since the same fluorescence intensity was recorded when GUVs of ePC:PE:Chl (50:25:25) with 15% of RBM4-35 were generated at both 70 ºC and 37ºC temperatures (data not shown).

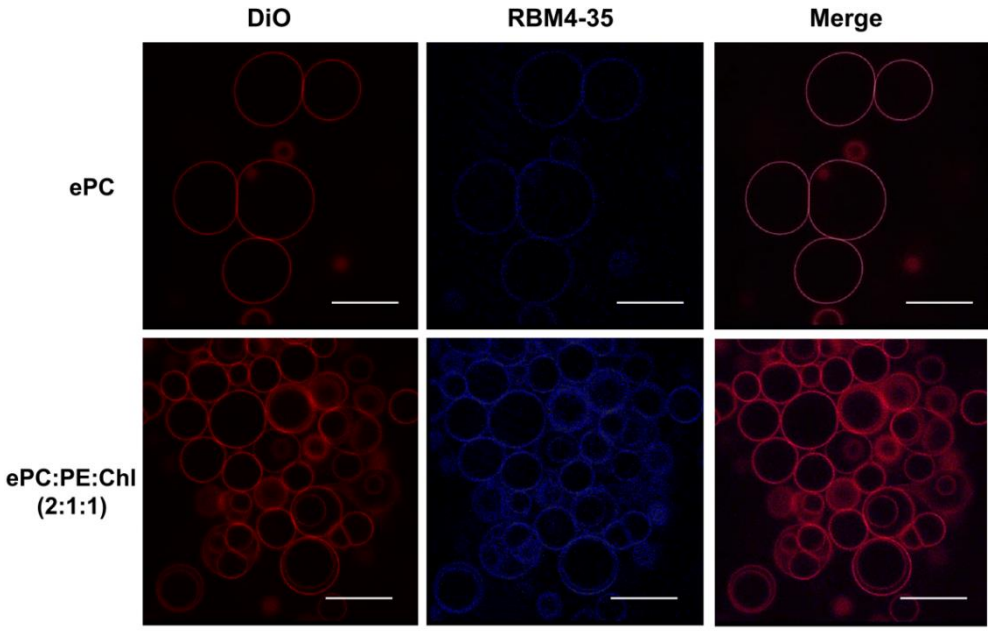

Figure 3.1.22 Representative confocal/multiphoton equatorial sections of GUVs of ePC (top) and ePC:PE:Chl (2:1:1) (bottom) containing DiO and RBM4-35. Scale bar = 10 µm.

In consideration of the above results, the use of 15% mol of pentaene probes differed greatly from physiological conditions. Therefore, we were encouraged to reduce the amount of probe incorporated, from 15% to 2%. For this goal, GUVs with different lateral phase separations and fluidities were generated.

When GUVs composed of DOPC:eSM:Chl (50:25:25) and RBM4-35 (2%, molar ratio) were examined, the mixture exhibited a lateral separation of liquid-disordered (L_d) (bright) and liquid-ordered (L_o) (dark) domains, as revealed by DiO (0.3% molar ratio) (Figure 3.1.23, left-hand panel). Interestingly, the L_o domains were preferentially stained by RBM4-35 (Figure 3.1.23, middle panel), initially suggesting a high partition of the polyene into ordered domains. However, the observed results could also be explained just by a higher fluorescence yield of the probe when it is present in the ordered domains. A quantitative average fluorescence intensity ratio of RBM4-35 between L_o/L_d domains gave a value of 3.9 ± 1.8 (for a total of 112 vesicles). These results suggested that RBM4-35 can be a suitable tracer to stain L_o domains, since many of the commonly available fluorescent probes partition mainly into L_d domains[215].

Despite probe RBM4-35 showed a photoselection process, (Figure 3.1.23, right-hand panel blue arrows), the fluorescence intensity at 2% probe incorporation was similar to that at 15% (data not shown). A photoselection process occurs when the extent of

excitation of a fluorophore depends on the orientation of its transition moment relative to the plane of polarization of the exciting light. Therefore, when the fluorophore keeps in a fixed orientation (as it happened with lipids in an ordered bilayer) the excitation efficiency will depend on the location of the probe along the liposome. Thus, dark areas can be seen in the L_o domains in the pentaene channel, located along an imaginary north-south axis. The disordered domains, on the contrary, did not exhibit such dark areas.

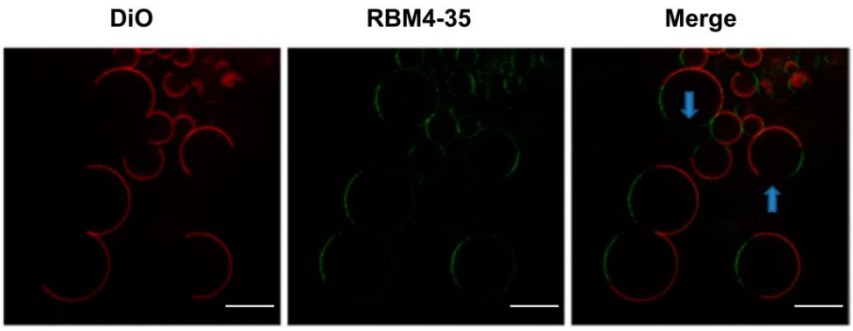

Figure 3.1.23 Staining of lipid domains by RBM4-35. Representative confocal/multiphoton equatorial sections of GUVs of DOPC:eSM:Chl (2:1:1) containing DiO and RBM4-35 are shown. Blue arrows show the photoselection effect on L_o domains. Scale bar = 10 µm.

In order to analysed the partition distribution of probe RBM4-35 when Cer-rich domains were generated, a mixture of phospholipid:pCer (palmitoyl ceramide) bilayers were examined. This composition led to lateral phase separation by generating Cer-rich and Cer-poor domains[49,151,216], where DiO preferentially stained the Cer-poor domains (Figure 3.1.24). However, RBM4-35 appeared to distribute rather evenly over the vesicle, albeit staining the two domains with different intensities.

Natural ceramides segregate laterally into highly enriched domains[49], through a network of hydrogen bonds[72,217]. However, GABA-pentaene probes lack the hydroxyl groups from the sphingoid backbone, so that the H-bonding network is severely perturbed. This relatively low level of intermolecular H-bonding allowed the even mixing of RBM4-35 in ceramide-rich and -poor domains, as illustrated in Figure 3.1.24. In addition, the ability of RBM4-35 to partition into both the Cer-rich and Cer-poor domains, differed from bulky chromophores such as NBD-Cer[216], that cannot partition into enriched Cer-domains. Therefore, probe RBM4-35 can be particularly useful given the potential presence of gel microdomains in live cell membranes[208,218].

Furthermore, when gel and fluid domains are formed in mixtures of saturated (DSPC) and unsaturated (DOPC) phospholipids (Figure 3.1.24, bottom panels), RBM4-35 emitted more intensely in gel phase domains, with a measured intensity ratio of 2.6 ± 0.8 for the gel/fluid domains (27 vesicles).

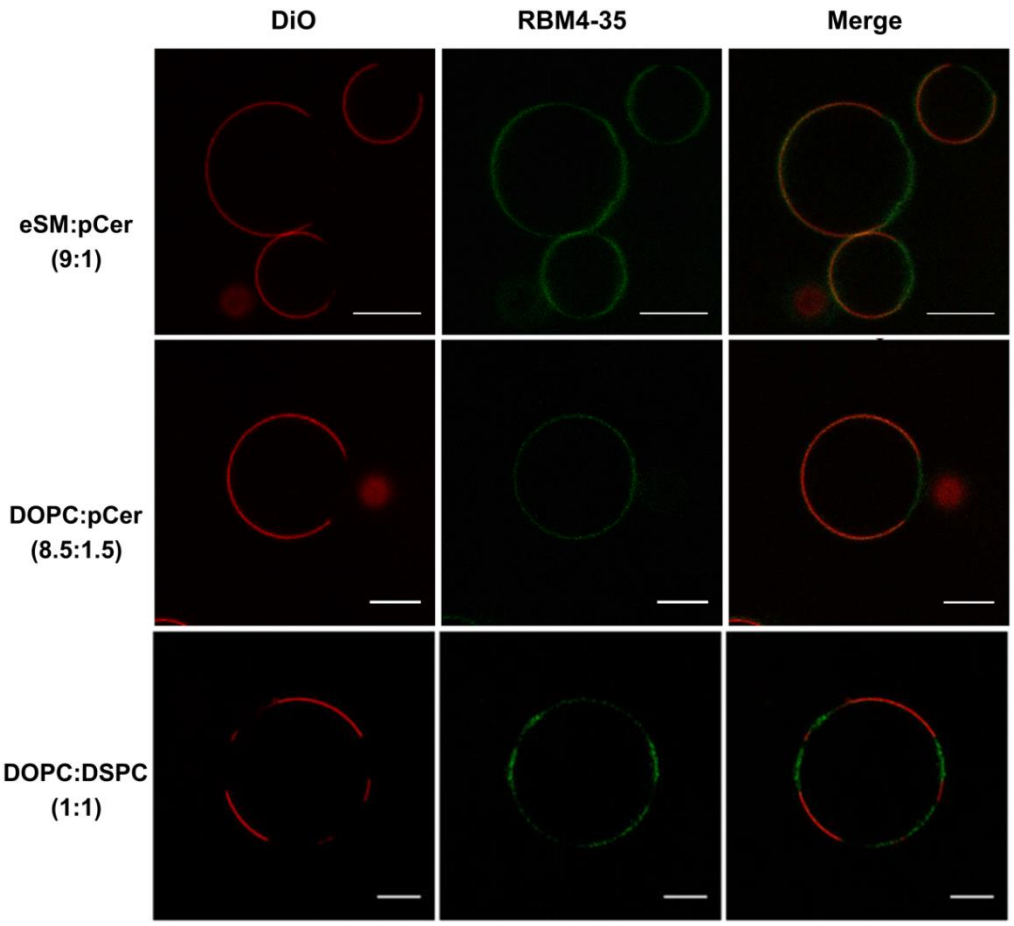

Figure 3.1.24 Staining of lipid domains by RBM4-35. Representative confocal/multiphoton equatorial sections of GUVs of different compositions containing 0.3% mol of DiO and 2% mol of RBM4-35 are shown. Scale bar = 10 μm.

GABA-pentaene RBM4-39 and RBM4-42 in microscopy studies

Microscopy studies with the GABA-pentaene-DOXYL probes, RBM4-39 and RBM4-42, were carried using the optimal parameters deduced from the model probe RBM4-35. In this context, GUVs of 0.2 mM with different lipid compositions, containing 0.3% of DiO and 2% of the desired polyene probe, were generated.

According to previous section, GUVs composed of DOPC:eSM:Chol (50:25:25, molar ratio) and DOXYL-probe (2% mol) were examined. This lipid mixture displays coexistence between L_d and L_o domains, where the DiO preferentially partitioned in disordered domains (Figure 3.1.25, left-hand panel). As shown in Figure 3.1.25, the emission of both GABA-pentaene pobes containing the free radical nitroxide, was similar throughout all the bilayer, staining equally L_o and L_d domains. Noteworthy, the position of the radical group in the *N*-acyl chain at 16C in RBM4-39 or at C5 in RBM4-42, did not appear to influence in the emission fluorescence in this lipid composition.

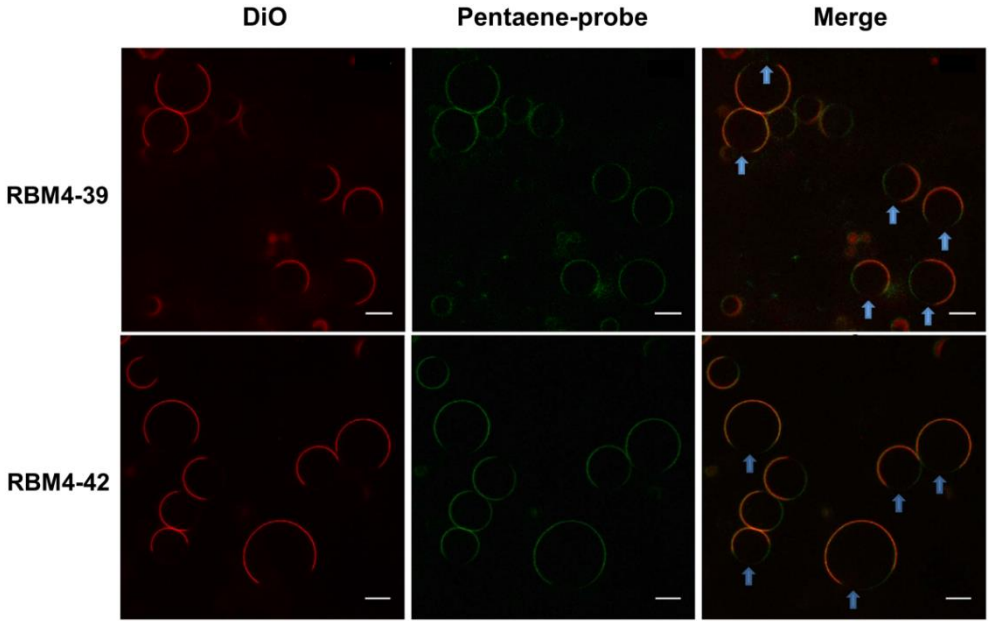

Figure 3.1.25 Staining of lipid domains by DOXYL-pentaene probes. Representative confocal/multiphoton equatorial sections of GUVs of DOPC:eSM:Chl (2:1:1) containing DiO (0.3% mol) and probes RBM4-39 or RBM4-42 (2% mol) are shown. Blue arrows show the effect of photoselection on Lo domains. Scale bar = 10 μm.

The partition of the DOXYL-GABA-pentaene probes differed from that of the palmitoyl-GABA-pentaene RBM4-35, which showed selectivity to L_o domains in the same lipid environment (Figure 3.1.23). Since the fluorescence quenching by the DOXYL group showed dependency on the fluidity of the membrane (Section 3.1.3.2), the apparent similar distributions observed for RBM4-39 and RBM4-42 throughout all the liposome, could be due to the enhanced quenching which would take place in the more ordered phase. However, it can also be due to a decreased partitioning into the ordered domains by the presence of the DOXYL group.

3.1.3.5 Electron paramagnetic resonance (EPR)

Electron paramagnetic resonance (EPR) spectroscopy is based on the absorption of electromagnetic radiation by paramagnetic species, such as systems with one or more unpaired electrons, in an external magnetic field.

Electrons possess an intrinsic spin angular momentum $\vec{S}$, which is associated with a magnetic dipole moment $\vec{\mu}$ with the same orientation. For a single unpaired electron with spin $\vec{S}$ = 1/2, the angular momentum (and, consequently, the magnetic dipole moment) can have two possible orientations, corresponding to two energy levels of the system, that are characterized by the magnetic spin quantum numbers m_S = ±1/2 (Figure 3.1.26). Application of an external magnetic field causes the two energy levels to split up, being separated by $g\beta B$, where g is the splitting factor (g = 2.0023 for a free electron), β is the Bohr magneton and B is the magnetic field strength. Transitions between these energy levels can be induced by applying electromagnetic radiation with the energy $h\upsilon$, where h is Planck's constant and υ is the frequency of the oscillating electromagnetic radiation. Consequently, the resonance condition in EPR spectroscopy is $h\upsilon = g\beta B$ (fundamental equation of EPR)[219,220].

Interaction of the electron spin with other nuclear spins (*hyperfine interactions*), gives rise to further splitting of the energy levels resulting in the appearance of multiple resonance lines and/or line broadening and narrowing effects. The number of EPR split lines depends on the nuclear spin *I.* In general, for the interaction with a nucleus with spin *I*, an EPR line is split into 2*I*+1 components.

In DOXYL-GABA-pentaene probes RBM4-39 and RBM4-42, the paramagnetic nitroxide group contains the unpaired electron coupled to a nitrogen atom. When the magnetic field is applied on the unpaired electron, the two energy levels of the system coupled with ^{14}N nucleus (I=1), with spin quantum numbers (m_I) equal to +1, 0, and - 1, lead to a ESR spectra consisting, ideally, of three essentially equivalent lines[140] (Figure 3.1.26).

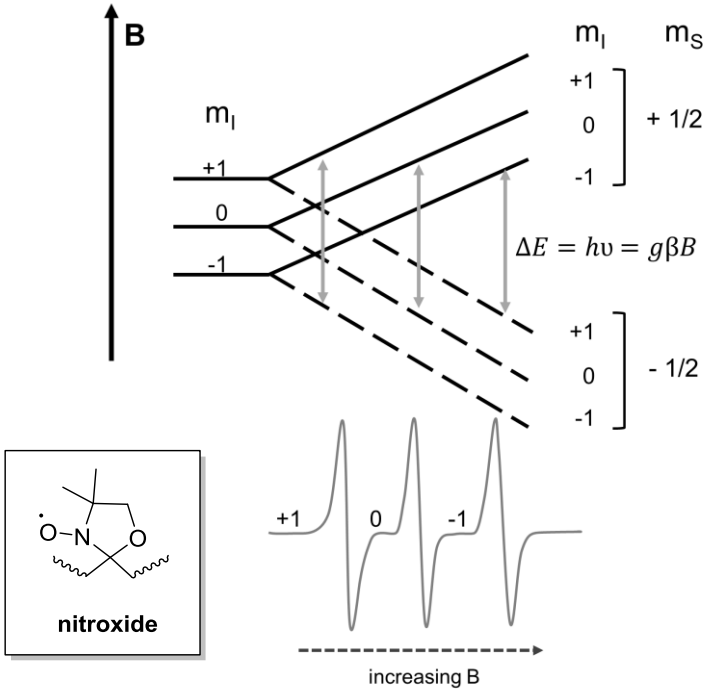

Figure 3.1.26 Hyperfine interactions between the unpaired electron and the ^{14}N nucleus of the nitroxide group, splitting each of the two energy (m_s = **±1/2)** levels into three new energy levels associated with the m_I spin quantum numbers of the nitrogen nucleus.

The EPR technique can be applied to monitor the molecular dynamics of the spin labels when are incorporated into lipid bilayers, providing valuable information about their environment[221–224]. The different fluidity and polarity in the inner membrane from each probe can be estimated by the following dynamic parameters.

The *rotational correlation time* τ_C, measures the motion of the nitroxide radical for fast movement, in weakly immobilized isotropic environments. This parameter is calculated from the following equation[225] **1**:

$$\tau_C = 6.5 \times 10^{-10} \Delta H_0 \left[\left(\frac{h_0}{h_{+1}} \right)^{1/2} + \left(\frac{h_0}{h_{-1}} \right)^{1/2} - 2 \right] \qquad \textbf{(1)}$$

where h_0, h_{+1}, and h_{-1} are the peak-to-peak heights of the 0, +1 and −1 transitions, in the first derivative EPR spectrum. ΔH_0 is the line width, in Gauss, of the 0 transition (Figure 3.1.27).

In the case of slow tumbling nitroxide group, when it is strongly immobilized into an anisotropic medium, the parameter τ_C was determined using the approximate expression[226,227] **2**:

$$\tau_C = a\left[1 - \left(\frac{A_{max}}{A_{ZZ}}\right)\right]^b \qquad \textbf{(2)}$$

where A_{max} is one-half the separation of the outer hyperfine extrema (Figure 3.1.27), and A_{ZZ} is the rigid limit value for the same quantity, with a and b values corresponding to a Lorentzian line width[226] (see Section 5.1.6).

An *empirical order parameter S*, obtained from the EPR spectra, was used to measure the molecular motion of the spin probe in the liposome membranes. This parameter is a measure of the anisotropy or random motion. The order parameter can be obtained from the experimental values of A_{max}, the *isotropic coupling constant* (a_N), and the maximum anisotropic coupling constant in the immobilized limit A_{ZZ}, as a relation between the observed anisotropy and the maximum anisotropy, according to the equation[228,229] **3**:

$$S = \frac{A_{max} - a_N}{A_{ZZ} - a_N} \qquad \textbf{(3)}$$

When *S* = 0, the motion is isotropic. The deviation of this value involves anisotropic molecular motion. Moreover, the a_N value (G) increases when the fluidity decreases[230], which represents a measure environmental polarity on the spin probe.

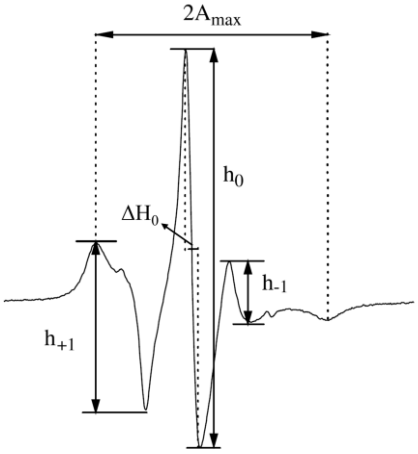

Figure 3.1.27 Typical EPR spectrum of spin-labelled liposomes at 300K. Image taken from Sulkowski *et al.*[231]

Electron paramagnetic resonance measurements

The EPR technique was applied to monitor the molecular dynamics of GABA-pentaene probes, in order to detect changes in the spin tropic movement of the unpaired electron depending on the lipid environment. For this purpose, LUVs (0,3 mM) of various glycerophospholipids containing 15% of the desired GABA-polyene-nDOXYL probes were prepared and analysed by an EPR/ESR Bruker EMX spectrometer.

The first step in the characterization of the DOXYL-GABA-pentaene probes, RBM4-39 and RBM4-42, was the measurement of their RPE spectra in THF solution. In this sense, a polar and isotropic profile, where the nitroxide group is not immobilised at RT, can be obtained as a reference (Figure 3.1.28, left panels). On the contrary, a hydrophobic and anisotropic spectra was obtained when the sample in THF solution was recorded at 140 K, where the nitroxide group was strongly immobilized (Figure 3.1.28, right panels).

In addition, the quantitative analysis of the spin probe concentration in LUVs was calculated using the spectrum of probes RBM4-39 and RBM4-42 in DCM (spectra not shown). The spin concentration was determined by the relationship **4**:

$$SS = SR\frac{(DI/N)S}{(DI/N)R} \qquad \textbf{(4)}$$

Where *SS* and *SR* are the number of spins (spin concentration) in the sample and reference, respectively, and $(DI/N)R$ and $(DI/N)S$ are the normalized double integrals with respect to the experimental conditions for the reference and sample spectra, respectively. The % probe incorporation into the liposome corresponds to the ratio between the concentration obtained by this method and the theoretical concentration of the liposome preparation (45 µM, corresponding to a 15 mol % probe concentration in a 0.3 mM lipids solution). The results are given in Table 3.1.3:

Table 3.1.3 The % of probe incorporated into the liposome

Probe	System	DI/N	[μM]	%
RBM4-39	DCM	41.81	1590	----
	ePC	0.6156	23.41	52
	DOPC	0.5988	22.77	50
	DPPC	0.8513	32.37	72
	DSPC	0.6147	23.38	52
RBM4-42	DCM	44.13	1590	----
	ePC	0.7905	28.48	63
	DOPC	0.9473	34.13	76
	DPPC	0.9837	35.44	79
	DSPC	0.2929	10.55	23

The EPR measurements for GABA-pentaene-DOXYLs, RBM4-39 and RBM4-42, into liposomes of different lipidic nature, are shown in Figure 3.1.28. As the rigidity of the membrane increased and the mobility of the nitroxide radical diminished (from left to right), the profile of the EPR spectrum became more anisotropic. In general, since the nitroxide group at C5 position in RBM4-42 was close to the amide bond, a reduced mobility is observed for this probe. Thus, the behaviour of probe RBM4-42 was less dependent on the lipid environment, showing in all cases an anisotropic profile.

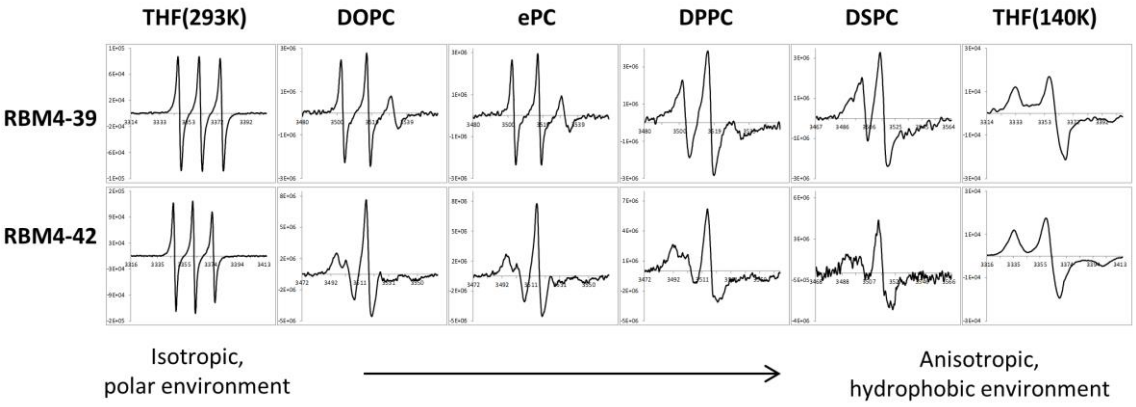

Figure 3.1.28 EPR spectrum of the polyene DOXYL probes in THF or in LUV with the lipids indicated on top. Spectra recorded at 20 °C (293 K) unless otherwise indicated.

Accordingly, the parameters of choice to study the spin dynamics of probe RBM4-42 in rigid systems (τ_C, $2A_{max}$, *S*) indicated that the probes were moving in a partially ordered structure, with an intermediate mobility between the slow and rigid limit movement (Table 3.1.4). These parameters exhibited an increasing immobilization in the chain segments closer to the lipid polar group in the order ePC~DOPC < DPPC < DSPC. In the latter two cases, the probe appeared to be almost fully immobilized.

Table 3.1.4 EPR parameters for RBM4-42 in different lipid nature of LUVs

System	τ_C (s)	*S*	$2A_{max}$ (G)
ePC	0.58 X 10^{-8}	0.69	53.94
DOPC	0.62 X 10^{-8}	0.70	54.48
DPPC	5.42 X 10^{-8}	0.93	62.73
DSPC	8.83 X 10^{-8}	0.95	63.73

In contrast, the shape of the spectra for RBM4-39 indicated that the probes were moving relatively fast. In this case, the use of τ_C, ΔH_0, and h_{-1} were diagnostic and the observed values indicated that the spin probes were tumbling in structures with intermediate mobility. All dynamic parameters were consistent with the different rigidity and polar environment in liposomes made of ePC, DOPC, DPPC, and DSPC, respectively (Table 3.1.5).

Table 3.1.5 EPR parameters for RBM4-39 in different lipid nature of LUVs

System	τ_C (s)	h_{-1}	ΔH_0 (G)
ePC	1.04 X 10^{-9}	1717	2.09
DOPC	1.23 X 10^{-9}	1477	2.09
DPPC	4.74 X 10^{-9}	845.4	3.52
DSPC	1.76 X 10^{-8}	209.2	5.97

Regarding the EPR results, the changes observed in the spin tropic movement of the unpaired electron, caused by the different lipid environment or the position of the nitroxide group in the acyl chain, correlated closely to the fluorescence studies discussed in section 3.1.3.2.

3.1.4 Summary & Conclusions

Synthesis of GABA-pentaene probes

- The (*all-E*)-pentaene alcohol RBM4-33 was obtained in 25% overall yield, starting from commercial 2,4-hexadienal, and elongation of the conjugated pentene moiety by applying two cycles of the HWE olefination reaction and final reduction with DIBAL-H (Figure 3.1.6).

- GABA-pentaene probes were obtained by esterification between the alcohol RBM4-33 and several *N*-acyl GABA intermediates, which in turn were prepared by *N*-acylation with different carboxylic acids. Starting from GABA, the palmitoyl-derivative RBM4-35 (15% overall yield), the 16-DOXYL stearic acid-derivative RBM4-39 (30% overall yield) and the 5-DOXYL stearic acid-derivative RBM4-42 (35% overall yield) were obtained in four synthetic steps. This method proved superior to the alternative *N*-acylation of an *N*-protected GABA esterified with the polyene alcohol RBM4-33.

Biophysical studies with GABA-pentaene probes

- The fluorescence spectroscopic properties of GABA-pentaene probes were analysed, exhibiting maximum excitation and emission wavelengths in phospholipid bilayers around 353 and 478 nm, respectively.

- The free radical *n*-DOXYL group was able to quench intramolecularly the fluorescence of the pentaene moiety when both chains were proximal in gel lipid bilayers (Figure 3.1.15 and Figure 3.1.16).

- The fluorescence quenching of RBM4-39 exhibited higher dependency on the membrane fluidity than RBM4-42 (Figure 3.1.16). Thus, 16-DOXYL stearic acid will be the radical of choice for the *N*-acylation of *erythro*-pentaene-sphingosine in order to obtain a suitable fluorescent polyene Cer analogue to monitor the changes in the fluidity on the lipid membrane.

- No intermolecular quenching is expected to take place in the resulting *erythro*-pentaene-sphingosine, once the radical quencher is released from the *erythro*-pentaene-ceramide after hydrolytic cleavage (Figure 3.1.17).

- The EPR studies correlated closely with the fluorescence spectroscopy results, showing that RBM4-42, with the nitroxide group at C5 of the acyl chain, exhibited lower sensitivity to the bilayer composition than RBM4-39 (Figure 3.1.28).
- The data in Figure 3.1.24 (DOPC:DSPC mixture) indicated that the fluorescence emission of RBM4-35 was more intense in the gel than in the fluid domains. Moreover, RBM4-35 emitted more intensely from liquid-ordered than from liquid-disordered phases (Figure 3.1.23).
- In mixtures containing natural ceramide, RBM4-35 partitions into both the ceramide-rich and ceramide-poor domains (Figure 3.1.24).
- The intensity of RBM4-35 fluorescence emission appeared to depend not only on the partition coefficient but also on the micro environmental effects on the quantum yield.
- In the lipid mixture with coexistence of liquid-ordered and liquid-disordered domains, the emission of RBM4-39 and RBM4-42, containing the free radical nitroxide, was similar throughout all the bilayer, staining equally L_o and L_d domains. However, RBM4-35 showed selectivity to partition in liquid-ordered domains (Figure 3.1.23 and Figure 3.1.25).
- In contrast to fluorescence spectroscopy and microscopy results, the DSC data (
- Figure **3.1.19**) suggested that RBM4-35 partitions preferentially in fluid over gel phases, since it caused a decrease in the gel−fluid transition temperature of DPPC.
- The GABA-pentaene probes appeared to occupy, mainly, with their polar moieties at the lipid−water interface, as amphipathic molecules. This is supported by the DSC data (
- Figure **3.1.19**) that showed a loss of the pretransition endotherm and a moderate widening of the DPPC main transition in the presence of 15 mol % RBM4-35.
- Although GABA-pentaene compounds were initially designed as models for a preliminary evaluation of the biophysical properties of the target pentaene-DOXYL systems, they have shown to be useful probes in fluorescence microscopy and spectroscopy, and EPR membrane studies. In particular, RBM4-35 may be particularly useful to observe highly-ordered bilayers by confocal microscopy, while the DOXYL-containing probes can give information on gel−fluid lipid transitions.

3.2 Synthetic approaches to polyene sphingolipids analogues

3.2.1 Introduction

3.2.1.1 Pentaene sphingolipids

One of the ultimate challenges for a biophysical tool is to directly visualise the molecular interactions under physiological conditions, in both model and natural environments. To address this need, suitable labelled SL analogues should be designed based on their natural counterparts. In this sense, the SLs labelled with fluorescent tags present high sensitivity and versatility of detection and wide applicability to many biological systems at low risk potential[103].

As described in the General Introduction (section 1.4), a conjugated double bond system, when introduced in a lipid as a fluorescent tag, minimizes structural alterations of the resulting probe, in comparison with commercially available bulky chromophores[124]. In this context, the pentaene moiety was reported to behave like their endogenous counterparts *in vivo*, with respect to uptake, metabolism, transport and localization in the membrane microdomains[109,132,133].

In light of the intrinsically fluorescent nature of the pentaene moiety, we considered of interest the design of sphingosine and ceramide analogues (Figure 3.2.1), labelled with the pentaene tag at the sphingoid base chain framework, as proper probes to directly visualise their distribution in lipid bilayers.

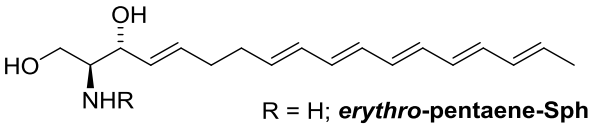

Figure 3.2.1 Unsaturated probes described in this section.

Additionally, regarding the results obtained in the previous section with GABA-pentaene probes, the design of Cer-like probes *N*-acylated with radical scavengers would enable interesting biophysical applications in natural or artificial membranes.

3.2.1.2 Synthetic approaches to sphingoid bases

Due to the biological importance of enantiopure Sph and Cer[232,233], a highly diastereoselective synthetic route is required to obtain the *erythro* (2*S*,3*R*)-configuration and the (*E*)-double bond at C4-C5 present in the natural sphingoid backbone.

Since the 1950s[234], numerous methods for synthesising the sphingoid base framework have been reported in the literature[235–237]. Collectively, they can be classified into two categories (Figure 3.2.2):

i. those that start from inexpensive chiral precursors, such as sugars and amino acids (L-serine). In this case, their C2 stereocenter may be directly conserved or it can influence into the C3 stereochemistry.
ii. those that are based on asymmetric induction using chiral auxiliaries or catalysts from achiral starting materials. For instance, the use of Sharpless asymmetric epoxidation, or aldol reactions in the presence of chiral auxiliaries. These methods allow the access to each of the diastereomers.

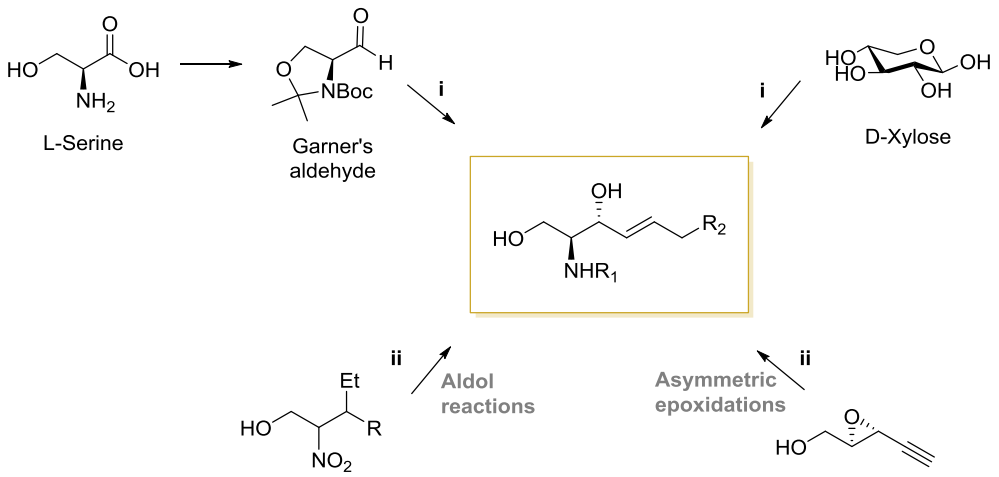

Figure 3.2.2 Some representative examples of synthetic approaches to introduce the sphingoid base backbone.

As part of our current interest in the development of synthetic protocols for the elaboration of new conformationally constrained pentaene *eryhtro*-Sph and *eryhtro*-Cer, the commercially available L-serine[238] was considered the starting material of choice. In this chapter, five building blocks derived from L-serine will be reported (Figure 3.2.3): Garner's aldehyde, along with the corresponding allylic alcohol **6** and

bicyclic RBM4-12, and the unreported aldehyde RBM4-54, together with its derived allylic alcohol RBM4-55.

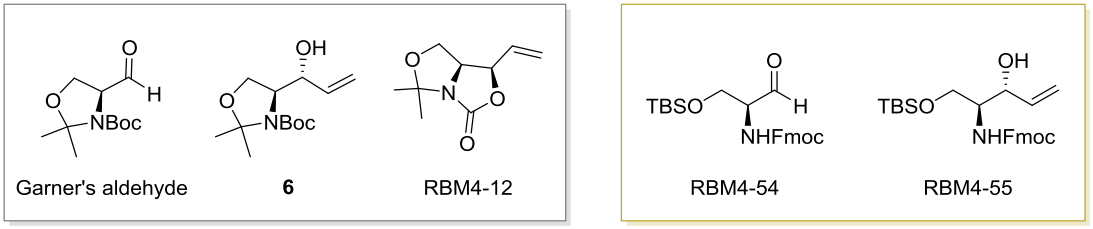

Figure 3.2.3 Building blocks derived from L-serine described in this chapter.

The well-described Garner's aldehyde[239–241] (4-formyl-2,2-dimethyloxazolidine-3-carboxylate) was synthesised according to the modification of McKillop *et al.*[179] and Campbell *et al.* [242], giving access to a wide variety of processes, such as cross-metathesis (CM) couplings (section 3.2.2 and 3.2.4), nucleophilic alkynylations (section 3.2.3) and hydrozirconation couplings (section 3.2.5).

The synthesis of the previously unreported aldehyde RBM4-54 (see section 3.2.4.5), bearing TBS and Fmoc as protecting groups, was envisaged to provide suitable mild conditions of deprotection compatible with polyene compounds. The building block RBM4-54 was subjected to hydrozirconation couplings (section 3.2.5), as well as to a CM process (section 3.2.4).

3.2.1.3 Synthetic approaches to the polyene moiety

Aside from the synthetic approaches envisioned for the sphingoid base framework, we focused on the elongation and assembly of the conjugated pentaene moiety. The present chapter is divided according to the different strategies devised for the construction of the *eryhtro*-pentaene-Sph or *eryhtro*-pentaene-Cer systems (Figure 3.2.4).

In section 3.2.2 and 3.2.4, the formation of C4-C5 (*E*)-double bond was planned to be accomplished by an olefin CM, since a high (*E*)-selectivity and compatibility with the amino diol functionality has been reported (see 3.2.2.1).

Nevertheless, in section 3.2.3, the C4-C5 (*E*)-double bond was envisioned by addition of a lithium-activated alkyne to Garner's aldehyde, followed by a selective reduction of the propargylic alcohol to the corresponding allylic alcohol. On the other hand, in section 3.2.5 the allylic alcohol framework can be obtained, in just one step by a hydrozirconation coupling, using the same alkyne as in section 3.2.3.

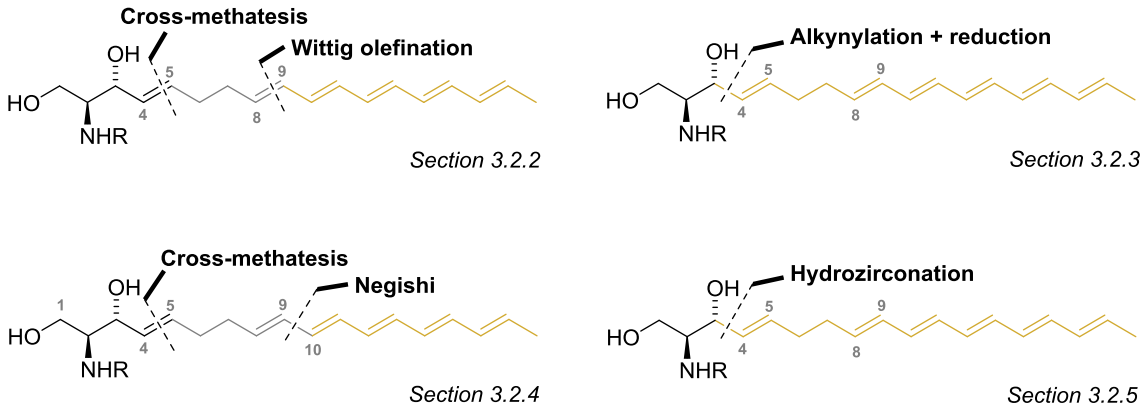

Figure 3.2.4 Synthetic strategies devised in this chapter for the construction of the target *erythro*-polyene-probes.

Different approaches for the elongation of the polyene chain were considered. As described in sections 3.2.2 and 3.2.3, a Wittig olefination between a polyene aldehyde and a suitable phosphonium ylide was used for the construction of the C8-C9 new double bond. Despite the poor *E*-selectivity of the Wittig olefination, the resulting isomeric mixtures can generally be isomerised with iodine to completely reverse the isomeric composition to the new mixtures where the *E*-isomer predominates. However, in section 3.2.4 the elongation of the polyene framework was planned by a Negishi cross-coupling, which provided an efficient method for the stereoselective one-pot conversion of a terminal acetylene into a conjugated polyene system by formation of the C9-C10 bond.

3.2.2 Cross-metathesis and Wittig olefination approach

3.2.2.1 Introduction and scope

Olefin cross-metathesis

The olefin metathesis is a process in which two alkylidene units undergo mutual exchange in the presence of a catalyst transition metal carbene complex to produce a new olefin[243–245].

Olefin metathesis can be applied in a variety of synthetic operations (Figure 3.2.5), such as cross-metathesis (CM), ring closing metathesis (RCM), ring opening metathesis (ROM) or intermolecular enyne metathesis. Amongst these processes, this section will focus on CM reaction.

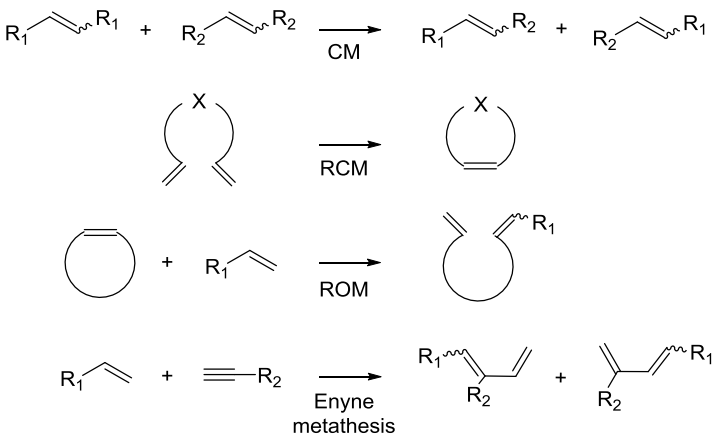

Figure 3.2.5 Variations of olefin metathesis.

A general CM mechanism was initially proposed by Hérisson and Chauvin[246], involving a [2+2] cycloaddition reaction between a metal carbene and an olefin to give a metallocyclobutane. This intermediate subsequently undergoes a retro [2+2] cycloaddition to generate ethylene and a substrate-loaded metal carbene, which reacts with the second olefin in the same fashion to release the metathesis product and regenerate the catalyst (Figure 3.2.6). All of the above reactions are reversible, so equilibrium mixtures are obtained. Nevertheless, the reaction is driven forward by evolution of the volatile ethylene, leading to a given product in high yields. This mechanism was later proved by Schrock with the isolation and structural characterization of the metallocyclobutane intermediate[247].

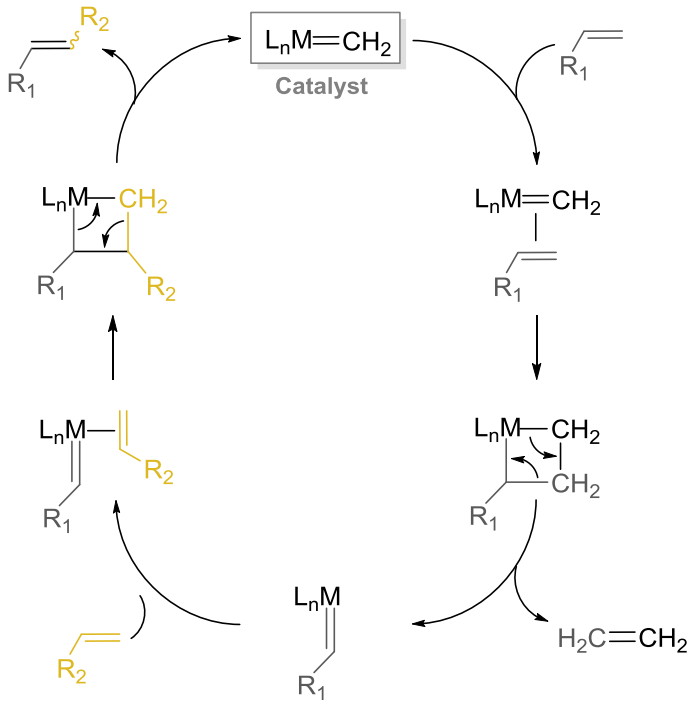

Figure 3.2.6 Cross-metathesis mechanism.

The successful application of CM hinges on both the regio- and stereoselectivity of the process. In this sense, the formation of self-metathesis (homodimerization) products must be reduced and the control of the *Z*/*E* olefin geometry in the newly formed double bond is required. To address this need, Chatterjee and coworkers[248] designed a general model in which the reactivity of different olefins was categorized in order to predict the selectivity of the CM process depending on the catalyst employed.

The number of catalyst systems able to initiate a CM is very large. Of the various catalysts, a series of molybdenum complexes developed by Schrock[249] were found to be very efficient for olefin metathesis. Nevertheless, due to their instability toward different functional groups, Mo was replaced by ruthenium, which circumvented this drawback. In addition, the Ru-carbene complexes exhibited high reactivity under mild conditions, as well as stability in the presence of air, humidity and solvent impurities.

The most frequently employed catalysts for olefin metathesis include the so called Grubbs' 1st and 2nd generation, and Hoveyda-Grubbs' 1st and 2nd generation catalysts (Figure 3.2.7). Focusing on the Grubbs' 2nd generation catalyst[250] (Figure 3.2.7, B), the introduction of the *N*-heterocyclic carbene ligand exhibited an increase of reactivity towards olefinic substrates, due to their higher basicity and σ-donating profile[251,252].

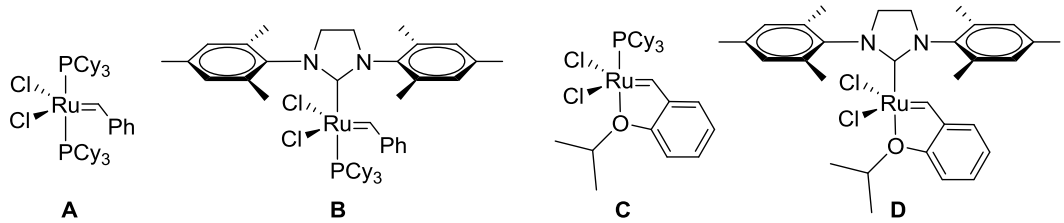

Figure 3.2.7 Selection of olefin metathesis catalysts. **A** and **B,** Grubbs' 1st and 2nd generation catalyst, respectively; **C** and **D**, Hoveyda-Grubbs' 1st and 2nd generation catalyst, respectively.

As a C-C bond-forming tool, the CM approach offers some attractive features, such its catalytic nature (it does not require co-catalysts or promoters), high yields and (*E*)-selectivity in relatively short reaction times. Moreover, a wide range of functional groups are tolerated.

Synthesis of sphingolipids by olefin cross-metathesis

In recent years, olefin CM has emerged as a convenient strategy to form the C4-C5 double bond of the sphingoid backbone[238], since high (*E*)-selectivities can be obtained and the Grubbs' 2nd generation catalyst is compatible with the amino diol functionality present in most of the building blocks used in the chemistry of SLs.

Accordingly, some authors have put their effort in the CM approach for the synthesis of diverse SLs starting from both Garner's aldehyde[253,254] or alternative building blocks[255–259].

Additionally, the alkyl or acyl chain present in the backbone of sphingosine derivatives can be exchanged with functionalised side chains in a single step under CM reaction conditions, affording labelled SLs analogues[258,260]. For instance, Peters[261] and Bandhuvula[262] introduced a BODIPY fluorescent tag and Tanaka and coworkers[263] modified the acyl chain of the sphingoid framework with the chromophore tetramethylrhodamine.

Wittig olefination

Since the 1950s[264], the Wittig olefination plays a central role in the synthesis of carbon-carbon double bonds. The reaction takes place between a carbonyl compound (generally an aldehyde or a ketone) and a phosphonium ylide (generated by the *in situ* deprotonation of an alkyl-triphenylphosphonium halide with a suitable base) to give an olefin, along with phosphine oxide as by-product (Figure 3.2.8).

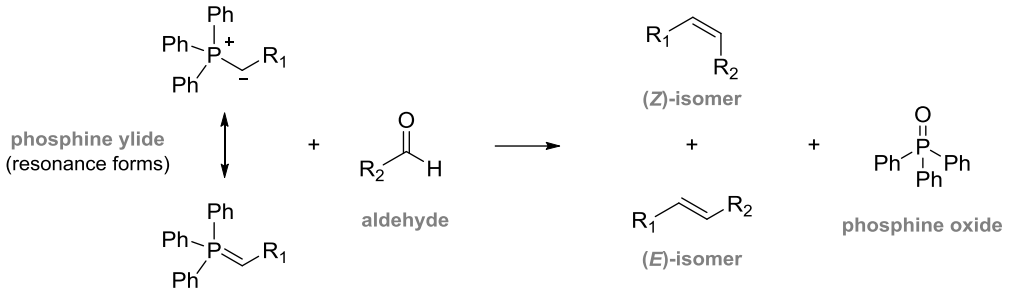

Figure 3.2.8 Example of Wittig reaction. (The negative charge in the phosphonium ylide is delocalised by d_{π}-p_{π}-bonding into the empty 3*d* orbitals of the phosphorous atom).

The attractiveness of the Wittig reaction relies on the regiospecific control of the new olefin formed. In addition, the reaction proceeds under mild conditions (appropriate for the synthesis of sensitive products), it generally requires readily accessible starting materials, and the new olefin is obtained in a single step, without isolation of the intermediate phosphorous ylide.

Despite the (*Z*/*E*)-selectivity of the Wittig olefination is frequently difficult to predict, it was soon discovered that the type of ylide and the reaction conditions could play a key role in determining the stereochemistry of the process. Thus, phosphorous ylides have been loosely classified in three groups according to their general reactivity: 'non-stabilised' or 'reactive' ylides, which lead to (*Z*)-isomers, 'semi-stabilised', and 'stabilised' ylides, which favour the formation of the (*E*)-isomers (Figure 3.2.9).

Although the Wittig reaction has been widespread used, its mechanism is still controversial. Initially, Wittig and co-workers postulated a model based on a 'betaine' as central intermediate of the mechanism[264]. Some years later, Schlosser used this model to study the stereoselectivity of the reaction[265]. Nevertheless, for a better understanding of the mechanism involved in the Wittig olefination, the 'betaine' model

was soon replaced by the participation of 1,2-oxaphosphetanes as crucial intermediates of the reaction[161,266].

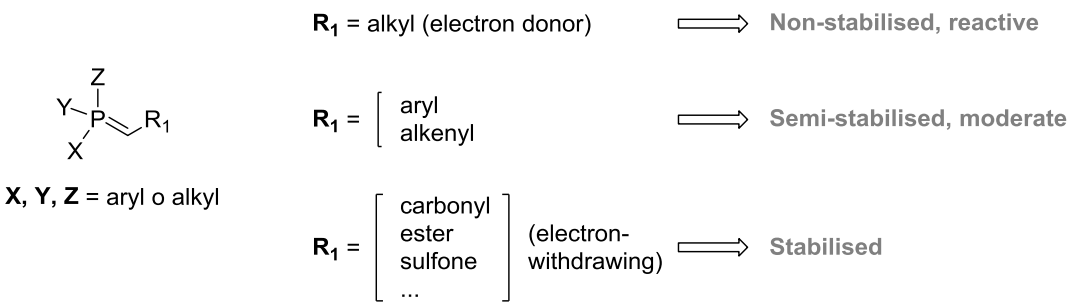

Figure 3.2.9 Classification of ylides based on their reactivity.

The mechanism outlined in Figure 3.2.10 represents the Wittig reaction between an aldehyde and a non-stabilised ylide[267]. The first step is a [2+2] cycloaddition that leads to the oxaphosphetane intermediates type A, which are in equilibrium with intermediates of type B. The chemistry of the pentacoordinated phosphorus compound influences the stability of cyclic intermediates with a trigonal bipyramidal arrangement of the substituents. Thus, the stereoselectivity of the reaction relies on the different decomposition rates of the two *cis/trans* cyclic isomeric trigonal bipyramidal phosphorane intermediates. When non-stabilised ylides are involved, the *cis* intermediate is less stable due to the major sterical overcrowding, decomposing at higher rate than the *trans* intermediate (k_2>k_1) and determining the formation of the (*Z*)-final product.

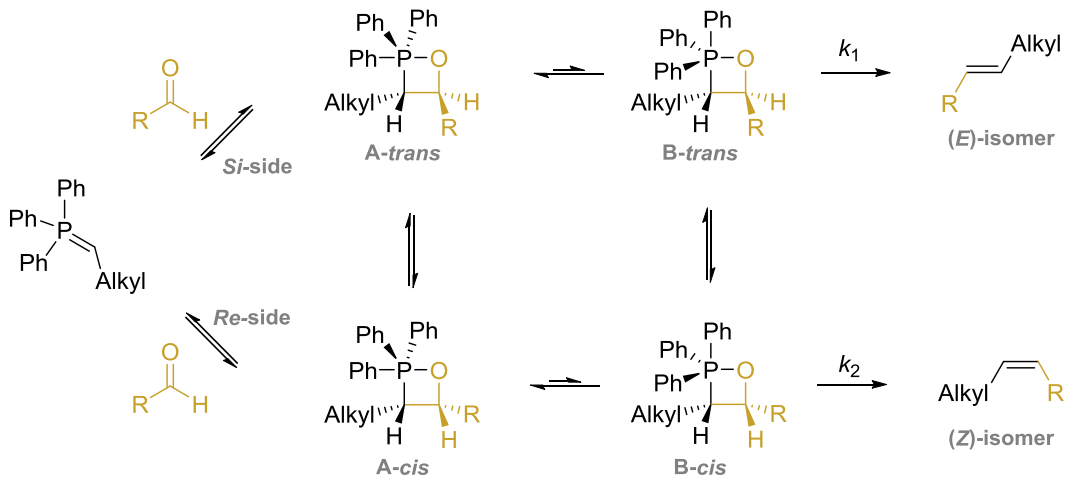

Figure 3.2.10 Wittig olefination mechanism based on 1,2-oxaphosphetanes as reaction intermediates. Image adapted from Baccolini *et al.*[267]

Noteworthy, many factors can influence on the success of the Wittig reaction, such as the presence of salts, the solvent, the temperature and the reagent concentration[161,265,268]. For instance, Oh *et al.*[269] reported that the (*Z*)-selectivity obtained with non-stabilised ylides can be reverted in favour to the (*E*)-isomer by quenching the reaction with excess methanol at -78ºC. In addition, Coyle *et al*.[270] recently described that the (*E*)-selectivity can be enhanced by using organosilanes as pre-catalysts.

Elongation of conjugated polyene moieties by Wittig olefination

Since polyene conjugated systems can display relevant physical properties, the preparation of (*all-E*)-compounds has become of great interest. Despite the poor (*Z/E*)-selectivity of the Wittig olefination, this reaction is one of the key approaches to assemble conjugated polyene moieties to functionalised building blocks.

The strategy of introducing a polyene framework as the last step of the synthesis by a Wittig reaction was applied to both the synthesis of natural products, such as carotenoids[125,271,272], and non-natural ones[109,131,273,274]. Interestingly, the resulting (*Z*>*E*)-isomeric mixtures can generally be isomerised with iodine[275–277] to completely reverse the isomeric composition to (*E*>*Z*) mixtures.

3.2.2.2 Retrosynthetic analysis of *erythro*-polyene ceramide

In consideration of the above reported synthetic strategies, the synthesis of the *erythro*-polyene-Cer was initially envisaged by assembling the conjugated tetraene aldehyde RBM4-4, described in section 3.1.2.3, with the triphenylphosphonium halide RBM4-14 or RBM4-15 by a Wittig olefination to generate the C8-C9 (*E*)-double bond (Scheme 3.2.1).

As depicted in the retrosynthetic analysis (Scheme 3.2.1), we planned to mask the 2-amino-1,3-diol framework of the triphenylphosphonium salts RBM4-14 and RBM4-15 by using two different protecting groups. This will allow us to evaluate the stability of the polyene moiety towards acidic deprotection (from RBM4-14) or basic deprotection (from RBM4-15).

The intermediates RBM4-14 and RBM4-15 could, in turn, be prepared by subjecting the corresponding functionalized serine-derived olefins **6** and RBM4-12 (Scheme 3.2.1) to a CM coupling[238] with commercial 5-bromo-1-pentene, followed by reaction with excess triphenylphosphine. In this way, the highly stereoselective olefin CM reaction would enable the introduction of the required (*E*)-double bond in C4-C5.

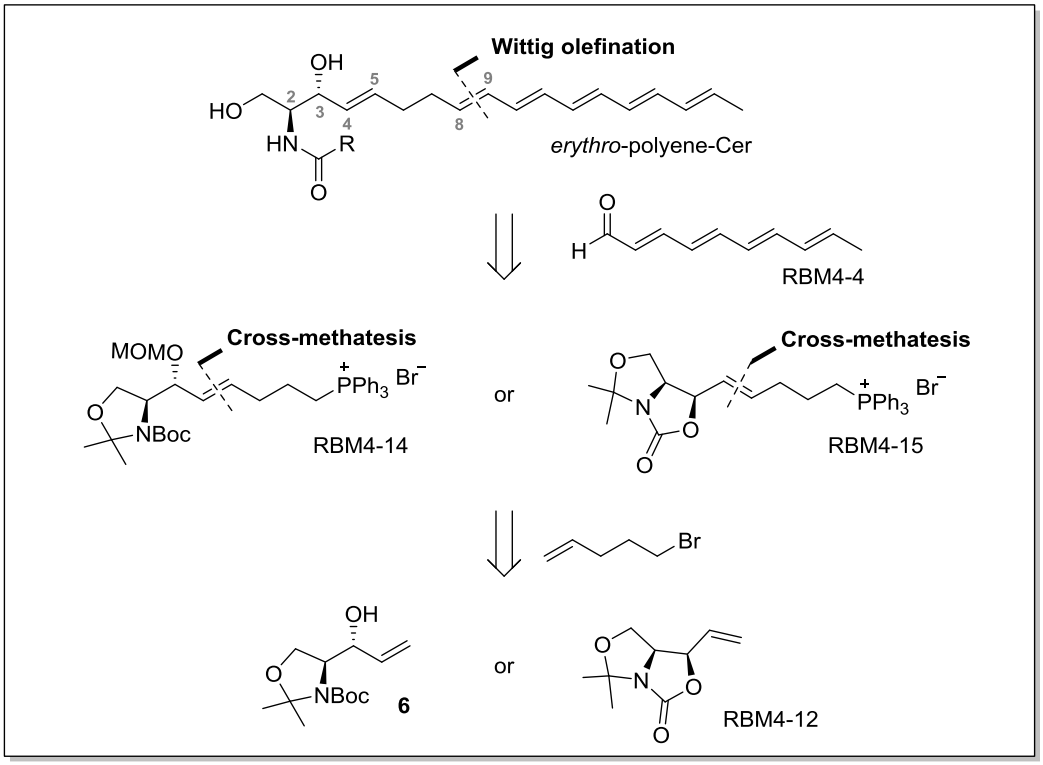

Scheme 3.2.1 Retrosynthetic analysis for the preparation of *erythro*-polyene-Cer.

In both cases, the *erythro* C2-C3 configuration of the sphingoid backbone was assumed to be determined by the chiral allylic alcohol **6**[278], derived from the conformationally rigid Garner's aldehyde.

3.2.2.3 Synthesis of triphenylphosphonium salt RBM4-14

According to the above retrosynthetic analysis, the allylic alcohol **6** was the building block of choice to introduce the desired *erythro* (2*S*,3*R*)-configuration at the sphingoid base backbone. The allylic alcohol **6** was readily obtained by the stereoselective addition of vinyl magnesium bromide to Garner's aldehyde,[242] as reported in the literature[278,279]. Despite the addition afforded a mixture of diastereomers in a (*anti/syn*) (6:1) ratio, the major *anti*-isomer was isolated after carefully chromatographic purification.

With allylic alcohol **6** in hand, we focused our attention on the synthesis of intermediate RBM4-7 (Figure 3.2.11). To address this need, an excess of commercial 5-bromo-1-pentene was assembled, in the presence of Grubbs' 2nd generation catalyst[250] (5% mol), to compound **6** by means of a CM reaction[238,248]. The intermediate RBM4-7 was isolated in excellent yield (80%) and total (*E*)-selectivity, as evidenced by the large ^{1}H NMR coupling constant (15 Hz) between H4-H5 protons.

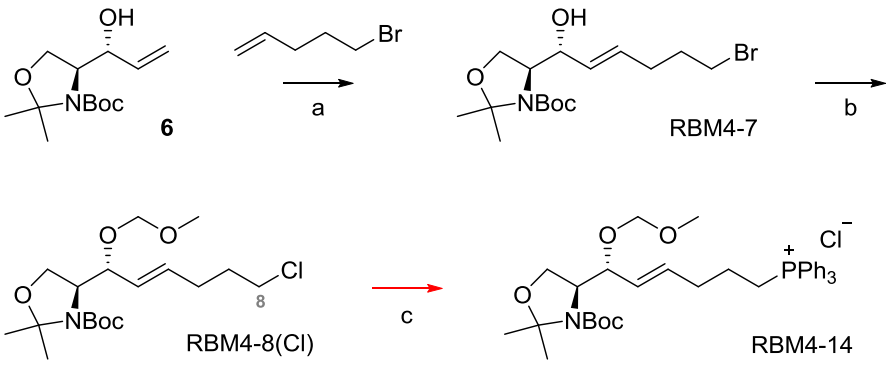

Figure 3.2.11 Initial synthetic strategy to RBM4-14. Reagents and conditions: (a) Grubbs' 2nd generation catalyst, DCM, reflux, 4h, 80%; (b) $ClCH_2OCH_3$, DIPEA, DCM, 16h, 95%; (c) see Table 3.2.3.

In order to prevent a competitive OH proton abstraction in the later ylide formation step, we considered the hydroxyl group protection in RBM4-7 as the corresponding methoxymethyl (MOM) derivative RBM4-8 (Figure 3.2.11). Despite the reaction with excess MOMCl (6 equiv/mol) afforded the required protected derivative, the nucleophilic substitution of the starting bromide by chloride was also observed, as confirmed by ESI-MS (*m/z* $C_{18}H_{32}ClNO_5$ $[M+H]^+$ Found: 378.2020; Calculated: 378.2047) (see also Figure 3.2.13). This apparently irrelevant transformation turned out to be crucial, since a sluggish reaction of chloride RBM4-8 with triphenylphosphine was observed under a variety of conditions (see Table 3.2.1).

Table 3.2.1 Attempts to form the bromide salt RBM4-14 from RBM4-8(Cl).

Entry	eq PPh_3	Solvent[280]	T (º C)	Additive	Time (h)	Yield (%) [a]
1	1.2	ACN	105	-----	16	-----
2	2.5	ACN	105	-----	48	25
3	2.5	ACN	105	NaI (0.2 eq)	24	25
4	2.5	Toluene	110	-----	24	20
5	2.5	-----	90	-----	16	40

[a] Isolated yield after chromatography

When the reaction was carried out in acetonitrile at 105ºC, long reaction times and excess PPh_3 were required in order to observe only a 25% conversion (entries 1 and 2). Exchanging chloride with the better leaving group iodide by addition of a 20% equiv/mol of NaI was also considered (entry 3). Although the rate of conversion increased, the yield was still poor. The use of toluene (entry 4) proved also fruitless. Finally, under solvent-free conditions, only a 40% yield in RBM4-14 was obtained after 16h (entry 5).

In order to circumvent this drawback, we considered to carry out the O-MOM protection of **6** prior to CM reaction with 5-bromo-1-pentene, as outlined in Figure 3.2.12. The protection of **6** proceeded smoothly, providing RBM4-9 in excellent yield. However, the CM between RBM4-9 and 5-bromo-1-pentene yielded RBM4-8(Br) at lower conversion (50%) than that obtained from unprotected **6** (80% yield). Formation of bromide RBM4-8 was confirmed by MS (ESI-MS *m/z* $C_{18}H_{32}BrNO_5$ $[M+H]^+$ Found: 422.1506; Calculated: 422.1542).

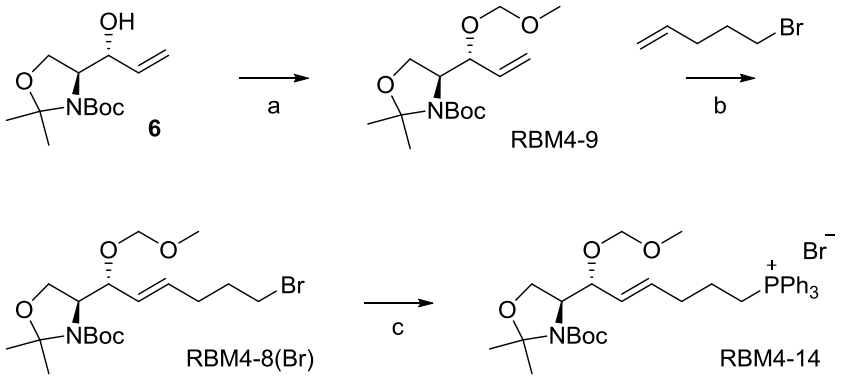

Figure 3.2.12 Second synthetic approach for RBM4-14. Reagents and conditions: (a) $ClCH_2OCH_3$, DIPEA, DCM, 16h, 95%; (b) Grubbs' 2nd generation catalyst, DCM, reflux, 4h, 50%; (c) PPh_3, 90 ºC, 16h, 80%.

Furthermore, significant differences in the NMR spectra of RBM4-8(Br) and RBM4-8(Cl) were observed for the -CH_2-X protons and carbon, where the shielding effect of the bulkier bromine atom is apparent (Figure 3.2.13).

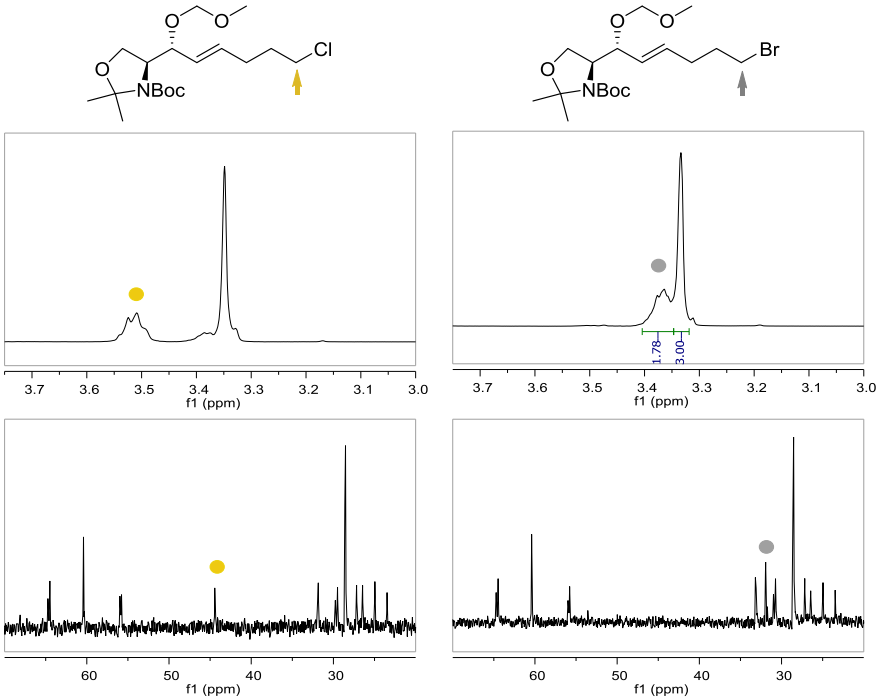

Figure 3.2.13 ^{1}H and ^{13}C-NMR spectrum of RBM4-8(Cl) and RBM4-8(Br).

With RBM4-8(Br) in hand, the preparation of triphenylphosphonium salt RBM4-14 was carried out using neat PPh_3, according to Table 3.2.3 (entry 5). This methodology afforded RBM4-14 in excellent yield (Figure 3.2.12, c).

3.2.2.4 Synthesis of triphenylphosphonium salt RBM4-15

In order to circumvent the presumed instability of the target polyene under the acidic conditions required for the final deprotection in the planned synthetic sequence from RBM4-14, [109,131] we undertook a parallel approach based on RBM4-15 as an alternative building block and suitable for deprotection under non-acidic conditions. To address this need, an oxazolidinone framework, readily obtained by cyclisation from building block **6** was considered (Figure 3.2.14).

Accordingly, the C3 hydroxyl group of the allylic alcohol **6** was transformed into the bicyclic intermediate RBM4-12 by treatment with NaH in THF[281,282]. Subsequent CM with 1-bromo-5-pentene, in the presence of Grubbs' 2nd generation catalyst, afforded RBM4-13 in acceptable yield (65%). In agreement with the NMR spectra data, CM provided only the (*E*)-double bond at C4-C5.

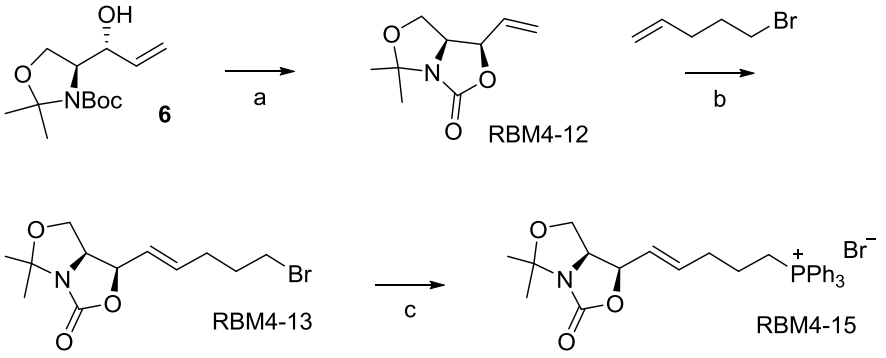

Figure 3.2.14 Synthesis of bromide RBM4-15. Reagents and conditions: (a) NaH, THF, 0 ºC to RT, 16h, 70%; (b) Grubbs' 2nd generation catalyst, DCM, reflux, 6h, 65%; (c) PPh_3, ACN, 90 ºC, 16h, 80%.

Initial attempts to the synthesis of the triphenylphosphonium bromide RBM4-15 were based on the results described for RBM4-14 in section 3.2.2.3. However, when RBM4-13 was heated with neat PPh_3 for 16h, only the product arising from the removal of the isopropylidene group of RBM4-15 was obtained. Fortunately, the use of ACN as solvent gave the desired phosphonium salt RBM4-15 in excellent yield.

3.2.2.5 Wittig olefination

Wittig olefination of aldehyde RBM4-4 with salt RBM4-14

A Wittig olefination of the polyene aldehyde RBM4-4 (see synthesis RBM4-4 in section 3.1.2.3) with the phosphine salt RBM4-14 was initially considered for the construction of the *erythro*-polyene-Cer like probes.

In order to obtain a high (*E*)-selectivity, the modification of Oh *et al.*[269] (quenching with excess MeOH at -78ºC, see section 3.2.2.1) was considered (Table 3.2.2, entry 1). However, despite the desired pentaene RBM4-10 was isolated in an acceptable *Z/E* ratio (*Z/E*: 1:2.5), the overall yield was very low (14%).

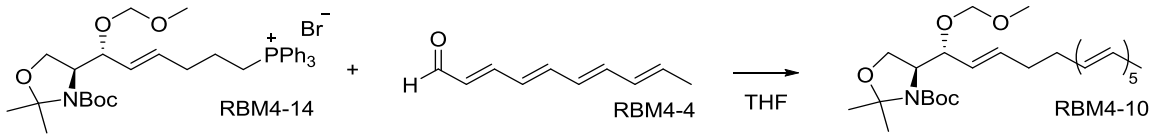

Table 3.2.2 Wittig olefination attempts.

Entry	eq/mol RBM4-14 (*)	eq/mol RBM4-4 (*)	eq/mol; Base	T (º C)	Time (h)	Yield (%) [a]
1	1.6	1 (0.1)	3.0; BuLi [b]	-78	2.5	14
2	1.2	1 (0.2)	1.5; BuLi [b]	-78	2.5	-----
3	1 (0.1)	1.5	1.1; BuLi [b]	-78	2.5	-----
4	1.8	1 (0.2)	2.0; BuLi [b]	-78	4	by-products
5	1.5	1 (0.2)	1.7; LiHMDS	0	1	by-products

(*) In parenthesis, mmol of the limiting reactive species
[a] Isolated yield after chromatography.
[b] Reaction quenched by addition of MeOH at -78ºC.
[c] Reactions were carried out at 0.1-0.2 mmol scale of the limiting reactive.

Attempts to improve the reaction conversion are summarised in Table 3.2.2 (entries 2-5). Initially, the reaction was scaled up (from 0.1 to 0.2 mmol) and the amount of butyllithium (BuLi) was reduced. However, despite the reaction turned dark-red when the phosphonium ylide was generated, no coupling adduct was observed, since unreacted starting aldehyde (entry 2) or unidentified by-products (entry 4) were isolated instead. Similarly, attempts to reverse the relative stoichiometry of the reactants also proved fruitless (entry 3). Finally, the use of LiHDMS[109] at 0 ºC was also fruitless, since a complex reaction mixture was obtained (entry 5).

Attempts to reproduce the results obtained in entry 1, at the same or at larger reaction scale, were also unsuccessful. Compound RBM4-10 was never isolated from the complex reaction mixtures. We have not been able to explain so far the lack of reproducibility observed in this reaction.

Wittig olefination of aldehyde RBM4-4 with salt RBM4-15

The synthesis of compound **7** was next considered by a Wittig olefination between the bicyclic salt RBM4-15 and the aldehyde RBM4-4 (Figure 3.2.15). The reaction was set into motion according to the attempts described for salt RBM4-14 in Table 3.2.2. Unfortunately, none of the above conditions led to the expected adduct **7** and complex reaction mixtures were obtained instead. In all cases, the polyene moiety was mostly deteriorated.

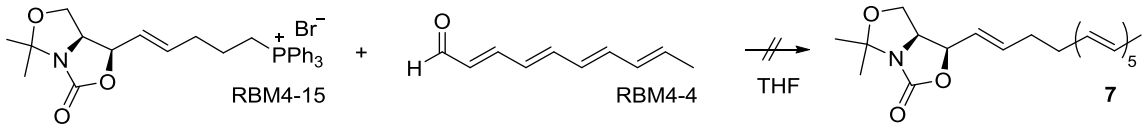

Figure 3.2.15 Synthesis of compound **7**. Reagents and conditions: see Table 3.2.2.

In light of the above results, we decided to rule out this synthetic approach for the construction of the *erythro*-polyene-Cer probes. Since triphenylphosphonium intermediates proved unreactive towards polyene aldehydes, an alternative disconnection analysis was required for the introduction of the polyene moiety into the sphingoid base backbone (See section 3.2.3).

3.2.3 Nucleophilic alkynylation approach

3.2.3.1 Introduction and scope

Nucleophilic alkynylation of α-amino aldehydes

Addition of organometallic reagents to α-amino aldehydes constitutes a straightforward method to synthesise vicinal amino alcohols[241]. Through the addition of a lithiated alkynyl species to a chiral aldehyde (e.g., Garner's aldehyde), the elongation of the carbon chain gives access to propargylic alcohols, whose stereochemistry is set in one step. The stereofacial selectivity observed in the attack of the nucleophile is usually explained by the Felkin-Anh or by the Cram-chelation models (Figure 3.2.16).

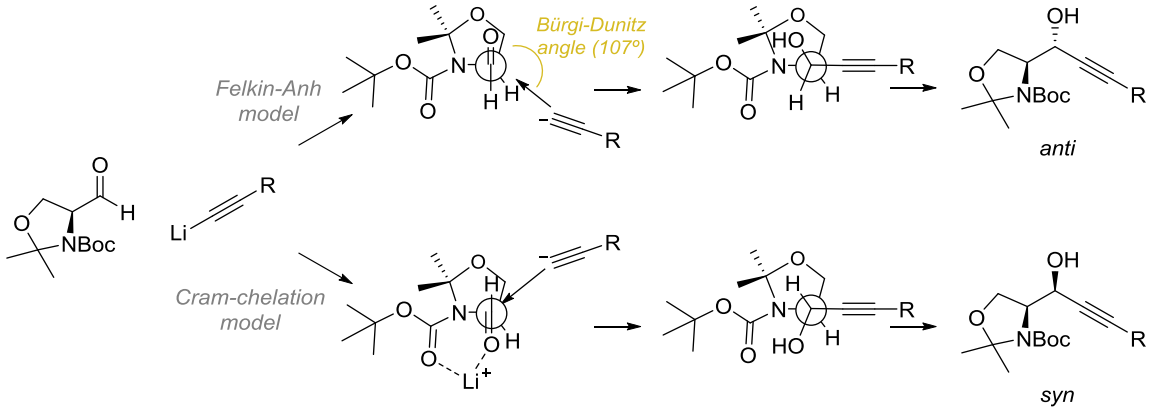

Figure 3.2.16 Diastereoselective models for the nucleophilic alkynylation of Garner's aldehyde.

The Felkin-Anh model postulates that the high *anti*-selectivity observed is due to the addition of the nucleophile along the sterically least hindered Bürgi-Dunitz trajectory, (*re*-side) in a reactive conformation in which the α-amino aldehyde nitrogen atom is placed perpendicular to the C=O carbonyl group (Figure 3.2.16). In this conformation, the π* orbital of the C=O bond and the σ* of C–N bond overlap to generate a new, lower-energy and more reactive molecular orbital (Figure 3.2.17). The formation of the *syn*-product can be rationalised by Cram's chelated model (Figure 3.2.16), where a chelating metal is coordinated between the carbonyl groups from the aldehyde and the carbamate protecting group. The addition of the nucleophile along the least hindered trajectory would indeed lead to the *syn*-compound[283].

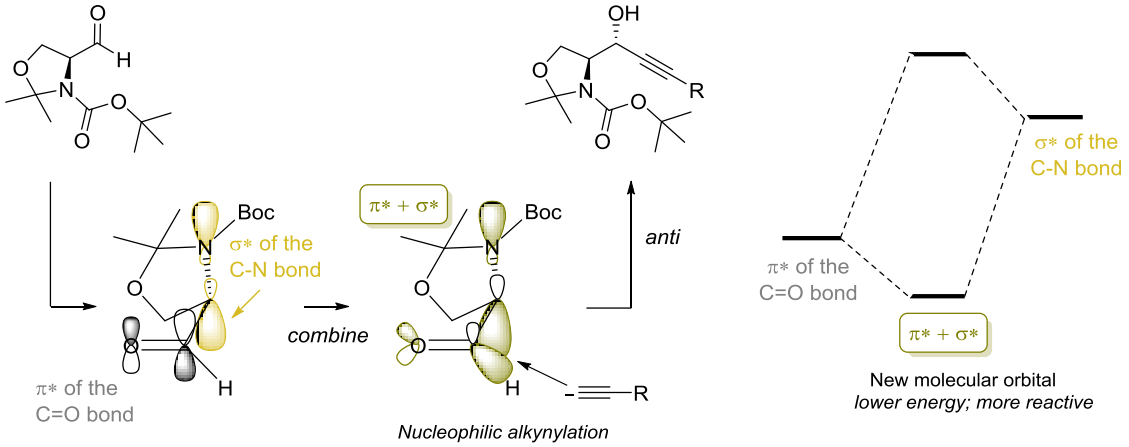

Figure 3.2.17 The effect of the nitrogen electronegativity in the Felkin-Anh transition state. Image adapted from Clayden *et al* [283].

Synthesis of sphingolipids by nucleophilic alkynylation

In agreement with the good diastereoselectivity observed in the addition of lithium-activated nucleophiles to Garner's aldehyde, this reaction has been applied to the synthesis of natural SLs, enabling an easy access to the 2-amino-1,3-dihydroxypropyl framework[240,284]. The stereochemical outcome of the coupling can be controlled by selecting the appropriate conditions. The influence of the steric, chelating and solvent effects has been highlighted by several authors, as discussed next.

In 1988, Herold[285], Garner[286] and Nimkar[287], independently observed that the addition of a lithiated alkynyl group to Garner's aldehyde in THF at low temperature was diastereoselective, favouring the *anti*-diastereomer. Herold also noticed an increase of the diastereoselectivity in the presence of hexamethylphosphorous triamide (HMPT), from an *anti*/*syn* = 8:1 ratio (Garner's methodology) or 9:1 (Nimkar's procedure) to an *anti*/*syn* = 20:1 ratio. HMPT coordinates to the Li cation, breaking the lithium aggregates and increasing the nucleophilicity of the alkyne favouring the kinetic *anti*-diastereomer through a Felkin-Anh transition state[240]. In 1990, Garner and coworkers[288] introduced hexamethyl-phosphoric triamide (HMPA) as a cosolvent, improving the *anti*-selectivity from an *anti*/*syn* = 8:1 ratio to 13:1.

To obtain the *syn*-diastereomer, Herold realized that the use of chelating metals, such as $ZnBr_2$ in Et_2O, was optimal to reverse the diastereoselectivity (*anti*/*syn* = 1:20). Garner applied a slightly different methodology[286], based on Newman's strategy[289,290], which consisted in the use of a transient vinylalane, resulting from the *in situ* reduction of 1-pentadecyne with $i Bu_2AlH$. However, this method provided a modest

diastereoselectivity (*anti*/*syn* = 1:2). In 1997, Gruza and coworkers[291] proposed the use of a Lewis acids, such as $SnCl_4$, to form a trans-metallated tin derivative from the original lithium acetylide. The trans-metallated nucleophile is presumably less reactive than the original lithium acetylide, thus increasing the *syn*-selectivity, albeit at reduced yields.

Recently, Wong and coworkers[292] found that the temperature played a crucial role in determining the diastereoselectivity of the addition of lithium acetylides to Garner's aldehyde. In this sense, the use of harmful additives, such as HMPT, could be avoided. Additionally, this was the first reported example of a complete inversion of the diastereoselectivity just by raising the reaction temperature. According to the authors, at low temperature (-40 ºC) the kinetic Felkin-Anh product predominates, whereas at -15º C the nucleophilic addition occurs via a thermodynamically more stable transition state resembling the chelation model.

Several syntheses of SL analogues have been carried out based on the pioneering work developed by the authors mentioned above[293–297]. However, a number of alternative methods for enantioselective additions of terminal acetylenes to chiral aldehydes have also been described in the literature using catalytic metals and chiral ligands[298,299].

3.2.3.2 Retrosynthetic analysis

As part of our effort towards the *erythro*-polyene-Cer system, we considered the construction of the C3-C4 bond by condensation of the Garner's aldehyde[242] with the unreported polyene alkyne RBM4-17 by means of a nucleophilic alkynylation reaction (Scheme 3.2.2). The configuration of the resulting C3 propargylic center will be determined by the C2 configuration of the conformationally rigid Garner's aldehyde, as well by the use of proper conditions in the nucleophilic alkynylation step to favour the *anti*-selectivity (see section 3.2.3.1).

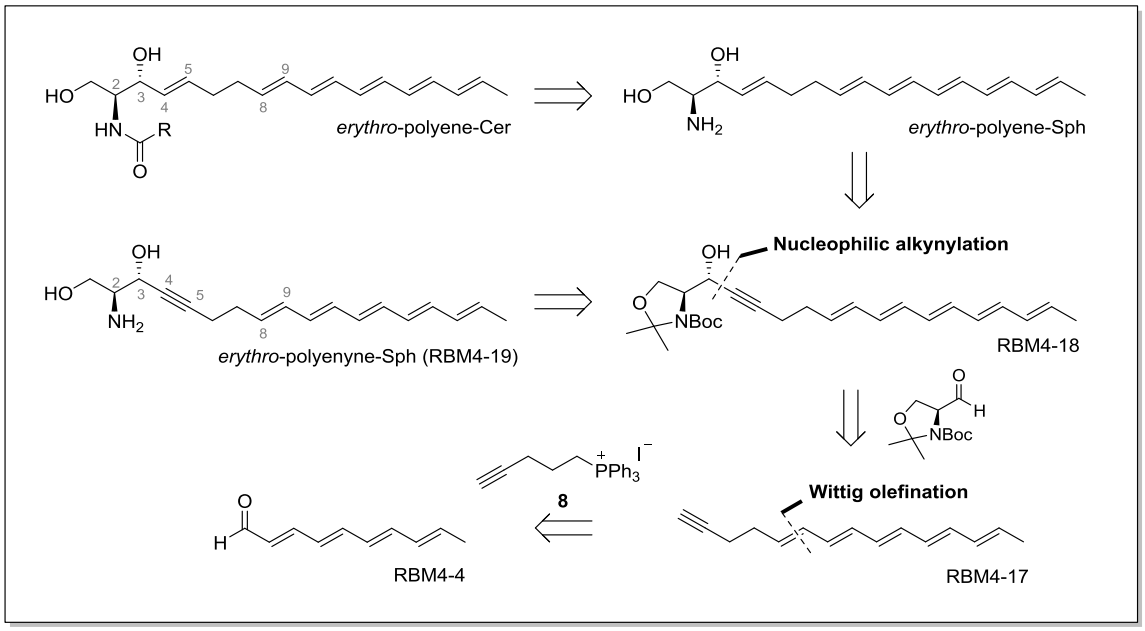

Scheme 3.2.2 Retrosynthetic analysis for the preparation of *erythro*-polyene-Cer and *erythro*-polyenyne-Sph.

Taking advantage of the (*all-E*)-decatetraenal RBM4-4 (see section 3.1.2.3), we were encouraged to synthesise the unreported polyene alkyne RBM4-17 by coupling the above aldehyde with the ylide resulting from the phosphonium salt **8** (Scheme 3.2.2) by a (*E*)-selective Wittig olefination[269]. As mentioned in section 3.2.2.2, compound RBM4-4 has been reported to react under Wittig olefination conditions[109,131,273]. Nonetheless, the access to this kind of polyene alkynes has been scarcely described in the literature[300–303].

In agreement with reported nucleophilic akynylations from lithiated polyunsaturated acetylides[300,304–307], we considered that lithiaded alkynyl RBM4-17 would add diastereoselectively to Garner's aldehyde to afford the propargylic alcohol intermediate RBM4-18.

The polyenyne intermediate RBM4-18 could be a versatile scaffold to prepare SL analogues. Removal of the protecting groups under mild acidic conditions[109,172] in one step, would give access to an interesting *erythro*-polyenyne-Sph probe. Chemical modification of the sphingoid backbone by incorporation of an acetylenic group has received considerable attention[281,292,308,309]. The triple bond increases the rigidity of the molecule, affecting its physicochemical and biological properties. Thereby, introduction of the fluorescent pentaenyne moiety can give rise to a useful tool for visualization studies.

In addition, we assumed that the selective reduction of the propargylic alcohol RBM4-18 to the corresponding (*E*)-allylic alcohol, would provide the precursors for the desired *erythro*-polyene-Sph and *erythro*-polyene-Cer probes. Reduction of the propargylic alcohol framework in the presence of conjugated double bonds is a well-studied transformation, leading to either *trans*[306,310] or *cis*[311,312] allylic alcohols upon appropriate conditions. However, to the best of our knowledge, a conjugated pentaene moiety has never been used under any of the above conditions. In the last step, we would attempt the sequential deprotection and *N*-acylation of the resulting sphingoid base to afford the required *erythro*-polyene systems.

3.2.3.3 Synthesis of the polyene alkynes RBM4-17 and RBM4-24

We first undertook the synthesis of the pentaene alkyne RBM4-17 by coupling the (*all-E*)-decatetraenal RBM4-4 with the triphenylphosphonium salt **8** under Wittig olefination conditions (Figure 3.2.18). The salt **8** was easily obtained in two steps, by formation of the 5-iodo-1-pentyne from the commercial 4-pentyn-1-ol[313] and transformation into the corresponding triphenylphosphonium iodide salt **8** in high yield (85%).

In order to elongate the polyene moiety of the aldehyde RBM4-4, the ylide formation of the phosphonium salt **8** was required. For this purpose, as a preventive measure, we used potassium *tert*-butoxide[314] (*t*-BuOK) to avoid the deprotonation of the acetylene group, since phosphonium ylides are more acidic than terminal acetylenes. However,

probably as a result of the inefficiency of *t*-BuOK to deprotonate the starting phosphonium salt (probable due to their similar pK_a values[315]), the Wittig olefination coupling was unsuccessful. Thereby, a stronger base, such as BuLi, was required to form the phosphonium ylide (Figure 3.2.18). The subsequent addition of RBM4-4 in the presence of HMPA, under conditions to favour the (*E*)-selectivity[269], afforded the desired pentaene alkyne RBM4-17 as a mixture of *Z* and *E* isomers (*Z*/*E* = 1:2) at the new double bond in 55% yield. The stereochemical assignment was made by comparison with the spectroscopic data for alkyne RBM4-17(*Z*)[316].

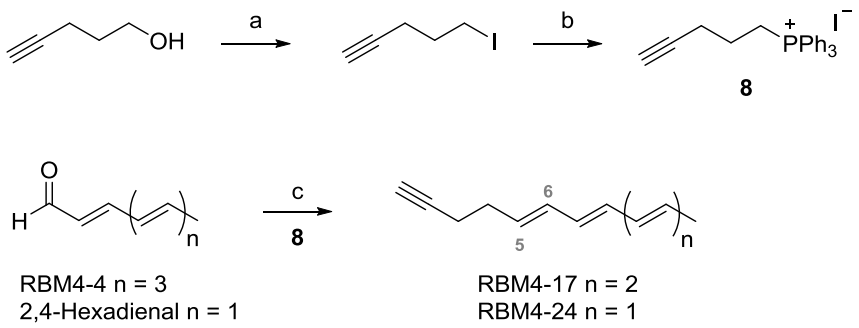

Figure 3.2.18 Synthesis of RBM4-17 and RBM4-24. Reagents and conditions: (a) I_2, PPh_3, imidazole, DCM, RT, 1h, 60%; (b) PPh_3, 86 ºC, 16h, 85%; (c) BuLi (2.5 M hexane), HMPA, THF, -78 ºC, 4h. RBM4-17: 55%, (5*Z*:*E* = 1:2); RBM4-24: 80%, (5*Z*:*E* = 1:1).

In order to set up the reaction conditions and also to gain knowledge of the reactivity of these systems, we decided to synthesise the polyene RBM4-24, with three conjugated double bonds, as a model probe.

Similarly as above, alkyne RBM4-24 was obtained by coupling the ylide **8** with the commercial aldehyde (*all-E*)-2,4-hexadienal (sorbic aldehyde) under Wittig olefination conditions[269], providing a 1.1 mixture of *Z,E* isomers at the new double bond in 80% yield (Figure 3.2.18). In consideration of the above results, we observed a direct relationship between the number of conjugated double bonds, the yield of the reaction and the selectivity of the new double bond generated. Basically, long conjugated polyene chains seem to favour the (*E*)-selectivity, albeit at the expense of yield.

The isomeric mixtures (5*Z*:5*E*) of the alkynes RBM4-17 and RBM4-24, were treated with iodine[275–277] in an attempt to force the isomerization into the corresponding (*all-E*)-alkynes. This isomerization was carried out according to the methodology reported by Souto *et al*[131], and the remaining iodine was removed by washing the crude reaction

mixture with a saturated aqueous sodium metabisulfite solution[317]. Ratios (*Z*:*E*) of (1:6) and (1:4) for RBM4-17 and RBM4-24, respectively, were obtained under these conditions. In both cases, this ratio was unaltered even after a second treatment with iodine.

We then focused our attention on the obtaining of the pure (*all-E*)-pentaene alkyne RBM4-17. For this purpose, the resulting (1:6) (5*Z*:5*E*) isomeric mixture of RBM4-17 was purified by preparative—HPLC, as described in the Experimental Section, isolating the (*all-E*)-isomer in 25% yield (Figure 3.2.19, B). It is particularly noteworthy that the pentaene alkyne RBM4-17 showed a relatively high instability, which required the use of the freshly prepared compound in the next reaction step.

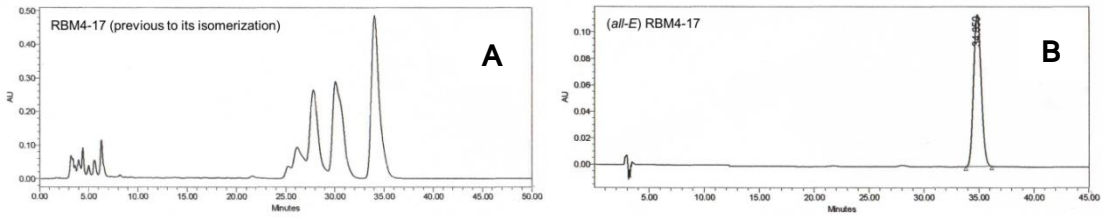

Figure 3.2.19 Preparative HPLC chromatograms of RBM4-17. **A:** Mixture of isomers (5'*Z*:5'*E*), (1:2). **B**: (*all-E*)-RBM4-17 after purification. Column (X-Bridge C18, 5µm OBD, 19 x 250 mm). Isocratic method (35:65, H_2O:ACN, 10 mL/min); Rt: 35.0 min; λ: 330 nm.

3.2.3.4 Nucleophilic alkynylation of Garner's aldehyde with RBM4-17 or RBM4-24

With the synthesis of the (*all-E*)-pentaene alkyne RBM4-17, we then targeted its nucleophilic alkynylation to Garner's aldehyde[242]. The reactivity and the stereochemical scope of the coupling was first examined using the model alkyne trienyne RBM4-24. All the attempts carried out are summarised in the table below (Table 3.2.3).

Based on Herold and Garner's protocols[285,288] to favour the *anti*-selectivity in the nucleophilic addition to α-aminoaldehydes, the lithiated acetylide from RBM4-24 was generated by using BuLi as a base. Next, addition of HMPA as co-solvent, followed by Garner's aldehyde at --78 ºC, afforded a complex mixture of compounds even after reducing the time for acetylide formation to only 5 min (entries 1 and 2).

Taking into account the method of Kuerschner *et al* in related systems[109], we were prompted to replace BuLi with lithium bis(trimethylsilyl)amide (LiHMDS). The lithiated polyene acetylide RBM4-24 was subsequently added at -78 ºC to the Garner's aldehyde without using any additive. Nonetheless, the conversion did not occur (entry 3).

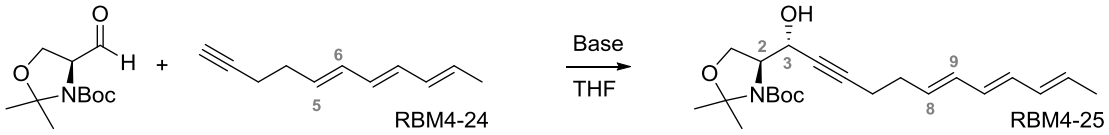

Table 3.2.3 Nucleophilic alkynylation of RBM4-24 to Garner's aldehyde

Entry	Base [a]	Additive (%vol)	T (ºC)	Acetylide formation (min)	Yield(%) [b]
1	BuLi	HMPA (5)	-78	60	-----
2	BuLi	HMPA (5)	-78	5	-----
3	LiHMDS		-78	5	-----
4	LDA		-78	5	10
5	LDA		-78	10	20
6	LDA		0→-78	30	-----
7	LDA		-78	30	45

[a] Bases were 1.0–1.3 eq. to the alkyne RBM4-24.
[b] Isolated yield after chromatography.

We next attempted the use of lithium diisopropylamide (LDA) as a hindered amide base that shows a much greater selectivity for proton abstraction versus nucleophilic addition (entries 4 to 7).

The best results were obtained by generation of the lithiated acetylide of RBM4-24 (5Z:5E; 1:1) for 30 min at -78 ºC and subsequent coupling with Garner's aldehyde (entry 7). In agreement with the results of Wong and coworkers on the effect of the low temperatures to favour a Felkin-Anh transition state[292], the trienyne *erytho*-RBM4-25 (8Z:8E; 1:1) was obtained as a single diastereomer in 45% yield.

With the optimized conditions in hand, the nucleophilic alkynylation of the pentaene alkyne RBM4-17 (5*Z*:5*E*; 1:1) to Garner's aldehyde was carried out as described above (Table 3.2.3, entry 7). The desired coupled pentaenyne *erythro*-RBM4-18 (8*Z*:8*E*; 1:1) was isolated as a single diastereomer in 25% yield (Figure 3.2.20). The configurational

assignment of C2 and C3 stereocenters was determined by comparison with the reported ^{1}H-NMR data for the corresponding saturated alkyne in $CDCl_3$[318].

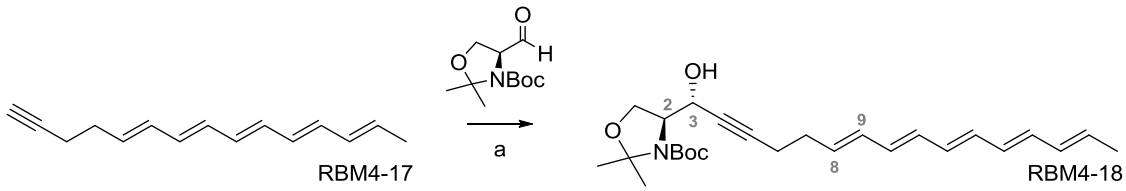

Figure 3.2.20. Reagents and conditions: (a) LDA, THF, -78 ºC, 3h, 25%.

From this point, our efforts were addressed at evaluating the suitability of RBM4-18 for the subsequent reaction steps (deprotection and triple to double bond reduction) rather than optimising the preparation of (*all-E*)-RBM4-18.

3.2.3.5 Selective reduction of the propargylic alcohol to the (*E*)-allylic alcohol

In consideration of our retrosynthetic analysis leading to the target Sph and Cer polyene probes (Scheme 3.2.2), we proceeded with the selective reduction of the propargylic alcohol RBM4-18 to the corresponding (*E*)-allylic alcohol.

Initial attempts were used with model trienyne RBM4-25 using Red-Al (sodium bis(2-methoxyethoxy)aluminum hydride), which is reported to reduce propargylic alcohols to allylic alcohols with *trans*-selectivity[306] (Figure 3.2.21). Despite a careful monitoring conditions (including the stepwise addition of Red-Al), complex reaction mixtures were obtained in all attempts.

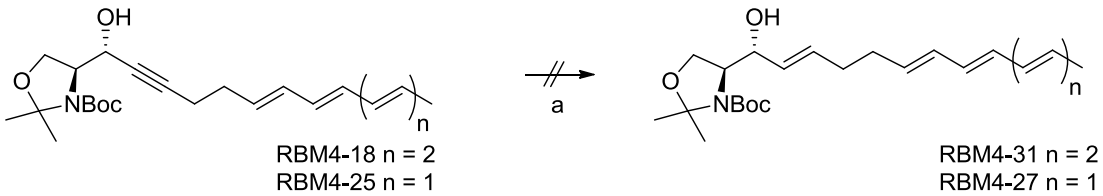

Figure 3.2.21 Attempts for the selective reduction of the propargylic alcohol. Reagents and conditions: (a) Red-Al, THF, 0 ºC, from 2 to 6h; or $LiAlH_4$, THF, 0ºC →RT, 3h.

The use of $LiAlH_4$ for this type of reduction[310] resulted again in a range of degradation by-products, as judged from the model RBM4-25. Similar results were obtained from the fully deprotected RBM-26, obtained as indicated in section 3.2.3.6.

After all the above unsuccessful attempts using pentaenyne RBM4-18 as starting material (Figure 3.2.21), we decided to disregard the nucleophilic alkynylation approach to obtain the desired Sph and Cer *erythro*-polyene probes.

3.2.3.6 Synthesis of the *erythro*-polyenyne-Sph RBM4-19

Despite we were not able to reach the required targets, this synthetic strategy led to their corresponding C4 acetylenic analogues. Due to the close structural analogy of polyene aminodiols RBM4-19 and RBM4-26 (Figure 3.2.22) with some reported acetylenic sphingolipid analogues[281,292,308,309], we considered that they could also find interesting applications as fluorescent surrogates thereof.

For this goal, we planned the simultaneous removal of both the isopropylidene and Boc groups from RBM4-18 and RBM4-25 (Figure 3.2.22). Commonly, *N*-Boc deprotection can be accomplished with strong acids, such as trifluoroacetic acid or HCl. Besides, according to several authors[109,172], acidic deprotection conditions can also be applied in polyene systems, despite conjugated double bonds are apparently sensitive under these conditions.

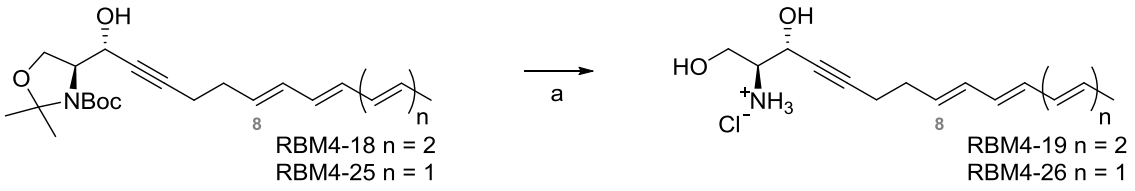

Figure 3.2.22 Deprotection conditions: (a) CH_3COCl (1.5%vol), MeOH, 0ºC to RT, 30 min. (*all-E*)-*erythro*-RBM4-19: 40%; (8*Z*:8*E*; 1:2)-*erythro*-RBM4-26: 60%.

Accordingly, deprotection of the model RBM4-25 under mild acidic conditions, using HCl in MeOH[319], afforded the desired aminodiol hydrochloride RBM4-26 (Figure 3.2.22). Gratifyingly, application of the same protocol to RBM4-18 led to the *erythro*-polyenyne Sph RBM4-19 (hydrochloride). This result showed the stability of the pentane moiety under the mild acidic conditions used in this deprotection step. Finally, this approach allowed, for the first time, the introduction of the pentaene moiety as part of the sphingoid backbone, thus providing access to new probes of interest for the biochemical and biophysical studies of SLs.

3.2.4 Negishi cross-coupling approach

3.2.4.1 Introduction and scope

Negishi cross-coupling reaction

The development of transition metal-mediated intermolecular cross-coupling reactions has provided an efficient method for the assembly of conjugated diene systems. The first observation of a zirconium—palladium transmetalation in alkene homocoupling reactions was reported by Schwartz and coworkers[320] in 1977. Subsequent reports by Negishi[321–324] described highly regio- and stereoselective nickel- or palladium-catalysed cross-coupling reactions between transition metals (Al, Zn, and Zr) as nucleophiles and organic halides (aryl, vinyl, benzyl, or allyl) as electrophiles for the synthesis of olefins (Figure 3.2.23). In the late 1990s, Panek and coworkers[325,326] optimized the experimental protocol of Negishi cross-coupling, executing a one-pot tandem process consisting of hydrometalation, followed by *in situ* transmetalation to the corresponding vinyl zincate, and Pd-catalysed alkenyl-alkenyl coupling[326] (Figure 3.2.24).

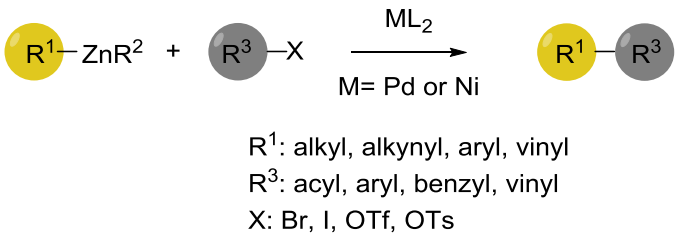

Figure 3.2.23 Negishi cross-coupling reaction. Image taken from Heravi *et al.*[327]

Generally, the accepted mechanism for the transition-metal catalysed cross-coupling reactions is described as a catalytic cycle[328] involving three elementary steps: the oxidative addition of the organic halide to a low valent transition metal, followed by a transmetalation with an organometallic reagent, and the final reductive elimination of the coupled product (Figure 3.2.24).

Nonetheless, in the Pd-catalysed cross-coupling between alkenylhalides and alkenylzirconocenes this catalytic process is unsatisfactory because of the slow Zr/Pd transmetalation. Negishi and coworkers[323] suggested that the single transmetalation process, of high activation energy, could be replaced by a double or multiple transmetalation processes of lower kinetic barriers, which could lead to an overall rate enhancement. Thus, the coupling can be significantly promoted by the addition of metal

salts of Zn or Cd. The resulting organozinc species, which shows a mild Lewis acidic character, is much more reactive towards transmetalation due to the empty low-lying p orbitals of the zinc, and the highly covalent character of the carbon–zinc bond[329,330].

Focusing on the slightly modified methodology of Panek and coworkers[325,326], the reactive organozinc intermediate is generated by transmetalation of an alkenylzirconocene, which in turn, is formed by hydrozirconation of an alkyne with Schwartz reagent[331] $Cp_2Zr(H)Cl$ (Figure 3.2.24). The hydrozirconation reaction is described in section 3.2.5. Subsequent *trans*/*cis* isomerization of the intermediate Pd-complex is required to favour the cross-coupling reaction[323] (Figure 3.2.24). Finally, the Pd (II)-π complex is converted by a reductive elimination to the corresponding coupled product along with the regeneration of the Pd(0) catalyst $Pd(Ph_3P)_4$.

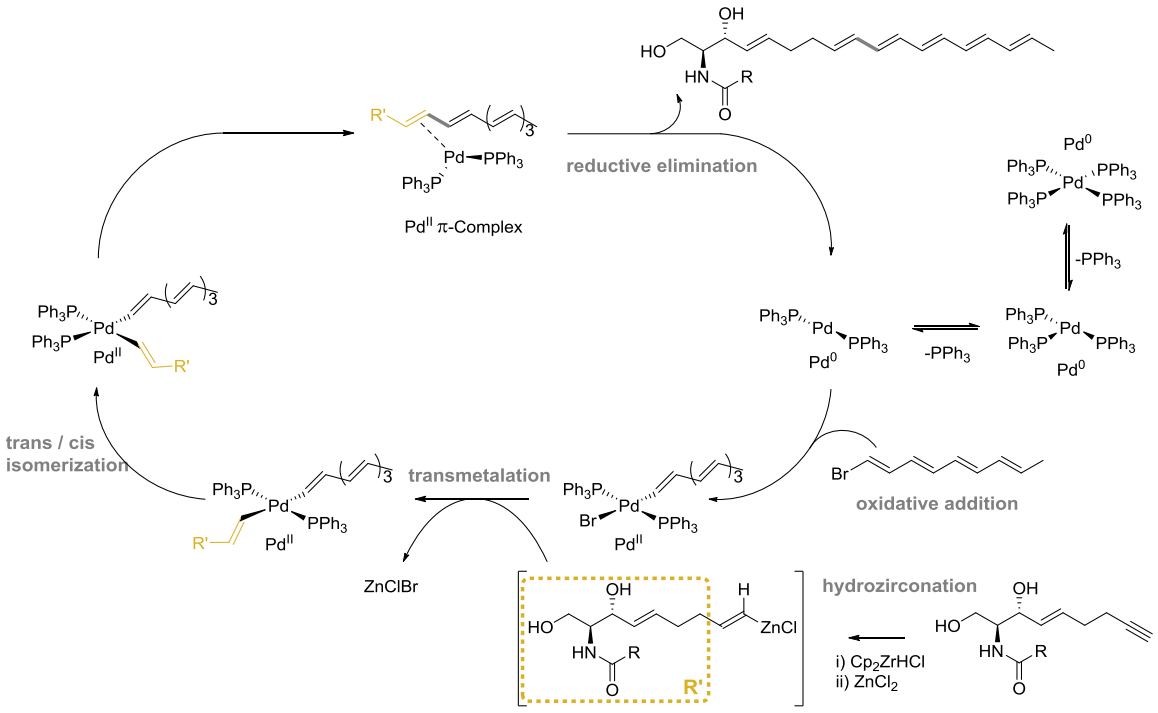

Figure 3.2.24 Negishi cross-coupling mechanism. Image adapted from Heravi *et al* [327].

The Negishi cross-coupling exhibits high tolerance towards a wide variety of functional groups. In addition, the reaction proceeds under mild conditions with high stereo- and regioselectivities. Additionally, the organozinc intermediates show a relatively low toxicity, although the procedure is particularly sensitive to the oxygen and water. Of no less significance, the Negishi cross-coupling can take place efficiently when using a nearly equimolar ratio of the two coupling partners, with no need to use a large excess of one or the other reagent[330,332].

Synthesis of conjugated polyene systems by Negishi cross-coupling

A particular attractive of the Negishi cross-coupling in the context of natural products synthesis, is the stereoselective one-pot conversion of terminal acetylenes into conjugated dienes and the ability to assemble conjugated polyene systems.

As the number of conjugated double bonds increases, the efficiency of the synthesis along with its selectivity becomes increasingly important. Despite common carbonyl olefinations, such as Wittig or HWE reactions, are often plagued by the formation of stereoisomeric mixtures, its combination with Pd-catalysed alkenylations can be mutually more complementary than competitive in the synthesis of polyene chains[155]. This combined strategy has been applied, for instance, to the preparation of ω-hydroxy di- and trienoic acid esters[158] or to obtain conjugated oligoenes[160].

An additional example of the utility of Negishi cross-coupling is the synthesis of carotenoids. The Zr-catalysed carboalumination enables the assembly of symmetrical and unsymmetrical ten conjugated double bonds[333]. In another example, the construction of the conjugated pentaene moiety of mycolactones A and B has been accomplished by successive application of carboalumination Pd-catalysed cross-coupling processes[334].

Zeng and coworkers[335] also reported a linear iterative hydrozirconation-Pd-catalysed cross-coupling methodology to synthesise a seven (*all-E*)-oligoenes, providing a general route to oligoene macrolide antibiotics and other related natural products.

To the best of our knowledge, however, sphingolipids containing conjugated polyene moieties do not appear to have been previously synthesized using the Negishi cross-coupling approach. Nonetheless, since all the works mentioned above show a wide compatibility with a variety of functional groups, we expected this method to be suitable for the synthesis of polyene-SLs.

3.2.4.2 Retrosynthetic analysis

In light of the labile nature of the conjugated pentaene compounds, we were prompted to design a convergent approach, which involved the introduction of the polyene moiety at the last step of the synthesis (Scheme 3.2.3).

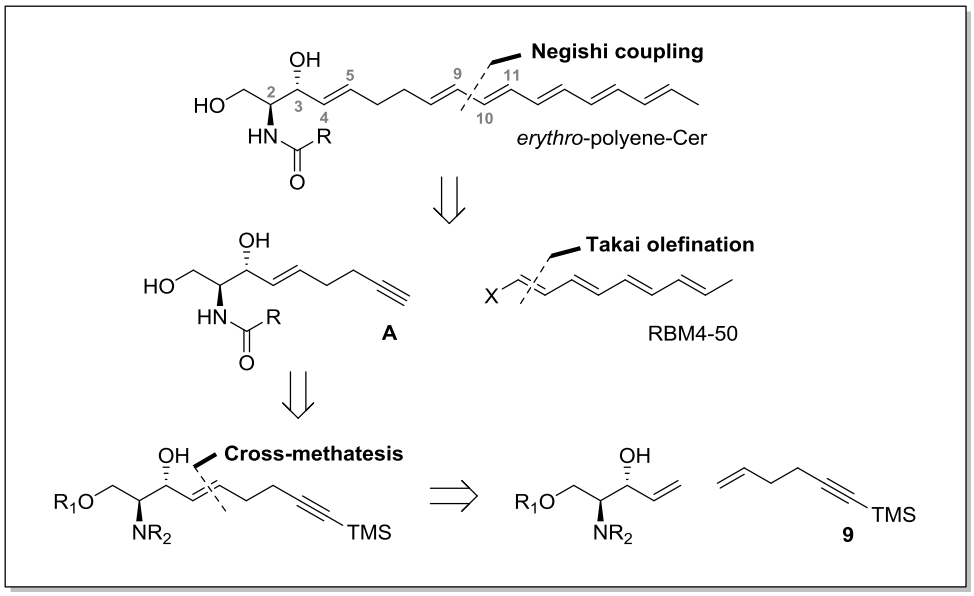

Scheme 3.2.3 Retrosynthetic analysis for the preparation of *erythro*-polyene-Cer.

For the construction of the sp^2-sp^2 C9-C10 bond, we envisaged the assembly of the polyene halide RBM4-50 and the sphingoid-alkyne **A** by a modified Negishi cross-coupling reaction[325,326]. The polyene halide RBM4-50 would arise by one-carbon homologation of (*all-E*)-octatrienal by means of the Takai olefination[336], which is reported to favour the (*E*)-selectivity of the resulting olefin.

We assumed that a CM between an allylic alkene and 5-hexen-1-ynyltrimethyl-silane[337–339] **9** would provide the C4-C5 (*E*)-double bond[238]. The resulting coupled product, bearing orthogonal protecting groups, should be selectively deprotected and *N*-acylated leading to the required terminal sphingoid-alkyne **A** precursor for the Negishi cross-coupling (Scheme 3.2.3).

3.2.4.3 Synthesis of the polyene halide RBM4-50

Amongst the wide range of synthetic strategies for the preparation of alkenyl halides,[302,336,340–344], we focused on those involving one—carbon homologation.

For this purpose, we first synthesised the (*all-E*)-octatrienal RBM4-2 by applying the methodology of Sun and coworkers[166] (Figure 3.2.25). Similarly as described in section 3.1.2.3, the commercial (*all-E*)-hexadienal was coupled with triethyl phosphonoacetate by a HWE reaction, followed by sequential ester reduction and oxidation of the intermediate alcohol with IBX to give the (2*Z*:2*E*; 1:10)-aldehyde RBM4-2.

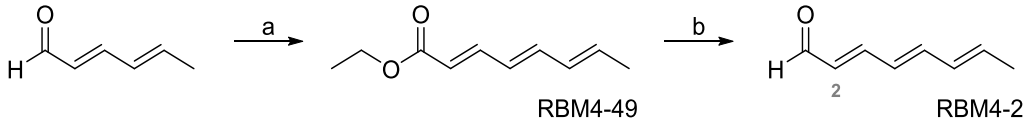

Figure 3.2.25 Synthesis of aldehyde RBM4-2. Reagents and conditions: (a) Triethyl phosphonoacetate, NaH, THF, 0º C, 3h, 84%; (b) i) DIBAL-H, hexane, -78º C, 1h; ii) IBX, EtOAc, refluxed, 12h, 60% (2*Z*:2*E*; 1:10).

Wittig[344] and Takai[336] olefinations are two of the most common reactions to prepare haloolefins from aldehydes. Since Takai reaction is reported to provide mainly the (*E*)-isomer[336,345], we decided to start with this strategy.

Takai olefination

The one-carbon homologation of the aldehyde RBM4-2 by Takai's protocol[336] is based on the $CrCl_2$-mediated aldehyde coupling with a haloform (Figure 3.2.26). The mechanism proposed by Takai consisted in the oxidation of Cr(II) to Cr(III) with replacement of two of the of the haloform halogen atoms. The geminal carbodianion complex reacts with the aldehyde, placing the bulky groups in an *anti*-periplanar conformation. A final E2-reductive elimination leads to the corresponding (*E*)-haloolefin.

Initials attempts were carried out using iodoform, due to the reported[336] reactivity of the starting haloform in the order I>Br>Cl. However, the iodoolefin RBM4-50-(I) was obtained as an inseparable mixture of *Z*:*E* isomers (1:2), which were unstable in the presence of solvents, oxygen and humidity.

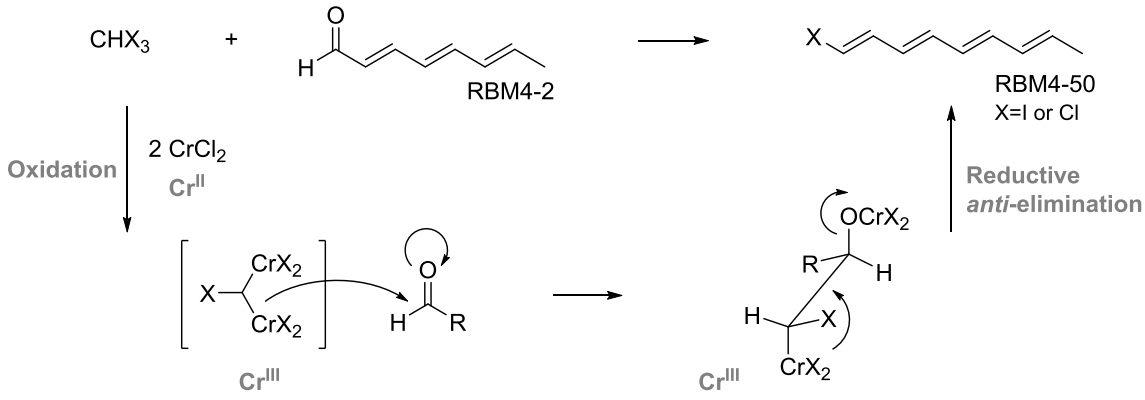

Figure 3.2.26 Synthesis of the haloforms RBM4-50. Reagents and conditions: CHI_3, $CrCl_2$, THF, 0ºC, 2h, 50% RBM4-50-(I) (*Z*:*E*; 1:2); or $CHCl_3$, THF, 65ºC, 5h, 35% RBM4-50-(Cl) (*Z*:*E*; 1:2).

In light of the instability of this iodoolefin, we tried the homologation of aldehyde RBM4-2 with chloroform. Both the original Takai's procedure, as well as a slightly modified protocol[346], afforded the 1-chlorononatetraene RBM4-50-(Cl) as mixture of isomers (*Z*:*E* 1:2). This compound showed a similar lability to that observed for the above iodo analog RBM4-50-(I).

Wittig olefination

In consideration of the above results, we expected to circumvent the instability of the haloolefins by avoiding the use of organochromium species. For this goal, Wittig olefination was devised as a possible strategy to homologate the polyene aldehyde RBM4-2, albeit a lower (*E*)-selectivity would be expected (see mechanism in Figure 3.2.10).

Quesada and coworkers[196,347] described the synthesis of the 1-bromononatetraene RBM4-50-(Br) using this approach. Accordingly, aldehyde RBM4-2 was coupled with the ylide obtained from commercial (bromomethyl)triphenylphosphonium bromide and *t*-BuOK as a base (Table 3.2.3, entry 2). Although the authors described RBM4-50-(Br) as a mixture of isomers (*Z*:*E*) (2.5:1) in 72% yield, we isolated this bromoolefin as a (4:1) (*Z*:*E*) mixture in very low yield (<5%). The configurational assignment of the new double bond was determined by comparison with the (*Z*)-1-bromononatetraene synthesised under Wittig conditions[316] (entry 1), as described in section 3.2.3.3.

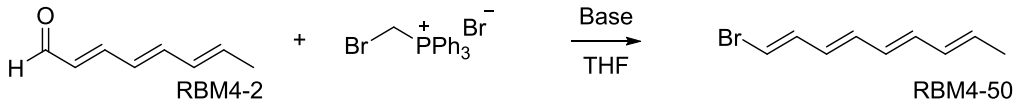

Table 3.2.4 Synthesis of the (*all-E*)-1-bromononatetraene RBM4-50 by Wittig olefination

Entry	Base [a]	T (ºC) Work-up	*Z*:*E*	Yield(%) [b]	References
1	BuLi [c]	RT [f]	4:1	70	(*Z*)-conditions[316]
2	*t*-BuOK [d]	RT [f]	4:1	<5	Quesada *et.al.*[196,347]
3	*t*-BuOK [d]	-78, MeOH	3:1	<5	Quesada and Oh[196,269,347]
4	*t*-BuOK [e]	RT [f]	4:1	70	Liu *et.al.*[348,349]
5	*t*-BuOK [e]	-78, MeOH	3:1	70	Liu and Oh [269,348]
6	BuLi [c]	-78, MeOH	1.5:1	70	Oh *et.al.*[269]
7	KHMDS	RT [f]		---	Lipshutz and Amans[302,35(

[a] 1.2–1.5 eq/mol relative to aldehyde RBM4-2.
[b] Isolated yield after chromatography.
[c] HMPA (5% vol) as co-solvent
[d] Added as powder
[e] Added as a 1M solution in THF
[f] Addition of water and extracted

In order to increase both the conversion rate and the (*E*)-selectivity of the Wittig olefination, we modified the methodology of Quesada *et. al*. by quenching the reaction with MeOH at -78ºC[269] (Table 3.2.3, entry 3, see section 3.2.3.3). Nonetheless, despite the (*Z*:*E*) ratio improved slightly from (4:1) to (3:1), the reaction yield was still very poor.

Unexpectedly, when *t*-BuOK was added as a 1M solution in THF[348], the yield increased to 70% (entries 4 and 5). Furthermore, the (*E*)-isomer was slightly favoured when the reaction was quenched with MeOH at -78ºC[269] (entry 5).

The modest (*E*)-stereoselectivity obtained under all the above conditions, however, still required improvement. Thereby, we next attempted the synthesis of the polyene bromide RBM4-50 using BuLi as a base in the presence of HMPA (5% vol) as co-solvent, following the same procedure as in section 3.2.3.3 for the synthesis of polyene alkynes RBM4-24 and RBM4-17. Despite BuLi is reported to lead to side reactions with α-bromoalkylide salts[344,351], we obtained the best *E* ratio (*Z*:*E*; 1.5:1) in 70% yield. The bromopolyene RBM4-50-(Br) should be used immediately, since degradation was observed even if stored at -20 ºC.

It is noteworthy that, by replacing BuLi with KHMDS[302,350] (entry 7), 1,1-dibromonona-tetraene was isolated as the unique reaction compound.

Regarding the observed instability of the polyene RBM4-50-(Br) during iodine-promoted double bond isomerization[131], we chose to address our efforts to the synthesis of the target polyene-Cer, thus postponing the isomerization of the C10-C11 double bond to a later step of the synthetic sequence.

3.2.4.4 Synthesis of 5-hexen-1-ynyltrimethylsilane 9

According to the above retrosynthetic analysis (Scheme 3.2.3), 5-hexen-1-ynyltrimethylsilane **9** was required for the CM coupling. The preparation of this building block has been reported by various authors[337–339]. Amongst the different approaches, we chose that of Peterson *et al.*[337], which involved the two-step process shown in Figure 3.2.27. First, 2-chloro-1,5-hexadiene was prepared by coupling of allylmagnesium bromide with 2,3-dichloropropene, and subsequent elimination under Neumann conditions[352] to provide compound **9** (Figure 3.2.27). Nonetheless, we decided to rule out this procedure due to the low yield (30%) of the intermediate 2-chloro-1,5-hexadiene and the large amount of byproducts observed in the elimination step.

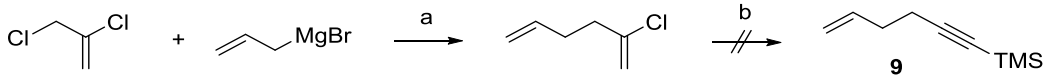

Figure 3.2.27 Synthesis of 5-hexen-1-ynyltrimethylsilane **9**. Reagents and conditions: (a) THF, -10ºC, 3h, 30%; (b) $(CH_3)_3SiCl$, BuLi (2.5 M hexane), Et_2O, -78ºC, 16h.

Taking into account the tedious and long alternative synthetic routes described in the literature for this compound[337–339], we tried the synthesis of **9** by the direct, albeit unreported, nucleophilic alkynylation of 4-bromo-1-butene with ethynyltrimethylsilane (Table 3.2.5).

In an attempt to find suitable conditions for the alkynylation reaction, we carried out a systematic survey of the reaction parameters, as shown in Table 3.2.5. The conversion rate was monitored by gas chromatography / mass spectrometry (GC/MS) and NMR.

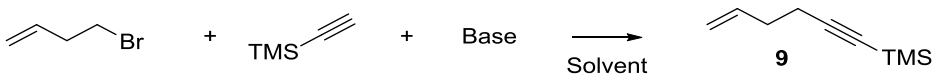

Table 3.2.5 Synthesis of 5-hexen-1-ynyltrimethylsilane **9**

Entry	Base [a]	Solvent	Additive (% vol)	Yield(%) [b]
1	LDA	THF		---
2	LDA	Et_2O		---
3	BuLi	THF		---
4	BuLi	THF	HMPA (50)	60
5	BuLi	Et_2O	HMPA (50)	60

[a] 1.2–2.5 eq/mol relative to ethynyltrimethylsilane.
[b] Isolated yield after distillation.

Based on the optimized conditions for the nucleophilic addition of an alkyne to Garner's aldehyde, described in section 3.2.3.4, we were prompted to generate the lithiated acetylide of ethynyltrimethylsilane using LDA as a base (entries 1 and 2). However, the starting 4-bromo-1-butene was totally recovered under these conditions. Moreover, when BuLi was employed as a base (entry 3), decomposition products were obtained. However, by adding HMPA (50 % of total volume) to the reaction mixture and using BuLi as a base[353], the desired 5-hexen-1-ynyl-trimethylsilane **9** was isolated in 60% yield (entries 4 and 5). In addition, the use of Et_2O as solvent resulted more suitable for the isolation of the volatile **9** by distillation (entry 5).

3.2.4.5 Synthesis of the allylic alcohol RBM4-55

In light of the difficulties associated with the observed instability of the conjugated pentaene system, we were encouraged to develop an alternative protection strategy for the amino diol moiety, which required mild basic conditions in the final deprotection step. For this purpose, the allylic alcohol RBM4-55 (Figure 3.2.28) bearing a *tert*-butyldimethylsilyl (TBS) and a fluorenylmethoxycarbonyl (Fmoc) as protecting groups was considered. The base-sensitive *O*-TBS and *N*-Fmoc protecting groups would enable a simultaneous or an orthogonal deprotection, depending on the conditions employed.

In this section, we describe two synthetic routes to the allylic alcohol RBM4-55.

Route I

The alcohol RBM4-55 was synthesized from L-serine through the intermediary aldehyde RBM4-54, following a similar strategy to that already optimized for allylic alcohol **6**[179,278] (Section 3.2.2.3), as shown in Figure 3.2.28.

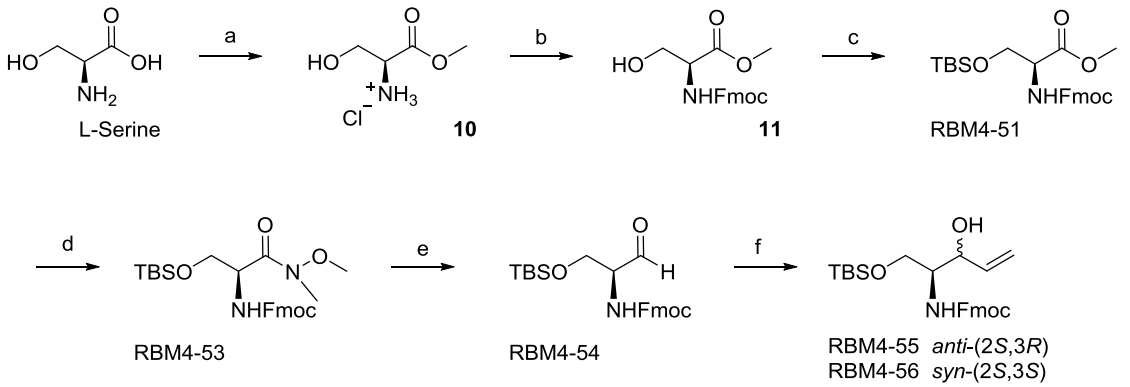

Figure 3.2.28 Synthesis of RBM4-55. Reagents and conditions: (a) $ClCOCH_3$, MeOH, 0º C to reflux, 16h, quantitative; (b) FmocCl, K_2CO_3, H_2O:dioxane, 0º C, 4h, 74%; (c) TBSCl, imidazole, DCM, 0º C to RT, 3h, 94%; (d) NH(OMe)Me·HCl, $AlMe_3$, DCM, 0ºC to reflux, 16h, 93%; (e) $LiAlH_4$, THF, -40º C, 2.5h, 90%; (f) $CH_2CHMgBr$, THF, -78º C, 60% (*anti/syn* = 1:1).

Formation of methyl serinate **10**[179], followed by *N*-Fmoc (**11**)[354,355] and *O*-TBS protection led to RBM4-51 in excellent yield over three steps. Next, the protected ester was readily converted into the Weinreb amide RBM4-53[356,357], which was next reduced to the corresponding aldehyde RBM4-54 in the presence of $LiAlH_4$ at low temperature[358]. Introduction of the vinyl group by means of the corresponding Grignard reagent provided the desired allylic alcohol RBM4-55 as an *anti*/*syn* = 1:1 mixture of diastereomers in 60% yield.

The absolute configuration of the resulting diastereomers, together with the quantification of the *anti*/*syn* ratio, was carried out by derivatization with (*R*) and (*S*)-α-methoxyphenylacetic acid (MPA), following the methodology of Riguera[359] (see Section 5.2.2).

Route II

In order to improve the diastereoselective formation of the allylic alcohol RBM4-55, the above route was modified from the Weinreb amide RBM4-53, as shown in Figure 3.2.29.

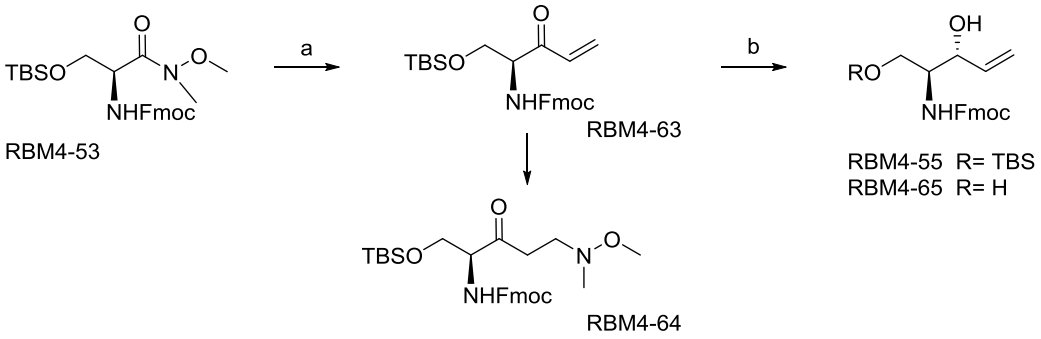

Figure 3.2.29 Optimization of the synthesis of RBM4-55. Reagents and conditions: (a) $CH_2CHMgBr$, THF, 0° C, 30 min, 83%; (b) $LiAl(^tOBu)_3H$, EtOH, -78 °C, 30min, 50% of RBM4-55 (*anti*/*syn* = 20:1) and 45% of RBM4-65 (only *anti*).

According to literature reports[258], the addition of vinyl magnesium bromide to Weinreb amide should provide the corresponding vinyl ketone RBM4-63 (Figure 3.2.29). However, when the reaction mixture was quenched at 0ºC by dropwise addition of 2M HCl or by addition of saturated aqueous NH_4Cl solution, the β-aminoketone RBM4-64 was isolated instead. The formation of RBM4-64 was rationalized by Gomtsyan and coworkers[360] as the result of a Michael addition of the liberated *N,O*-dimethyl hydroxylamine to the initially formed vinyl ketone RBM4-63. This adduct could be avoided by a modification of the reaction workup, namely by a dropwise addition of the reaction mixture into an equal volume of 1 M HCl at 0°C[361]. Using these conditions, the desired vinyl ketone RBM4-63 was obtained in good yield.

The vinyl ketone was next subjected to the *anti*-selective reduction[258,362] with lithium tri-*tert*-butoxyaluminohydride in distilled EtOH at -78 ºC, providing the allylic alcohol RBM4-55 as an *anti*/*syn* = 20:1 diastereomeric mixture, along with the partially TBS-deprotected RBM4-65 (Figure 3.2.29).

3.2.4.6 Synthesis of sphingoid-alkynes from the allylic alcohol 6

*Cross-metathesis between alcohol **6** and alkene **9***

With compound 5-hexen-1-ynyltrimethylsilane **9** in hand, its CM with vinyl alcohol **6**[278] was examined (Figure 3.2.30). This transformation was first carried out in DCM using an excess of **9** (3-4 equiv/mol relative to **6**) in the presence of 5% mol of Grubbs' 2nd generation catalyst[250] (see Section 3.2.2). Nonetheless, the conversion proved fruitless, recovering mainly the starting material in all the attempts.

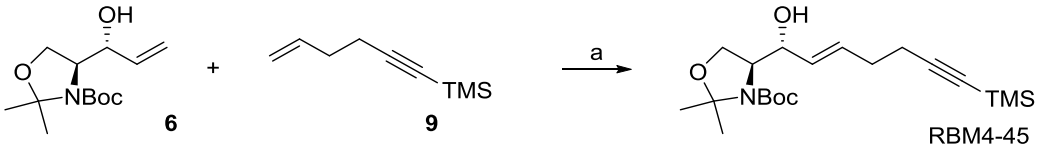

Figure 3.2.30 Synthesis of RBM4-45. Reagents and conditions: (a) Grubbs' 2nd generation catalyst, DCM, 45 ºC, 5h.

When the volatile 5-hexen-1-ynyltrimethylsilane **9** was used as a limiting reagent and coupled with an excess of **6** (2.5 eq/mol), we observed the formation of the desired olefin RBM4-45. However, even after careful chromatographic separations, the desired compound was always contaminated with the excess starting allylic alcohol **6**. At this point, we decided not to devote additional efforts to the purification of RBM4-45 with the hope that the excess **6** would be more easily removed along the subsequent reaction steps.

Noteworthy, compound RBM4-45 was obtained in excellent (*E*)-selectivity, since no (*Z*)-isomer was observed by ^{1}H-NMR in the crude reaction mixture. The presence of the *trans* double bond at C4-C5 was unambiguously confirmed by the large ^{1}H NMR coupling constant (> 15 Hz) between H4 and H5 protons.

Deprotection and N-acylation

Once obtained RBM4-45, the synthesis of the Negishi cross-coupling precursors RBM4-47 and RBM4-48 (Figure 3.2.31) was attempted. For this goal, the crude RBM4-45 was first subjected to desilylation using tetrabutylammonium fluoride (TBAF)[363], furnishing the terminal alkyne RBM4-46 in 40% yield over the two reaction steps. At this point, the excess alcohol **6** was totally removed after careful chromatographic purification of the crude desilylation mixture.

We then examined the simultaneous removal of both the isopropylidene and Boc protecting groups by *in situ* generated HCl, as described in section 3.2.3.6. The reaction proceeded smoothly, and the desired aminodiol RBM4-47 was isolated in quantitative yield and good purity without further purification.

The aminodiol RBM4-47 was *N*-acylated with palmitic acid to provide the ceramide precursor RBM4-48 in 70% yield. Both RBM4-47 and RBM4-48 are versatile building blocks for Negishi cross-coupling reactions with bromopolyene RBM4-50, as detailed in the section 3.2.4.8.

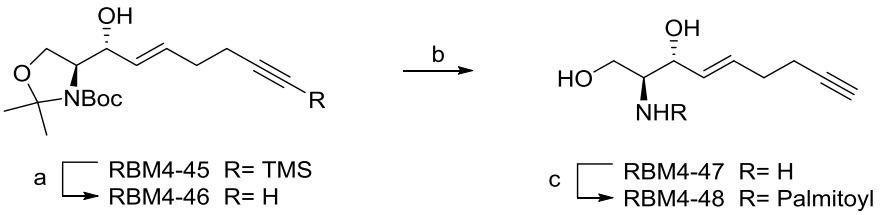

Figure 3.2.31 Synthesis of RBM4-47 and RBM4-48. Reagents and conditions: (a) TBAF, THF, RT, 1h, 40% from allylic alcohol **6**; (b) CH_3COCl (5%vol), MeOH, RT, 1.5 h, quantitatively; (c) Palmitic acid, HOBt, EDC, Et_3N, DCM, RT, 1h, 70%.

3.2.4.7 Synthesis of sphingoid-alkynes from the allylic alcohol RBM4-55

In order to evaluate the influence of the amino and/or hydroxyl functionalization in the Negishi cross—coupling reaction, we considered of interest the preparation of alternative precursors in addition to those reported in the above section.

*Cross-metathesis between allylic alcohol RBM4-55 and alkene **9***

Cross-metathesis between the allyl alcohol RBM4-55 and 5-hexen-1-ynyltrimethylsilane **9** was initially carried out based on the optimized conditions outlined in section 3.2.4.6. However, the use of 5% mol of Grubbs' 2nd generation catalyst proved inefficient since unreacted starting olefins were mainly recovered. Gratifyingly, by increasing the amount of catalyst from 5 to 20% mol, the desired olefin RBM4-57 was obtained in 50% yield (Figure 3.2.32).

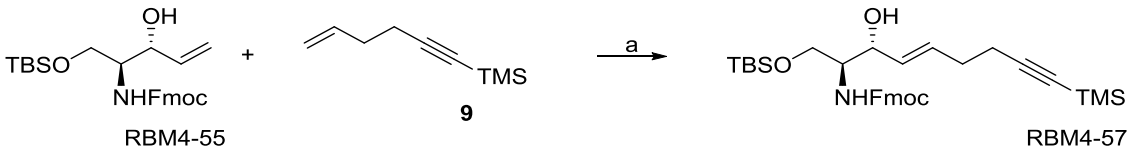

Figure 3.2.32 Synthesis of RBM4-57. Reagents and conditions: (a) Grubbs' 2nd generation catalyst, DCM, 45 ºC, 5h, 50%.

Deprotection and N-acylation

Once obtained RBM4-57, we focused our attention on the sphingoid precursors RBM4-58, RBM4-48 and RBM4-61, as Negishi cross-coupling substrates (Figure 3.2.33).

The amino alcohol RBM4-58 was easily reached in good yield from RBM4-57 by selective TMS removal with $AgNO_3$/2,6-lutidine[364,365].

The versatility of RBM4-57 encouraged us to selectively remove the Fmoc group with piperidine[355,366], to give the amine RBM4-67 with excellent conversion (Figure 3.2.33). Subsequent *N*-acylation of RBM4-67 with palmitic acid and EDC/HOBt as coupling reagents, afforded RBM4-68. The simultaneous TBS and TMS silyl deprotection was carried out with TBAF as a source of fluoride ions. This sequence furnished the same ceramide precursor RBM4-48, already described in section 3.2.4.6.

The selective alkyne desilylation mentioned above ($AgNO_3$/2,6-lutidine), was also applied to RBM4-68, to give the RBM4-69, which was used without further purification to give RBM4-61 in 55% yield over the two steps (Figure 3.2.33).

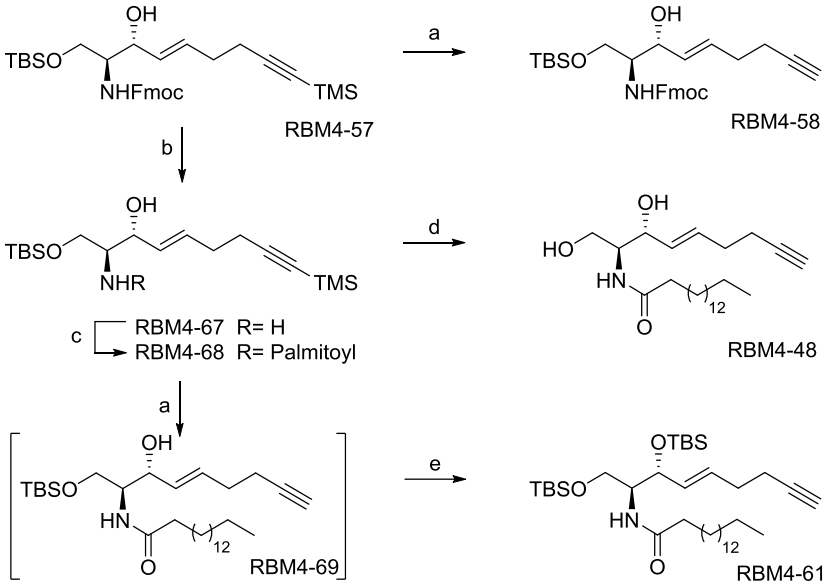

Figure 3.2.33 Synthesis of Negishi cross-coupling precursors RBM4-48, RBM4-58, RBM4-61. Reagents and conditions: (a) $AgNO_3$ 2,6-lutidine, THF, H_2O, EtOH, RT, 4h, 80%; (b) piperidine, THF, RT, 2h, 90%; (c) Palmitic acid, HOBt, EDC, Et_3N, DCM, RT, 3h, 70%; (d) TBAF, THF, RT, 1h, 85%; (e) TBSCl, imidazole, DCM, 0 ºC to RT, 3h, 65% over two steps.

Noteworthy, attempts to obtain RBM4-47 from RBM4-57 by the simultaneous removal of the Fmoc[367] and silyl groups with TBAF were hampered by the isolation of crude reaction mixtures in which the target amino diol was apparently contaminated with remaining TBAF and related by-products.

3.2.4.8 Pd-catalysed cross–coupling

Optimization of the Negishi cross-coupling reaction

As outlined in the retrosynthetic analysis (Scheme 3.2.3), the construction of the sp^2-sp^2 C9-C10 bond was planned based on a modified Negishi-type coupling. In preliminary assays designed to optimize the reaction conditions, the coupling between the bromotetraene RBM4-50 and the commercial *N*-(4-pentynyl)-phthalimide as alkyne partner was studied in some detail (Table 3.2.6).

In agreement with the methodology of Hu and co-workers[368], the model alkyne *N*-(4-pentynyl)-phthalimide was subjected to hydrozirconation using Schwartz reagent to form the corresponding vinylzirconocene. The zirconate intermediate was then transmetalated with strictly anhydrous $ZnCl_2$ to afford the corresponding vinylzinc species, which was used directly in the coupling step with freshly prepared polyene bromide RBM4-50 in the presence of $Pd(Ph_3P)_4$ (see introduction Figure 3.2.24).

In consideration with the results summarized in Table 3.2.6, two optimal conditions were devised:

1) When anhydrous THF was used as solvent, 0.6 mmol of alkyne and 0.3 mmol of the vinyl bromide RBM4-50 were required (entry 3). Attempts to reduce the reaction scale (entry 5) or to reverse the stoichiometry (entry 4) proved fruitless. Furthermore, the *in situ* generation of $Pd(Ph_3P)_4$ by reduction of $PdCl_2(Ph_3P)_2$[335] resulted in the recovery of the starting materials (entry 2).

2) When anhydrous DCM was used as solvent, the insolubility of $ZnCl_2$ in this solvent hampered the transmetalation step, despite the intermediate vinylzirconocene was generated (as evidenced by the isolation of the corresponding alkene *N*-(4-pentenyl)-phthalimide) (entry 6). For this reason, $ZnCl_2$ was incorporated in the reaction as a THF solution. Under these conditions, the polyene **12** was obtained in 50% yield (entry 7). Based on this result, a fine tuning of the reaction stoichiometry (entries 8-11) led to the conditions shown in entry 9 as the most suitable ones for the Negishi cross-coupling of this model reaction in DCM.

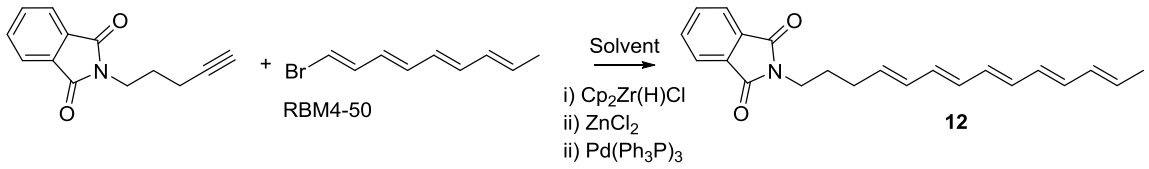

Table 3.2.6 Negishi cross-coupling between *N*-(4-pentynyl)-phthalimide and RBM4-50

Entry	Solvent	eq/mol Alkyne	eq/mol RBM4-50 (mmol)	eq/mol $Cp_2Zr(H)Cl$	eq/mol $ZnCl_2$ (THF)	Yield(%) [a]
1	THF	2	1 (0.1)	3	3	---
2	THF	1	1.05 (0.1)[b]	1.1	1	---
3	THF	2	1 (0.3)	3	3	50
4	THF	1	2 (0.3)	2	2	---
5	THF	2	1 (0.05)	3	3	---
6	DCM	2	1 (0.3)	3	3[c]	---
7	DCM	2	1 (0.3)	3	3	50
8	DCM	1	2 (0.6)	3	3	---
9	DCM	1.5	1 (0.3)	2.25	2.25	50
10	DCM	1.5	1 (0.05)	2.25	2.25	---
11	DCM	1.1	1 (0.3)	2.25	2.25	---

[a] Isolated yield after chromatography

[b] *In situ* generated Pd(0).

[c] Solution of $ZnCl_2$ in DCM

Attempts of Negishi cross-coupling to obtain sphingoid adducts

With the optimal conditions in hand, we evaluated the reactivity of the above sphingoid-derived alkynes with the freshly prepared polyene bromide RBM4-50 (Figure 3.2.34).

Nevertheless, application of the optimized conditions in THF (Table 3.2.6, entry 3) to the all above terminal alkynes, the reaction failed to afford the expected vinylzirconocene intermediate, as evidenced by the recovery of unreacted starting materials, probably due to the low solubility in THF.

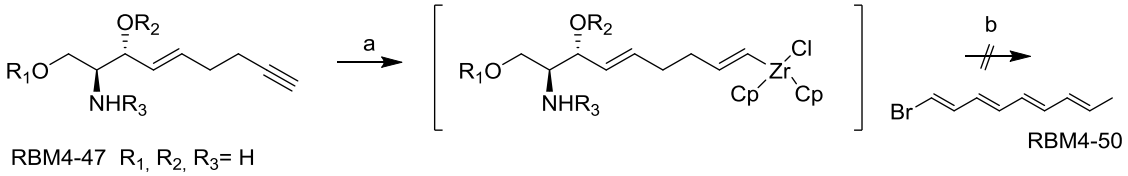

RBM4-47 R_1, R_2, R_3= H
RBM4-48 R_1, R_2= H, R_3= Palmitoyl
RBM4-58 R_1= TBS, R_2= H, R_3= Fmoc
RBM4-61 R_1, R_2= TBS, R_3= Palmitoyl

Figure 3.2.34 Negishi cross-coupling between sphingoid-derived alkynes and RBM4-50. Reagents and conditions: (a) $Cp_2Zr(H)Cl$, THF or DCM, 0ºC to RT, 1-3h; (b) i) $ZnCl_2$, THF, RT, 15-30 min; ii) RBM4-50, $Pd(Ph_3P)_4$, DCM, RT, 4-16h.

The use of DCM (Table 3.2.6, entry 9) led to the formation of the corresponding intermediate vinylzirconocenes, as evidenced by the recovery of the terminal alkenes. However, subsequent transmetalation with $ZnCl_2$ (in THF) and coupling with RBM4-50, in the presence of $Pd(Ph_3P)_4$, proved fruitless both at room and at reflux temperature (Figure 3.2.34).

In light of the above results and taking into account the apparent sensitivity of the process to the reaction scale, additional experimentation is required to improve this interesting coupling.

3.2.5 Hydrozirconation approach

3.2.5.1 Introduction and scope

Hydrozirconation

The hydrozirconation of alkynes and alkenes with Schwartz reagent, $Cp_2Zr(H)Cl$, affords organozirconocene (IV) complexes[331] as versatile scaffolds for a range of organic reactions (Figure 3.2.35).

The $Cp_2Zr(H)Cl$ complex was first synthesised in 1969 by Wailes and coworkers[369,370] and used directly in reactions with alkenes[371] and alkynes[372]. Subsequently, Schwartz and coworkers extended the scope of the reaction by addition of inorganic electrophiles or by transmetalation[373–375]. Because of these contributions, $Cp_2Zr(H)Cl$ is commonly referred to as “Schwartz reagent”.

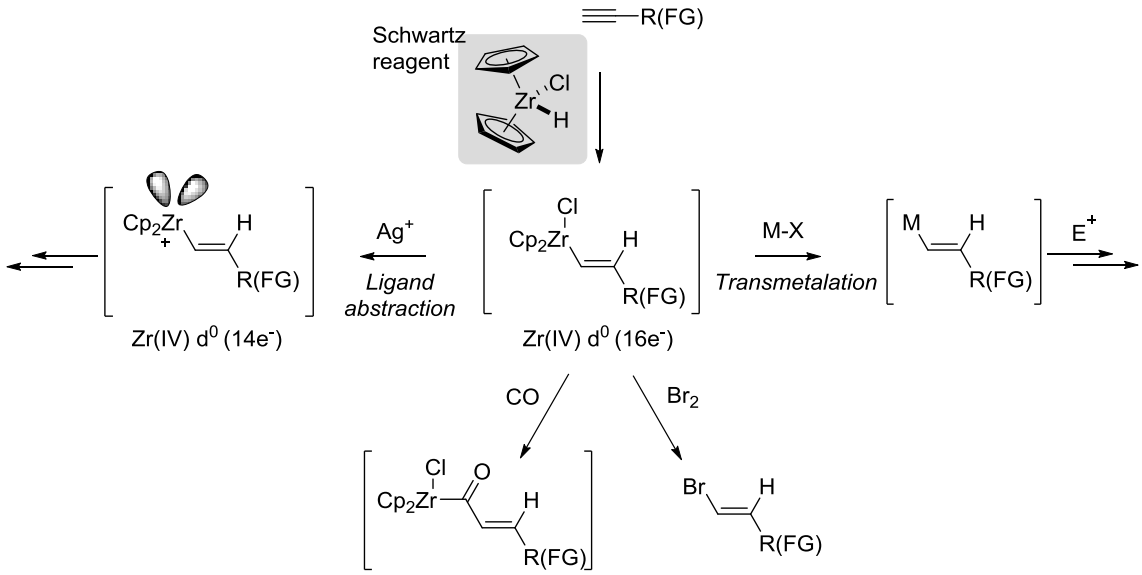

Figure 3.2.35 Summary of organozirconocene reactions. FG: functional group. Image taken from Wipf et al.[376]

The Schwartz reagent is considered as a weak nucleophile due to the steric shielding at the metal atom exerted by the two cyclopentadienyl (Cp) ligands. However, activation of the C—Zr bond by addition of metal salts, by ligand substitution or abstraction, favours the formation of bridged bimetallic complexes[377]. In addition, small electrophiles can also be directly added to the C—Zr bond (Figure 3.2.35)[378,379].

Generally, alkynes are more reactive than alkenes towards hydrozirconation. In addition, the reactions show higher regioselectivity and broader compatibility with different functional groups (FG)[379–381]. For these reasons, this section will focus on the hydrozirconation of alkynes and its applications to the synthesis of SLs.

Synthesis of sphingolipids by hydrozirconation

The hydrozirconation reductive coupling is a suitable synthetic approach to obtain the allylic alcohol framework present in some SLs backbone (Figure 1.1)[377,379,382–385]. Unlike the nucleophilic alkynylation method mentioned in section 3.2.3, hydrozirconation affords the allylic alcohol framework in just one step, avoiding the additional reduction step required in the nucleophilic alkynylation for the conversion of the initially formed propargylic alcohol into an allylic alcohol of (*E*)-configuration.

Basically, the new C—C bond is formed by cross-coupling between an aldehyde (electrophile) and the corresponding vinylzirconocene intermediate (nucleophile) arising from a starting alkyne. Most of the syntheses of Sphs described in the literature, employ Garner's aldehyde as a conformationally restricted α-nitrogen-substituted aldehyde[239], which represents a good substrate for probing the stereochemical outcome of the hydrozirconation reaction[377,379,382–384].

The stereoselectivity of the hydrozirconation of aldehydes can also be explained on the basis of the Felkin-Ahn and the Cram's chelation models already discussed in section 3.2.3.1 and Figure 3.2.16, Figure 3.2.17.

The stereoselectivity observed in the hydrozirconation of aldehydes has been shown to be rather reagent dependent, since both chelated and non-chelated processes can occur simultaneously[279,377]. In this context, Coleman and coworkers suggested an alternative transition state to explain the *si*-side attack. This is described as a coordinated delivery of the nucleophile, where the reagent precomplexes with the carbamate carbonyl, and is thereby delivered to the opposite face of the aldehyde carbonyl to afford *syn*-configuration[279] (Figure 3.2.36).

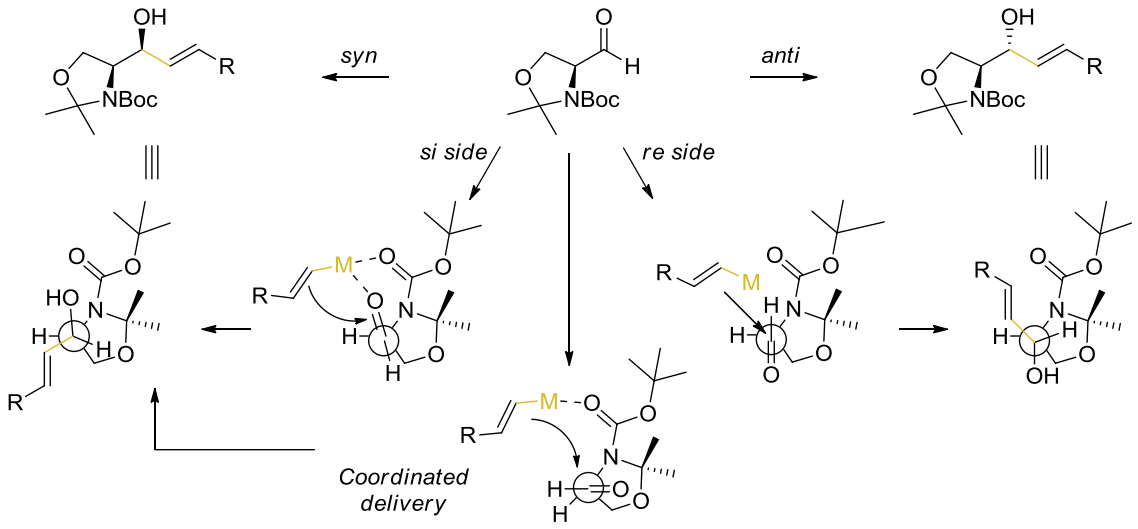

Figure 3.2.36 Stereochemical outcome of the cross-coupling between a vinylzirconocene and Garner's aldehyde. Image adapted from Passiniemi *et al.*[240] and Coleman *et al*[279].

Despite the addition of alkenylzirconocenes to aldehydes is sluggish, the reaction can be accelerated either by transmetalation to an alkenylzinc reagent or by addition of a catalyst to afford, in all cases, the corresponding (*E*)-allylic alcohols.

Carbonyl activation by addition of $ZnBr_2$ or $ZnCl_2$[386] has been applied in the syntheses of Sphs[377], gangliosides HLG-2[383], the α-glucosidase inhibitor (+)-valienamine[382] and spisulosines[385]. On the other hand, transmetalation of an alkenylzirconocene to an alkenylzinc intermediate can be achieved with dialkylzinc reagents (Me_2Zn or Et_2Zn), which have been used in the syntheses of Sphs[377], spisulosines[385] or deoxygalactono-jirimycines[387]. The stereoselectivity reported in these works shows that the addition of alkenylzirconocene-zinc reagents is strongly dependent on the solvent employed, the conformation of the aldehyde, but also on the stoichiometry of Zn.

In order to increase the electrophilicity of the aldehydes, Ag(I) salts can be added to activate the carbonyl group, improving its reactivity against of vinylzirconocenes. Some of the salts commonly used are $AgAsF_6$[388] and $AgClO_4$[389], the latter being a catalyst tested in the synthesis of spisulosines[385]. However, this procedure affords lower stereoselectivity in the cross-coupling process compared with transmetalation or the coordination with Zn additives.

3.2.5.2 Retrosynthetic analysis

An alternative synthetic strategy for our target *erythro*-polyene-Cer was based on the use of a hydrozirconation reaction as the key step (Scheme 3.2.4). Access to the C3-C5 (*E*)-allylic alcohol framework would be enabled by using the same building blocks from the nucleophilic alkynylation approach (see section 3.2.3.2). The chiral and conformationally constrained Garner's aldehyde will determine the C2 configuration, whereas the alkyne RBM4-17 will be the precursor of the (*all-E*)-polyene system. We expected to cross-couple the vinylzirconocene intermediate arising from RBM4-17 with Garner's aldehyde[242] to afford the (*E*)-allylic alcohol moiety in one synthetic step, thus avoiding the additional reduction of the triple bond to an (*E*)-olefin. Based on mechanistic considerations, the new C3 stereocenter thus generated would present the proper configuration to provide the required *erythro* (*anti*)-backbone. Finally, despite the expected instability of the polyene moiety, a final deprotection step under the same mild acidic conditions reported in section 3.2.3.6 and also in the literature[109,172,390,391] will be attempted. Finally, *N*-acylation with different carboxylic acids would afford the desired *erythro*-polyene-Cers.

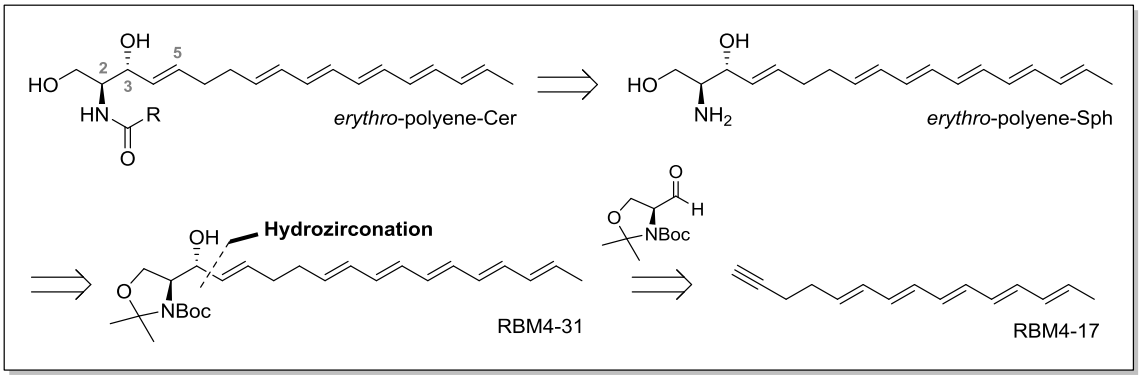

Scheme 3.2.4 Retrosynthetic analysis for *erythro*-polyene-Cer.

Polyene systems were expected to be compatible with hydrozirconation conditions, as reported in the literature. Thus, homologation of conjugated double bonds by hydrozirconation was described by Maeta and coworkers[390] using $AgClO_4$ as catalyst to afford a conjugated hexaene system. Based on this procedure, Díaz and coworkers[391] synthesised a carbazolyl–oxazolone system with nine conjugated double bonds. In addition, construction of polyunsaturated chains by Zr-Zn transmetalation has been applied to the preparation of manumycin A antibiotics[392,393]. Moreover, a double

addition of palladium and zinc to a zirconium intermediate has been described in the synthesis of (*all-E*)-oligoenes, providing seven conjugated double bonds[335].

3.2.5.3 Synthesis of a *erythro*-polyene ceramide from Garner's aldehyde

Cross-coupling between Garner's aldehyde and polyene alkyne RBM4-17

Initial attempts to evaluate the compatibility of the hydrozirconation reaction towards polyene systems were carried out using the triene alkyne RBM4-24 (see preparation in section 3.2.3.3) and Garner's aldehyde[242] as models. According to Murakami and coworkers[377,384], treatment of Garner's aldehyde with a 1-alkenylzirconocene chloride in the presence of $ZnBr_2$ in THF[386], provides the natural *erythro* (*anti*) configuration in high diastereoselectivity. Nonetheless, in our hands, no cross-coupling between RBM4-24 and Garner's aldehyde took place under these conditions. Further attempts changing several reaction conditions, such as solvent (DCM)[387], the use of *in situ* generated Schwartz reagent[394], or $ZnBr_2$ stoichiometry (0.4, 1, 2 eq/mol), were also unsuccessful.

In consideration of the above results, we were prompted to use a silver salt as catalyst, in accordance with the procedure of Maeta and coworkers[389,390], albeit a drop in the diastereselectivity was expected under these conditions [377,388]. Thus, hydrozirconation of the alkyne RBM4-24 in DCM, followed by addition of the aldehyde and $AgClO_4$ (20% mol), afforded readily the desired cross-coupled product RBM4-27 in 50% yield (*anti*/*syn* = 1:1) (Figure 3.2.37). The ratio *anti*/*syn* was assigned by comparison of the NMR data with those of the protected isopropylidene-Boc *erythro*- and *threo* Sph, previously synthesised in our group following Herold's methodology[285].

Stimulated by this result, we next focused our attention on the coupling of the pentaene alkyne RBM4-17 with Garner's aldehyde. Uneventfully, the silver-catalysed hydrozirconation in DCM afforded the desired coupled compound RBM4-31 (Figure 3.2.37). However, the target compound was isolated after silica gel chromatography in a modest 20% yield and as an inseparable mixture of diastereomers. The ^{1}H-NMR of RBM4-31 showed a similar pattern to that of RBM4-27, with an estimated *anti*/*syn* ~ 1:1 ratio. The complexity of the pentaene system made difficult the complete assignment of the mixture. However, in light of the presumed instability of the conjugated pentaene system, we used the above mixture in the next synthetic step. Moreover, when the hydrozirconation reaction was scaled-up (from 0.3 to 1.0 mmol), the resulting coupling

adduct showed an apparent deterioration of the polyene system, thus restricting the optimum scale of the process.

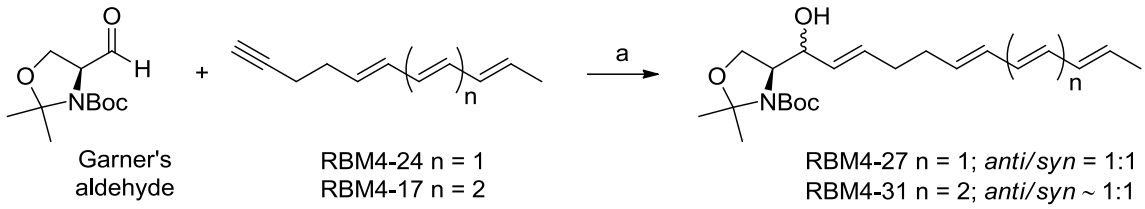

Figure 3.2.37 Synthesis of RBM4-27 and RBM4-31. Reagents and conditions: (a) $Cp_2Zr(H)Cl$, $AgClO_4$, DCM, 0 ºC to RT, 40 min. RBM4-27: 50%; RBM4-31: 20%.

Isopropylidene and N-Boc deprotection

With the required coupled products RBM4-27 and RBM4-31 in hand, we examined the simultaneous removal of the isopropylidene and Boc groups to obtain the corresponding polyene-Sphs. According to the results obtained in section 3.2.3.6 and to reported deprotections of polyene systems under acidic conditions[109,172,390,391], we were prompted to use HCl, despite the apparent sensitivity of conjugated double bonds to strong acids.

Taking into account all these considerations, we first planned to deprotect the model compound RBM4-27 by the *in situ* generation of HCl by the addition of acetyl chloride (3% vol) to a methanolic solution of the starting material[319] (Figure 3.2.38). Gratifyingly, the reaction afforded the desired 2-amino-1,3-diol (hydrochloride) RBM4-29 without further purification. Prompted by this result, we attempted the deprotection of RBM4-31 following the same methodology. Unfortunately, the conjugated pentaene system proved unstable under the acidic conditions, giving rise to a range of byproducts. Therefore, this route was disregarded for the synthesis of the polyene RBM4-11.

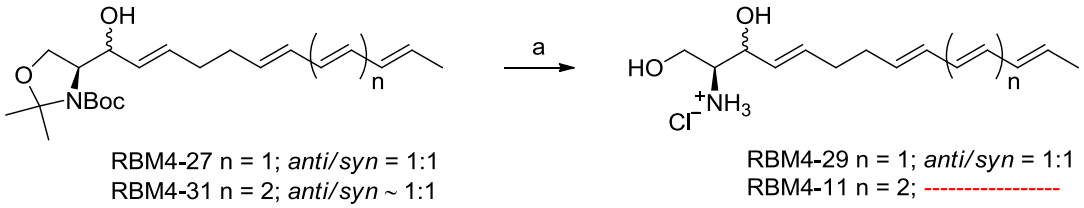

Figure 3.2.38 Deprotection conditions: (a) CH_3COCl (3%vol), MeOH, RT, 1h. RBM4-29: quantitative; RBM4-11: byproducts were isolated.

3.2.5.4 Synthesis of an *erythro*-polyene ceramide from aldehyde RBM4-54

Cross-coupling between aldehyde RBM4-54 and the polyene alkyne RBM4-17

Based on the previous synthetic strategy and with the aim of avoiding the final acidic deprotection step, we planned an alternative approach starting from aldehyde RBM4-54 (see preparation in section 3.2.4.5). Aldehyde RBM4-54 is a serinal derivative with an *O*-TBS and a *N*-Fmoc, two orthogonal protecting groups that can be deprotected under non acidic conditions.

Hydrozirconation of the pentaene alkyne RBM4-17 with Schwartz reagent in DCM, followed by addition of RBM4-54 and $AgClO_4$ (20% mol) as catalyst, afforded the desired sphingoid base RBM4-59 as a mixture of diastereomers in 20% yield (Figure 3.2.39). This yield was comparable to that obtained from the Garner's aldehyde approach (see section 3.2.5.3).

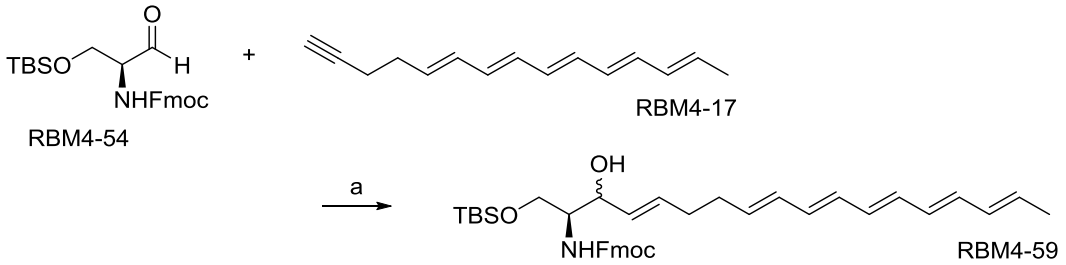

Figure 3.2.39 Synthesis of RBM4-59. Reagents and conditions: (a) $Cp_2Zr(H)Cl$, $AgClO_4$, DCM, 0 ºC to RT, 40 min, 20%, mixture of diastereomers.

Diastereoselectivity of the cross-coupling between RBM4-54 and RBM4-17

Since the configuration of the starting enantiopure aldehyde RBM4-54 is known (2*S*), the stereoselectivity of the process can be inferred by determination of the absolute configuration at C3 of any of the diastereomers formed. Because of the instability of the conjugated pentaene system, we decided to study the stereochemical outcome of the reaction by using a model system. In this context, the above hydrozirconation conditions were applied to the condensation of 1-tetradecyne with aldehyde RBM4-54 (Figure 3.2.40, a). Following the standard methodology, the resulting cross-coupled product **13** was isolated in 50% yield as a mixture of diastereomers, which were separated after careful chromatographic purification.

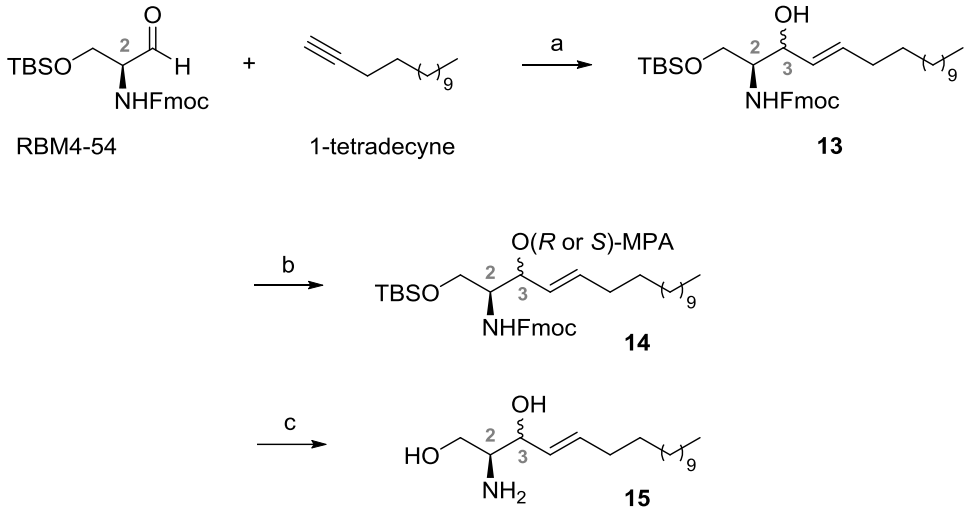

Figure 3.2.40 Assignment of the absolute configuration at C3 from the diastereomeric mixture of isomers **13**. Reagents and conditions: (a) $Cp_2Zr(H)Cl$, $AgClO_4$, DCM, 0 ºC to RT, 40 min, 50%, (*anti*/*syn* = 1:4); (b) (*R*)(-)-MPA or (*S*)(+)-MPA, EDC, DMAP, DCM, 0 ºC to RT, 12h; (c) TBAF, THF, RT, 1.5h.

Derivatization of the less polar, major diastereomer of compound **13** with (*R*)-MPA and (*S*)-MPA (Figure 3.2.40, b), following the methodology of Riguera[359], allowed the assignment of the absolute configuration of the secondary alcohol as 3*S* (Table 3.2.7) (see also Section 5.2.2). Thus, we can conclude that compound **13** was obtained as an *anti*/*syn* = 1:4 diastereomeric mixture.

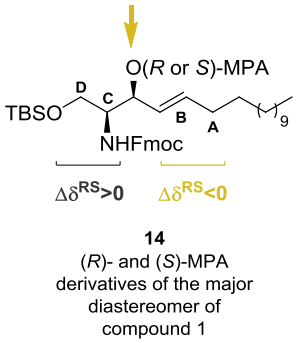

14
(*R*)- and (*S*)-MPA derivatives of the major diastereomer of compound 1

Table 3.2.7 $\Delta\delta^{RS}$ values from 1H-NMR spectra for the major diastereomer derivatized.

	δH_A	δH_B	δH_C	δH_D
R-MPA	1.88	5.54	3.85	3.52
S-MPA	2.01	5.80	3.79	3.22
$\Delta\delta^{RS}$	-0.13	-0.26	0.06	0.30

The reported Ag catalysed condensations between Garner's aldehyde and the corresponding vinylzirconocenes from 1-pentadecyne[377] or 1-hexadecyne[388], led to *anti*/*syn* ≈ 1:1 mixtures. Our results indicate a higher *syn*-selectivity (*anti*/*syn* = 1:4) in the coupling of the less conformationally rigid aldehyde RBM4-54 with 1-(*E*)-tetradecenyl-zirconocene.

To unambiguously confirm the diastereoselective course of the hydrozirconation coupling between RBM4-54 and 1-tetradecyne, the major diastereomer was fully deprotected (Figure 3.2.40, c) to afford a diastereomerically pure Sph **15**. Its NMR data (in CD_3OD), differed from those of a *erythro*-Sph, obtained following a diastereoselective route[285,286] (Table 3.2.8). Thus, the major diastereomer of the hydrozirconation reaction of RBM4-54 is in agreement with a *syn*-configuration, this confirming the above ratio *anti*/*syn* = 1:4.

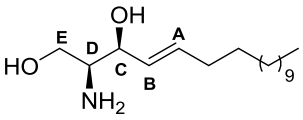

Sph **15**

Table 3.2.8 δ(ppm) values from ^{1}H and ^{13}C-NMR spectrum (CD_3OD) of Sph **15**.

	δH_A	δH_B	δH_C	δH_D	δH_E
erythro-Sph	5.49	5.77	4.06	2.88	3.63
Sph **15**	5.45	5.85	4.11	3.03	3.66
	δC_A	δC_B	δC_C	δC_D	δC_E
erythro-Sph	130.1	135.7	73.9	58.2	62.9
Sph **15**	129.7	137.0	71.0	59.0	60.1

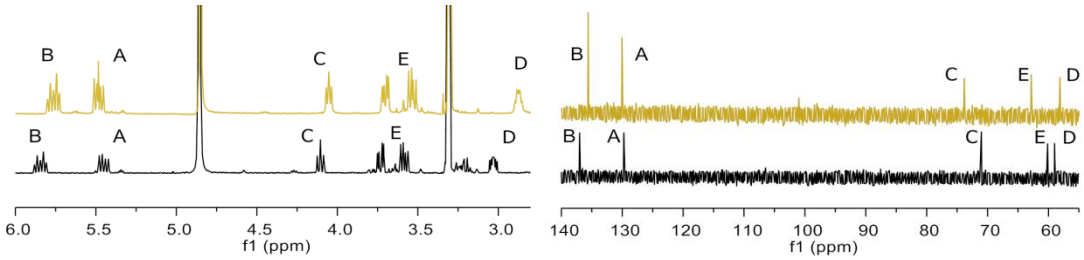

Comparison of the above RMN data with those of crude RBM4-59 (Figure 3.2.39), allowed us to determine a diastereoselectivity *anti*/*syn* = 1:2.3, taking the integration of the diastereotopic C1 protons as diagnostic signals.

Optimization of the diastereoselectivity of the hydrozirconation coupling

We next based our efforts on the search of optimal conditions to increase the *anti* diastereoselectivity in the hydrozirconation coupling with aldehyde RBM4-54. Mechanistically, our goal was to favour a non-chelating transition state to improve the *anti*-selectivity, as mentioned in the introduction (see Section 3.2.5.1). Nonetheless, we needed to slightly modify Murakami's methodology in consideration of the unsuccessful attempts described in section 3.2.5.3, in which the use of $ZnBr_2$ proved fruitless.

The reaction with 1-(*E*)-tetradecenyl-zirconocene chloride (A) (Table 3.2.9), obtained from 1-tetradecyne following standard protocols, with aldehyde RBM4-54 was first considered under a diversity of reaction conditions, as summarized in Table 3.2.9.

We first examined the reaction scope by changing the zinc source from $ZnBr_2$ to $ZnCl_2$, following the protocol of Murakami[377] and Zheng[386], and taking into account the related Negishi's procedure[323]. Although using THF as solvent impressively reversed the stereochemical reaction outcome, favouring the *anti*-diastereomer (entry 1), the yields were very low and numerous side products were obtained. Moreover, despite reducing the amount of $ZnCl_2$ [377] from 50 to 25% mol (entry 2), no increase in the diastereoselectivity or yield were observed in THF.

In order to improve the reactivity, we tried to increase the electrophilicity of aldehyde RBM4-54 by activating the carbonyl group with $ZnCl_2$, prior to the addition to intermediate (A). However, the reaction failed in THF (entry 3). Interestingly, by changing the solvent to DCM, an *anti*/*syn* = 1:1.5 mixture of diastereomers was obtained in 30% yield (entry 4). Although the major *syn*-configuration still prevailed, an enriched fraction with an *anti*/*syn* = 1:1 ratio could be isolated by silica gel chromatography. Despite this experiment was designed to mimic a Felkin-anh transition state model, the selectivity apparently followed a chelation control. This is probably due to DCM, which has been reported to be prone to give chelated adducts as intermediates[240,377,387].

To completely evaluate the stereochemical outcome of the hydrozirconation reaction with the aldehyde RBM4-54, we finally tested the transmetalation conditions (entry 5). Thus, the zirconium intermediate (A) was transmetalated to the corresponding zinc species by treatment with Et_2Zn at – 40 ºC. After addition of the aldehyde RBM4-54 in DCM, at – 40 ºC, compound **13** was obtained as an *anti*/*syn* = 1:2.5 mixture of diastereomers in an overall 25% yield. In agreement with the literature[377,385,387], the transmetalation pathway favoured the *syn*-selectivity.

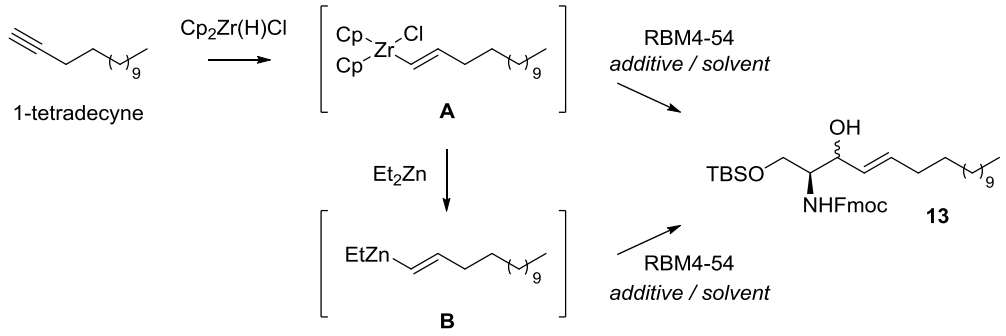

Table 3.2.9 Addition of 1-(*E*)-tetradecenyl-metal to RMB4-54 aldehyde

Entry	Alquenyl [a]	Additive (%mol) [b]	Solvent	Yield of 13 (%) [c]	*anti/syn* [d]
1	A	$ZnCl_2$ (50)	THF	6	2:1
2	A	$ZnCl_2$ (25)	THF	6	2:1
3	A	$ZnCl_2$ (50)	THF	-----*	
4	A	$ZnCl_2$ (50)	DCM	30*	1:1.5
5	B		DCM	25**	1:2.5

[a] 1.1–1.5 eq/mol relative. to RBM4-54.
[b] Relative to RBM4-54.
[c] Isolated yield after chromatography.
[d] Ratio determined by ^{1}H NMR.

* Aldehyde previously activated with $ZnCl_2$.
** Conditions: - 40 ºC.
.

In light of the above results, we considered the use of $ZnCl_2$ as additive in DCM (entry 4) as the most suitable conditions to obtain the desired *anti* diastereomer. These conditions were applied to the reductive coupling between polyene alkyne RBM4-17 and aldehyde RBM4-54, as outlined in Figure 3.2.41.

In this case, the polyene RBM4-59 was isolated as an *anti*/*syn* = 1:1.5 mixture of diastereoisomers in 20% yield. As expected for a polyene compound, the reaction yield was slightly lower than that obtained from 1-tetradecyne, albeit with a similar diastereoselectivity (Table 3.2.9, entry 4). Attempts to scale-up the reaction (from 0.3 to 1.2 mmol) resulted in the formation of a major byproduct with the same retention factor as RBM4-59, but showing a clear deterioration of the polyene system, as revealed by the ^{1}H-NMR spectrum. Therefore, as already observed with Garner's aldehyde (see section 3.2.5.3), the working scale of the hydrozirconation coupling of aldehydes with polyene systems is determinant to the success of the process.

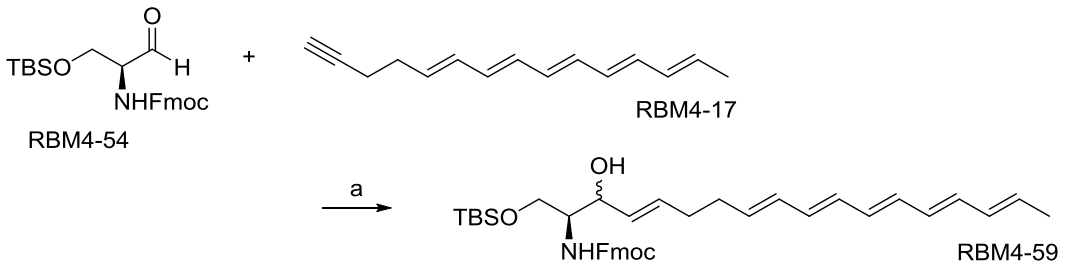

Figure 3.2.41 Synthesis of RBM4-59. Reagents and conditions: (a) $Cp_2Zr(H)Cl$, $ZnCl_2$, DCM, 0 ºC to RT, 40 min, 20%, (*anti/syn* = 1:1.5).

Deprotection and N-acylation

With the required coupled adduct RBM4-59 in hand, we then investigated the simultaneous deprotection of the TBS and Fmoc groups in order to obtain the corresponding polyene-Sph in one step. Neutral conditions for the cleavage of silyl ethers or carbamate bonds are desirable when dealing with sensitive substrates like polyene compounds. In this regard, a source of fluoride ion can be suitable for this pourpose. Commonly, the Fmoc group is susceptible of removal by weak bases, such as TBAF[367], and the progress of the reaction can be monitored by detection of the resulting dibenzofulvene intermediate by UV absorbance at 365 nm. Furthermore, TBS deprotection is also reported to take place in the presence of a source of fluoride ion[395–397].

These considerations prompted us to optimize the experimental conditions using the model compound **13** (Figure 3.2.42). In this case, two equiv/mol of a 1M TBAF solution in THF were required for the complete removal of both the TBS and Fmoc groups. However, the work-up procedure, consisting of an aqueous washing of the organic phase to eliminate the excess TBAF and its by-products, was incompatible with the highly water soluble nature of the resulting Sph. Thus, the protocol[398,399] was modified by neutralizing the crude reaction mixture with calcium carbonate, prior to the scavenging of the resulting Sph with an acidic ion-exchange resin (Amberlyst 15), followed by final treatment with 2M NH_4Cl in MeOH[400]. However, this procedure was unable to completely remove the excess TBAF and a subsequent chromatographic purification was still required.

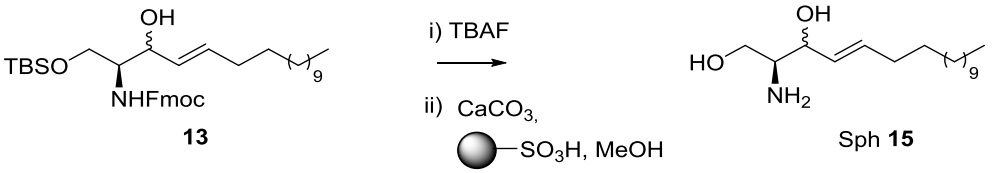

Figure 3.2.42 Simultaneous TBS and Fmoc deprotection. Reagents and conditions: i) TBAF, THF, RT, 90 min; ii) $CaCO_3$, Amberlyst 15, 2M NH_4Cl in MeOH, RT, 1h.

Since isolation of the putative amino diol sphingoid base was tedious and not feasible for polyene compounds, we decided to carry out an "one-pot" deprotection-acylation process in order to circumvent the above purification problems. In this way, the *N*-acylation with palmitic acid of the crude deprotection reaction of RBM4-59 would afford the desired polyene-Cer RBM4-60 (Figure 3.2.43).

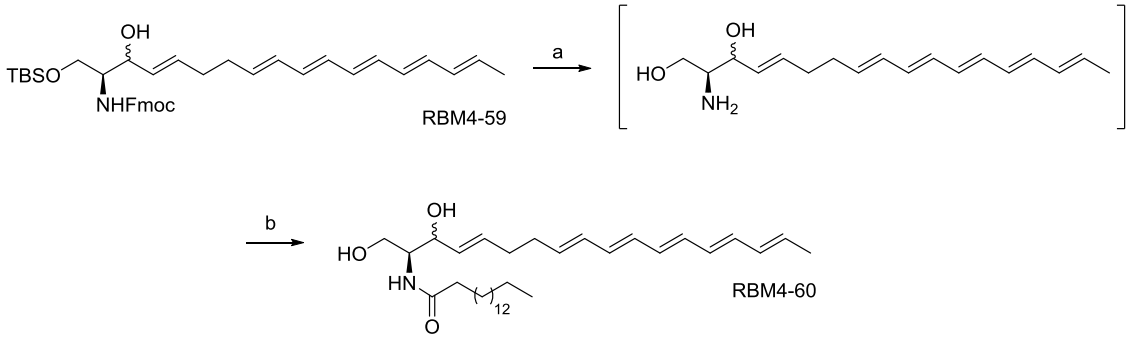

Figure 3.2.43 Synthesis of RBM4-60. Reagents and conditions: (a) TBAF (1M in THF), THF, RT, 90 min; (b) Palmitic acid, HOBt, EDC, Et_3N, DCM, RT, 90 min, low yield (*anti/syn* = 1:1.5).

In practice, treatment of RBM4-59 (*anti/syn* = 1:1.5) with TBAF (1.5 equivalents) was suitable to accomplish the simultaneous removal of both protecting groups. Subsequently, the crude reaction mixture was *N*-acylated with palmitic acid, in the presence of EDC-HOBt in DCM, to give polyene ceramide RBM4-60 after chromatographic purification (Figure 3.2.43). Since the chromatographic separation of the diastereomers was not possible at this stage, an *anti/syn* = 1:1.5 ratio was inferred for this diastereomeric mixture of polyene ceramides RBM4-60. Despite the limitations of the approach, this is the first time that a pentaene moiety has been introduced in the sphingoid base of a ceramide.

Further attempts to increase the diastereoselectivity and the overall yield of this hydrozirconation approach will be necessary to improve the efficiency of the process.

3.2.6 Summary & Conclusions

Cross-metathesis and Wittig olefination approach

- Triphenylphosphonium bomide salt RBM4-14 was obtained in three steps in 40% overall yield, starting from the allylic alcohol **6**, derived from Garner's aldehyde. A crucial step was the protection of compound **6** prior to the subsequent CM and salt formation (Figure 3.2.11 and Figure 3.2.12).
- The constrained bicyclic triphenylphosphonium bromide salt RBM4-15 was obtained from the allylic alcohol **6** in three steps in 40% overall yield (Figure 3.2.14).
- Suitable conditions for the preparation of triphenylphosphonium salt RBM4-14 required the use of neat PPh_3, whereas RBM4-15 was preferably formed using ACN as solvent (Table 3.2.3 and Figure 3.2.14).
- Despite we were able to isolate, albeit in low yield, the Wittig olefination adduct RBM4-10 (Table 3.2.2, entry 1), we were unable to optimize and not even reproduce this transformation.
- The Wittig olefination between salt RBM4-15 and polyene aldehyde RBM4-4 proved fruitless under a variety of reaction conditions (Figure 3.2.15).

Nucleophilic alkynylation approach

- A (*E*)-selective Wittig olefination between a (*all-E*)-polyene aldehyde and the triphenylphosphonium salt **8**, provided the model triene RBM4-24 (*Z*:*E*; 1:1) and the target pentaene RBM4-17 (*Z*:*E*; 1:2) alkynes in 55% and 80% yield, respectively (Figure 3.2.18).
- The (*all-E*)-pentaene alkyne RBM4-17 was isolated after isomerization with iodine and purification by prep-HPLC in 25% yield. Due to the instability of the alkyne group, RBM4-17 must be used directly and freshly prepared to next reaction.
- Lithitated RBM4-24 and RBM4-17 alkynes were generated using LDA as a base. Diastereomeric alkynylation to Garner's aldehyde under Felkin-Anh control,

afforded in 45% and 25% yield the *erythro*-RBM4-25 and *erythro*-RBM4-18, respectively, as a unique diastereomer (Table 3.2.3 and Figure 3.2.20).

- Either the triene RBM4-25 or the pentaene RBM4-18 compounds, resulted unstable under selective reduction of the propargylic alcohol framework to the corresponding (*E*)-allylic alcohol by diverse hydrides. Thus, rejecting nucleophilic alkynylation as a possible approach to obtain the *erythro*-polyene Sph and –Cer.

- Interestingly, the intermediate pentaenyne RBM4-18 proved to be a versatile scaffold to obtain the fluorescent aminodiol pentaenyne RBM4-19, by simultaneous removal of the protecting groups under mild acidic conditions (Figure 3.2.22).

Negishi cross-coupling approach

- Tetraene halide RBM4-50-(Br) has been synthesised as (*Z:E*) (1.5:1) mixture of isomers in the C1-C2 double bound, by one-carbon homologation of the aldehyde RBM4-2 applying Wittig olefination strategy. The polyene bromide RBM4-50 resulted more stable under Wittig olefination conditions than under Takai's (see Table 3.2.4).

- The completion of synthon 5-hexen-1-ynyltrimethylsilane **9** was achieved by an unreported nucleophilic alkynylation of ethynyltrimethylsilane to the 4-bromo-1-butene in anhydrous Et_2O, in just one step. BuLi was used as a base, and 50% of HMPA (of total volume) was required to succeed (Table 3.2.5).

- Cross-metathesis between Garner's allylic alcohol and the 5-hexen-1-ynyltrimethylsilane **9** took place when the volatile compound 1 was used as a limiting reagent with 5% mol Grubbs' 2nd generation catalyst, providing the coupled product RBM4-45 with excellent (*E*)-selectivity, albeit an excess of Garner's allylic alcohol was required (Figure 3.2.30). Totally deprotection and *N*-acylation of RBM4-45 proceeded smoothly, affording the Negishi precursors RBM4-47 and RBM4-48 (Figure 3.2.31).

- The unreported allylic alcohol RBM4-55 was synthesised as a diastereomeric mixture (*anti/syn;* 20:1) in six steps from L-serine in 50% overall yield (Figure 3.2.28 and Figure 3.2.29).

- When cross-metathesis was carried out between the allylic alcohol RBM4-55 and the synthon 5-hexen-1-ynyltrimethylsilane **9**, 20% mol of Grubbs' 2nd generation catalyst was required to succeed (Figure 3.2.32). The resulting RBM4-57 was subjected to diverse protecting strategies to afford versatile precursors to the Negishi cross-coupling (Figure 3.2.33).

- Two different synthetic approaches were devised for intermediate RBM4-48. The first one, after four reaction steps from Garner's allylic alcohol, *eryhtro*-RBM4-48 was isolated as a unique diastereomer in 28% yield (Figure 3.2.31). Similarly, starting from the alternative allylic alcohol RBM4-55 and subsequent four reaction steps, *eryhtro*-RBM4-48 was obtained in 27% (Figure 3.2.33).

- Initial attempts to optimize the Negishi cross-coupling conditions were devised using the polyene bromide RBM4-50 and the *N*-(4-pentynyl)-phthalimide as alkyne partner. Optimal conditions were set at around 0.6 mmol of alkyne and 0.3 mmol of vinyl halide RBM4-50 in THF (Table 3.2.6), and 0.45 mmol of alkyne and 0.3 mmol of polyene halide RBM4-50 (Table 3.2.3, entry 9) when DCM was used as solvent.

- Negishi cross-coupling in anydrous THF failed to afford the corresponding vinylzirconocenes intermediates. Gratifyingly, when DCM was used as solvent (Figure 3.2.34) the viniylzirconocenes of totally, partially or non-protected alkynes were generated, but next transmetalation and coupling to vinyl halide RBM4-50 proved fruitless, probably due to a limiting factor of the reaction scale.

- We decided to address our efforts to an alternative approach, aside from Negishi cross-coupling, due to both limiting factors: the CM step (sections 3.2.4.6 and 3.2.4.7), which demanded high amounts of allylic alcohol, and the Wittig olefination step which provided tetraene bromide RBM4-50 as mixture of (*Z*:*E*)-isomers (3.2.4.3), thus leading poor overall yield and selectivity to the synthesis.

Hydrozirconation approach

- Silver perchlorate catalysed hydrozirconation of triene and pentane alkynes RBM4-24 and RBM4-17 with Garner's aldehyde, in DCM, afforded the corresponding coupled (*E*)-allylic alcohols RBM4-27 and RBM4-31 as a 1:1 mixture of diastereomers (Figure 3.2.37).

- Unlike the triene compound RBM4-27, the simultaneous isopropylidene and *N*-Boc deprotection of the pentaene adduct RBM4-31 under mild acidic conditions resulted unpracticable, giving rise to a range of degradation byproducts (Figure 3.2.38).

- Silver perchlorate catalysed hydrozirconation of pentaene alkyne RBM4-17 with aldehyde RBM4-54, in DCM, provided the sphingoid framework RBM4-59 as a diastereomeric mixture in an *anti/syn* = 1:2.3 ratio (Figure 3.2.39).

- The configuration of RBM4-59 was inferred from that of the model reaction of aldehyde RBM4-54 with 1-tetradecyne, after derivatization as (*R*) and (*S*)-MPA esters (Figure 3.2.40, Table 5.2, Table 3.2.8).

- Presumably, coupling of vinylzirconocenes with less conformationally rigid aldehydes, such as RBM4-54 in comparison with Garner's aldehyde, might favour the observed *syn*-selectivity.

- The stereochemical outcome of the hydrozirconation of alkyne RBM4-17 with aldehyde RBM4-54 was evaluated. The best *anti*-selectivity and yield of RBM4-59 was achieved by adding $ZnCl_2$ as additive in DCM (*anti/syn* = 1:1.5 / 30% yield) (Table 3.2.9).

- Deprotection of pentaene RBM4-59 with TBAF and subsequent *N*-acylation with palmitic acid, afforded the new fluorescent polyene-Cer probe in an estimated *anti/syn* =1:2.3 ratio, albeit in low yield (Figure 3.2.43).

- The reaction scale of the hydrozirconation-coupling reaction with polyene systems and aldehydes turned out to be crucial for the outcome of the process.

- Generally, as the number of conjugated double bonds increased, the stability of the compound decreased.

4. GENERAL CONCLUSIONS

The most remarkable general conclusions of the present thesis are highlighted in this section. A detailed analysis of the conclusions derived from each of the topics presented in this dissertation is outlined at the end of the corresponding sections.

4.1 GABA-pentaene analogues as membrane probes

- Three GABA-pentaene probes have been synthesised as fluorescent ceramide analogues. These were obtained by esterification between a pentaene alcohol and different *N*-acyl GABA intermediates. Probe RBM4-35, containing a *N*-palmitoyl acyl chain, was taken as reference of maximum fluorescence intensity, whereas probes RBM4-39 and RBM4-42, containing the 16-DOXYL and 5-DOXYL free radicals, respectively, in the *N*-acyl chain were designed as fluorometric probes.

- Calorimetric and fluorescence quenching experiments suggested that the lipids under study orient themselves in lipid bilayers with their polar moieties located at the lipid−water interface, as amphipathic molecules.

- The nitroxide radical quenched intramolecularly the fluorescence of the conjugated pentaene group when they were in close proximity. Furthermore, no noticeable intermolecular quenching was observed upon release of the radical from the pentaene partner.

- The quenching of RBM4-39 showed higher dependency on the fluidity of the lipid bilayers in comparison with RBM4-42. Electron paramagnetic resonance measurements of the DOXYL-probes confirmed their sensitivity to the physical state of the bilayer. The ability of probes to detect membrane lipids in the gel phase becomes relevant in view of the novel evidences pointing at the existence of gel microdomains in cell membranes.

- Concerning the coexistence of lipid domains in different physical states, probe RBM4-35 may be particularly useful for the observation of highly-ordered bilayers by confocal microscopy, since its emission was higher in gel than in fluid domains, and in liquid-ordered than in liquid-disordered areas. In addition, RBM4-35 did not segregate from the other lipids in the way natural ceramide did, but rather mixed with them in a selective way according to the lipid phases involved.

4.2 Synthetic approaches to polyene sphingolipids analogues

- Synthetic protocols for the construction of novel conformationally constrained polyene Sph and Cer analogues were designed.
- The triene and pentaene acetylenes RBM4-24 and RBM4-17, respectively, were found to be versatile synthons for the preparation of SLs analogues by means of nucleophilic alkynylations or hydrozirconation reactions.
- The nucleophilic alkynylation approach, based on the addition of lithium polyene acetylides to Garner's aldehyde, gave access to the unreported *anti*-polyenyne Sph, RBM4-26 (triene) and RBM4-19 (pentaene) as a single diastereomers.
- Despite the polyenye systems could be deprotected under acidic conditions, these conditions were not suitable for the deprotection of polyene compounds.
- The unreported serinal *N*-Fmoc *O*-TBS derivatives (aldehyde RBM4-54 and allylic alcohol (2*R*, 3*S*)-RBM4-55) represent alternative building blocks that require mild basic conditions for their deprotection.
- The stereochemical outcome of the hydrozirconation of alkyne RBM4-17 with aldehyde RBM4-54 was evaluated. When $AgClO_4$ was used as catalyst, the unnatural *threo* configuration was favoured (*anti/syn* 1:4). Nevertheless, addition of $ZnCl_2$ afforded an *anti/syn* mixture of RBM4-59 diastereomers in 1:1.5 ratio.
- The novel pentaene-Cer analogue was obtained in an estimated *anti/syn* =1:1.5 ratio, by deprotection of pentaene RBM4-59 with TBAF and subsequent *N*-acylation with palmitic acid.

5. EXPERIMENTAL SECTION

5.1 Biophysical assays

5.1.1 Materials

Dioleoylphosphatidylcholine (DOPC), distearoylphosphatidylcholine (DSPC), egg phosphatidylcholine (ePC), dipalmitoylphosphatidylcholine (DPPC), egg sphingomyelin (eSM), and cholesterol (Chol) were purchased from Avanti Polar Lipids (Alabaster, AL). The lipophilic fluorescent probe DiO (3,3′-dioctadecyloxacarbocyanine perchlorate) was purchased from Molecular Probes (Eugene, OR). Stock solutions were prepared by dissolving pure lipids and (when required) DiO in chloroform/methanol (2:1 v/v) and stored at −20 °C. The pentaene fluorophores used in this work, due to their labile nature, were dissolved in THF (tetrahydrofuran) stabilized with BHT (butylated hydroxytoluene) and stored at −80 °C. GABA-pentaene compounds were constantly protected from the exposure to light. The buffer solution used in the biophysical studies was HEPES 50 mM, pH 7.4.

5.1.2 Lipid vesicles (liposomes)

5.1.2.1 Multilamellar vesicles (MLVs)

The desired amount of lipid was pipetted from the stock in organic solution into a glass test tube. The organic solvent was evaporated by putting the solution under a nitrogen gas flow. To completely remove any traces of organic solvent, the sample was introduced into a high vacuum desiccator for 2 hours. A dried lipid film at the bottom of the test tube was obtained. Then, the lipid was hydrated by pipetting the desired amount of HEPES buffer solution at a temperature above the lipid main phase transition temperature (65 ºC for DSPC, 45 ºC for all other samples) and shaken by vigorous vortexing for lipid detachment from the bottom of the test tube. The samples were then sonicated for 10 min in a bath sonicator at the same temperature.

5.1.2.2 Large unilamellar vesicles (LUVs)

The desired amount of lipid was pipetted from the stock in organic solution into a plastic eppendorf tube. The organic solvent was evaporated by putting the solution under a nitrogen gas flow. To completely remove any traces of organic solvent, the sample was introduced into a high vacuum desiccator for 2 hours. A dried lipid film at the bottom of the tube was obtained. The desired amount of HEPEs buffer solution, at

a temperature above that of the lipid with the highest main phase transition temperature (65 ºC for DSPC, 45 ºC for all other samples), was pipetted into the eppendorf tube at once. By vigourous vortexing the lipid film was detached from the bottom of the tube and a MLV suspension generated. In order to reduce the size and the amount of lamellas within the MLVs, the sample was subjected to 10 freeze-thaw cycles. In this sense, the sample tube was immersed in liquid nitrogen for 1 minute. Once frozen, the sample was transferred into a water bath for 5 min until total defreezing and sample equilibration at a temperature above that of the lipid with the highest main phase transition temperature. The sample was vortexed and the same procedure was repeated for 10 times. The vesicles were finally extruded by passing the sample 10 times through polycarbonate filters of 0.1 µm pore diameter (Nucleopore, Pleasanton, CA), in an extruder (Northern Lipids, Vancouver, Canada) with the help of a nitrogen gas flow (15-20 bars). By using a water bath, the extruder is maintained at a temperature above that of the lipid with the highest main phase transition temperature at every time.

Since some lipid might be lost within the polycarbonate filters while extruding, the final concentration was then determined in terms of lipid phosphorous by the Fiske assay (see next section). In addition, by dynamic light scattering (DLS) was determined the homogeneity of the diameter size of the vesicles in solution, namely its polydispersity. These measurements were carried out in a Nano-S Zetasizer (Malvern Instruments, UK) using standard acryl-cuvettes, typically measuring 1 ml of a 100 µM vesicle suspension in buffer at room temperature.

Phospholipid concentration determination (Fiske assay)

The assay consists of hydrolysing the phospholipids until the lipid phosphate group is free to interact with specific reagents that will colour the solution in a concentration-dependent manner.

A calibration curve, to determine the exact lipid sample concentration, was prepared by pipetting 0, 25, 50, 75 and 100 nmol phosphorous into duplicate separate test tubes from a 1 mM NaH_2PO_4 standard solution. The sample was then pipetted into separate tubes (at least triplicate) to contain approximately 50 nmol lipid phosphorous, which will be in the centre of the calibration curve. To each tube, 500 µl of a 60 % perchloric acid ($HClO_4$) were pipetted. The tubes were vigorously vortexed and introduced into a heating block at 205 ºC for 45 min. In this way phospholipid hydrolysis was achieved

leaving free inorganic phosphate. The tubes were then collected, cooled down to room temperature and thereafter the following solutions were pipetted:

- 4 ml of an ammonium heptamolybdate solution [$(NH_4)_6Mo_7O_{24}.4H_2O$]
- 500 µl of a 10 % ascorbic acid (added while vortexing)

The inorganic phosphate reacted with molybdate which subsequently reacted with the ascorbic acid giving a yellow-coloured solution. The tubes were introduced into a boiling water bath and left for 6 min. During that period, the solution colour was blue-shifted depending on the amount of phosphorous. Finally, tubes were cooled in water, and thereafter, the samples were measured at 812 nm in a Ultrospec 500 pro spectrophotometer from Amersham Biosciences (Piscataway, NJ, USA).

To obtain the sample phospholipid concentration, the standards absorbance is plotted against the phosphorous concentration and adjusted to a straight line. The slope of the curve and the sample absorbance are used to find out the sample concentration.

5.1.2.3 Giant unilamellar vesicles (GUVs)

GUVs were prepared following the electroformation method described previously[213], using a homemade chamber that allows direct visualization under the microscope. 3 µL of the desired stock solution were added to the surface of platinum electrodes and the solvent was removed under vacuum for 90 min. Electroformation was then performed using a wave generator (TG330 function generator; Thurlby Thandar Instruments, Huntingdon, UK). The buffer solution used for electroformation was first preheated above the lipid main phase transition temperature. The electric field and water bath are disconnected and vesicles left to equilibrate for 30 min. The chamber was finally mounted on top of the microscope and direct confocal fluorescence microscopy performed on vesicles attached to the platinum wire (see 5.1.5).

5.1.3 Fluorescence spectroscopy

5.1.3.1 Fluoerscence measurements in solution

Absorption and fluorescence spectra of probe solution, in different organic solvents, were registered in QuantaMaster 40 spectrofluorometer (Photon Technology International, Lawrenceville, NJ). The samples (0.9 µM) absorbed and emitted at λex =

353 nm, λem = 474 nm using a cutoff filter at 385 nm. The measurements were done under continuous stirring and at a constant temperature of 23 °C.

5.1.3.2 Molar extinction coefficient (*ε*)

The molar extinction coefficient (*ε*) of pentane probes in ethanol solution was calculated according to Lambert-Beer's law. For this purpose a range of solutions between 0.8 and 80 μM were prepared. The ethanol (absolute for analysis) was deoxygenated prior to use. Then, the maximum of absorbance was registered for each concentration at same wavelength. The background signal of the absorbance intensities was subtracted from a control solution without probe. The absorption measurements were registered in a SpectraMax M5 spectrophotometer using 1 cm path length quartz cuvette.

The maximum absorbance was plotted against the corresponding concentration and adjusted to a straight line. Since they behave proportionally, according to Lambert-Beer's law, the slope of the curve is the *ε* value of the probe in ethanol.

5.1.3.3 Fluorescence quantum yield measurements(Φ_F)

Absorption and fluorescence spectra were registered in a SpectraMax M5 spectrophotometer using 1 cm path length quartz cuvette. 9,10-Diphenylanthracene (9,10-DPA) was obtained from Sigma-Aldrich and used without further purification. Ethanol (absolute for analysis) was deoxygenated prior to use.

Fluorescence quantum yields were calculated using eq **5** below, where Φ_F^S and Φ_F^{ref} ref are the quantum yield of the sample and that of the standard (9,10-DPA[201] Φ_F^{ref} = 0.95), respectively. F_S and F_{ref} represent the area of fluorescent emission in units of photons; *η*s and *η*ref are the refractive indices of the solvent (ethanol[202] *η*=1.361). β_S and β_{ref} are the correction absorption factors, $\beta = 1 - 10^{-A}$ where A= absorbance. In order to minimize reabsorption effects, the solutions for quantum yield measurements were prepared such that the optical density was generally about A = 0.04 at λex = 346 nm, but was never higher than 0.05 for our 1 cm path length.

$$\Phi_F^S = \frac{F_s \cdot \beta_{ref} \cdot \eta_s^2}{F_{ref} \cdot \beta_s \cdot \eta_{ref}^2} \cdot \Phi_F^{ref} \qquad (\mathbf{5})$$

Due to 9-10-DPA has a similar spectra region of emission and excitation towards polyene samples, ensured that the standard absorb at the excitation wavelength of choice. Quantum yields calculated by this probes described in the literature. Quantum yields calculated by this method are reliable to ±10%.

5.1.3.4 Fluoerscence measurements in liposomes

Fluorescence measurements were performed in LUVs suspensions 0.3 mM in lipid with 0.3 mol % of the polyene probes using a QuantaMaster 40 spectrofluorometer (Photon Technology International, Lawrenceville, NJ). Excitation spectra were collected between 250 and 400 nm, emitting at 468 nm. Emission spectra were collected between 360 and 700 nm, exciting at 353 nm and using a 385 nm cutoff filter to minimize detection of dispersed light. In both cases excitation and emission slits were set to 8 nm and a step size of 1 nm and an integration time of 0.5 s were used. The measurements were done at a constant temperature of 23 ºC and under continuous stirring. Once the emission spectra were obtained, the background signal was subtracted with a control liposome without probe. Three independent experiments were done for each of the four lipid compositions used and the average and SD values were calculated.

For experiments involving *n*-DOXYL-probes, the quenching efficiency was calculated as follows:

$$\%\, Quenching = \left(1 - \frac{Area\ (n{-}DOXYL{-}probe)}{Area\ (RBM4{-}35)}\right) \times 100 \qquad \textbf{(6)}$$

When the quenching efficiency was calculated using the maximum intensity instead of the area the result did not change significantly.

5.1.4 Differential scanning calorimetry (DSC)

All measurements were performed in a VP-DSC high-sensitivity scanning microcalorimeter (MicroCal, Northampton, MA). MLVs to a final concentration of 1 mM were prepared as described above (5.1.2.1). Both the samples and buffer solutions (HEPES) were fully degassed before loading into the appropriate cell. Three heating scans were performed for each sample at 45 °C/h; after the first scan, successive ones always yielded superimposable thermograms. The final lipid concentration, determined by a lipid phosphorus assay (see 5.1.2.2), and data from the third scan were used to

obtain normalized thermograms. The data were processed using the software ORIGIN (MicroCal) provided with the calorimeter.

5.1.5 Fluorescence confocal and multiphoton microscopy

GUVs attached to the platinum electrodes were visualized under an inverted confocal microscope with a high-efficiency spectral detector (Leica TCS SP5; Leica Microsystems, Manheim, Germany) and a two-photon excitation mode (MaiTai HP DS laser; Spectra Physics,Mountain View, CA). A 63x water immersion, N.A. 1.2 objective was used, and the images were collected and analyzed with the LAS AF software.

DiO was excited at 488 nm using an argon laser and its emission was collected in the 500-600 nm channel with the pinhole set at 1 Airy unit. Polyene probes were excited using two-photon excitation mode at 706 nm, and their emission was collected in the 467−499 nm range with the pinhole completely opened. Control GUVs with only DiO were used to confirm that DiO emission did not significantly contribute to the signal observed on the polyene channel.

Two independent experiments were done for each sample, and within each experiment duplicates or triplicates of the samples were prepared. During visualization, several images were taken at different places of the platinum wire in order to ensure that the sample did not display significant heterogeneity.

In GUVs exhibiting lateral phase separation, detected through differential fluorescence intensities, the intensity ratios between the different domains were calculated measuring local intensities with the Leica LAS AF software.

5.1.6 Electron paramagnetic resonance (EPR)

The EPR measurements were carried out on an EPR/ESR Bruker EMX spectrometer, equipped with an X-band (~9 GHz) EMX X Premium microwave bridge, a 10″ ER073 magnet with a 12 KW ER083 source power and an ER4102ST standard cavity. The spectra were recorded in the following operating conditions: microwave power (MP) 20 mW, modulation amplitude of magnetic field (MA) 0.5 G, modulation frequency (MF) 100 kHz, time constant (TC) 20.48 ms, conversion time (CT) 100 ms, sweep time (ST) 102.40 s, field width (FS) 100 G, gain (RG) 5.02 × 104, and a resolution of 1024 points. Processing was carried out using Bruker WIN-EPR system (v 2.22 rev. 12) software.

The measurements were carried out at room temperature in a capillary quartz tube with 40−500 spectra accumulation. Samples from LUVs were prepared as described above (5.1.2.2) and transferred to a capillary quartz tube.

For experiments with LUVs containing RBM4-42 probe, where the nitroxide group slow tumbled, the a and b values in equation **2** (see 3.1.3.5) were: 5.4×10^{-10} and −1.36 for ePC and DOPC, 1.9×10^{-9} and 1.05 for DPPC and DSPC, respectively. These values corresponded to a Lorentzian line width of 3 G in the first case, and a line width of 8 G in the second group of compounds, for Brownian diffusion[226].

5.2 Synthesis and product characterisation

5.2.1 General remarks

All chemicals were purchased from commercial sources and used as received unless otherwise noted. Dry solvents were obtained by passing through an activated alumina column on a Solvent Purification System (SPS). Synthesis grade or HPLC–grade solvents were used for extractions and purifications. Anhydrous EtOH and Et_3N were prepared by distillation at atmospheric pressure over calcium hydride under N_2 atmosphere, and stored over 4Å molecular sieves and argon atmosphere. Molecular sieves were previously dried in a dry flask, heated to 120 ºC under high vacuum for 5 h, and refilled with argon.

All reactions were monitored by TLC analysis using ALUGRAM® SIL G/UV_{254} precoated aluminum sheets (0.2 mm-thickness) (Machery-Nagel). UV light was used as the visualizing agent, and a 5% (w/v) ethanolic solution of phosphomolybdic acid or as the developing agent. Flash column chromatography was carried out with the indicated solvents using flash-grade silica gel 60 Å (37-70 μm).Yields refer to chromatographically and spectroscopically pure compounds, unless otherwise stated.

NMR spectra were recorded at room temperature on a Varian Mercury 400 instrument. The chemical shifts (δ) are reported in parts per million (ppm) relative to the solvent signal, and coupling constants (J) are reported in Hertz (Hz). For $CDCl_3$/CD_3OD solvent mixtures, chemical shifts are expressed relative to the residual peak of CD_3OD. The following abbreviations are used to define the multiplicities in ^1H NMR spectra: s = singlet, d = doublet, t = triplet, q = quartet, dd = doublet of doublets, ddd = doublet of

doublet of doublets, m = multiplet, br = broad signal and app = apparent, or combinations of these descriptive names.

Specific optical rotations were recorded on a digital Perkin-Elmer 34 polarimeter at 25 ºC in 1-dm 1-mL cell, using a sodium light lamp (λ=589 nm). Specific optical rotations values ($[\alpha]_D$) are expressed in 10^{-1} deg cm^3 g^{-1}, and concentrations (*c*) are reported in g/100 mL of solvent.

High Resolution Mass Spectrometry analyses were recorded on an Acquity UPLC system coupled to a LCT Premier orthogonal accelerated time-of-flight mass spectrometer (Waters) using electrospray ionization (ESI) technique. Data were acquired in positive ESI. Samples were analysed by FIA (Flow Injection Analysis), using ACN/water (70:30) as mobile phase. Samples were analysed using a 10 μL volume injection. *m/z* ratios are reported in atomic mass units.

Polyene compounds are sensitive to oxidation and strong acids. Storage should be in THF (stabilized with BHT, butylated hydroxytoluene) solution at mM concentrations under argon at —80 °C. Polyene systems should be constantly protected from bright light. Silica gel used to purify, by flash column chromatography, should be neutralized with Et_3N (1% vol, using hexane as solvent). Since commercial $CDCl_3$ often contain HCl, must be neutralised with an aqueous $NaHCO_3$ solution and dried over anhydrous $MgSO_4$, before use.

5.2.2 Synthesis and product characterisation

Decyl 4-((((9H-fluoren-9-yl)methoxy)carbonyl)amino)butanoate (2)

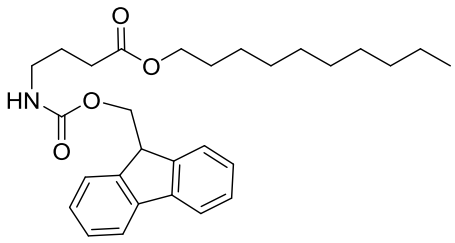

To a solution of EDC (25 mg, 0.13 mmol) and HOBt (13 mg, 0.1 mmol) in anhydrous DCM (3 mL) was added, dropwise, a solution of the commercial 4-(Fmoc-amino)butyric acid (30 mg, 0.09 mmol) in DCM (2 mL). After 10 min of stirring, this mixture was added at RT to a solution containing 1-decanol (16 μL, 0.08 mmol) and Et_3N (24 μL, 0.1 mmol) in DCM (10 mL). The mixture was vigorously stirred overnight and then

quenched with H_2O. The organic phase was extracted with 3 X 10 mL DCM, washed with brine, dried over $MgSO_4$ and concentrated under reduced pressure. The resulting crude was purified by flash column chromatography (hexane:EtOAc; 85:15) to give compound **2** as a white solid in 65% yield.

Rf: 0.66 (hexane:EtOAc; 7:3)

^{1}H NMR ($CDCl_3$) δ 7.76 (dt, *J* = 7.5, 1.0 Hz, 2H), 7.59 (ddd, *J* = 7.5, 2.0, 1.0 Hz, 2H), 7.40 (tdd, *J* = 7.5, 1.0, 0.5 Hz, 2H), 7.31 (td, *J* = 7.5, 1.0 Hz, 2H), 4.90 (m, 1H), 4.40 (d, *J* = 7.0 Hz, 2H), 4.21 (t, *J* = 7.0 Hz, 1H), 4.07 (t, *J* = 7.0 Hz, 2H), 3.25 (dd, *J* = 13.0, 6.5 Hz, 2H), 2.35 (t, *J* = 7.0 Hz, 2H), 1.89 – 1.80 (m, 2H), 1.66 – 1.57 (m, 2H), 1.37 – 1.22 (m, 14H), 0.88 (t, *J* = 7.0 Hz, 3H).

^{13}C NMR (**$CDCl_3$**) δ 173.5 (C), 156.6 (C), 144.1 (C), 141.4 (C), 141.3 (C), 127.8 (CH), 127.1 (CH), 125.1 (CH), 120.1 (CH), 66.7 (CH_2), 64.9 (CH_2), 47.4 (CH), 40.5 (CH_2), 32.2 (CH_2), 32.0 (CH_2), 29.7 (CH_2), 29.7 (CH_2), 29.6 (CH_2), 29.4 (CH_2), 28.7 (CH_2), 26.0 (CH_2), 25.3 (CH_2), 22.8 (CH_2), 14.2 (CH_3).

4-Methoxy-4-oxobutan-1-aminium chloride (3)

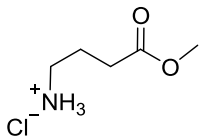

Acetyl chloride (4.1 mL, 58.2 mmol) was added dropwise over a cooled (0 ºC) solution of 4-aminobutyric acid (2 g, 19.4 mmol) in MeOH (20 mL). The reaction mixture was then stirred at reflux temperature for 16 h, cooled to RT and concentrated under reduce pressure to give a quantitative **3** as a white solid, which was used in the next step without purification.

Rf: 0.26 (DCM:MeOH; 9:1)

^{1}H NMR (CD_3OD): *δ* 3.70 (s, 3H), 3.00 (t, *J* = 7.5 Hz, 2H), 2.50 (t, *J* = 7.0 Hz, 2H), 2.01 – 1.91 (m, 2H).

^{13}C NMR (CD_3OD): *δ* 174.5 (C), 52.3 (CH_3), 40.1 (CH_2), 31.4 (CH_2), 23.7 (CH_2).

Methyl 4-palmitamidobutanoate (4)

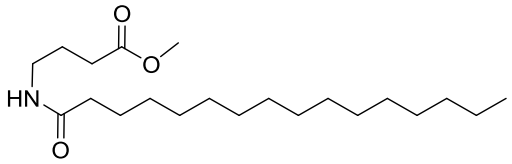

A solution of the palmitic acid (1.2 g, 4.7 mmol) in anhydrous DCM (20 mL) was added dropwise over a solution of EDC (1.3 g, 6.8 mmol) and HOBt (680 mg, 5.1 mmol) in DCM (30 mL). The mixture was allowed to react for 10 min and next added dropwise at RT over a solution of ester **3** (500 mg, 4.3 mmol) in DCM (50 mL) containing Et_3N (1.2 mL, 8.5 mmol). After 1h, the reaction mixture was quenched with H_2O (30 mL) and extracted with DCM (3 x 50 mL). The combined organic phases were washed with brine, dried and concentrated to give a residue. Flash-chromatography (DCM:MeOH; 96:4) afforded **4** as a white solid in 60% yield.

Rf: 0.81 (DCM:MeOH; 95:5)

^{1}H NMR ($CDCl_3$) δ 5.86 (s, 1H), 3.68 (s, 3H), 3.31 (dd, *J* = 12.5, 6.5 Hz, 2H), 2.38 (t, *J* = 7.0 Hz, 2H), 2.22 – 2.16 (m, 2H), 1.85 (p, *J* = 7.0 Hz, 2H), 1.67 – 1.57 (m, 2H), 1.33 – 1.23 (m, 24H), 0.88 (t, *J* = 7.0 Hz, 3H).

^{13}C NMR ($CDCl_3$) δ 174.1 (C), 173.8 (C), 51.9 (CH_3), 39.2 (CH_2), 39.2 (CH_2), 36.9 (CH_2), 36.8 (CH_2), 32.1 (CH_2), 31.7 (CH_2), 31.7 (CH_2), 29.9 (CH_2), 29.84 (CH_2), 29.83 (CH_2), 29.81 (CH_2), 29.77 (CH_2), 29.6 (CH_2), 29.51 (CH_2), 29.49 (CH_2), 29.44 (CH_2), 26.0 (CH_2), 24.72 (CH_2), 24.70 (CH_2), 22.8 (CH_2), 14.3 (CH_3).

4-Palmitamidobutanoic acid (5)

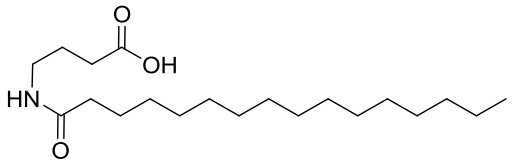

Lithium hydroxide (70 mg, 2.9 mmol) was added in one portion over a solution of compound **4** (265 mg, 0.7 mmol) in a mixture of THF (3.5 mL) and H_2O (1.5 mL) at RT. The resulting yellow reaction mixture was allowed to stir at RT for 1.5 h and next concentrated under reduced pressure to give a solid, which was taken up in H_2O and acidified to pH=3 by addition of 1*M* HCl aqueous solution. The acidic aqueous phase was extracted with EtOAc (3 x 5 mL) and the combined organic layers were dried and

concentrated to afford crude, which were purified by flash column chromatography (DCM:MeOH; 97:3) to give **5** as a white solid in 80% yield.

Rf = 0.28 (DCM:MeOH; 95:5).
^{1}H NMR ($CDCl_3$): δ 5.88 (s, 1H), 3.23 (dd, *J* = 12.5, 7.0 Hz, 2H), 2.34 (t, *J* = 7.0 Hz, 2H), 2.24 - 2.14 (m, 2H), 1.81 (p, *J* = 7.0 Hz, 2H), 1.62 (dt, *J* = 14.5, 7.0 Hz, 2H), 1.31 – 1.19 (m, 24H), 0.92 (t, *J* = 7.0 Hz, 3H).
^{13}C NMR (CD_3OD): δ 176.9 (C), 176.4 (C), 39.7 (CH_2), 37.1 (CH_2), 33.0 (CH_2), 32.2 (CH_2), 30.77 (CH_2), 30.75 (CH_2), 30.71 (CH_2), 30.6 (CH_2), 30.5 (CH_2), 30.4 (CH_2), 30.3 (CH_2), 27.0 (CH_2), 25.8 (CH_2), 23.7 (CH_2), 14.4 (CH_3).

***tert*-Butyl (*S*)-4-((*R*)-1-hydroxyallyl)-2,2-dimethyloxazolidine-3-carboxylate (6)**

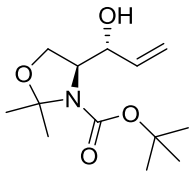

To a solution of Garner's aldehyde (5.0 g, 22 mmol) in anhydrous THF (70 mL) and under argon atmosphere was dropwise added a solution of vinylmagnesium bromide (40 mL, 1M in THF) at -78ºC. After the reaction mixture was vigorously stirred at -78ºC for 3 h, was quenched by addition of saturated aqueous NH_4Cl solution, and next allowed to warm to RT. The resulting suspension was taken up in water, and the aqueous phase was extracted with Et_2O (3 x 100 mL). The combined organic layers were dried over $MgSO_4$ and concentrated under reduced pressure. The reaction crude was carefully purified by flash column chromatography (hexane:EtOAc; 85:15) to isolate the (2*S*,3*R*)-compound **6** in 70% yield, from the (2*S*,3*S*)-diastereomer (minor). The physical and spectroscopic data of compound **6** were identical to those reported in the literature[401].

Rf: 0.42 (hexane:EtOAc; 7:3); **$[\alpha]_D$:** -22.0 (*c* 1.2, $CHCl_3$); **$[\alpha]_D$:** -23.8(*c* 1.0, $CHCl_3$) lit.[401]
^{1}H NMR ($CDCl_3$): δ 5.91 – 5.80 (m, 1H), 5.38 (d, *J* = 17.0 Hz, 1H), 5.22 (d, *J* = 10.5 Hz, 1H), 4.23 (m, 2H), 3.95 (m, 3H), 1.55 (s, 6H), 1.49 (s, 9H).

5-Iodo-1-pentyne

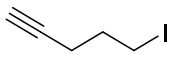

A solution of 4-pentyn-1-ol (2.5 g, 29.7 mmol) in DCM (30 mL) was added to a rapidly stirred suspension of triphenylphosphine (10.1 g, 38.9 mmol), imidazole (2.6 g, 38.6 mmol) and iodine (9.8 g, 38.6 mmol) in DCM (120 mL). After stirring for 1 h, the solvent was evaporated and the residue purified by flash column chromatography (hexane:EtOAc; 95:5) to give the iodide as an orange oil (60 %).

Rf: 0.86 (hexane:EtOAc; 9:1)
^{1}H NMR ($CDCl_3$): δ 3.44-3.11 (m, 2H), 2.33 (qt, J = 7.0, 3.0 Hz, 3H), 2.09 – 1.92 (m, 3H).
^{13}C NMR ($CDCl_3$): δ 82.2 (C), 69.5 (CH), 31.8 (CH_2), 19.4 (CH_2), 5.1 (CH_2).

Pent-4-yn-1-yltriphenylphosphonium iodide (8)

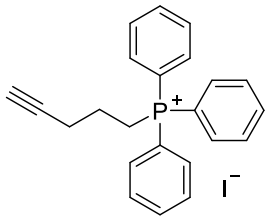

A mixture of 5-iodo-1-pentyne (2.7 g, 14.0 mmol) and triphenylphosphine (11 g, 42.0 mmol) was heated at 86 ºC for 16h under argon atmosphere. The wax mixture was cooled down to RT and then was added hexane (50 mL) affording a precipitate. The supernatant was discarded and the crude was concentrated under reduced pressure. The residue was purified by flash column chromatography (DCM:MeOH; 96:4) to give a yellowish solid (85%).

Rf: 0.72 (DCM:MeOH; 9:1)
^{1}H NMR ($CDCl_3$) δ 7.87 – 7.78 (m, 9H), 7.74 – 7.68 (m, 6H), 3.96 – 3.87 (m, 2H), 2.66 (ddd, J = 12.0, 6.5, 1.0 Hz, 2H), 2.01 (t, J = 3.0 Hz, 1H), 1.96 – 1.84 (m, 2H).
^{13}C NMR ($CDCl_3$) 135.2 ($J_{C\text{-}P}$ = 2.2 Hz, CH), 133.5 ($J_{C\text{-}P}$ = 9.8 Hz, CH), 130.5 ($J_{C\text{-}P}$ = 12 Hz, CH), 118.2 (C), 117.1 (C), 82.3 (C), 70.6 (CH), 21.8 ($J_{C\text{-}P}$ = 51.8 Hz, CH_2), 21.7 ($J_{C\text{-}P}$ = 2.3 Hz, CH_2), 19.2 ($J_{C\text{-}P}$ = 18.8 Hz, CH_2).

5-Hexen-1-yn-1-yltrimethylsilane (9)

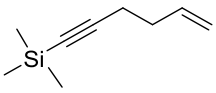

To a solution of ethynyltrimethylsilane (4 mL, 28.3 mmol) in anhydrous Et_2O (40 mL) was added 22 ml of dry HMPA. The mixture was cooled at 0ºC and then was added dropwise 21.2 mL of BuLi (1.6M in hexane, 34.0 mmol). The solution turned dark red immediately. After 30 min it was added 4-bromo-1-butene (3.4 mL, 34.0 mmol) at 0ºC. Stirring was continued for 6 h and the reaction mixture was extracted with HCl (1N) (2 x 10 mL). The organic layers were dried over $MgSO_4$ and distilled at 35ºC (Atm). The concentrated crude was purified by flash column chromatography with hexane to remove the byproduct bis(trimethylsilyl)acetylene and the desired product in hexane was next distilled at 65ºC (Atm) giving 5-hexen-1-yn-1-yltrimethylsilane (60% of yield). The reaction was also monitored by GC-MS. (carrier 1mL/min He, column ID-BPX5 30m x 0.25mm, gradient from 60ºC to 100 ºC at 3 ºC/min followed by a gradient from 100 ºC to 260 ºC at 20 ºC/min).

Rf: 0.66 (Hexane)

^{1}H NMR ($CDCl_3$): δ 5.93 – 5.78 (m, 1H), 5.07 (dq, J = 17.0, 1.5 Hz, 1H), 5.04 – 5.00 (m, 1H), 2.34 – 2.22 (m, 4H), 0.15 (s, 9H).

^{13}C NMR ($CDCl_3$): δ 137.0 (CH), 115.7 (CH_2), 106.8 (C), 85.0 (C), 33.0 (CH_2), 19.9 (CH_2), 0.3 (CH_3).

Analytical GC-MS for 9: carrier 1mL/min He, column ID-BPX5 30m x 0.25mm. Program: from 60 to 100 °C at 3 °C/min and then to 260 °C at 20 °C/min after an initial delay of 1 min. Retention time: 5.62 min. *m/z* $C_9H_{16}Si$ [M^-] Found: 151; Calculated: 152.10.

(*S*)-3-Hydroxy-1-methoxy-1-oxopropan-2-aminium chloride (10)

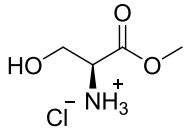

To a 200 mL of cold MeOH it was added 40.5 mL of acetyl chloride (571 mmol) at 0 ºC. The solution was stirred for 10 min, treated with commercially available L-Serine (20 g, 190.3 mmol) and heated to reflux for 16 h. The mixture reaction was next cooled to RT

and concentrated under reduced pressure. The desired product was obtained quantitatively as a white solid, which was used without further purification.

Rf: 0.24 (DCM:MeOH; 9:1) **$[\alpha]_D$** +4.1 (*c* 1, CH_3OH)
^{1}H NMR (CD_3OD): *δ* 8.53 (s, 2H), 4.12 (t, *J* = 4.0 Hz, 1H), 3.95 (qd, *J* = 12.0, 4.0 Hz, 2H), 3.81 (s, 3H).
^{13}C NMR (CD_3OD): *δ* 169.4 (C), 60.6 (CH_2), 56.1 (CH), 53.7 (CH).

(*S*)-Methyl 2-((((9H-fluoren-9-yl)methoxy)carbonyl)amino)-3-hydroxypropanoate (11)

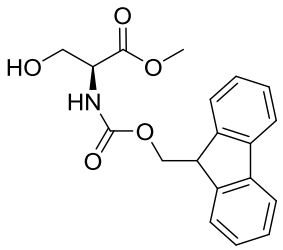

To a solution of (*S*)-methyl 2-amino-3-hydroxypropanoate hydrochloride (5 g, 32.1 mmol) in water (31mL) was added a solution of K_2CO_3 (9.7 g, 70.1 mmol) in a mixture of water (15.5 mL) and 1,4-dioxane (62 mL) at 0ºC. The reaction mixture was treated with fluorenylmethyloxycarbonyl chloride (7.6 g, 29.2 mmol) and stirred for 4 h at 0 ºC. Subsequently, it was diluted with 150 mL of water and extracted with Et_2O (3 x 100 ml). The combined organic layers were acidified to pH 2-3 with HCl (1N), extracted with EtOAc, dried and concentrated to give a residue. Purification by flash chromatography (DCM:MeOH; 96:4) gave 8.1 g (23.7mmol, 74%) of the desired product as a white solid.

Rf: 0.74 (DCM:MeOH; 9:1) **$[\alpha]_D$** +7.2 (*c* 1, $CHCl_3$)
^{1}H NMR ($CDCl_3$): *δ* 7.75 (d, *J* = 8.0 Hz, 2H), 7.59 (d, *J* = 6.0 Hz, 2H), 7.39 (tdd, *J* = 8.0, 2.0, 1.0 Hz, 2H), 7.31 (tt, *J* = 7.5, 1.5 Hz, 2H), 5.65 (d, *J* = 8.0 Hz, 1H), 4.51 – 4.35 (m, 3H), 4.22 (t, *J* = 7.0 Hz, 1H), 4.04 – 3.85 (m, 2H), 3.79 (s, 3H).
^{13}C NMR ($CDCl_3$): *δ* 171.2 (C), 156.4 (C), 143.9 (C), 143.8 (C), 141.4 (C), 141.4 (C), 127.8 (CH), 127.2 (CH), 127.2 (CH), 125.2 (CH), 120.1 (CH), 120.1 (CH), 67.3 (CH_2), 63.2 (CH_2), 56.1 (CH), 52.9 (CH_3), 47.2 (CH).

2-((5*E*,7*E*,9*E*,11*E*,13*E*)-pentadeca-5,7,9,11,13-pentaen-1-yl)isoindoline-1,3-dione (12)

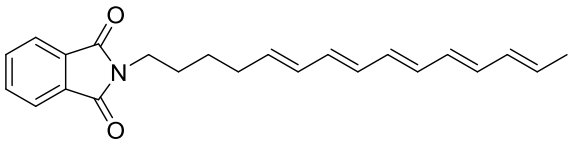

To a flame-dried Schlenk with a suspension of $Cp_2Zr(H)Cl$ (158 mg, 0.6 mmol) in DCM (0.6 mL), was added a solution of the alkyne *N*-(4-pentynyl)-phthalimide (93 mg, 0.4 mmol) in anhydrous DCM (1 mL), at 0 ºC under argon atmosphere and protected from light. During warming to room temperature, the zirconocene complex gradually dissolved to give a clear orange solution (60 min). To the mixture was added anhydrous $ZnCl_2$ (84 mg, 0.6 mmol, dried under vacuum for 1 h before use) dissolved in THF (2.4 mL). After stirring 15 min at RT, a solution of polyene bromide RBM4-50 (54 mg, 0.3 mmol), which was previously activated with $Pd(PPh_3)_4$ (16 mg, 0.05 mmol) for 10 min, was added. The resulting mixture was allowed to stir at RT for 4 h, while the reaction turned to dark-brown mixture, which was diluted with water and stirred for 10 min. Then, the mixture was extracted with DCM (3 x 5 mL), and the organic extracts were combined, dried over $MgSO_4$ and concentrated under reduced pressure. The crude product was purified by flash column chromatography on silica-gel neutralized (hexane:EtOAc; stepwise gradient from 0 to 8 % of AcOEt) to afford coupling product **12** in 50% yield as a yellow solid.

Rf: 0.56 (hexane:EtOAc; 8:2).

^{1}H NMR ($CDCl_3$): δ 7.84 (app. dd, J = 5.5, 3.0 Hz, 2H), 7.70 (app. dd, J = 5.5, 3.0 Hz, 2H), 6.28 – 6.01 (m, 8H), 5.78 – 5.58 (m, 2H), 3.71 – 3.66 (m, 2H), 2.19 – 2.11 (m, 2H), 1.78 (app. d, J = 6.0 Hz, 3H), 1.74 – 1.63 (m, 2H), 1.50 – 1.39 (m, 2H).

^{13}C NMR ($CDCl_3$): δ 168.6 (2 x C), 138.4 (C), 134.6 (CH), 134.0 (2 CH), 133.1 (CH), 132.8 (CH), 132.7 (CH), 132.5 (CH), 132.3 (CH), 132.1 (CH), 131.4 (CH), 131.3 (CH), 130.8 (CH), 130.1 (CH), 123.3 (2 CH), 38.0 (CH_2), 33.4 (CH_2), 28.2 (CH_2), 26.3 (CH_2), 18.5 (CH_3).

(9H-fluoren-9-yl)methyl ((2*S*,3*R*:*S*,*E*)-1-((*tert*-butyldimethylsilyl)oxy)-3-hydroxy-heptadec-4-en-2-yl)carbamate (13)

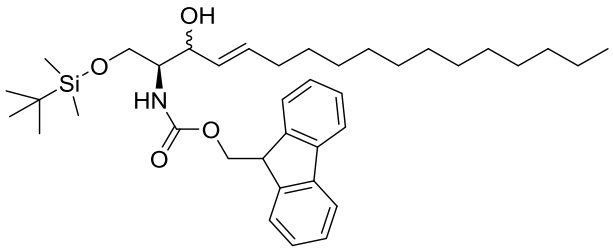

Procedure using $AgClO_4$ as catalyst:

To a flame-dried Schlenk with $Cp_2Zr(H)Cl$ (85 mg, 0.33 mmol) in anhydrous DCM (0.3 mL), was added 1-tetradecyne (75 μL, 0.3 mmol), at 0 ºC under argon and protected from light. During warming to room temperature, the zirconocene complex gradually dissolved to give a clear red solution (60 min). A solution of the aldehyde RBM4-54 (100 mg, 0.2 mmol) in DCM (0.3 mL) was added followed by $AgClO_4$ (10 mg, 20% mol). After 20 min, the reaction mixture turned dark red, was diluted with Et_2O and was quenched by addition of 0.5 mL saturated $NaHCO_3$ aqueous solution. The mixture was filtered through a Celite® pad, and the products were extracted with Et_2O (5 mL x 3). The combined ethereal solution were washed with brine, dried and concentrated *in vacuo*. Purification with flash column chromatography with silica-gel (hexane:EtOAc; 100:0 to 90:10 gradient) gave compound **13** (50%) as a mixture of diastereomers (*anti*:*syn*; 1:4).

Procedure using $ZnCl_2$ as additive:

To a flame-dried Schlenk with a suspension of $Cp_2Zr(H)Cl$ (63 mg, 0.25 mmol) in DCM (250 μL), was added 1-tetradecyne (56 μL, 0.2 mmol) at 0 ºC, under argon, and protected from light. During warming to room temperature, the zirconocene complex gradually dissolved to give a clear red solution (60 min). A solution of the aldehyde RBM4-54 (75 mg, 0.18 mmol) in DCM (500 μL), which was activated previously with $ZnCl_2$ (12 mg, 0.1 mmol, dried under vacuum for 1 h before use) for 10 min, was added to the reaction mixture. The solution was stirred for 30 min at RT and turned clear orange. Next dilution with DCM (2 mL) and addition of aqueous potassium sodium tartrate (2 mL) was stirred for 10 min. The resulting suspension was filtered through Celite® pad and washed thoroughly with DCM (5 mL). The combined filtrate was successively washed with H_2O and brine. The aqueous phase was extracted with DCM

(3x10 mL), and the combined organic layers were dried over Mg_2SO_4. Purification with flash column chromatography with silica-gel (hexane:EtOAc; 100:0 to 93:7 gradient) gave compound **13** as a mixture of diastereomers (15% *anti*:*syn*; 2:1) and (15% *anti*:*syn*; 1:1).

Transmetalation procedure using Et_2Zn

To an ice-cooled stirred suspension of $Cp_2Zr(H)Cl$ (68 mg, 0.3 mmol) in DCM (300 μL) under argon was added 1-tetradecyne (56 μL, 0.2 mmol), and the mixture was stirred at room temperature for 1 h protected from light, and then cooled to -40 ºC. To the resulting yellow solution was added 1.0M solution in hexane Et_2Zn (230 μL, 0.2 mmol) followed by the aldehyde RBM4-54 (75 mg, 0.18 mmol) in DCM (500 μL), and the mixture was stirred for 20 min at -40 ºC. The mixture was diluted with DCM (2 mL) and aqueous potassium sodium tartrate (2 mL). The resulting suspension was filtered through Celite® pad and washed thoroughly with DCM (5 mL). The combined filtrate was successively washed with H_2O and brine. The aqueous phase was extracted with DCM (3x10 mL), and the combined organic layers were dried over Mg_2SO_4. Purification with flash column chromatography with silica-gel (hexane:EtOAc; 100:0 to 93:7 gradient) gave compound **13** (25%) as a mixture of diastereomers (*anti*:*syn*; 2:5).

Rf: (2*S*, 3*S*) 0.53; **(2*S*, 3*R*)** 0.49 (hexane:EtOAc; 8:2).

^{1}H NMR ($CDCl_3$): Diastereomers assignment from a mixture (*anti*:*syn*; 1:1). **(2*S*, 3*R*)** δ 7.75 (d, *J* = 5.2 Hz, 2H), 7.62 – 7.56 (m, 2H), 7.41 – 7.36 (m, 2H), 7.33 – 7.28 (m, 2H), 5.81 – 5.66 (m, 1H), 5.56 – 5.43 (m, 1H), 5.26 – 5.17 (m, 1H), 4.43 – 4.27 (m, 3H), 4.24 (t, *J* = 7.1 Hz, 1H), 4.04 – 3.91 (m, 1H), 3.82 – 3.72 (m, 1H), 3.69 – 3.59 (m, 1H), 3.23 (d, *J* = 8.4 Hz, 1H), 2.12 – 1.95 (m, 2H), 1.40 – 1.31 (m, 2H), 1.24 (d, *J* = 7.1 Hz, 18H), 0.98 – 0.82 (m, 12H), 0.11 (s, 3H), 0.10 (s, 3H). **(2*S*, 3*S*)** δ 7.77 (d, *J* = 7.5 Hz, 2H), 7.60 (dd, *J* = 7.6, 3.7 Hz, 2H), 7.40 (t, *J* = 7.5 Hz, 2H), 7.31 (td, *J* = 7.5, 1.2 Hz, 2H), 5.77 (dt, *J* = 14.1, 6.7 Hz, 1H), 5.49 (dd, *J* = 15.4, 6.2 Hz, 1H), 5.40 (d, *J* = 8.7 Hz, 1H), 4.48 – 4.42 (m, 1H), 4.37 (dd, *J* = 7.2, 4.9 Hz, 2H), 4.24 (t, *J* = 7.1 Hz, 1H), 3.89 – 3.81 (m, 2H), 3.71 – 3.63 (m, 1H), 2.03 (q, *J* = 7.1 Hz, 2H), 1.42 – 1.32 (m, 2H), 1.32 – 1.19 (m, 18H), 0.92 (s, 9H), 0.88 (t, *J* = 6.9 Hz, 3H), 0.08 (s, 6H).

^{13}C NMR ($CDCl_3$): (2*S*, 3*R*) δ 156.7 (C), 144.1 (C), 144.0 (C), 141.4 (C), 133.6 (CH), 129.3 (CH), 127.3 (CH), 125.1 (CH), 120.3 (CH), 73.4 (CH), 67.1 (CH_2), 63.5 (CH_2), 55.4 (CH), 47.4 (CH), 32.5 (CH_2), 32.1 (CH_2), 29.8 (3 CH_2), 29.7 (CH_2), 29.5 (CH_2), 29.4 (CH_2), 29.3 (CH_2), 26.0 (CH_3), 22.8 (CH_2), 18.3 (CH_2), 14.3 (CH_3), -5.4 (2 CH_3). **(2*S*, 3*S*)** δ 156.7 (C), 144.1 (C), 144.0 (C), 141.4 (C), 133.9 (CH), 128.8 (CH), 127.8

(CH), 127.2 (CH), 125.3 (CH), 120.1 (CH), 73.5 (CH), 67.1 (CH_2), 65.2 (CH_2), 55.3 (CH), 47.4 (CH), 32.5 (CH_2), 32.1 (CH_2), 29.8 (3 CH_2), 29.7 (CH_2), 29.5 (CH_2), 29.4 (CH_2), 29.3 (CH_2), 26.0 (CH_3), 22.8 (CH_2), 18.3 (CH_2), 14.3 (CH_3), -5.4(2 CH_3).

(2*S*,3*S*,*E*)-2-((((9H-fluoren-9-yl)methoxy)carbonyl)amino)-1-((*tert*-butyldimethylsilyl) oxy)heptadec-4-en-3-yl (*R* or *S*)-2-methoxy-2-phenylacetate (14)

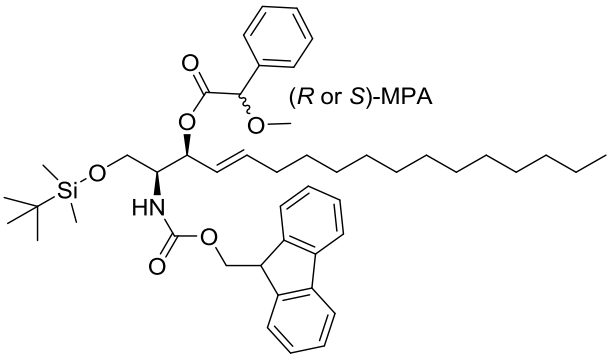

To a solution of (-)*R* or (+)*S*-α-methoxyphenylacetic acid (MPA) (20mg, 0.1 mmol) in anhydrous DCM (0.7 mL) was added dropwise a solution of EDC (25 mg, 0.1 mmol) in DCM (0.7mL) at 0ºC, under argon atmosphere. The resulting mixture was vigorously stirred at RT for 20 min, and then was added a solution of compound **13** (less polar major diastereomer) (50 mg, 0.08 mmol) in DCM (1.4mL) at 0ºC. The reaction mixture was stirred at RT for 8 h and then was diluted by addition of DCM (5 mL), and washed successively with water (5 mL) and brine (5 mL). The organic layer was dried over $MgSO_4$, and filtered and concentrated *in vacuo*. The crude was purified by flash column chromatography with silica-gel (hexane:EtOAc; 100:0 to 94:6 gradient) yielding the corresponding esters as a colourless oil.

Rf: (-)*R*-MPA 0.2; **(+)*S*-MPA** 0.26 (hexane:EtOAc; 9:1).

^{1}H NMR ($CDCl_3$): (+)*S*-MPA δ 7.78 (d, *J* = 7.3 Hz, 2H), 7.58 – 7.51 (m, 2H), 7.46 – 7.36 (m, 4H), 7.35 – 7.28 (m, 5H), 5.85 – 5.72 (m, 1H), 5.50 (d, *J* = 5.7 Hz, 1H), 5.42 (dd, *J* = 15.4, 7.5 Hz, 1H), 4.75 (d, *J* = 11.0 Hz, 1H), 4.37 – 4.26 (m, 1H), 4.24 – 4.13 (m, 2H), 3.84 – 3.73 (m, 1H), 3.47 – 3.34 (m, 4H), 3.21 (dd, *J* = 10.2, 6.2 Hz, 1H), 2.06 – 1.93 (m, 2H), 1.37 – 1.13 (m, 24H), 0.85 (d, *J* = 7.1 Hz, 9H), -0.04 (d, *J* = 3.0 Hz, 6H). **(-)*R*-MPA** δ 7.77 (d, *J* = 7.5 Hz, 2H), 7.57 (d, *J* = 7.5 Hz, 2H), 7.45 – 7.37 (m, 4H), 7.36 – 7.28 (m, 5H), 5.57 – 5.45 (m, 1H), 5.27 (dd, *J* = 15.3, 7.1 Hz, 1H), 5.02 (d, *J* = 9.7 Hz, 1H), 4.75 (s, 1H), 4.42 – 4.26 (m, 2H), 4.22 (q, *J* = 7.7 Hz, 1H), 3.89 – 3.78 (m, 1H),

3.63 (dd, *J* = 10.2, 3.3 Hz, 1H), 3.51 (dd, *J* = 10.3, 5.4 Hz, 1H), 3.38 (s, 3H), 1.88 (d, *J* = 6.2 Hz, 2H), 1.33 – 1.04 (m, 24H), 0.88 (s, 9H), 0.01 (s, 6H).

Absolute configuration determination

After carefully chromatographic purification the single diastereomers were isolated. The absolute configuration was assigned by derivatization of the major diastereomers with (*R*)-MPA and (*S*)-MPA, following the Riguera and coworkers procedure[359].

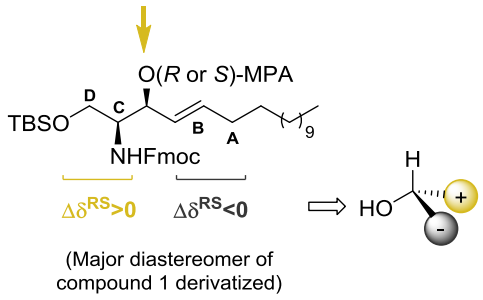

Table 5.1 $\Delta\delta^{RS}$ values from 1H-NMR spectra for the major diastereomer derivatized.

	δ H_A	δ H_B	δ H_C	δ H_D
R-MPA	1.88	5.54	3.85	3.52
S-MPA	2.01	5.80	3.79	3.22
$\Delta\delta^{RS}$	-0.13	-0.26	0.06	0.30

(2*S*,3*S*,*E*)-2-aminoheptadec-4-ene-1,3-diol (15)

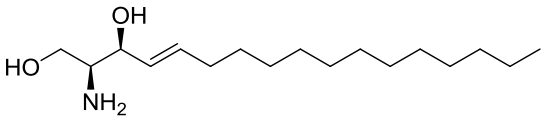

(2*S*, 3*S*) Compound **13** (20 mg, 0.03 mmol) was dissolved in anhydrous THF (0.5 mL) under argon atmosphere. Next, 30 µL of TBAF solution (1M in THF) was added via syringe (0.04 mmol, 1M in THF). The solution turned orange immediately. After being stirred for 1 h at RT, it was observed by TLC that the conversion was not completed, then to the reaction mixture was added an additional 30 µL of TBAF solution (1M in THF). After 30 min, a saturated aqueous NH_4Cl (0.5 mL) solution was added. The mixture was then extracted with DCM (3 x 5 mL), and washed with brine (5 mL). The organic layer was dried over $MgSO_4$ and concentrated *in vacuo*. Purification by flash column chromatography with silica-gel (DCM:MeOH:NH_3; 100:0:1 to 85:15:1 gradient) yielded the corresponding **15**.

Rf: 0.48 (DCM:MeOH:NH_3; 80:20:1)

^{1}H NMR (CD_3OD): δ 5.85 (ddd, *J* = 15.6, 7.0, 6.8 Hz, 1H), 5.45 (ddt, *J* = 15.2, 7.4, 1.2 Hz, 1H), 4.11 (t, *J* = 8.0 Hz, 1H), 3.73 (dd, *J* = 11.7, 3.8 Hz, 1H), 3.58 (dd, *J* = 11.6, 6.5

Hz, 1H), 3.03 (ddd, *J* = 8.3, 6.5, 3.8 Hz, 1H), 2.10 (q, *J* = 7.1 Hz, 2H), 1.48 – 1.37 (m, 2H), 1.30 (d, *J* = 7.4 Hz, 18H), 0.90 (t, *J* = 6.8 Hz, 3H).

^{13}C NMR (CD_3OD): 137.0 (CH), 129.7 (CH), 71.0 (CH), 60.1 (CH_2), 59.0 (CH), 33.3 (CH_2), 33.1 (CH_2), 30.8 (3 CH_2), 30.7 (CH_2), 30.6 (CH_2), 30.5 (CH_2), 30.3 (CH_2), 30.2 (CH_2), 23.7(CH_2), 14.4 (CH_3).

(2*E*,4*E*,6*E*)-Octa-2,4,6-trienal (RBM4-2)

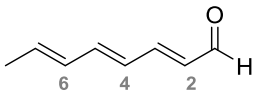

To a solution of the ester RBM4-49 (2 g, 12.0 mmol) in hexane (50 mL) at -78 °C was added DIBAL-H solution (1.0 M in toluene, 30 mL). The reaction mixture was stirred for 1h at -78 °C before being quenched with 50 mL of saturated Rochelle's salt solution. The resultant mixture was stirred at room temperature for 1.5 h before Et_2O (100 mL) was added. The organic layer was separated, dried, concentrated and used directly in the next step. To a solution of alcohol (1.5 g, 12.0 mmol) in 80 mL of EtOAc was added IBX (4.8 g, 18.0 mmol) in one portion, the mixture was refluxed overnight and then cooled to room temperature. The white precipitate was removed by filtration through a Celite® pad and the pad was rinsed with 3 x 50 mL of EtOAc. The combined organic filtrates were concentrated, the residue was purified by flash column chromatography (hexane:EtOAc; 96:4), to afford a yellow solid RBM4-2 (61%; (2 *Z:E*; 1:10). The spectroscopic data of RBM4-2 was identical to those reported in the literature[166]

Rf: 0.47 (hexane:EtOAc; 9:1)

^{1}H NMR ($CDCl_3$): Signals deduced from the (2 *Z:E*;1:10) mixture **(2*E*,4*E*,6*E*)** *δ* 9.55 (d, *J* = 8.0 Hz, 1H), 7.11 (dd, *J* = 15.5, 11.0 Hz, 1H), 6.64 (ddt, *J* = 15.0, 10.5, 0.5 Hz, 1H), 6.33 (ddt, *J* = 15.0, 11.0, 0.5 Hz, 1H), 6.25 – 5.99 (m, 3H), 1.86 (dd, *J* = 6.5, 1.0 Hz, 3H). **(2*Z*,4*E*,6*E*)** *δ* 9.57 (d, *J* = 8.0 Hz, 1H), 7.18 (ddd, *J* = 15.5, 11.0, 1.0 Hz, 1H), 6.99 (dd, *J* = 15.0, 11.5 Hz, 1H), 6.42 (dd, *J* = 14.5, 11.0 Hz, 1H), 6.27 – 6.18 (m, 2H), 5.92 – 5.81 (m, 1H), 1.88 (d, *J* = 4.0 Hz, 3H).

^{13}C NMR ($CDCl_3$): (2*E*,4*E*,6*E*) *δ* 193.7 (CH), 152.6 (CH), 143.2 (CH), 137.3 (CH), 131.3 (CH), 130.8 (CH), 127.8 (CH), 18.9 (CH_3). **(2*Z*,4*E*,6*E*)** δ 193.7 (CH), 152.4 CH), 137.7 (CH), 133.7 (CH), 131.2 (CH), 129.7 (CH), 128.9 (CH), 14.1 (CH_3).

(2*E*,4*E*,6*E*,8*E*)-Deca-2,4,6,8-tetraenal (RBM4-4)

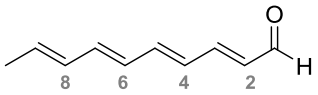

To a solution of the ester RBM4-5 (1.9 g, 10.0 mmol) in hexane (80 mL) at -78 °C was added DIBAL-H solution (1.0 M in toluene, 25 mL). The reaction mixture was stirred for 1h at -78 °C before being quenched with 40 mL of saturated Rochelle's salt solution. The resultant mixture was stirred at room temperature for 1.5 h before Et_2O (80 mL) was added. The mixture was filtered through a Celite® pad and the organic layer was separated, dried, concentrated and used directly in the next step. To a solution of alcohol (1.5 g, 10.0 mmol) in 70 mL of EtOAc was added IBX (4.0 g, 15.0 mmol) in one portion, the mixture was refluxed overnight and then cooled to room temperature. The white precipitate was removed by filtration through a Celite® pad and the pad was rinsed with 3 x 50 mL of EtOAc. The combined organic filtrates were concentrated, the residue was purified by flash column chromatography (hexane:EtOAc; 94:6), to afford a yellow solid RBM4-4 (80%; (4 *Z:E*; 1:7). The spectroscopic data of RBM4-4 was identical to those reported in the literature[174].

Rf: 0.19 (hexane:EtOAc; 9:1)

^{1}H NMR ($CDCl_3$): Signals deduced from the (4*Z:E*; 1:7) mixture **(2*E*,4*E*,6*E*,8*E*)** δ 9.55 (d, J = 8.0 Hz, 1H), 7.13 (dd, J = 15.2, 11.2 Hz, 1H), 6.68 (dd, J = 14.7, 11.0 Hz, 1H), 6.43 (td, J = 14.6, 11.1 Hz, 2H), 6.27 – 6.10 (m, 4H), 5.92 (dq, J = 14.0, 7.0 Hz, 1H), 1.83 (d, J = 7.0 Hz, 3H). **(2*E*,4Z,6*E*,8*E*)** δ 9.57 (d, J = 8.0 Hz, 1H), 7.14 (dd, J = 15.2, 11.3 Hz, 1H), 6.78 (td, J = 15.7, 11.3 Hz, 1H), 6.31 (dd, J = 15.3, 11.3 Hz, 1H), 6.22 – 6.10 (m, 4H), 5.73 (dq, J = 11.6, 8.0 Hz, 1H), 1.87 (d, J = 7.9 Hz, 3H).

^{13}C NMR ($CDCl_3$): (2*E*,4*E*,6*E*,8*E*) δ 193.7 (CH), 152.2 (CH), 143.2 (CH), 139.3 (CH), 134.6 (CH), 131.7 (CH), 130.7 (CH), 129.3 (CH), 129.2 (CH), 18.7 (CH_3). **(2*E*,4Z,6*E*,8*E*)** δ 193.6 (CH), 152.0 (CH), 143.1 (CH), 133.9 (CH), 131.3 (CH), 131.2 (CH), 131.0 (CH), 129.7 (CH), 129.3 (CH), 14.0 (CH_3).

ESI-MS *m/z* $C_{10}H_{12}O$ $[M+Na]^+$ Found: 171.0784; Calculated: 171.0786; $[M+H]^+$ Found: 149.0959; Calculated: 149.0966.

Ethyl (2*E*,4*E*,6*E*,8*E*)-deca-2,4,6,8-tetraenoate (RBM4-5)

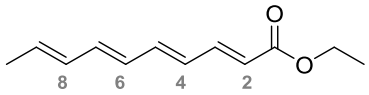

To a suspension of NaH (60% in mineral oil, 2.0 g, 50.0 mmol) in anhydrous THF (250 mL) at 0 °C was slowly added the triethyl 4-phosphonocrotonate (10.0 g, 40.0 mmol). The suspension was stirred at 0 °C for 1 h, and then the *trans,trans*-2,4-hexadienal (2.8 mL, 25.0 mmol) was added. The reaction mixture was stirred at 0 °C for 2 h, protected from light, before being quenched by saturated NH_4Cl (100 mL). The product was extracted with EtOAc (3 x 100 mL). The combined extracts were washed with brine, dried and concentrated under reduce pressure. The crude was purified by flash column chromatography (hexane:EtOAc; 97:3), to afford RBM4-5 (40% (4*Z:E*; 1:4) as a yellowish solid.

Rf: 0.77 (hexane:EtOAc; 9:1)

^{1}H NMR ($CDCl_3$): Data deduced from the (4*Z:E;* 1:4) mixture of isomers **(2*E*,4*E*,6*E*,8*E*)** δ 7.29 (dd, J = 15.2, 11.3 Hz, 1H), 6.54 (dd, J = 14.8, 11.0 Hz, 1H), 6.40 – 6.07 (m, 4H), 5.83 (dd, J = 15.0, 6.9 Hz, 2H), 4.18 (qd, J = 7.2, 0.7 Hz, 2H), 1.79 (d, J = 7.2 Hz, 3H), 1.27 (t, J = 7.1 Hz, 3H). **(2*E*,4*Z*,6*E*,8*E*)** δ 7.29 (dd, J = 15.2, 11.4 Hz, 1H), 6.70 (td, J =14.9, 11.4 Hz, 1H), 6.36 – 5.89 (m, 5H), 5.64 (dq, J = 11.2, 7.5 Hz, 1H), 4.19 (q, J = 7.2 Hz, 2H), 1.83 (d, J = 7.1 Hz, 3H), 1.28 (t, J = 7.1 Hz, 3H).

^{13}C NMR ($CDCl_3$): (2*E*,4*E*,6*E*,8*E*) δ 167.4 (C), 144.7 (CH), 141.2 (CH), 137.6 (CH), 133.3 (CH), 131.7 (CH), 129.5 (CH), 129.2 (CH), 120.2 (CH), 60.4 (CH_2), 18.7 (CH_3), 14.5 (CH_3).

ESI-MS *m/z* $C_{12}H_{16}O_2$ $[M+H]^+$ Found: 193.1218 Calculated: 193.1229.

***tert*-Butyl (*S*)-4-((*R*,*E*)-6-bromo-1-hydroxyhex-2-en-1-yl)-2,2-dimethyloxazolidine-3-carboxylate (RBM4-7)**

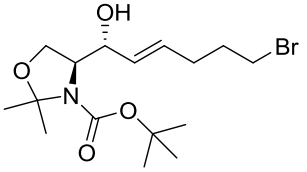

A two necked round bottom flask fitted with a reflux condenser under argon atmosphere, was charged with allylic alcohol **6** (970 mg, 3.8 mmol) in 100 mL of DCM previously degassed. To the solution was added 5-bromo-1-pentene (1.8 mL, 15.1

mmol) and Grubbs' 2nd generation catalyst (320 mg, 0.04 mmol). The resulting mixture was stirred at reflux temperature for 4 h and then cooled down to RT. The mixture was concentrated under reduced pressure to afford a crude, which was purified by flash column chromatography (hexane:EtOAc; 85:15) yielding RBM4-7 (80%) as a colourless oil.

Rf: 0.46 (hexane:EtOAc; 7:3); **$[\alpha]_D$:** -35.4 (*c* 1.1, $CHCl_3$).
^{1}H NMR ($CDCl_3$): δ 5.71 (dt, *J* = 15.0, 7.0 Hz, 1H), 5.53 (dd, *J* = 15.0, 6.0 Hz, 1H), 4.39 – 4.24 (m, 1H), 4.23 – 4.10 (m, 1H), 4.08 – 3.97 (m, 1H), 3.87 – 3.77 (m, 1H), 3.40 (t, *J* = 7.0 Hz, 2H), 2.22 (td, *J* = 7.5, 7.0 Hz, 2H), 1.99 – 1.89 (m, 2H), 1.53 (s, 6H), 1.50 – 1.45 (m, 9H).
^{13}C NMR ($CDCl_3$): δ 154.3 (C), 130.7 (CH), 130.1 (CH), 94.5 (C), 81.2 (C), 74.1 (CH), 65.0 (CH), 62.2 (CH_2), 33.2 (CH_2), 32.2 (CH_2), 30.7 (CH_2), 28.4 (CH_3), 25.7 (CH_3).

tert-Butyl (*S*)-4-((*R*,*E*)-6-bromo-1-(methoxymethoxy)hex-2-en-1-yl)-2,2-dimethyl-oxazolidine-3-carboxylate (RBM4-8(Br))

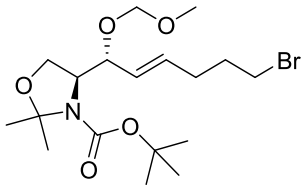

A two necked round bottom flask fitted with a reflux condenser under argon atmosphere, was charged with RBM4-9 (170 mg, 0.6 mmol) in 12 mL of DCM previously degassed. To the solution was added 5-bromo-1-pentene (0.3 mL, 2.2 mmol) and Grubbs' 2nd generation catalyst (25 mg, 0.03 mmol). The resulting mixture was stirred at reflux temperature for 5 h and then cooled down to RT. The mixture was concentrated under reduce pressure to afford a crude, which was purified by flash column chromatography (hexane:EtOAc; 88:12) yielding RBM4-8(Br) (50%) as pale yellowish oil.

Rf: 0.65 (hexane:EtOAc; 7:3); **$[\alpha]_D$:** -46.2 (*c* 1.0, $CHCl_3$).
^{1}H NMR ($CDCl_3$): δ 5.69 – 5.55 (m, 1H), 5.45 – 5.32 (m, 1H), 4.68 (d, *J* = 7.0 Hz, 1H), 4.50 (d, *J* = 6.0 Hz, 1H), 4.29 – 4.19 (m, 1H), 4.04 (dd, *J* = 9.0 Hz, 1H), 4.00 – 3.93 (m, 1H), 3.92 – 3.86 (m, 2H), 3.86 – 3.79 (m, 1H),.3.44 – 3.35 (m, 2H), 3.33 (s, 3H), 2.27 – 2.11 (m, 2H), 1.96 – 1.87 (m, 2H), 1.57 (s, 3H), 1.49 (s, 3H), 1.45 (s, 9H).

^{13}C NMR ($CDCl_3$): Some splitting observed due to rotamers. δ 152.6 (C), 133.9 (CH), 128.8 (CH), 94.5 (C), 93.9 (CH_2), 80.2 (C), 76.6 (CH), 64.5 (CH_2), 60.4 (CH), 55.8 (CH_3), 33.2 (CH_2) 31.9 (CH_2), 30.7 (CH_2), 28.5 (CH_3), 27.2 (CH_3), 25.0 (CH_3).
ESI-MS *m/z* $C_{18}H_{32}BrNO_5$ $[M+H]^+$ Found: 422.1506; Calculated: 422.1542.

tert-Butyl (*S*)-4-((*R*,*E*)-6-chloro-1-(methoxymethoxy)hex-2-en-1-yl)-2,2-dimethyl-oxazolidine-3-carboxylate (RBM4-8(Cl))

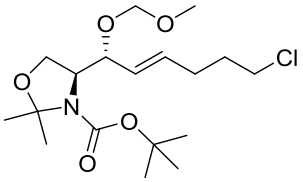

To a stirred solution of RBM4-7 (370 mg, 1.0 mmol) in anhydrous DCM (40 mL), was added 2.9 mL of DIPEA (12.0 mmol) under argon atmosphere. Then, the solution was cooled down to 0ºC and the methoxymethyl chloride (0.9 mL, 12.0 mmol) was added dropwise. After stirring at RT overnight, the reaction mixture was quenched by addition of saturated aqueous NH_4Cl solution and extracted with DCM. The organic phase was washed with brine, dried and concentrated under reduce pressure. The residue was purified by flash column chromatography (hexane:EtOAc; 88:12) to afford a colourless oil (yield: 95%), which resulted in a mixture of (3:1); (6-Cl, 6-Br).

Rf: 0.65 (hexane:EtOAc; 7:3);
^{1}H NMR ($CDCl_3$): Signals corresponding to $C_{18}H_{32}ClNO_5$. δ 5.76 – 5.55 (m, 1H), 5.50 – 5.28 (m, 1H), 4.70 (d, *J* = 7.0 Hz, 1H), 4.52 (d, *J* = 7.0 Hz, 1H), 4.32 – 4.19 (m, 1H), 4.05 (dd, *J* = 9.0, 2.0 Hz, 1H), 4.01 – 3.94 (m, 1H), 3.94 – 3.88 (m, 2H), 3.88 – 3.81 (m, 1H), 3.56 – 3.46 (m, 2H), 3.35 (s, 3H), 2.29 – 2.10 (m, 2H), 1.90 – 1.78 (m, 2H), 1.59 (s, 3H), 1.54 (s, 3H), 1.47 (s, 9H).
^{13}C NMR ($CDCl_3$): Some splitting observed due to rotamers. δ 152.6 (C), 134.1 (CH), 128.7 (CH), 94.5 (C), 93.9 (CH_2), 80.2 (C), 76.6 (CH), 64.5 (CH_2), 60.4 (CH), 55.8 (CH_3), 44.4 (CH_2), 31.8 (CH_2), 29.5 (CH_2), 28.5 (CH_3), 27.2 (CH_3), 25.0 (CH_3).
ESI-MS *m/z* $C_{18}H_{32}ClNO_5$ $[M+H]^+$ Found: 378.2020; Calculated: 378.2047.

***tert*-Butyl (*S*)-4-((*R*)-1-(methoxymethoxy)allyl)-2,2-dimethyloxazolidine-3-carboxylate (RBM4-9)**

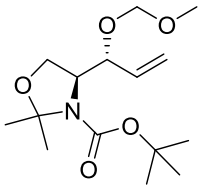

To a stirred solution of compound **6** (150 mg, 0.6 mmol) in anhydrous DCM (40 mL), was added 1.7 mL of DIPEA (7.0 mmol) under argon atmospehere. The solution was then cooled down to 0ºC and the methoxymethyl chloride (0.5 mL, 7.0 mmol) was added dropwise. After stirring at RT overnight, the reaction mixture was quenched by addition of saturated aqueous NH_4Cl solution and extracted with DCM. The organic phase was washed with brine, dried and concentrated under reduce pressure. The residue was purified by flash column chromatography (hexane:EtOAc; 90:10) to afford RBM4-9 as a colourless oil (yield: 96%). The physical and spectroscopic data of compound RBM4-9 were identical to those reported in the literature[402].

Rf: 0.75 (hexane:EtOAc; 7:3); **$[\alpha]_D$:** -65.2 (*c* 1, $CHCl_3$); **$[\alpha]_D$**: -66.4 (*c* 0.8, $CHCl_3$) lit[402].
^{1}H NMR ($CDCl_3$): Some splitting observed due to rotamers. δ 5.81 – 5.62 (m, 1H), 5.35 – 5.15 (m, 2H), 4.72 (d, *J* = 6.5 Hz, 1H), 4.56 (d, *J* = 7.0 Hz, 1H), 4.44 – 4.20 (brm, 1H), 4.11 – 3.82 (m, 3H), 3.37 (s, 3H), 1.61 (s, 3H), 1.52 (s, 15H), 1.47 (s, 9H).

***tert*-Butyl (*S*)-4-((*R*,2*E*,6*E*,8*E*,10*E*,12*E*,14*E*)-1-(methoxymethoxy)hexadeca-2,6,8,10,12,14-hexaen-1-yl)-2,2-dimethyloxazolidine-3-carboxylate (RBM4-10)**

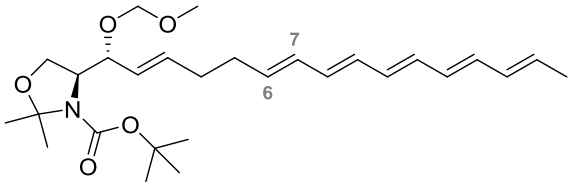

To a suspension of phosphonium RBM4-14 salt (100 mg, 0.15 mmol) in anhydrous THF (2 mL) under argon atmosphere, was added dropwise a solution of BuLi (2.5 M in hexane, 0.14 mmol) at -78 ºC. The reaction mixture was stirred at 0 ºC for 30 min. To the resulting reddish solution was added dropwise the aldehyde RBM4-4 (14 mg, 0.09 mmol) in THF (1 mL) at -78ºC and protected from light. After 2 h, MeOH (1 mL) was added at -78 ºC and the mixture was gradually warmed to RT and concentrated under reduce pressure. The residue was extracted with Et_2O (3 x 5 mL) and the combined

organic layers were washed with brine, dried over $MgSO_4$, and concentrated. The crude was purified by flash column chromatography (hexane:AcOEt; 95:5) to afford RBM4-10 as a yellowish oil (14%, 6*Z:E*;1:2.5).

Rf: 0.83 (hexane:EtOAc; 7:3)

^{1}H NMR ($CDCl_3$): Some splitting observed due to rotamers. Data described for (*all-E*) isomer *δ* 6.31 – 5.95 (m, 8H), 5.78 – 5.57 (m, 3H), 5.34 (d, *J* = 29.0 Hz, 1H), 4.71 (d, *J* = 7.0 Hz, 1H), 4.50 (d, *J* = 6.5 Hz,1H), 4.33 – 4.18 (m, 1H), 4.09 – 3.78 (m, 3H), 3.35 (s, 3H), 2.25 – 2.07 (m, 4H), 1.78 (d, *J* = 7.0 Hz, 3H), 1.59 (s, 3H), 1.54 (s, 3H), 1.47 (s, 9H).

ESI-MS *m/z* $C_{28}H_{43}NO_5$ $[M+H]^+$ Found: 474.3212; Calculated: 474.3206.

(1*R*,7a*S*)-5,5-Dimethyl-1-vinyldihydro-1H,3H,5H-oxazolo[3,4-c]oxazol-3-one (RBM4-12)

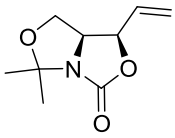

To a suspension of NaH (60% in mineral oil, 780 mg, 19.4 mmol) in anhydrous THF (40 mL) was added a solution of compound **6** (500 mg, 1.94 mmol) in THF (10 mL) at 0 ºC. The reaction mixture was vigorously stirred at RT overnight under argon atmosphere. The mixture was quenched by dropwise addition of saturated aqueous $NaHCO_3$ solution at 0ºC, until H_2 evolution was not observed. The aqueous phase was next extracted with EtOAc (3 x 30 mL). The combined organic layers were dried over $MgSO_4$, filtered and concentrated under reduce pressure. The resulting residue was purified by flash column chromatography (hexane:EtOAc; 87:13) to afford RBM4-12 (71%) as a colourless oil. RBM4-12 was isolated as a mixture of diastereomers (1*R*,7a*S:* 1*S*,7a*S;* 17:1), since compound **6** was not diastereomerically pure.

Rf: 0.31 (hexane:EtOAc; 7:3)

^{1}H NMR ($CDCl_3$): Signals deduced from a (1*R*,7a*S:* 1*S*,7a*S;* 17:1) mixture. **(1*R*,7a*S*)** *δ* 5.78 (ddd, *J* = 17.0, 10.5, 5.5 Hz, 1H), 5.50 (dd, *J* = 17.0, 2.5 Hz, 1H), 5.38 (dd, *J* = 10.5, 2.5 Hz, 1H), 5.10 – 5.04 (m, 1H), 4.42 (td, *J* = 8.5, 6.5 Hz, 1H), 3.88 (dd, *J* = 8.5, 6.5 Hz, 1H), 3.71 – 3.65 (m, 1H), 1.70 (s, 3H), 1.45 (s, 3H). **(1S,7a*S*)** δ 5.95 (ddd, *J* = 17.0, 10.5, 7.0 Hz, 1H), 5.44 (dd, *J* = 17.0, 1.0 Hz, 1H), 5.36 (dd, *J* = 10.5, 1.0 Hz, 1H), 4.72 – 4.66 (m, 1H), 4.18 – 4.06 (m, 2H), 3.72 – 3.67 (m, 1H), 1.73 (s, 3H), 1.43 (s, 3H).

^{13}C NMR ($CDCl_3$): (1*R*,7a*S*) δ 156.8 (C), 130.8 (CH), 119.9 (CH_2), 95.2 (C), 74.9 (CH), 64.4 (CH), 61.5 (CH), 28.0 (CH_3), 23.5 (CH_3). **(1S,7a*S*)** δ 156.8 (C), 130.5 (CH), 120.6 (CH_2), 79.2 (C), 68.1 (CH), 62.0 (CH), 56.9 (CH), 31.1 (CH_3), 25.7 (CH_3).
ESI-MS *m/z* $C_9H_{13}NO_3$ $[M+H]^+$ Found: 184.0961; Calculated: 184.0974.

(1*R*,7a*S*)-1-((*E*)-5-Bromopent-1-en-1-yl)-5,5-dimethyldihydro-1H,3H,5H-oxazolo[3,4-c]oxazol-3-one (RBM4-13)

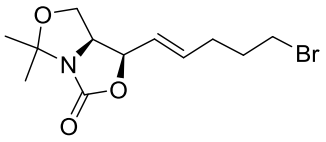

A two necked round bottom flask fitted with a reflux condenser under argon atmosphere, was charged with compound RBM4-12 (150 mg, 0.8 mmol) in 15 mL of DCM previously degassed. To the solution was added 5-bromo-1-pentene (0.4 mL, 3.3 mmol) and Grubbs' 2nd generation catalyst (40 mg, 5 µmol). The resulting mixture was stirred at reflux temperature for 6 h and then cooled down to RT. The mixture was concentrated under reduced pressure affording a crude, which was purified by flash column chromatography (hexane:EtOAc; 85:15)to yield RBM4-13 (65%) as a mixture of diastereomers in a ratio (1*R*,7a*S:*1*S*,7a*S; 9*:1).

Rf: 0.30 (hexane:EtOAc; 7:3)
^{1}H NMR ($CDCl_3$): Signals deduced from a (1*R*,7a*S:*1*S*,7a*S; 9*:1) mixture. **(1*R*, 7a*S*)** δ 5.86 (dtd, *J* = 15.0, 7.0, 1.0 Hz, 1H), 5.49 (ddt, *J* = 15.5, 7.0, 1.5 Hz, 1H), 5.06 – 5.00 (m, 1H), 4.38 (td, *J* = 8.5, 6.5 Hz, 1H), 3.87 (dd, *J* = 8.5, 6.5 Hz, 1H), 3.69 (dd, *J* = 8.5, 8.5 Hz, 1H), 3.39 (dd, *J* = 7.0, 6.5 Hz, 2H), 2.30 – 2.23 (m, 2H), 1.99 – 1.90 (m, 2H), 1.70 (s, 3H), 1.43 (s, 3H).
^{13}C NMR ($CDCl_3$): (1*R*, 7a*S*) δ 160.3 (C), 136.5 (CH), 124.1 (CH), 95.1 (C), 79.9 (CH), 64.3 (CH), 61.6 (CH), 33.0 (CH_2), 31.4 (CH_2), 30.6 (CH_2), 27.9 (CH_3), 23.5 (CH_3).
ESI-MS *m/z* $C_{12}H_{18}BrNO_3$ $[M+H]^+$ Found: 304.0515; Calculated: 304.0504

((*R*,*E*)-6-((*S*)-3-(*tert*-Butoxycarbonyl)-2,2-dimethyloxazolidin-4-yl)-6-(methoxymethoxy)hex-4-en-1-yl)triphenylphosphonium bromide (RBM4-14)

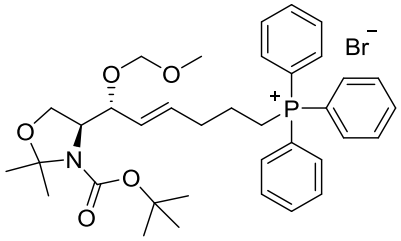

A stirred mixture of the compound RBM4-8(Br) (290 mg, 0.7 mmol) and triphenylphosphine (540 mg, 2.1 mmol) were heated to 90 ºC for 16 h, under argon atmosphere. The reaction mixture was cooled down to RT. The resulting yellowish precipitate was washed with hexane (3 x 25 mL) and the supernatants were discarded. The precipitate was completely dried under reduce pressure and the crude was purified by flash column chromatography (DCM:MeOH; 95:5) to afford RBM4-14 (80%) as a white solid.

Rf: 0.47 (DCM:MeOH; 9:1); **$[\alpha]_D$:** -55.6 (*c* 1.2, $CHCl_3$).

^{1}H NMR ($CDCl_3$): *δ* 7.86 – 7.80 (m, 6H), 7.78 (app.t, *J* = 7.5 Hz, 3H), 7.68 (dt, *J* = 10.0, 5.0 Hz, 6H), 5.61 – 5.45 (m, 1H), 5.43 – 5.29 (m,1H), 4.52 (dd, *J* = 63.0, 7.0 Hz, 2H), 4.30 – 4.14 (brm, 1H), 4.04 –3.69 (brm, 3H), 3.25 (s, 3H), 2.62 – 2.31 (m, 4H), 1.81 – 1.59 (m, 2H), 1.50 (s, 3H), 1.44 (s, 3H), 1.39 (s, 9H).

^{13}C NMR ($CDCl_3$): Some splitting observed due to rotamers. *δ* 152.6 (C), 135.1 (CH), 133.9 (CH), 133.1 (CH), 130.7 (CH), 129.2 (CH), 118.9 (C), 117.8 (C), 103.3 (C), 94.1 (CH_2), 80.2 (C), 76.3 (CH), 64.1 (CH_2), 60.5 (CH), 55.6 (CH_3), 32.8 (CH_2), 32.3 (CH_2), 28.5 (CH_3), 27.0 (CH_3), 24.9 (CH_3), 22.0 (CH_2).

ESI-MS *m/z* $C_{36}H_{47}BrNO_5P$ $[M+Na]^+$ Found: 706.2339; Calculated: 706.2273.

((*E*)-5-((1*R*,7a*S*)-5,5-Dimethyl-3-oxodihydro-1H,3H,5H-oxazolo[3,4-c]oxazol-1-yl)pent-4-en-1-yl)triphenylphosphonium bromide (RBM4-15)

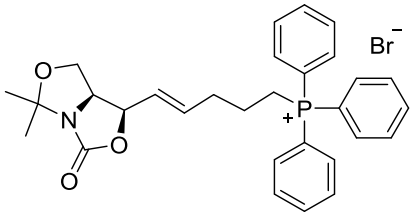

A stirred mixture of the compound RBM4-13 (380 mg, 1.2 mmol) and triphenylphosphine (980 mg, 3.6 mmol) in ACN (2.5 mL) were heated to 100ºC for 16 h, under argon. The reaction mixture was cooled down to RT. The resulting precipitate was washed with hexane (3 x 30 mL) and the supernatants were discarded. The precipitate was completely dried under reduce pressure and the crude was purified by flash column chromatography (DCM:MeOH; 97:3) to afford RBM4-15 (80%) as a white solid.

Rf: 0.68 (DCM:MeOH; 9:1); **$[\alpha]_D$:** -25.2 (*c* 1.0, $CHCl_3$).
^{1}H NMR ($CDCl_3$): The spectral data showed signals from a mixture RBM4-15: partially deprotected*;* (7:3). Data described for RBM4-15. *δ* 7.88 – 7.76 (m, 9H), 7.75 – 7.67 (m, 6H), 5.96 – 5.86 (m, 1H), 5.70 (dd, *J* = 15.5, 6.5 Hz, 1H), 5.12 (dd, *J* = 7.5, 7.0 Hz, 1H), 4.46 (td, *J* = 8.0, 6.5 Hz, 1H), 3.92 (dd, *J* = 9.0, 6.5 Hz, 1H), 3.72 (dd, *J* = 9.0, 8.0 Hz, 1H), 2.66 – 2.40 (m, 4H), 1.80 – 1.67 (m, 2 H), 1.64 (s, 3H), 1.41 (s, 3H).
^{13}C NMR ($CDCl_3$): *δ* 157.1 (C), 135.2 (CH), 134.1 (CH), 133.8 (CH), 133.6 (CH), 130.6 (CH), 125.7 (CH), 118.7 (C), 117.8 (C), 94.8 (C), 75.2 (CH), 64.5 (CH_2), 61.5 (CH), 32.3 (CH_2), 32.2 (CH_2), 27.6 (CH_3), 23.4 (CH_3), 22.1 (CH_2).
ESI-MS *m/z* $C_{30}H_{33}BrNO_3P$ $[M+H]^+$ Found: 566.1489; Calculated: 566.1502.

(5*E*,7*E*,9*E*,11*E*,13*E*)-Pentadeca-5,7,9,11,13-pentaen-1-yne (RBM4-17)

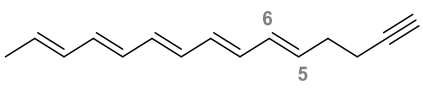

To a suspension of 4-pentyn-1-yltriphenylphosphonium iodide (3.9 g, 8.6 mmol) in anhydrous THF (60 mL) under argon atmosphere was added HMPA (5 mL, 5% final vol) at RT and then cooled to -78 ºC. To the reaction mixture was added dropwise a solution of BuLi (2.5 M in hexane, 3.7 mL, 9.2 mmol) and then was warmed to 0 ºC with

stirring for 1 h. After cooling the reddish orange solution to -78 ºC, the aldehyde RBM4-4 (800 mg, 5.4 mmol) in THF (40 mL) was added dropwise under argon atmosphere and protected from light. Although after 4 h the reaction was not complete, MeOH (40 mL) was added at -78 ºC and then the resulting mixture was gradually warmed overnight to RT. The mixture was concentrated under reduced pressure, and extracted with Et_2O (3 x 30 mL). The combined organic layers were washed with brine, dried over $MgSO_4$, and concentrated. The residue was purified by flash column chromatography (hexane) to afford RBM4-17 as a pale yellow solid (55%, (5*Z:E*,7*E*,9*E*,11*E*,13*E*); (1:2,1,1,1,1)).

(E)-Isomerization of C5-C6 double bond:

To a mixture of isomers RBM4-17 (300 mg, 1.5 mmol) (5*Z*:*E*,7*E*,9*E*,11*E*,13*E*), (1:2,1,1,1,1) in hexane (50 mL) under argon atmosphere, was added a saturated solution of iodine in hexane (55 µL). The resulting solution was heated at 69 ºC for 15 min, after which the solution was cooled to RT. The mixture was washed thoroughly with saturated aqueous sodium metabisulfite ($Na_2S_2O_5$), destroying the remaining iodine. The yellowish solution was washed with water, dried, and concentrated under reduced pressure furnishing a quantitative RBM4-17 as a pale yellow solid (5*Z*:*E*,7*E*,9*E*,11*E*,13*E*); (1:6,1,1,1,1). The product was purified by preparative-HPLC using a reverse phase column (X-Bridge C18, 5µm OBD, 19x250 mm) and eluted following an isocratic method (35:65, H_2O:ACN, 10 mL/min). (*all-E*) RBM4-17 isomer was isolated in 60% yield (λ: 330 nm) and Rt: 35.0 min.

Rf: 0.30 (hexane)

^{1}H NMR ($CDCl_3$): (5*E*,7*E*,9*E*,11*E*,13*E*) *δ* 6.37 – 6.03 (m, 8H), 5.73 (dq, *J* = 14.5, 7.0 Hz, 2H), 2.40 – 2.24 (m, 4H), 1.97 (t, *J* = 2.5 Hz, 1H), 1.78 (dd, *J* = 7.0, 1.4 Hz, 3H). **(5*Z*,7*E*,9*E*,11*E*,13*E*)** *δ* 6.75 – 6.35 (m, 2H), 6.33 – 5.86 (m, 7H), 5.49 (ddd, *J* = 18.0, 9.0, 7.0 Hz, 1H), 2.50 – 2.40 (m, 2H), 2.39 – 2.31 (m, 2H), 1.97 (t, *J* = 2.5 Hz, 1H), 1.82 (d, *J* = 7.0 Hz, 3H).

^{13}C NMR ($CDCl_3$): (5*E*,7*E*,9*E*,11*E*,13*E*) *δ* 133.3 (CH), 133.1 (CH), 132.5 (CH), 132.4 (CH), 132.3 (CH), 132.1 (CH), 132.0 (CH), 131.9 (CH), 130.7 (CH), 130.3 (CH), 83.92 (C), 68.9 (CH), 32.0 (CH_2), 18.8 (CH_2), 18.5 (CH_3). **(5*Z*,7*E*,9*E*,11*E*,13*E*)** *δ* 133.8 (CH), 133.7 (CH), 133.6 (CH), 132.1 (CH), 132.0 (CH), 130.6 (CH), 130.5 (CH), 130.3 (CH), 129.8 (CH), 127.6 (CH), 83.9 (C), 68.8 (CH), 27.2 (CH_2), 18.9 (CH_2), 18.6 (CH_3).

Preparative-HPLC for (*all-E*):Column (X-Bridge C18, 5µm OBD, 19 x 250 mm). Isocratic method (35:65, H_2O:ACN, 10 mL/min); Rt: 35.0 min; λ: 330 nm

(*S*)-*tert*-Butyl 4-((*R*,6*E*,8*E*,10*E*,12*E*,14*E*)-1-hydroxyhexadeca-6,8,10,12,14-pentaen-2-yn-1-yl)-2,2-dimethyloxazolidine-3-carboxylate (RBM4-18)

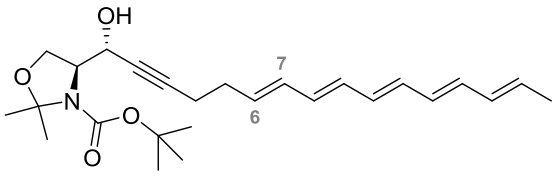

To a stirred solution of alkyne RBM4-17 (96mg, 0.5 mmol) in anhydrous THF (6 mL), was added dropwise a solution of LDA (325 µL, 1.8 M in THF/heptane/ethylbenzene) at -78 ºC under argon atmosphere. The mixture was stirred at -78 ºC for 30 min, and then was added a solution of Garner's aldehyde (170 mg, 0.7 mmol) in THF (6 mL). After 3 h, a saturated aqueous NH_4Cl (5 mL) solution was added to the reaction mixture at -78ºC and was warmed to RT. The resulting white suspension was diluted with H_2O, and extracted with Et_2O (3X15 mL). The combined organic layers were dried over $MgSO_4$ and concentrated under reduced pressure. The residue was purified by flash column chromatography (hexane:EtOAc; 85:15) to afford the *erythro*-RBM4-18 (25%) and mixture of isomers (6*Z*:*E*; 1:1).

Rf: 0.24 (hexane:EtOAc; 8:2); **$[\alpha]_D$:** -28.2 (*c* 1, $CHCl_3$, mixture of isomers).

^{1}H NMR ($CDCl_3$): Data described for (*all-E*)-isomer. δ 6.34 – 6.00 (m, 8H), 5.83 – 5.62 (m, 2H), 4.74 - 4.58 (m, 1H), 4.59 - 4.45 (m, 1H), 4.24 – 3.81 (m, 3H), 2.35 – 2.24 (m, 4H), 1.78 (dt, *J* = 7.0, 2.0 Hz, 3H), 1.63 – 1.53 (m, 6H), 1.56 – 1.39 (m, 9H).

^{13}C NMR ($CDCl_3$): (*all-E*)-isomer. δ 154.3(C), 133.8 (CH), 133.7 (CH), 132.3 (CH), 132.1 (CH), 132.0 (CH), 131.9 (CH), 130.7 (CH), 130.6 (CH), 130.5 (CH), 130.3 (CH), 95.1 (C), 86.0 (C), 81.4 (C), 79.3 (C), 65.2 (CH_2), 64.4 (CH), 62.9 (CH), 53.6 (C), 32.1 (CH_2), 29.8 (CH_3), 26.0 (CH_3), 19.3 (CH_2), 18.5 (CH_3).

ESI-MS *m/z* $C_{26}H_{37}NO_4$ $[M+Na]^+$ Found:450.2610; Calculated: 450.2620.

Analytical HPLC for RBM4-18: Column (Kromasil 100, C18, 5 µm, 15 x 0.4 cm). Isocratic method (30:70, H_2O:ACN). Sample volume: 25 µL; RBM4-18 (1mg/ mL DMSO); Rt:20.9 min (*Z*-isomer); Rt: 23.6 min (*E*-isomer) (λ: 331 nm).

(2*S*,3*R*,8*E*,10*E*,12*E*,14*E*,16*E*)-1,3-dihydroxyoctadeca-8,10,12,14,16-pentaen-4-yn-2-aminium chloride (RBM4-19)

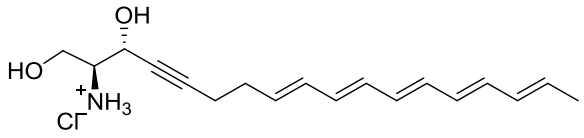

To a solution of the protected amino diol RBM4-18 (20 mg, 0.04 mmol) in MeOH (3mL) was added dropwise acetyl chloride (45 µL, 1.5% vol) at -30 ºC. The resulting mixture was vigorously stirred and warmed to RT for 30 min. Next addition of a saturated $NaHCO_3$ aqueous solution and concentration under reduce pressure, afforded a dark green crude. The crude was dissolved in DCM, dried over $MgSO_4$, filtrated through a cotton pad and then the solvent was concentrated under reduced pressure. The resulting solid (*all-E*)-RBM4-19 hydrochloride was obtained in 40% yield and characterized without further purification.

Rf: 0.46 (DCM:MeOH; 8:2); **$[\alpha]_D$:** -4.2 (*c* 1, CH_3OH)

^{1}H NMR (CD_3OD): (*all-E*) isomer. δ 6.38 – 5.94 (m, 8H), 5.84 – 5.63 (m, 2H), 4.71 – 4.62 (m, 1H), 4.02 – 3.87 (m, 1H), 3.86 – 3.71 (m, 2H), 2.45 – 2.13 (m, 4H), 1.77 (d, *J* = 6.5 Hz, 3H).

ESI-MS *m/z* $C_{18}H_{25}NO_2$ $[M+Na]^+$ Found: 310.1779; Calculated: 310.1783; $[M+H]^+$ Found:288.1954; Calculated: 288.1964.

Analytical HPLC for RBM4-19: Column (Kromasil 100, C18, 5 µm, 15 x 0.4 cm). Isocratic method (60:40, Buffer sodium acetate (pH=4.8, 140 mM):ACN). Sample volume: 50 µL; RBM4-19 (1mg/ mL DMSO); Rt: 8.8 min (*E*-isomer) (λ: 331 nm).

(5*E*,7*E*,9*E*)-undeca-5,7,9-trien-1-yne (RBM4-24)

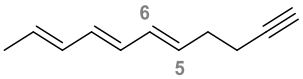

To a suspension of 4-pentyn-1-yltriphenylphosphonium iodide (6.3 g, 13.8 mmol) in anhydrous THF (150 mL) under argon atmosphere was added HMPA (7.5 mL, 5% vol) at RT and then cooled to -78 ºC. To the reaction mixture was added dropwise a solution of BuLi (2.5 M in hexane, 5.8 mL, 14.6 mmol) and then was warmed to 0 ºC with stirring for 1 h. After cooling the reddish orange solution to -78 ºC, *trans,trans*-2,4-hexadienal (1 mL, 8.6 mmol) was added dropwise under argon atmosphere and

protected from light. After 4 h the conversion was complete. Then MeOH (60 mL) was added at -78 ºC and the resulting mixture was gradually warmed overnight to RT. The mixture was concentrated under reduced pressure and then extracted with Et_2O (3 x 50 mL). The combined organic layers were washed with brine, dried over $MgSO_4$, and concentrated. The residue was purified by flash column chromatography (hexane) to afford RBM4-24 as a pale yellow oil (80%, (5*Z:E*,7*E*,9*E*); (1:1,1,1)).

*(E)-Isomerization C5-C6 double bond***:**

To a mixture of isomers RBM4-24 (50 mg, 0.3 mmol) (5*Z*:*E*,7*E*,9*E*), (1:1,1,1) in hexane (125 mL) under argon atmosphere, was added a saturated solution of iodine in hexane (5 µL). The resulting solution was heated at 69 ºC for 20 min, after which the solution was cooled to RT. The mixture was washed thoroughly with saturated aqueous sodium metabisulfite ($Na_2S_2O_5$), destroying the remaining iodine. The yellow solution was washed with water, dried, and concentrated under reduced pressure furnishing a quantitative RBM4-24 as a pale yellow oil (5*Z*:*E*,7*E*,9*E*); (1:4,1,1).

Rf: 0.36 (hexane)

^{1}H NMR ($CDCl_3$): (5*E*,7*E*,9*E*) δ 6.23 – 6.00 (m, 4H), 5.78 – 5.62 (m, 2H), 2.37 – 2.22 (m, 2H), 1.97 (t, *J* = 2.5 Hz, 1H), 1.77 (dd, *J* = 7.0, 1.5 Hz, 3H). **(5*Z*,7*E*,9*E*)** δ 6.42 – 6.29 (m, 1H), 6.23 – 6.02 (m, 3H), 5.81 – 5.66 (m, 1H), 5.49 – 5.38 (m, 1H), 2.47 – 2.39 (m, 2H), 2.29 – 2.22 (m, 2H), 1.97 (t, *J* = 3.0 Hz, 1H), 1.79 (d, *J* = 7.0 Hz, 3H).

^{13}C NMR ($CDCl_3$): (5*E*,7*E*,9*E*) 131.9 (CH), 131.8 (CH), 131.5 (CH), 130.2 (CH), 130.1 (CH), 129.6 (CH), 84.0 (C), 68.8 (CH), 31.9 (CH_2), 18.8 (CH_2), 18.4 (CH_3). **(5*Z*,7*E*,9*E*)** 133.8 (CH), 131.8 (CH), 130.3 (CH), 130.2 (CH), 129.0 (CH), 125.4 (CH), 84.0 (C), 68.8 (CH), 27.1 (CH_2), 19.0 (CH_2), 18.5 (CH_3).

Analytical HPLC for RBM4-24: Column (Kromasil 100, C18, 5 µm, 15 x 0.4 cm). Isocratic method (30:70, H_2O:ACN). Sample volume: 25 µL; RBM4-24 (1mg/ mL DMSO); Rt:6.6 min (*Z*-isomer); Rt: 7.1 min (*E*-isomer) (λ: 254 nm).

(*S*)-*tert*-Butyl 4-((*R*,6*E*,8*E*,10*E*)-1-hydroxydodeca-6,8,10-trien-2-yn-1-yl)-2,2-dimethyloxazolidine-3-carboxylate (RBM4-25)

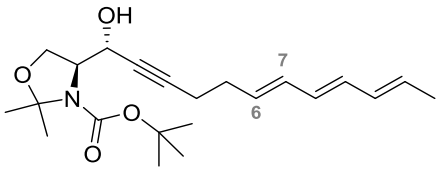

To a stirred solution of alkyne RBM4-24 (400mg, 2.4 mmol) in anhydrous THF (40 mL), was added dropwise a solution of LDA (3.3 mmol, 1.8 M in THF/heptane/ethylbenzene) at -78 ºC under argon atmosphere. The mixture was stirred at -78 ºC for 30 min, and then was added a solution of Garner's aldehyde (815 mg, 3.6 mmol) in THF (20 mL). After 3 h, a saturated aqueous NH_4Cl (5 mL) solution was added to the reaction mixture at -78ºC and was warmed to RT. The resulting white suspension was diluted with H_2O, and extracted with Et_2O (3X50 mL). The combined organic layers were dried over $MgSO_4$ and concentrated under reduced pressure. The residue was purified by flash column chromatography (hexane:EtOAc; 90:10) to afford *erythro*-RBM4-25 in 45% yield as a mixture of isomers (6*Z*:*E*; 1:1). Despite performing a carefully purification, the desired product was isolated with part of the Garner's aldehyde excess.

Rf: 0.34 (hexane:EtOAc; 8:2); **$[\alpha]_D$:** -22.6 (*c* 1.3, $CHCl_3$, mixture of isomers)

^{1}H NMR ($CDCl_3$): Data described for (*all-E*)-isomer. *δ* 6.25 – 5.95 (m, 4H), 5.77 – 5.60 (m, 2H), 4.62 – 4.40 (m, 1H), 4.21 – 3.82 (m, 3H), 2.33 – 2.25 (m, 4H), 1.76 (d, *J* = 7.0 Hz, 3H), 1.51 (s, 6H), 1.49 (s, 9H).

^{13}C NMR ($CDCl_3$): Some splitting observed due to rotamers. *δ* 154.2 (C), 133.6 (CH), 131.8 (CH), 131.7 (CH), 130.1 (CH), 129.4 (CH), 125.4 (CH), 95.0 (C), 85.8 (C), 81.3 (C), 78.7 (C), 64.8 (CH_2), 64.0 (CH), 62.8 (CH), 32.0 (CH_2), 28.5 (CH_3), 28.3 (CH_3), 19.1(CH_2), 18.3 (CH_3).

ESI-MS *m/z* $C_{22}H_{33}NO_4$ $[M+Na]^+$ Found:398.2315; Calculated: 398.2307.

(2*S*,3*R*,8*E*,10*E*,12*E*)-1,3-dihydroxytetradeca-8,10,12-trien-4-yn-2-aminium chloride (RBM4-26)

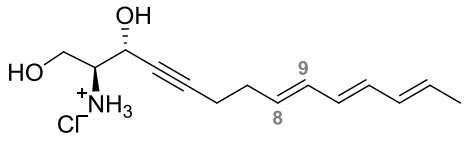

To a solution of the protected amino diol RBM4-25 (200 mg, 0.5 mmol) in MeOH (36mL) was added dropwise acetyl chloride (540 µL, 1.5% vol) at -30 ºC. The resulting mixture was vigorously stirred and warmed to RT for 30 min. Next addition of a saturated $NaHCO_3$ aqueous solution and concentration under reduce pressure, afforded a dark green crude. The crude was dissolved in DCM, dried over $MgSO_4$, filtrated through a cotton pad and then the solvent was concentrated under reduced pressure. The resulting solid RBM4-26 hydrochloride (mixture of isomers 8*Z:E*; 1:2) was obtained in 60% yield and characterized without further purification

Rf: 0.60 (DCM:MeOH; 8:2); **$[\alpha]_D$:** -3.1 (*c* 1.2, CH_3OH, mixture of isomers)

^{1}H NMR (CD_3OD): Data described for (*all-E*)-isomer. δ 6.46 – 5.93 (m, 4H), 5.86 – 5.60 (m, 2H), 4.71 – 4.60 (m, 1H), 3.99 – 3.74 (m, 2H), 3.35 – 3.27 (m, 1H), 2.46 – 2.23 (m, 4H), 1.77 (d, *J* = 7.0 Hz, 3H).

^{13}C NMR (CD_3OD): δ 131.7 (CH), 131.7 (CH), 131.6 (CH), 131.1 (CH), 129.9 (CH), 128.6 (CH), 87.4 (C), 76.4 (C), 59.3 (CH), 58.4 (CH_2), 57.2 (CH), 31.3 (CH_2), 18.3 (CH_2), 17.0 (CH_3).

ESI-MS *m/z* $C_{14}H_{21}NO_2$ $[M+H]^+$ Found:236.1655; Calculated: 236.1651.

(*S*)-*tert*-Butyl 4-((*R*:*S*,2*E*,6*E*,8*E*,10*E*)-1-hydroxydodeca-2,6,8,10-tetraen-1-yl)-2,2-dimethyloxazolidine-3-carboxylate (RBM4-27)

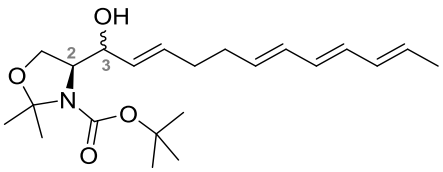

To a flame-dried Schlenk with $Cp_2Zr(H)Cl$ (350 mg, 1.4 mmol), was added a solution of alkyne RBM4-24 (200 mg, 1.4 mmol) in anhydrous DCM (1.7 mL) at 0 ºC under argon atmosphere and protected from light. During warming to room temperature, the zirconocene complex gradually dissolved to give a clear orange solution (20 min). A solution of the Garner's aldehyde (224 mg, 1.0 mmol) in DCM (1.2 mL) was added

followed by $AgClO_4$ (20% mol). After 20 min, the reaction mixture turned dark red and was monitored by TLC. The system was diluted with Et_2O and quenched by addition of 3 mL saturated $NaHCO_3$ aqueous solution. The mixture was filtered through a Celite ® pad, and the products were extracted with Et_2O (10 mL x 3). The combined ethereal solution were washed with brine, dried and concentrated under reduced pressure. Purification with flash column chromatography (hexane:EtOAc; stepwise gradient from 0 to 12% of EtOAC) afforded RBM4-27 (50%) as a mixture of diastereomers (*anti:syn* = 1:1) and additional 15% of byproducts.

Rf: (2*S*, 3*R*) 0.38; **(2*S*, 3*S*)** 0.32 (hexane:EtOAc; 8:2)

^{1}H NMR ($CDCl_3$): Signals corresponding to the mixture (*anti:syn* = 1:1). **(2*S*,3*R:S*)** δ 6.19 – 5.93 (m, 4H), 5.77 – 5.57 (m, 3H), 5.51 – 5.38 (m, 1H), 4.45 – 3.73 (m, 5H), 2.24 – 1.96 (m, 4H), 1.74 (d, *J* = 6.5 Hz, 3H), 1.47 (s, 6H), 1.46 (s, 9H).

^{13}C NMR ($CDCl_3$): (2*S*,3*R:S*) δ 152.8 (C), 133.0 (CH), 132.4 (CH), 131.9 (CH), 131.3 (CH), 131.2 (CH), 130.5 (CH), 130.4 (CH), 129.9 (CH), 94.6 (C), 81.2 (C), 74.1 (CH), 65.0 (CH_2), 62.4 (CH), 32.5 (CH_2), 32.3 (CH_2), 28.5 (2 CH_3), 18.4 (CH_3).

ESI-MS *m/z* $C_{22}H_{35}NO_4$ $[M+Na]^+$ Found: 400.2379; Calculated: 400.2464.

Analytical HPLC for (*all-E*) RBM4-27: Column (Kromasil 100, C18, 5 µm, 15 x 0.4 cm). Isocratic method (30:70, H_2O:ACN). Sample volume: 25 µL; RBM4-27 (1mg/ mL DMSO); Rt: 11.5 min (2*S*,3*S*); Rt: 12.3 min (2*S*,3*R*) (λ: 254 nm).

(2*S*,3*R*:*S*,4*E*,8*Z*:*E*,10*E*,12*E*)-1,3-Dihydroxytetradeca-4,8,10,12-tetraen-2-aminium chloride (RBM4-29)

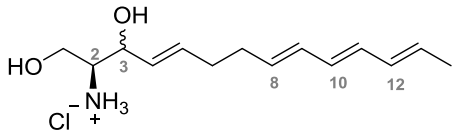

To a solution of the protected amino diol RBM4-27 (2*S*, 3*R:S* 1:1) (4*E*,8*Z:E*,10*E*,12*E*) (1,4:3,1,1) (185 mg, 0.5 mmol) in MeOH (30 mL) was added dropwise acetyl chloride (900 µL, 3% vol). The resulting mixture was vigorously stirred at RT for 30 min. Next addition of a saturated $NaHCO_3$ aqueous solution and concentration under reduce pressure, afforded a dark green crude. The crude was dissolved in DCM, dried over $MgSO_4$, filtrated through a cotton pad and then the solvent was concentrated under reduced pressure. RBM4-29 hydrochloride (8*Z:E*; 1:2) was obtained as a solid in quantitative yield and characterized without further purification.

Rf: (2*S*,3*R:S*) 0.40 (DCM:MeOH; 85:15)

^{1}H NMR ($CDCl_3$): Mixture (*anti:syn* = 1:1). **(2*S*,3*R:S*) (4*E*,8*E*,10*E*,12*E*)** *δ* 6.26 – 5.80 (m, 5H), 5.76 – 5.42 (m, 3H), 4.47 – 4.26 (m, 1H), 3.92 (s, 1H), 3.84 – 3.42 (m, 2H), 3.31 – 3.20 (m, 1H), 2.27 – 2.04 (m, 4H), 1.76 (d, *J* = 7.0 Hz, 3H). **(2*S*,3*R:S*) (4*Z*,8*E*,10*E*,12*E*)** *δ* 6.54 – 6.27 (m, 2H), 6.21 – 6.02 (m, 3H), 5.81 – 5.53 (m, 2H), 5.53 – 5.42 (m, 1H), 5.40 – 5.30 (m, 1H), 4.13 – 4.05 (m, 1H), 3.77 – 3.58 (m, 2H), 3.01 (s, 1H), 2.94 – 2.71 (m, 1H), 2.32 – 2.23 (m, 2H), 2.20 – 2.10 (m, 2H), 1.77 (d, *J* = 7.0 Hz, 3H).

^{13}C NMR ($CDCl_3$): (2*S*,3*R:S*) (4*E*,8*E*,10*E*,12*E*) *δ* 133.5 (CH), 133.0 (CH), 131.9 (CH), 131.3 (CH), 130.5 (CH), 130.4 (CH), 129.9 (CH), 129.5 (CH), 73.2 (CH), 63.8 (CH_2), 56.8 (CH), 32.4 (CH_2), 32.2 (CH_2), 18.4 (CH_3). **(2*S*,3*R:S*) (4*Z*,8*E*,10*E*,12*E*)** *δ* 133.5 (CH), 133.4 (CH), 131.8 (CH), 131.4 (CH), 130.4 (CH), 130.3 (CH), 130.2 (CH), 125.6 (CH), 74.6 (CH), 63.4 (CH_2), 56.3 (CH), 32.4 (CH_2), 27.5 (CH_2), 18.5 (CH_3).

ESI-MS *m/z* $C_{14}H_{23}NO_2$ $[M+Na]^+$ Found**:** 260.1610; Calculated: 260.1626.

Analytical HPLC for (*all-E*) RBM4-29: Column (Kromasil 100, C18, 5 µm, 15 x 0.4 cm). Isocratic method (25:75, buffer sodium acetate (pH:4.8, 140 mM) : ACN). Sample volume: 25 µL; RBM4-29 (1mg/ mL DMSO); Rt: 17.6 min (2*S*,3*S*); Rt: 19.7 min (2*S*,3*R*) (λ: 254 nm).

(*S*) *tert*-Butyl 4-(*R*:*S*(2*E*,6*E*,8*E*,10*E*,12*E*,14*E*)-1-hydroxyhexadeca-2,6,8,10,12,14-hexaen-1-yl)-2,2-dimethyloxazolidine-3-carboxylate (RBM4-31)

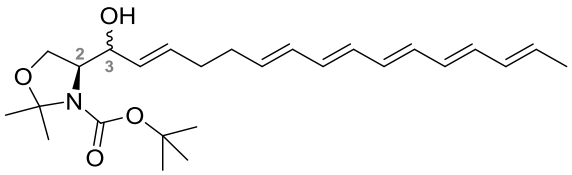

To a flame-dried Schlenk containing 100 mg of $Cp_2Zr(H)Cl$ (0.4 mmol), was added a solution of the alkyne RBM4-17 (75 mg, 0.4 mmol) in anhydrous DCM (0.4 mL) at 0 ºC under argon atmosphere and protected from light. During warming to room temperature, the zirconocene complex gradually dissolved to give a pale orange solution after 20 min of stirring. A solution of the Garner's aldehyde (60 mg, 0.3 mmol) in DCM (0.3 mL) was added followed by $AgClO_4$ (20% mol). After 20 min, the reaction mixture turned dark red, was diluted with Et_2O and was quenched by addition of 1 mL saturated $NaHCO_3$ aqueous solution. The mixture was filtered through a Celite ® pad, and the products were extracted with Et_2O (5 mL x 3). The combined ethereal solution

were washed with brine, dried and concentrated under reduced pressure. Purification with flash column chromatography (hexane:EtOAc; stepwise gradient from 0 to 18% of EtOAc) afforded (*all-E*)-RBM4-31 (20%) as a mixture of diastereomers (*anti:syn* ~ 1:1) and additional 20% of byproducts.

Rf: (2*S*,3*R:S*) 0.30 (hexane:EtOAc; 8:2)

^{1}H NMR ($CDCl_3$): Signals corresponding to the (*all-E*)-(mixture *anti:syn* ~ 1:1). **(2*S*,3*R:S*)** δ 6.28 – 6.00 (m, 7H), 5.80 – 5.58 (m, 3H), 5.56 – 5.37 (m, 2H), 4.44 – 4.30 (m, 1H), 4.26 – 4.06 (m, 2H), 4.06 – 3.77 (m, 3H), 2.25 – 2.11 (m, 4H), 1.78 (dd, *J* = 7.5, 1.5 Hz, 3H), 1.50 (s, 6H), 1.48 (s, 9H).

^{13}C NMR ($CDCl_3$): (2*S*,3*R:S*) δ 159.3 (C), 133.1 (CH), 132.9 (CH), 132.8 (CH), 132.8 (CH), 132.8 (CH), 132.7 (CH), 132.5 (CH), 132.1 (CH), 131.4 (CH), 131.2 (CH), 130.8 (CH), 130.1 (CH), 118.0 (C), 94.6 (C), 74.0 (CH), 65.0 (CH_2), 62.4 (CH), 32.6 (CH_2), 32.3 (CH_2), 28.6 (CH_3), 26.5 (CH_3), 18.6 (CH_3).

ESI-MS *m/z* $C_{26}H_{39}NO_4$ $[M+Na]^+$ Found: 452.2776; Calculated: 452.2777; $[M+H]^+$ Found:430.2995; Calculated: 430.2957.

Ethyl (2*E*,4*E*,6*E*,8*E*,10*E*)-dodeca-2,4,6,8,10-pentaenoate (RBM4-32)

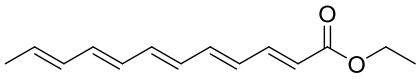

To a suspension of NaH (60% in mineral oil, 750 mg, 19 mmol) in anhydrous THF (60 mL) at 0 °C was slowly added the triethyl phosphonoacetate (3 mL, 15 mmol). After 1 h of stirring at 0 ºC, a solution of aldehyde RBM4-4 (1.4 g, 9.5 mmol) in THF (20 mL) was added to the system. The reaction mixture was stirred at 0 °C for 2 h, protected from light, before being quenched by saturated NH_4Cl (50 mL). The product was extracted with ethyl acetate (3 x 30 mL). The combined extracts were washed with brine, dried and concentrated. The crude was purified by flash column chromatography (hexane:EtOAc; 98:2), to afford (*all-E*)-RBM4-32 (75%) as a yellow solid.

Rf: 0.68 (hexane:EtOAc; 9:1)

^{1}H NMR ($CDCl_3$) δ 7.31 (dd, *J* = 15.5, 12.0 Hz, 1H), 6.58 (dd, *J* = 15.0, 11.0 Hz, 1H), 6.45 – 6.08 (m, 6H), 5.85 (d, *J* = 15.5 Hz, 1H), 5.85 – 5.75 (m, 1H), 4.20 (q, *J* = 7.0 Hz, 2H), 1.80 (dd, *J* = 6.0, 1.0 Hz, 3H), 1.29 (t, *J* = 7.0 Hz, 3H).

^{13}C NMR ($CDCl_3$) *δ* 167.3 (C), 144.6 (CH), 141.0 (CH), 137.7 (CH), 136.0 (CH), 132.2 (CH), 131.9 (CH), 131.2 (CH), 130.1 (CH), 129.5 (CH), 120.4 (CH), 60.4 (CH_2), 18.6 (CH_3), 14.5 (CH_3).

ESI-MS *m/z* $C_{14}H_{18}O_2$ $[M+H]^+$ Found: 219.1366 Calculated: 219.1385.

(2*E*,4*E*,6*E*,8*E*,10*E*)-Dodeca-2,4,6,8,10-pentaen-1-ol (RBM4-33)

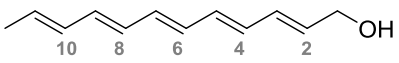

A solution of 1*M* DIBAL-H in toluene (5.7 mL, 5.7 mmol) was added dropwise over a solution of ethyl ester RBM4-32 (248 mg, 1.1 mmol) in DCM (8 mL) at -78 ºC. After stirring for 2h at this temperature, the mixture was quenched with an aqueous solution of Rochelle's salt (7 mL) and allowed to warm to RT. The reaction mixture was extracted with DCM (3 x 10 mL) and the combined organic phases were washed with brine, dried and concentrated to give a yellowish solid RBM4-33 as a mixture of isomers (2*Z:E*; 1:6). The product was used in the next step without further purification.

Rf: 0.44 (hexane:EtOAc; 7:3)

^{1}H NMR ($CDCl_3$): Data for (*all-E*) deduced from a (2*Z:E*; 1:6) mixture of isomers. **(2*E*,4*E*,6*E*, 8*E*,10*E*)** *δ* 6.34–6.06 (m, 8H), 5.89–5.80 (m, 1H), 5.79–5.69 (m, 1H), 4.21 (d, *J* = 6.0 Hz, 2H), 1.79 (dd, *J* = 7.0, 1.5 Hz, 3H).

^{13}C NMR ($CDCl_3$): **(2*E*,4*E*,6*E*, 8*E*,10*E*)** *δ* 134.0 (CH), 133.6 (CH), 132.6 (CH), 132.5 (CH), 132.2 (CH), 131.9 (CH), 131.9 (CH), 129.8 (CH), 128.7 (CH), 128.7 (CH), 63.6 (CH_2), 18.6 (CH_3).

(2*E*,4*E*,6*E*,8*E*,10*E*)-dodeca-2,4,6,8,10-pentaen-1-yl 4-((((9H-fluoren-9-yl)methoxy)-carbonyl)amino)butanoate (RBM4-34)

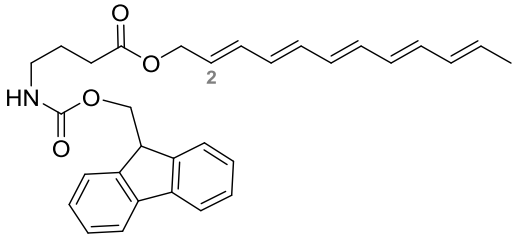

To a solution of EDC (990 mg, 5.2 mmol) and HOBt (517 mg, 5.1 mmol) in anhydrous DCM (10 mL) was added, dropwise, a solution of the commercial 4-(Fmoc-

amino)butyric acid (770 mg, 2.4 mmol) in DCM (5 mL). After 10 min of stirring, this mixture was added at RT to a solution containing alcohol RBM4-33 (570 mg, 3.2 mmol) and Et_3N (0.93 mL, 6.5 mmol) in DCM (10 mL). The mixture was vigorously stirred overnight and then quenched with H_2O. The organic phase was extracted with 3 X 30 mL DCM, washed with Brine, dried over $MgSO_4$ and concentrated under reduced pressure. The resulting crude was purified by flash column chromatography (DCM:MeOH; 99:1) to give RBM4-34 (2*Z:E*; 1:6) as a yellowish solid in <20% yield.

Rf: 0.64 (hexane:EtOAc; 7:3)

^{1}H NMR ($CDCl_3$) Data for (*all-E*) deduced from a (2*Z:E*; 1:6) mixture of isomers **(2*E*,4*E*,6*E*, 8*E*,10*E*)**.*δ* 7.76 (dd, *J* = 7.5, 1.5 Hz, 2H), 7.59 (dd, *J* = 7.5, 1.0 Hz, 2H), 7.40 (td, *J* = 7.5 Hz, 1.0 Hz, 2H), 7.31 (td, *J* = 7.5, 1.0 Hz, 2H), 6.38 – 6.03 (m, 8H), 5.81 – 5.69 (m, 2H), 4.95 (s, 1H), 4.61 (d, *J* = 7.0 Hz, 2H), 4.40 (d, *J* = 7.0 Hz, 2H), 4.21 (t, *J* = 7.0 Hz, 1H), 3.25 (dd, *J* = 12.5, 6.0 Hz, 2H), 2.37 (t, *J* = 7.0 Hz, 2H), 1.89 – 1.82 (m, 2H), 1.79 (dd, *J* = 7.0, 1.0 Hz, 3H).

^{13}C NMR (**$CDCl_3$**) **(2*E*,4*E*,6*E*, 8*E*,10*E*)** *δ* 173.1 (C), 156.5 (C), 144.1 (C), 141.4 (C), 135.0(CH), 134.7 (CH), 134.5 (CH), 134.1 (CH), 132.0 (CH), 131.7 (CH), 131.3 (CH), 130.9 (CH), 130.9 (CH), 130.4 (CH), 129.7 (CH), 129.0 (CH), 128.7 (CH), 127.8 (CH), 127.2 (CH), 126.1 (CH), 125.1 (CH), 120.1 (CH), 66.7 (CH_2), 65.1 (CH_2), 47.4 (CH), 40.5 (CH_2), 31.6 (CH_2), 25.2 (CH_2), 18.5 (CH_3).

ESI-MS *m/z* $C_{31}H_{33}NO_4$ $[M+Na]^+$ Found: 506.2320 Calculated: 506.2307; $[M+H]^+$ Found: 484.2491 Calculated: 484.2488.

(2*E*,4*E*,6*E*,8*E*,10*E*)-Dodeca-2,4,6,8,10-pentaen-1-yl 4-palmitamidobutanoate (RBM4-35)

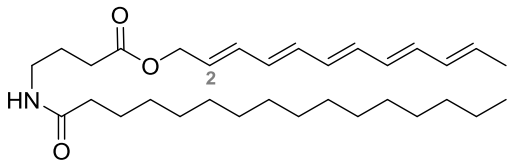

A solution of EDC (10 mg, 50 µmol) in anhydrous DCM (600 µL) was added dropwise over a solution of acid **5** (13 mg, 40 µmol) in DCM (600 µL) at 0 ºC. After 30 min stirring at RT, the mixture was cooled to 0 ºC and treated with 100 µL of a 0.35 *M* solution of RBM4-33 in THF (equivalent to 6 mg, 35 µmol) followed by the addition of solid DMAP (4.5 mg, 40 µmol). The resulting reaction mixture was allowed to stir at RT for 16h and next quenched with H_2O (1 mL) and extracted with DCM (3 x 3 mL). The combined organic phases were dried and concentrated to give crude, which were flash

chromatographed (hexane:EtOAc; 8:2) to afford RBM4-35 (2*Z:E*; 1:6) as a yellowish solid in 30% yield.

Rf = 0.26 (Hexane:EtOAc, 7:3).

^{1}H NMR ($CDCl_3$): Data for (*all-E*) deduced from a (2*Z:E*; 1:6) mixture of isomers. **(2*E*,4*E*,6*E,* 8*E*,10*E*)** *δ* 6.38 – 6.03 (m, 6H), 5.80 – 5.69 (m, 2H), 5.63 (s, 1H), 4.62 (dd, *J* = 7.0, 1.0 Hz, 2H), 3.29 (dd, *J* = 13.0, 6.5 Hz, 2H), 2.42 – 2.35 (m, 2H), 2.16– 2.11 (m, 2H), 1.87 – 1.82 (m, 2H), 1.79 (dd, *J* = 7.0, 1.5 Hz, 3H), 1.46 – 1.39 (m, 2H), 1.25 (s, 26H), 0.88 (t, *J* = 7.0 Hz, 3H).

^{13}C NMR ($CDCl_3$): (2*E*,4*E*,6*E,* 8*E*,10*E*) *δ* 173.4 (C), 173.4 (C), 135.1 (CH), 134.8 (CH), 134.6 (CH), 134.2 (CH), 132.0 (CH), 131.7 (CH), 131.0 (CH), 130.9 (CH), 130.4 (CH), 126.0 (CH), 65.2 (CH_2), 39.1 (CH_2), 37.0 (CH_2), 32.1 (CH_2), 31.9 (CH_2), 29.9 (CH_2), 29.82 (CH_2), 29.79 (CH_2), 29.7 (CH_2), 29.52 (CH_2), 29.49 (CH_2), 29.48 (CH_2), 25.9 (CH_2), 24.8 (CH_2), 22.9 (CH_2), 18.6 (CH_3), 14.3 (CH_3).

ESI-MS *m/z* $C_{32}H_{53}NO_3$ $[M+Na]^+$ Found: 522.3849 Calculated: 522.3923; $[M+H]^+$ Found: 500.4093 Calculated: 500.4104.

Φ_F (λ_{ex}: 346 nm, ethanol, ref 9,10-DPA): 0.060; ***ε*** (λ_{ex} max = 325nm): 16028 M^{-1}•cm^{-1}.

Decyl 4-octanamidobutanoate (RBM4-36)

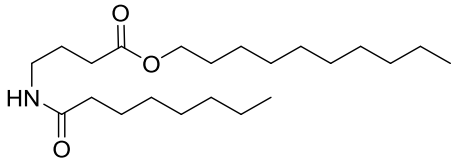

To a solution of EDC (9 mg, 0.05 mmol) and HOBt (5 mg, 0.04 mmol) in anhydrous DMF (500 μL) was added, dropwise, a solution of octanoic acid (6 μL, 0.04 mmol). After 10 min of stirring, this mixture was added at RT to a solution containing compound **2** (14 mg, 0.03 mmol), KF (7 mg, 0.1 mmol) and Et_3N (8 μL, 0.06 mmol) in DMF (500 μL). The mixture was vigorously stirred overnight. After dilution with EtOAc (5 mL), the mixture was washed with 5% aqueous HCl solution (2 X 1 mL) and 5% aqueous $NaHCO_3$ solution (2 X 1 mL). The aqueous layers were combined and extracted with EtOAc (2 X 2 mL). The organic layer was dried, filtered, and concentrated. The resulting crude was purified by flash column chromatography (hexane:EtOAc; 7:3) to afford RBM4-36 in 40% yield as a white solid.

Rf: 0.3 (hexane:EtOAc; 7:3)

^{1}H NMR ($CDCl_3$) δ 5.64 (s, 1H), 4.04 (t, *J* = 7.0 Hz, 2H), 3.28 (dd, *J* = 12.5, 7.0 Hz, 2H), 2.34 (t, *J* = 7.0 Hz, 2H), 2.16 – 2.10 (m, 2H), 1.82 (p, *J* = 7.0 Hz, 2H), 1.60 (dt, *J* = 13.5, 6.9 Hz, 4H), 1.34 – 1.19 (m, 22H), 0.89 – 0.83 (m, 6H).

^{13}C NMR ($CDCl_3$) δ 173.6 (C), 173.2 (C), 64.8 (CH_2), 38.9 (CH_2), 36.8 (CH_2), 31.84 (CH_2), 31.78 (CH_2), 31.7 (CH_2), 29.49 (CH_2), 29.48 (CH_2), 29.3 (CH_2), 29.23 (CH_2), 29.21 (CH_2), 29.0 (CH_2), 28.6 (CH_2), 25.9 (CH_2), 25.7 (CH_2), 24.6 (CH_2), 22.64 (CH_2), 22.57 (CH_2), 14.1 (CH_3), 14.0 (CH_3).

ESI-MS *m/z* $C_{22}H_{43}NO_3$ $[M+Na]^+$ Found: 392.3138 Calculated: 392.3141; $[M+H]^+$ Found: 370.3310 Calculated: 370.3321.

Synthesis of intermediate RBM4-38

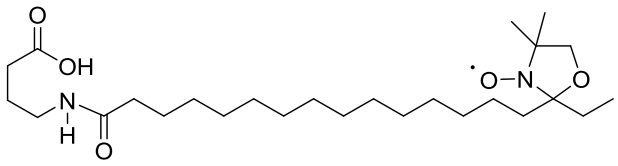

a) ***N*-acylation**: A solution of the free radical 16-DOXYL stearic acid (20 mg, 50 μmol) in anhydrous DCM (500 μL) was added dropwise over a solution of EDC (16 mg, 80 μmol) and HOBt (8 mg, 60 μmol) in DCM (1 mL). The mixture was allowed to react for 10 min and next added dropwise at RT over a solution of ester **3** (9.5 mg, 62 μmol) in DCM (1.5 mL) containing Et_3N (15 μL, 100 μmol). After 2h, the reaction mixture was quenched with H_2O (5 mL) and extracted with DCM (3 x 3 mL). The combined organic phases were washed with brine, dried and concentrated to give a residue. Flash-chromatography (DCM:MeOH; 98:2) afforded a quantitative amidoester RBM4-37, which was used immediately in the next synthetic step.

b) **Hydrolysis of amidoester RBM4-37**: Lithium hydroxide (5 mg, 200 μmol) was added in one portion over a solution of RBM4-37 (25 mg, 50 μmol) in a mixture of THF (240 μL) and H_2O (110 μL) at RT. The resulting yellow reaction mixture was allowed to stir at RT for 1.5 h and next concentrated under reduced pressure to give a solid, which was taken up in H_2O and acidified to pH=3 by addition of 1*M* HCl aqueous solution. The acidic aqueous phase was extracted with EtOAc (3 x 5 mL) and the combined organic layers were dried and concentrated to afford crude, which were purified by flash column chromatography (DCM:MeOH; 96:4) to give RBM4-38 as a yellowish solid in 65% yield.

Rf: 0.42 (DCM:MeOH; 95:5)

^{1}H NMR ((1:1) CD_3OD: $CDCl_3$): δ 3.19 (app.t, J = 7.0 Hz, 2H), 2.48 – 2.38 (m, 4H), 2.36 – 2.26 (m, 2H), 2.14 (app.t, J = 7.5 Hz, 2H), 1.78 (p, J = 7.0 Hz, 2H), 1.64 – 1.50 (m, 4H), 1.38 – 1.17 (m, 27H), 1.01 (t, J = 7.5 Hz, 3H), 0.94 – 0.84 (m, 3H).

^{13}C NMR ((1:1) CD_3OD: $CDCl_3$): Some splitting observed due to rotamers δ 175.7 (C), 119.0 (C), 70.4 (C), 42.9 (CH_2), 39.3 (CH_2), 36.99 (CH_2), 36.3 (CH_2), 32.2 (CH_2), 30.4 (CH_2), 30.23 (CH_2), 30.18 (CH_2), 30.14 (CH_2), 30.11 (CH_2), 30.08 (CH_2), 30.04 (CH_2), 29.99 (2 CH_3), 29.93 (CH_2), 29.89 (CH_2), 29.84 (CH_2), 29.81 (CH_2), 29.75 (CH_2), 26.5 (CH_2), 25.2 (CH_2), 24.4 (CH_2), 8.00 (CH_3).

Synthesis of compound RBM4-39

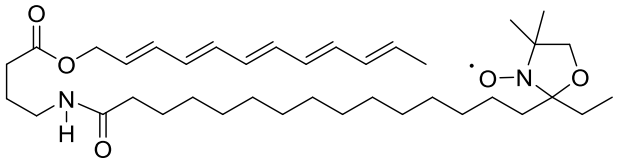

A solution of EDC (8 mg, 42 µmol) in anhydrous DCM (600 µL) was added dropwise over a solution of acid RBM4-38 (13 mg, 28 µmol) in DCM (400 µL) at 0 ºC. After 30 min stirring at RT, the mixture was cooled to 0 ºC and treated with 100 µL of a 0.35 *M* solution of RBM4-33 in THF (equivalent to 6 mg, 35 µmol) followed by the addition of solid DMAP (3.5 mg, 30 µmol). The resulting reaction mixture was allowed to stir at RT for 6h and next quenched with H_2O (1 mL) and extracted with DCM (3 x 3 mL). The combined organic phases were dried and concentrated to give crude, which were flash chromatographed (hexane:EtOAc; 65:35) to afford RBM4-39 (*all-E*) as a yellowish solid in 40% yield.

Rf = 0.18 (Hexane:EtOAc; 7:3).

^{1}H NMR ($CDCl_3$): δ 6.39–6.04 (m, 8H), 5.82–5.68 (m, 2H), 4.62 (d, J = 6.0 Hz, 2H), 3.36–3.26 (m, 2H), 2.44–2.33 (m, 2H), 2.20–2.09 (m, 2H), 2.08–1.98 (m, 2H), 1.80 (d, J = 6.5 Hz, 3H), 1.66–1.52 (m, 2H), 1.48–1.40 (m, 10H), 1.37–1.18 (m, 24H), 0.89 (t, J= 6.5 Hz, 3H).

^{13}C NMR ($CDCl_3$): δ 173.3 (C), 173.2 (C), 134.9 (CH), 134.7 (CH), 134.5 (CH), 134.1 (CH), 131.9 (CH), 131.6 (CH), 130.9 (CH), 130.8 (CH), 130.3 (CH), 125.9 (CH), 68.0(CH_2), 65.1 (CH_2), 38.9 (CH_2), 37.0 (CH_2), 31.9 (CH_2), 29.8 (CH_2), 29.7 (2 x CH_2), 29.65 (CH_2), 29.62 (CH_2), 29.60 (CH_2), 29.57 (CH_2), 29.52 (CH_2), 29.5 (CH_2), 29.4 (CH_2), 29.3 (CH_2), 25.8 (CH_2), 24.7 (CH_2), 18.5 (CH_2), 18.4 (CH_3), 14.1 (CH_3).

ESI-MS *m/z* $C_{38}H_{63}N_2O_5$ $[M+Na]^+$ Found: 650.4633; Calculated: 650.4635; $[M+H]^+$ Found: 628.4819; Calculated: 628.4815.

EPR: g= 2.00575, ΔH_{pp}= 1.40 G, a_N= 14.58 ($1.6x10^{-3}$ mM, DCM)

EPR (140 K in THF): A_{ZZ} = 31.80 G

Φ_F (λ_{ex}: 346 nm, ethanol, ref 9,10-DPA): 0.048; $\boldsymbol{\varepsilon}$ (λ_{ex} max = 325nm): 14972 M^{-1}•cm^{-1}.

Synthesis of intermediate RBM4-41

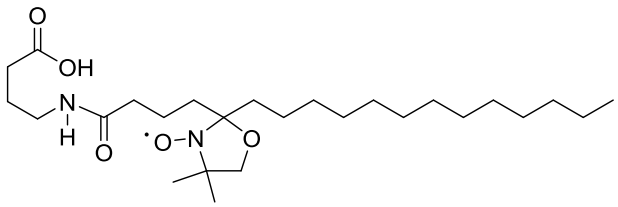

a) ***N*-acylation**: A solution of the free radical 5-DOXYL stearic acid (20 mg, 50 μmol) in anhydrous DCM (500 μL) was added dropwise over a solution of EDC (16 mg, 80 μmol) and HOBt (8 mg, 60 μmol) in DCM (1 mL). The mixture was allowed to react for 10 min and next added dropwise at RT over a solution of ester **3** (9.5 mg, 62 μmol) in DCM (1.5 mL) containing Et_3N (15 μL, 100 μmol). After 2h, the reaction mixture was quenched with H_2O (5 mL) and extracted with DCM (3 x 3 mL). The combined organic phases were washed with brine, dried and concentrated to give a residue. Flash-chromatography (DCM:MeOH; 98:2) afforded a quantitative amidoester RBM4-40, which was used immediately in the next synthetic step.

b) **Hydrolysis of amidoester RBM4-40**: Lithium hydroxide (5 mg, 200 μmol) was added in one portion over a solution of RBM4-40 (25 mg, 50 μmol) in a mixture of THF (240 μL) and H_2O (110 μL) at RT. The resulting yellow reaction mixture was allowed to stir at RT for 1.5 h and next concentrated under reduced pressure to give a solid, which was taken up in H_2O and acidified to pH=3 by addition of 1*M* HCl aqueous solution. The acidic aqueous phase was extracted with EtOAc (3 x 5 mL) and the combined organic layers were dried and concentrated to afford crude, which were purified by flash column chromatography (DCM:MeOH; 97:3) to give RBM4-41 as a white solid in 85% yield.

Rf: 0.52 (DCM:MeOH; 95:5)

^{1}H NMR ((1:1) CD_3OD: $CDCl_3$): δ 4.09 (q, *J* = 7.0 Hz, 2H), 3.19 (t, *J* = 7.0 Hz, 2H), 2.46 (app.t, *J* = 7.0 Hz, 2H), 2.40 (app.t, *J* = 7.5 Hz, 2H), 2.30 (app.t, *J* = 7.5 Hz, 2H), 2.15

(app.t, *J* = 7.5 Hz, 2H), 1.91 – 1.71 (m, 4H), 1.60 – 1.47 (m, 2H), 1.36 – 1.10 (m, 27H), 0.85 (t, *J* = 6.5 Hz, 3H).

^{13}C NMR ($CDCl_3$): Some splitting observed due to rotamers *δ* 174.6 (C), 172.6 (C), 112.9 (C), 75.7 (CH_2), 74.4 (C), 61.2 (CH_2), 43.3 (CH_2), 42.1 (CH_2), 39.3 (CH_2), 35.6 (CH_2), 32.4 (CH_2), 30.2 (CH_2), 30.13 (CH_2), 30.09 (CH_2), 29.97 (CH_2), 29.9 (CH_2), 29.8 (CH_2), 29.7 (CH_2), 25.2 (CH_2), 24.3 (CH_2), 23.2 (CH_2), 21.1 (CH_2), 20.4 (CH_2), 14.32 (CH_3), 14.31 (CH_3), 14.29 (CH_3).

Synthesis of compound RBM4-42

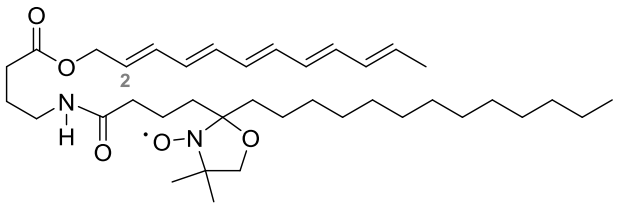

A solution of EDC (9 mg, 50 µmol) in anhydrous DCM (700 µL) was added dropwise over a solution of acid RBM4-41 (15 mg, 32 µmol) in DCM (500 µL) at 0 ºC. After 30 min stirring at RT, the mixture was cooled to 0 ºC and treated with 100 µL of a 0.35 *M* solution of RBM4-33 in THF (equivalent to 6 mg, 35 µmol) followed by the addition of solid DMAP (4 mg, 32 µmol). The resulting reaction mixture was allowed to stir at RT for 5h and next quenched with H_2O (1 mL) and extracted with DCM (3 x 3 mL). The combined organic phases were dried and concentrated to give crude, which were flash chromatographed (hexane:EtOAc; 55:45) to afford RBM4-42 (2*Z*:*E*, 1:6) as a yellowish solid in 40% yield.

Rf = 0.30 (Hexane:EtOAc; 1:1).

^{1}H NMR ($CDCl_3$): *δ* 6.39–6.06 (m, 7H), 5.81–5.70 (m, 2H), 5.37–5.32 (m, 1H), 4.62 (d, *J* = 6.0 Hz, 2H), 3.32–3.26 (m, 2H), 2.50–2.45 (m, 2H), 2.41–2.32 (m, 4H), 2.24-2.18 (m, 2H), 2.04–1.98 (m, 2H), 1.79 (d, *J* = 7.0 Hz, 3H), 1.25 (m, 36H), 0.88 (t, *J* = 6.5 Hz, 3H).

^{13}C NMR ($CDCl_3$): *δ* 169.7 (C), 169.6 (C), 135.1 (CH), 134.7 (CH), 134.3 (CH), 133.3 (CH), 132.2 (CH), 131.9 (CH), 131.1 (CH), 131.0 (CH), 130.5 (CH), 130.1 (CH), 110.5 (C), 75.3 (C), 70.2 (C), 65.2 (CH_2), 39.1 (CH_2), 43.0 (CH_2), 41.6 (CH_2), 36.1 (CH_2), 34.0 (CH_2), 32.1 (CH_2), 29.8 (CH_2), 29.4 (CH_2), 27.4 (CH_2), 26.9 (CH_2), 25.7 (CH_2), 24.0 (CH_2), 22.8 (CH_2), 18.5 (CH_3), 17.2 (CH_3), 14.2 (CH_3)

ESI-MS *m/z* $C_{38}H_{63}N_2O_5$ $[M+Na]^+$ Found: 650.4639; Calculated: 650.4635.

EPR: g= 2.00575, ΔH_{pp}= 1.37 G, a_N= 14.57 ($1.6x10^{-3}$ mM, DCM)

EPR (140 K in THF): A_{ZZ} = 32.71 G

Φ_F (λ_{ex}: 346 nm, ethanol, ref 9,10-DPA): 0.031; $\boldsymbol{\varepsilon}$ (λ_{ex} max = 325nm): 23659 M^{-1}•cm^{-1}.

tert-Butyl (*S*)-4-((*R,E*)-1-hydroxy-7-(trimethylsilyl)hept-2-en-6-yn-1-yl)-2,2-dimethyl-oxazolidine-3-carboxylate (RBM4-45)

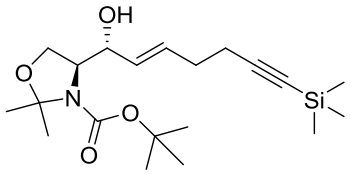

A two necked round bottom flask fitted with a reflux condenser under argon atmosphere, was charged with allylic alcohol **6** (2 g, 7.6 mmol) in 70 mL of DCM previously degassed. To the solution was added 5-hexen-1-ynyltrimethylsilane (470 mg, 3.0 mmol) and Grubbs' 2nd generation catalyst (123 mg, 0.15 mmol). The resulting mixture was stirred at reflux temperature for 5 h and then cooled down to RT. The mixture was concentrated under reduced pressure to afford a crude, which was used without further purification to next reaction, due to even after careful chromatographic separations, the desired compound was always contaminated with the excess starting allylic alcohol **6**.

Rf: 0.44 (hexane:EtOAc; 7:3)

tert-Butyl (*S*)-4-((*R,E*)-1-hydroxyhept-2-en-6-yn-1-yl)-2,2-dimethyloxazolidine-3-carboxylate (RBM4-46)

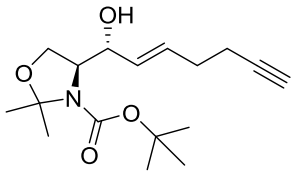

The crude mixture of RBM4-45 (900 mg, 2.4 mmol), along with the allylic alcohol **6** excess, was dissolved in 30 mL of anhydrous THF under argon atmosphere. Next, 2.6 mL of TBAF solution was added via syringe (2.6 mmol, 1M in THF). The solution turned orange immediately. The mixture was stirred for 1 h at room temperature. Then, 5 mL of a saturated aqueous NH_4Cl solution was added, and the aqueous layer was

extracted with diethyl ether. The combined organic phase was washed with brine, dried over $MgSO_4$ and then filtered. The solvent was concentrated under reduced pressure and the crude was purified by flash column chromatography (hexane:EtOAc; 100:0 to 85:15 gradient) to afford a colourless oil. The overall yield was 40% over two steps.

Rf: 0.42 (hexane:EtOAc; 7:3); **$[\alpha]_D$:** -7.8 (*c* 1, $CHCl_3$).
^{1}H NMR ($CDCl_3$): δ 5.80 (ddd, *J* = 15.5, 7.0, 5.5 Hz, 1H), 5.54 (dd, *J* = 15.5, 6.0 Hz, 1H), 4.32 – 4.19 (m, 1H), 4.18 – 4.11 (m, 1H), 4.09 – 3.80 (m, 2H), 2.35 – 2.22 (m, 4H), 1.95 (t, *J* = 2.5 Hz, 1H), 1.54 (s, 6H), 1.49 (s, 9H).
^{13}C NMR ($CDCl_3$): δ 154.3 (C), 130.8 (CH), 130.0 (CH), 94.6(C), 83.9 (C), 81.3 (C), 73.9 (CH), 68.8 (CH), 65.0 (CH_2), 62.3 (CH), 31.5 (CH_2), 28.5 (CH_3), 26.5 (CH_3), 18.6 (CH_2).
ESI-MS *m/z* $C_{17}H_{27}NO_4$ $[M+Na]^+$ Found: 332.1813; Calculated: 332.1838.

(2*S*,3*R*,*E*)-2-aminonon-4-en-8-yne-1,3-diol (RBM4-47)

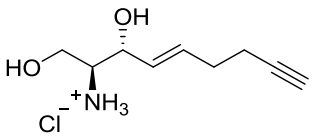

To a solution of protected amino diol RBM4-46 (120 mg, 0.4 mmol) in MeOH (22 mL) was added dropwise acetyl chloride (1.1 mL, 5%). The resulting mixture was vigorously stirred at RT for 1.5 h. Concentration under reduce pressure afforded the crude RBM4-47 in quantitative yield, which was used without further purification.

Rf: 0.14 (DCM:MeOH; 9:1); **$[\alpha]_D$:** -4.6 (*c* 1, CH_3OH).
^{1}H NMR (CD_3OD): δ 5.98 – 5.88 (m, 1H), 5.59 (dd, *J* = 15.5, 6.5 Hz, 1H), 4.34 (dd, *J* = 6.5 Hz, 1H), 3.84 (dd, *J* = 11.5, 4.0 Hz, 1H), 3.70 (dd, *J* = 11.5, 8.5 Hz, 1H), 3.29 – 3.19 (m, 1H), 2.34 – 2.28 (m, 4H), 2.27 (t, *J* = 2,5 Hz, 1H).
^{13}C NMR (CD_3OD): δ 133.9 (CH), 130.2 (CH), 84.4 (C), 71.1 (CH), 70.2 (CH), 59.8 (CH_2), 58.4 (CH), 32.4 (CH_2), 19.0 (CH_2).

***N*-((2*S*,3*R*,*E*)-1,3-dihydroxynon-4-en-8-yn-2-yl)palmitamide (RBM4-48)**

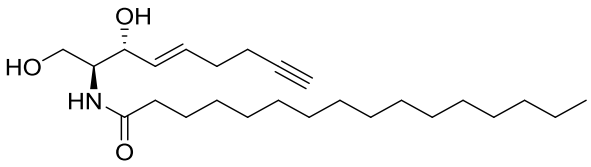

From RBM4-47:

To a solution of EDC (92 mg, 0.5 mmol) and HOBt (48 mg, 0.4 mmol) in anhydrous DCM (4mL) was added palmitic acid (85 mg, 0.3 mmol) in DCM (2mL) under argon atmosphere. The resulting mixture was vigorously stirred at RT for 10 min, and next added dropwise to a solution of the amino diol chlorate RBM4-47 (62 mg, 0.3 mmol) and Et_3N (86 µL, 0.6 mmol) in anhydrous DCM (4 mL). The reaction mixture was stirred at RT for 1h and diluted by addition of DCM (15mL), washed successively with water (15 mL) and brine (15 mL). The organic layer was dried over $MgSO_4$, and filtered and concentrated under reduced pressure. The crude was purified by flash column chromatography (DCM:MeOH; 97:3) yielding 70 % of white solid RBM4-48.

From RBM4-68:

To a stirred solution of RBM4-68 (39 mg, 0.07 mmol) in anhydrous THF (1 mL), a solution of TBAF (1.0M in THF, 99 µL, 0.1 mmol) was added dropwise at RT. After stirring at this temperature for 1 h, the reaction was quenched with water, and the resulting mixture was extracted with EtOAc. The combined organic extract was successively washed with water and brine, dried with $MgSO_4$, and concentrated under reduced pressure. The residue was purified by flash column chromatography (DCM:MeOH; 97:3) yielding 85 % of the white solid RBM4-48.

Rf: 0.74 (DCM:MeOH; 9:1); **$[\alpha]_D$:** -7.36 (*c* 1, $CHCl_3$).
^{1}H NMR ($CDCl_3$): δ 6.32 (d, *J* = 7.5 Hz, 1H), 5.88 – 5.78 (m, 1H), 5.63 (dd, *J* = 15.5, 6.0 Hz, 1H), 4.34 (td, *J* = 4.5, 2.0 Hz, 1H), 4.02 – 3.88 (m, 2H), 3.70 (dd, *J* = 11.5, 3.0 Hz, 1H), 2.31 – 2.28 (m, 4H), 2.23 (t, J = 7.5 Hz, 2H), 1.97 (t, *J* = 2.5 Hz, 1H), 1.63 (p, *J* = 7.5 Hz, 2H), 1.35 – 1.20 (m, 24H), 0.87 (t, *J* = 7.0 Hz, 3H).
^{13}C NMR ($CDCl_3$): δ 174.3 (C), 131.4 (CH), 130.8 (CH), 83.8 (C), 74.4 (CH), 69.2 (CH), 62.5 (CH_2), 54.6 (CH), 37.0 (CH_2), 32.1 (CH_2), 31.2 (CH_2), 29.8 (CH_2), 29.8 (CH_2), 29.8 (CH_2), 29.8 (CH_2), 29.7 (CH_2), 29.5 (CH_2), 29.5 (CH_2), 29.4 (CH_2), 25.9 (CH_2), 22.8 (CH_2), 18.6 (CH_2), 14.3 (CH_3).

ESI-MS *m/z* $C_{25}H_{45}NO_3$ $[M+H]^+$ Found: 408.3481 Calculated: 408.3478.

Ethyl (2*E*,4*E*,6*E*)-octa-2,4,6-trienoate (RBM4-49)

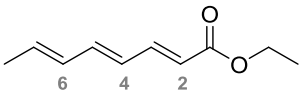

To a suspension of NaH (60% in mineral oil, 2.2 g, 54.4 mmol) in anhydrous THF (150 mL) at 0 °C was slowly added the triethyl phosphonoacetate (8.6 mL, 43.5 mmol). After 1 h of stirring at 0 ºC the *trans,trans*-2,4-hexadienal (3 mL, 27.2 mmol) was added. The reaction mixture was stirred at 0 °C for 2 h, protected from light, before being quenched by saturated NH_4Cl (100 mL). The product was extracted with ethyl acetate (3 x 70 mL). The combined extracts were washed with brine, dried and concentrated. The crude was purified by flash column chromatography (hexane:EtOAc; 95:5), to afford RBM4-49 (84% (2 *Z:E*;1:10) as a white solid.

Rf: 0.60 (hexane:EtOAc; 9:1)

^{1}H NMR ($CDCl_3$): Signals deduced from (2*Z:E*; 1:10) mixture **(2*E*,4*E*,6*E*)** δ 7.29 (dd, *J* = 15.5, 11.5 Hz, 1H), 6.52 (dd, *J* = 15.0, 11.0 Hz, 1H), 6.25 – 6.10 (m, 2H), 5.93 (dq, *J* = 14.5, 7.0 Hz, 1H), 5.83 (d, *J* = 15.0 Hz, 1H), 4.19 (qd, *J* = 7.0, 1.0 Hz, 2H), 1.82 (d, *J* = 7.0 Hz, 3H), 1.29 (td, *J* = 7.0, 1.0 Hz, 3H). **(2*Z*,4*E*,6*E*)** δ 7.36 (dd, *J* = 15.5, 11.5 Hz, 1H), 6.87 (dd, *J* = 15.0, 11.5 Hz, 1H), 6.29 (dd, *J* = 15.0, 11.5 Hz, 2H), 5.80 – 5.68 (m, 1H), 5.60 (d, *J* = 11.0 Hz, 1H), 4.19 (qd, *J* = 7.0, 1.0 Hz, 2H), 1.82 (d, *J* = 7.0 Hz, 3H), 1.29 (td, *J* = 7.0, 0.5 Hz, 3H).

^{13}C NMR ($CDCl_3$): (2*E*,4*E*,6*E*) δ 167.4 (C), 144.9 (CH), 141.2 (CH), 135.2 (CH), 131.4 (CH), 127.7 (CH), 120.2 (CH), 60.3 (CH_2), 18.7 (CH_3), 14.5 (CH_3). **(2*Z*,4*E*,6*E*)** δ 167.3 (C), 144.9 (CH), 135.7 (CH), 131.8 (CH), 129.7 (CH), 129.0 (CH), 120.7 (CH), 60.4 (CH_2), 18.7 (CH_3), 13.9 (CH_3).

ESI-MS *m/z* $C_{10}H_{14}O_2$ $[M+H]^+$ Found: 167.1033 Calculated: 167.1072.

(1*E*,3*E*,5*E*,7*E*)-1-Bromonona-1,3,5,7-tetraene (RBM4-50)

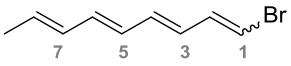

To a suspension of (bromomethyl)triphenylphosphonium bromide (2.9 g, 6.5 mmol) in anhydrous THF (40 mL), under argon atmosphere, was added HMPA (3 mL, 5% vol) at

RT and subsequently cooled to -78 ºC. To the reaction mixture was added dropwise a solution of BuLi (2.5 M in hexane, 2.8 mL, 6.9 mmol) and then was warmed to 0 ºC with stirring for 1 h. After cooling the reddish orange solution to -78 ºC, the aldehyde RBM4-2 (500 mg, 4.1 mmol) in THF (20 mL) was added dropwise under argon and protected from light. After 3 h the reaction was completed, methanol (31 mL) was added at -78 ªC and the resulting mixture was gradually warmed overnight to RT. The mixture was concentrated under reduced presure and the residue was extracted with Et_2O (3 x 20 mL). The combined organic layers were washed with brine, dried over $MgSO_4$, and concentrated. The crude was purified by flash column chromatography (hexane) to afford a yellow solid RBM4-50 as a mixture of isomers (1*Z*:*E*; 1.5:1) in 70% yield.

Rf: 0.70 (hexane)
1H NMR (CDCl3): Signals deduced from (1*Z*:*E*; 7:3) mixture. **(1*E*,3*E*,5*E*,7*E*)** *δ* 6.74 (dd, *J* = 13.5, 11.0 Hz, 1H), 6.66 – 6.01 (m, 6H), 5.62 (ddd, *J* = 15.0, 10.5, 7.5 Hz, 1H), 1.78 (d, *J* = 6.0 Hz, 3H). **(1*Z*,3*E*,5*E*,7*E*)** *δ* 6.66 (dd, *J* = 10.0, 7.0 Hz, 1H), 6.52 – 6.36 (m, 2H), 6.35 – 6.05 (m, 4H), 5.80 (dq, *J* = 14.0, 7.0 Hz, 1H), 1.79 (dd, *J* = 7.0, 1.5 Hz, 3H).
13C NMR (CDCl3): (1*E*,3*E*,5*E*,7*E*) *δ* 137.9 (CH), 135.0 (CH), 134.2 (CH), 131.4 (CH), 130.4 (CH), 129.6 (CH), 128.6 (CH), 108.1 (CH), 18.6 (CH3). **(1*Z*,3*E*,5*E*,7*E*)** *δ* 136.8 (CH), 135.6 (CH), 132.9 (CH), 131.9 (CH), 131.8 (CH), 130.1 (CH), 127.2 (CH), 107.6 (CH), 18.6 (CH3).
ESI-MS *m/z* $C_9H_{11}Br$ $[2M^+H]^+$ Found: 399.1880 Calculated: 399,1752.

Methyl *N*-(((9H-fluoren-9-yl)methoxy)carbonyl)-*O*-(*tert*-butyldimethylsilyl)-*L*-serinate (RBM4-51)

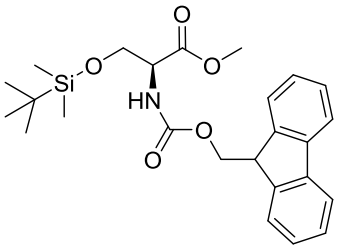

To a solution of *(S)*-methyl 2-((((9H-fluoren-9-yl)methoxy)carbonyl)amino)-3-hydroxy-propanoate (8.1 g, 23.7 mmol) in anhydrous DCM (180 mL) was added TBSCl (7.1 g, 47.1 mmol) followed by imidazole (4.8 g, 71.2 mmol) at 0 ºC. The reaction mixture was warmed to RT and stirred for 3 h. The reaction was quenched by the addition of saturated aqueous NH_4Cl solution and then was extracted with DCM (3x150 mL).The combined organic phases were washed with brine, dried with Mg_2SO_4 and

concentrated. The residue was purified by flash column chromatography (hexane:EtOAc; 95:5) to afford RBM4-51 (10.3 g, 94%) as a white solid.

Rf: 0.81 (hexane:EtOAc; 7:3); **$[\alpha]_D$** +19.6 (*c* 1, $CHCl_3$).
^{1}H NMR ($CDCl_3$): *δ* 7.77 (d, *J* = 7.5 Hz, 2H), 7.62 (t, *J* = 8.0 Hz, 2H), 7.40 (t, *J* = 7.5 Hz, 2H), 7.32 (td, *J* = 7.5, 1.0 Hz, 2H), 5.64 (d, *J* = 9.0 Hz, 1H), 4.48 – 4.43 (m, 1H), 4.42 – 4.33 (m, 2H), 4.26 (t, *J* = 7.5 Hz, 1H), 4.08 (dd, *J* = 10.0, 3.0 Hz, 1H), 3.87 (dd, *J* = 10.0, 3.0 Hz, 1H), 3.77 (s, 3H), 0.89 (s, 9H), 0.06 (s, 3H), 0.04 (s, 3H).
^{13}C NMR ($CDCl_3$): *δ* 171.1 (C), 156.1 (C), 144.1 (C), 143.9 (C), 141.4 (C), 127.9 (CH), 127.2 (CH), 125.3 (CH), 125.3(CH), 120.1 (CH), 67.4 (CH_2), 63.8 (CH_2), 56.1 (CH), 52.6 (CH_3), 47.3 (CH), 25.9 (CH_3), 18.4 (C), -5.4 (CH_3), -5.5 (CH_3).
ESI-MS *m/z* $C_{25}H_{33}NO_5Si$ $[M+Na]^+$ Found: 478.2008; Calculated: 478.2026; $[M+H]^+$ Found: 456.2193; Calculated: 456.2206.

(9H-Fluoren-9-yl)methyl (*S*)-(3,8,8,9,9-pentamethyl-4-oxo-2,7-dioxa-3-aza-8-siladecan-5-yl)carbamate (RBM4-53)

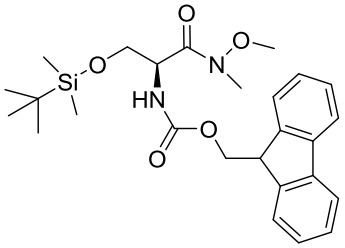

A solution of *N,O*-dimethylhydroxylamine·(HCl) (13.5 g, 138.3 mmol) in DCM (50 mL) under argon atmosphere, was treated at 0 ºC with 69.1 mL Me_3Al (2M in toluene, 138.3 mmol). The reaction mixture was stirred at RT for 30 min, treated with a solution of RBM4-51 (21 g, 46.1 mmol) in DCM (150 mL) and heated to reflux for 16 h. The reaction mixture was cooled to 0 °C and carefully quenched with aqueous sodium potassium tartrate (10%, 75 mL). After stirring at RT for 1 h, the resulting suspension was filtered through a pad of Celite ®, which was then washed with DCM. The filtrate was concentrated under reduced pressure to give the crude product, which upon purification by flash chromatography (hexane:EtOAc; 85:15) gave the Weinreb amide RBM4-53 (20.8 g, 93%) as a colorless oil.

Rf: 0.35 (hexane:EtOAc; 7:3); **$[\alpha]_D$** +13.9 (*c* 1, $CHCl_3$).
^{1}H NMR ($CDCl_3$): *δ* 7.76 (d, *J* = 7.5 Hz, 2H), 7.61 (t, *J* = 8.0 Hz, 2H), 7.40 (tq, *J* = 7.5, 1.0 Hz, 2H), 7.31 (tt, *J* = 7.5, 1.0 Hz, 2H), 5.69 (d, *J* = 9.0 Hz, 1H), 4.89 – 4.79 (m, 1H),

4.36 (d, *J* = 7.5 Hz, 2H), 4.24 (t, *J* = 7.0 Hz, 1H), 3.88 (qd, *J* = 10.0, 5.0 Hz, 2H), 3.77 (s, 3H), 3.24 (s, 3H), 0.89 (s, 9H), 0.05 (d, *J* = 2.0 Hz, 6H).

^{13}C NMR ($CDCl_3$): The methyl group bonded to the Weinreb amide is not observed in the ^{13}C spectra. *δ* 156.1 (C), 156.1 (C), 144.1 (C), 144.0 (C), 141.4 (C), 127.8 (CH), 127.2 (CH), 125.4 (CH), 125.3 (CH), 120.1 (CH), 67.3 (CH_2), 63.5 (CH_2), 61.7 (CH_3), 53.2 (CH), 47.3 (CH), 25.9 (CH_3), -5.4 (CH_3).

ESI-MS *m/z* $C_{26}H_{36}N_2O_5Si$ $[M+Na]^+$ Found: 507.2280; Calculated: 507.2291; $[M+H]^+$ Found: 485.2451; Calculated: 485.2472.

(*S*)-(9H-fluoren-9-yl)methyl (1-((*tert*-butyldimethylsilyl)oxy)-3-oxopropan-2-yl)-carbamate (RBM4-54)

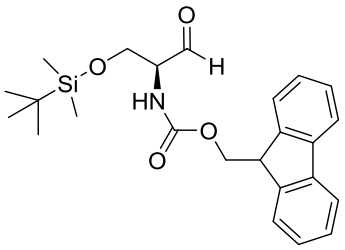

To a solution of Weinreb amide RBM4-53 (5g, 10.3 mmol) in anhydrous THF (100 mL) at -40ºC, was added dropwise a solution of $LiAlH_4$ (0.7g, 19.6 mmol) in 20 mL of THF. After being stirred for 2.5 h at the same temperature, the reaction was monitored by TLC and then quenched by addition of saturated aqueous Na_2SO_4 solution. The resulting white solid was filtered through a pad of Celite ®, which was then washed with EtOAc. The filtrated was concentrated under reduced pressure to give the crude product, which upon purification by chromatography on silica gel column (hexane:EtOAC; 98:12) gave the aldehyde RBM4-54 (3.9 g, 90%) as a colorless oil.

Rf: 0.44 (hexane:EtOAc; 8:2); **$[\alpha]_D$** +19.3 (*c* 1, $CHCl_3$).

^{1}H NMR ($CDCl_3$): *δ* 9.67 (s, 1H), 7.77 (d, *J* = 8.0 Hz, 2H), 7.65 – 7.57 (m, 2H), 7.41 (t, *J* = 7.5 Hz, 2H), 7.37 – 7.28 (m, 2H), 5.65 (d, *J* = 7.0 Hz, 1H), 4.42 (d, *J* = 7.0 Hz, 2H), 4.35 (dt, *J* = 7.0, 4.0 Hz, 1H), 4.29 – 4.18 (m, 3H), 3.90 (dd, *J* = 10.5, 4.0 Hz, 1H), 0.88 (s, 9H), 0.06 (s, 6H).

^{13}C NMR ($CDCl_3$): *δ* 198.9 (CH), 156.2 (C), 144.0 (C), 143.9 (C), 141.5 (C), 127.9 (CH), 127.2 (CH), 125.3 (CH), 125.2 (CH), 120.2 (CH), 67.4 (CH_2), 62.0 (CH), 61.4 (CH_2), 47.3 (CH), 25.9 (CH_3), -5.4 (CH_3), -5.4 (CH_3).

ESI-MS *m/z* $C_{24}H_{31}NO_4Si$ $[M+H]^+$ Found: 426.2087; Calculated: 426.2101.

(9H-Fluoren-9-yl)methyl ((2*S*,3*R*)-1-((*tert*-butyldimethylsilyl)oxy)-3-hydroxypent-4-en-2-yl)carbamate (RBM4-55)

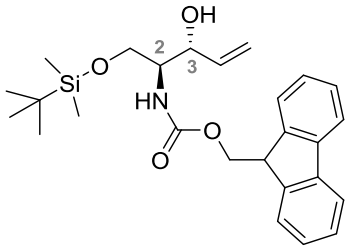

Route I

RBM4-54 aldehyde (600 mg, 1.5 mmol) was dissolved in anhydrous THF (10 mL) under argon atmosphere. The solution was cooled to -78ºC, followed by dropwise addition of vinylmagnesium bromide solution (0.7M in THF, 3.9 mL). The reaction was stirred at -78ºC for 4 h and then the temperature was allowed to gradually rise to -40ºC. Saturated aqueous NH_4Cl solution (5 mL) was added to quench the reaction, the mixture was warmed to RT and extracted with Et_2O (3 x 25 mL). The ether solutions were combined and dried over Mg_2SO_4. The concentrated residue was purified by flash column chromatography (hexane:EtOAc; stepwise gradient from 0 to 15 of EtOAc) affording a mixture of diastereomers *anty/syn* = 1:1 (RBM4-55 :RBM4-56, 60%) as a white solid.

Absolute configuration determination

After carefully chromatographic purification the single diastereomers were isolated. The absolute configuration was assigned by derivatization of one of the diastereomers with (*R*)-MPA and (*S*)-MPA, following the Riguera and coworkers procedure[359].

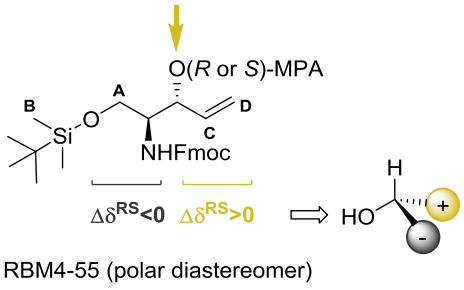

RBM4-55 (polar diastereomer)

Table 5.2 $\Delta\delta^{RS}$ values from 1H-NMR spectra for the derivatized polar *anti*-diastereomer

	δH_A	δH_B	δH_C	δH_D
R-MPA	3.23	-0.10	5.84	5.39
S-MPA	3.51	0.02	5.67	5.11
$\Delta\delta^{RS}$	-0.28	-0.12	0.17	0.28

Route II

EtOH was distilled and dried with CaH_2 prior to use. Lithium tri-*tert*-butoxyaluminohydride (2.1 g, 8.1 mmol) was cooled at –78ºC under argon atmosphere and then it was dissolved in EtOH (50 mL). To this suspension, a solution of RBM4-63 (1.8 g, 4.0 mmol) in EtOH (40 mL) was added dropwise at -78ºC. After the reaction mixture was stirred at the same temperature for 30 min, was warmed to 0ºC and quenched with 10% citric acid (32mL). The resulting mixture was extracted with EtOAc (3 x 75mL). The organic layers were combined, washed with H_2O (100 mL) and brine (100 mL), dried over $MgSO_4$ and concentrated to provide a white solid. Flash column chromatography (hexane:EtOAc; 89:11) gave 293 mg of RBM4-55 as mixture of diastereomers *anty/syn* = 3:1, and 603 mg of only *anti*-RBM4-55. Moreover, it was isolated (DCM:MeOH; 95:5) 600 mg of partially TBS-deprotected vinylalcohol RBM4-65.

RBM4-55 (2*S*, 3*R*) Rf: 0.24 (hexane:EtOAc; 8:2); **$[\alpha]_D$** +10.0 (*c* 0.5, $CHCl_3$).
^{1}H NMR ($CDCl_3$): *δ* 7.77 (d, *J* = 7.5 Hz, 2H), 7.60 (dd, *J* = 7.0, 3.5 Hz, 2H), 7.41 (t, *J* = 7.5 Hz, 2H), 7.31 (td, *J* = 7.5, 1.0 Hz, 2H), 5.94 (ddd, *J* = 16.0, 10.0, 5.0 Hz, 1H), 5.55 (d, *J* = 8.5 Hz, 1H), 5.34 (dd, *J* = 56.0, 14.0 Hz, 2H), 4.40 (dd, *J* = 7.0, 2.5 Hz, 2H), 4.36 – 4.28 (m,1H), 4.24 (t, *J* = 7.0 Hz, 1H), 3.88 (ddd, *J* = 75.5, 10.5, 2.5 Hz, 2H), 3.76 – 3.68 (m, 1H), 0.91 (s, 9H), 0.07 (s, 6H).
^{13}C NMR ($CDCl_3$): *δ* 156.3 (C), 144.1 (C), 144.0 (C), 141.5 (C), 137.8 (CH), 127.8 (CH), 127.2 (CH), 125.3 (CH), 125.2 (CH), 120.1 (CH), 116.3 (CH_2), 74.8 (CH), 67.1 (CH_2), 63.5 (CH_2), 54.6 (CH), 47.4 (CH), 25.9 (CH_3), 18.3 (C), -5.5 (CH_3).
ESI-MS *m/z* $C_{26}H_{35}NO_4Si$ $[M+Na]^+$ Found: 476.2237; Calculated: 476.2233; $[M+H]^+$ Found: 454.2416; Calculated: 454.2414.

RBM4-56 (2*S*, 3*S*) Rf: 0.28 (hexane:EtOAc; 8:2); **$[\alpha]_D$** +4.6 (*c* 0.7, $CHCl_3$).
^{1}H NMR ($CDCl_3$): *δ* 7.77 (d, *J* = 7.5 Hz, 2H), 7.63 – 7.53 (m, 2H), 7.44 – 7.37 (m, 2H), 7.35 – 7.28 (m, 2H), 5.93 – 5.79 (m, 1H), 5.64 (d, *J* = 7.0 Hz, 1H), 5.41 – 5.34 (m, 1H), 5.23 (d, *J* = 11.0 Hz, 1H), 4.55 – 4.50 (m, 1H), 4.38 (app.dt, *J* = 25.5, 9.0 Hz, 2H), 4.29 – 4.19 (m, 1H), 3.90 – 3.86 (m, 2H), 3.72 (dd, *J* = 9.0, 4.0 Hz, 1H), 0.92 (s, 9H), 0.09 (s, 6H).
^{13}C NMR ($CDCl_3$): Some splitting observed due to rotamers. *δ* 156.6 (C), 144.1 (C), 144.0 (C), 141.5 (C), 137.3 (CH), 127.8 (CH), 127.2 (CH), 125.2 (CH), 120.1 (CH), 116.5 (CH_2), 73.5 (CH), 67.1 (CH_2), 65.4 (CH_2), 54.8 (CH), 47.4 (CH), 26.0 (CH_3), -5.4 (CH_3).

ESI-MS *m/z* $C_{26}H_{35}NO_4Si$ $[M+Na]^+$ Found: 476.2243; Calculated: 476.2233; $[M+H]^+$ Found: 454.2426; Calculated: 454.2414.

(9H-fluoren-9-yl)methyl ((2*S*,3*R*,*E*)-1-((*tert*-butyldimethylsilyl)oxy)-3-hydroxy-9-(trimethylsilyl)non-4-en-8-yn-2-yl)carbamate (RBM4-57)

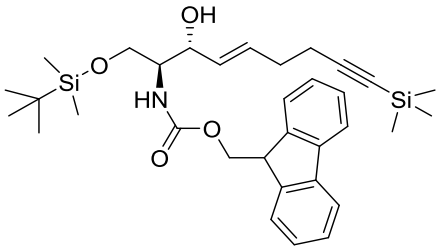

A two necked round bottom flask fitted with a reflux condenser under argon atmosphere, was charged with the allylic alcohol RBM4-55 (900 mg, 2.0 mmol) in 25 mL of DCM previously degassed. To the solution was added 5-hexen-1-yn-1-yltrimethylsilane (100 mg, 0.7 mmol) and Grubbs' 2nd generation catalyst (112 mg, 0.14 mmol). The resulting mixture was stirred at reflux temperature for 5h and then cooled down to RT. The mixture was concentrated under reduced pressure to afford dark brown crude, which was purified by flash column chromatography (hexane:EtOAc; stepwise gradient from 0 to 9 of EtOAc) giving RBM4-57 (50%) as a colourless oil.

Rf: 0.48 (hexane:EtOAc; 8:2); **$[\alpha]_D$** +8.2 (*c* 0.8, $CHCl_3$).

^{1}H NMR ($CDCl_3$): *δ* 7.77 (dd, *J* = 7.5, 1.5 Hz, 2H), 7.60 (d, *J* = 7.5 Hz, 2H), 7.41 (td, *J* = 7.5, 0.5 Hz, 2H), 7.32 (td, *J* = 7.5, 1.0 Hz, 2H), 5.89 – 5.77 (m, 1H), 5.61 (dd, *J* = 15.5, 6.0 Hz, 1H), 5.53 (d, *J* = 8.5 Hz, 1H), 4.39 (d, *J* = 7.0 Hz, 2H), 4.32 – 4.24 (m, 1H), 4.24 (t, *J* = 7.0 Hz, 1H), 3.99 (dd, *J* = 10.5, 3.0 Hz, 1H), 3.78 (dd, *J* = 10.5, 3.5 Hz, 1H), 3.69 (dd, *J* = 8.0, 4.0 Hz, 1H), 3.38 – 3.27 (m, 1H), 2.30 (m, 4H), 0.92 (s, 9H), 0.15 (t, 6H), 0.08 (s, 9H).

^{13}C NMR ($CDCl_3$): *δ* 156.3 (C), 144.1 (C), 144.0 (C), 141.5 (C), 131.0 (CH), 130.8 (CH), 127.8 (CH), 127.2 (CH), 125.3 (CH), 125.2 (CH), 120.1 (CH), 106.6 (C), 85.2 (C), 74.5 (CH), 67.1 (CH_2), 63.6 (CH_2), 54.8 (CH), 47.4 (CH), 31.7 (CH_2), 26.0 (CH_3), 20.1 (CH_2), 0.3 (CH_3), -5.5 (CH_3).

ESI-MS *m/z* $C_{33}H_{47}NO_4Si_2$ $[M+Na]^+$ Found: 600.2939; Calculated: 600.2941; $[M+H]^+$ Found: 578.3160; Calculated: 578.3122.

(9H-fluoren-9-yl)methyl ((2*S*,3*R*,*E*)-1-((*tert*-butyldimethylsilyl)oxy)-3-hydroxynon-4-en-8-yn-2-yl)carbamate (RBM4-58)

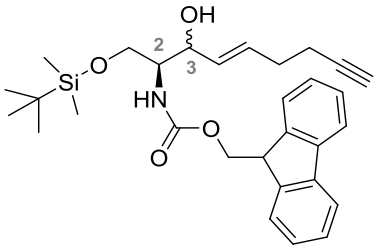

To a solution of (trimethylsilyl)acetylene RBM4-57 (1:1.5, *syn:anti*) (30 mg, 0.05 mmol) in 2.5 mL of a (1:1:1:0.1) mixture of (THF:H_2O:EtOH:2,6-lutidine) was added in one portion $AgNO_3$ (88 mg, 0.5 mmol). After stirring the white suspension vigorously for 3.5 h was added 1.5 mL of aqueous KH_2PO_4 (1.0 M) solution. The resulting yellow mixture was stirred for an additional 30 min, filtered through Celite ® pad removing most of the yellow precipitate. The filtrate was extracted with Et_2O (3 x 5 mL), and the combined organic layers were washed once with saturated aqueous NaCl (10 mL) and dried over $MgSO_4$. Evaporation of the solvent under reduced pressure afforded a pale yellow oil, which was purified by flash column chromatography (hexane:EtOAc; 88:12) to yield 20 mg (80%) of RBM4-58 (1:1.5, *syn:anti*).

Rf: (2S, 3S) 0.61; **(2*S*, 3*R*)** 0.57 (hexane:EtOAc; 7:3)

^{1}H NMR ($CDCl_3$): Mixture of diastereomers (1:1.5, *syn:anti*). **(2*S*, 3*S*)** δ 7.77 (d, *J* = 7.5 Hz, 2H), 7.63 – 7.56 (m, 2H), 7.41 (t, *J* = 7.5 Hz, 2H), 7.31 (td, *J* = 7.5, 1.0 Hz, 2H), 5.90 – 5.76 (m, 1H), 5.63 – 5.52 (m, 1H), 5.38 (d, *J* = 9.0 Hz, 1H), 4.47 (m, 1H), 4.39 (dd, *J* = 7.0, 3.0 Hz, 2H), 4.23 (t, *J* = 7.0 Hz, 1H), 3.89 – 3.81 (m, 2H), 3.69 (dd, *J* = 9.0, 5.0 Hz, 1H), 3.23 (s, 1H), 2.34 – 2.22 (m, 4H), 1.94 (s, 1H), 0.91 (s, 9H), 0.08 (s, 9H). **(2*S*, 3*R*)** δ 7.77 (d, *J* = 7.5 Hz, 2H), 7.63 – 7.56 (m, 2H), 7.41 (t, *J* = 7.5 Hz, 2H), 7.31 (td, *J* = 7.5, 1.0 Hz, 2H), 5.89 – 5.76 (m, 1H), 5.67 – 5.53 (m, 1H), 5.50 (d, *J* = 8.5 Hz, 1H), 4.39 (dd, *J* = 7.0, 3.0 Hz, 2H), 4.29 (m, 1H), 4.23 (t, *J* = 7.0 Hz, 1H), 4.00 (dd, *J* = 10.5, 3.0 Hz, 1H), 3.77 (dd, *J* = 10.5, 3.0 Hz, 1H), 3.69 (dd, *J* = 8.5, 4.5 Hz, 1H), 3.30 (d, *J* = 8.0 Hz, 1H), 2.34 – 2.22 (m, 4H), 1.94 (s, 1H), 0.91 (s, 9H), 0.08 (s, 6H).

^{13}C NMR ($CDCl_3$): (2*S*, 3*S*) δ 156.6 (C), 144.1 (C), 144.0 (C), 141.5 (C), 131.1 (CH), 130.6 (CH), 127.9 (CH), 127.2 (CH), 125.2 (CH), 120.1 (CH), 83.9 (C), 73.3 (CH), 69.0 (CH), 67.0 (CH_2), 65.2 (CH_2), 55.0 (CH), 47.4 (CH), 31.3 (CH_2), 26.0 (CH_3), 18.6 (CH_2), -5.5 (CH_3). **(2*S*, 3*R*)** δ 156.4 (C), 144.1 (C), 144.0 (C), 141.5 (C), 131.1 (CH), 130.7 (CH), 129.0 (CH), 127.9 (CH), 127.2 (CH), 125.3 (CH), 125.2 (CH), 120.1 (CH), 83.9

(C), 74.3 (CH), 69.0 (CH), 67.0 (CH_2), 63.6 (CH_2), 55.1 (CH), 47.4 (CH), 31.3 (CH_2), 26.0 (CH_3), 18.6 (CH_2), -5.5 (CH_3).
ESI-MS *m/z* $C_{30}H_{39}NO_4Si$ $[M+H]^+$ Found: 506.2719; Calculated:506.2727.

(9H-fluoren-9-yl)methyl ((2*S*,3 *R*:*S*,4*E*,8*E*,10*E*,12*E*,14*E*,16*E*)-1-((*tert*-butyldimethyl-silyl)oxy)-3-hydroxy-octadeca-4,8,10,12,14,16-hexaen-2-yl)carbamate (RBM4-59)

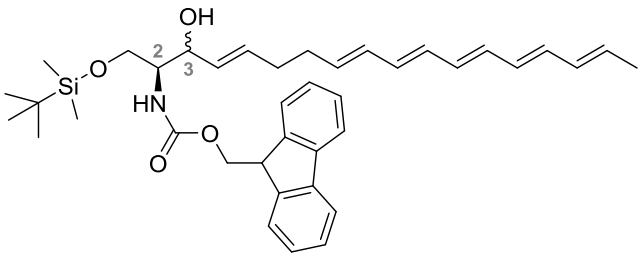

Procedure using $AgClO_4$ as catalyst:

To a flame-dried Schlenk containing 175 mg of $Cp_2Zr(H)Cl$ (0.7 mmol), was added a solution of the alkyne RBM4-17 (125 mg, 0.6 mmol) in anhydrous DCM (0.7 mL), at 0 ºC under argon atmosphere and protected from light. During warming to room temperature, the zirconocene complex gradually dissolved to give a clear red solution (20 min). A solution of the aldehyde RBM4-54 (206 mg, 0.5 mmol) in DCM (10.6 mL) was added followed by $AgClO_4$ (20 mg, 20% mol). After 20 min, the reaction mixture turned dark red, was diluted with Et_2O and was quenched by addition of 1 mL saturated $NaHCO_3$ aqueous solution. The mixture was filtered through a Celite ® pad, and the products were extracted with Et_2O (5 mL x 3). The combined ethereal solution were washed with brine, dried and concentrated under reduced pressure. Purification with flash column chromatography (hexane:EtOAc; stepwise gradient from 0 to 10% of EtOAc) gave RBM4-59 (20%) as a mixture of diastereomers (*anti*:*syn*; 1:2.3)

Procedure using $ZnCl_2$ as additive:

To a flame-dried Schlenk with a suspension of $Cp_2Zr(H)Cl$ (100 mg, 0.4 mmol) in DCM (0.4 mL), was added a solution of the alkyne RBM4-17 (55 mg, 0.3 mmol) in anhydrous DCM (0.4 mL), at 0 ºC under argon atmosphere and protected from light. During warming to room temperature, the zirconocene complex gradually dissolved to give a clear red solution (20 min). A solution of the aldehyde RBM4-54 (91 mg, 0.2 mmol) in DCM (0.6 mL), which was activated previously with $ZnCl_2$ (15 mg, 0.1 mmol, dried under vacuum for 1 h before use) for 10 min, was added to the reaction mixture. The

solution was stirred for 30 min at RT and turned clear orange. Next dilution with DCM (2 mL) and addition of aqueous potassium sodium tartrate (2 mL) was stirred for 10 min. The resulting suspension was filtered through Celite ® pad and washed thoroughly with DCM (5 mL). The combined filtrate was successively washed with H_2O and brine. The aqueous phase was extracted with DCM (3x10 mL), and the combined organic layers were dried over Mg_2SO_4. Purification with flash column chromatography (hexane:EtOAc; stepwise gradient from 0 to 10% of EtOAc) gave RBM4-59 (20%) as a mixture of diastereomers (*anti*:*syn*; 1:1.5).

Rf: (2*S*, 3*S*) 0.43; **(2*S*, 3*R*)** 0.37 (hexane:EtOAc; 8:2)

^{1}H NMR ($CDCl_3$): Mixture of diastereomers (*anti*:*syn*; 1:1) **(2*S*, 3*R*)** *δ* 7.77 (d, *J* = 8.0 Hz, 2H), 7.60 (d, *J* = 7.5 Hz, 2H), 7.40 (ddt, *J* = 8.5, 7.5, 1.5 Hz, 2H), 7.31 (tt, *J* = 7.5, 2.0 Hz, 2H), 6.30 – 5.88 (m, 8H), 5.91 – 5.21 (m, 4H), 5.05 (d, *J* = 13.0 Hz, 1H), 4.54 – 4.30 (m, 3H), 4.23 (t, *J* = 7.0 Hz, 1H), 3.96 (d, *J* = 10.0 Hz, 1H), 3.76 (d, *J* = 10.0 Hz, 1H), 3.71 – 3.62 (m, 1H), 3.26 (d, *J* = 5.0 Hz, 1H), 2.24 – 1.94 (m, 3H), 1.78 (dd, *J* = 7.0, 1.5 Hz, 3H),0.91 (s, 9H), 0.08 (s, 6H). **(2*S*, 3*S*)** *δ* 7.77 (d, *J* = 8.0 Hz, 2H), 7.60 (d, *J* = 7.5 Hz, 2H), 7.40 (ddt, *J* = 8.5, 7.5, 1.5 Hz, 2H), 7.31 (tt, *J* = 7.5, 2.0 Hz, 2H), 6.30 – 5.88 (m, 8H), 5.91 – 5.21 (m, 4H), 4.97 (d, *J* = 12.0 Hz, 2H), 4.54 – 4.30 (m, 3H), 4.23 (t, *J* = 7.0 Hz, 1H), 3.89 – 3.81 (m, 2H), 3.70 – 3.61 (m, 1H), 3.17 (d, *J* = 12.5 Hz, 1H), 2.24 – 1.94 (m, 4H), 1.78 (dd, *J* = 7.0, 1.4 Hz, 3H), 0.91 (s, 9H), 0.08 (s, 6H).

^{13}C NMR ($CDCl_3$): (2*S*, 3*R*:*S*) *δ* 156.3 (C), 144.1 (C), 141.5 (C), 133.1 (CH), 133.1 (CH), 132.8 (CH), 132.5 (CH), 132.4 (CH), 132.1 (CH), 132.1 (CH), 131.0 (CH), 130.8 (CH), 130.2 (CH), 129.9 (CH), 129.6 (CH), 127.85 (CH), 127.2 (CH), 125.23 (CH), 120.1 (CH), 73.4 (CH), 67.1 (CH_2), 65.5 (CH_2), 55.2 (CH), 47.4 (CH), 32.2 (CH_2), 32.1 (CH), 26.0 (CH_3), 18.3 (CH_3), -5.4 (CH_3).

ESI-MS *m/z* $C_{39}H_{51}NO_4Si$ $[M+Na]^+$ Found: 648.3478; Calculated: 648.3485; $[M+H]^+$ Found: 626.3668; Calculated: 626.3666.

***N*-((2*S*,3*R*:*S*,4*E*,8*E*,10*E*,12*E*,14*E*,16*E*)-1,3-dihydroxyoctadeca-4,8,10,12,14,16-hexaen-2-yl) palmitamide (RBM4-60)**

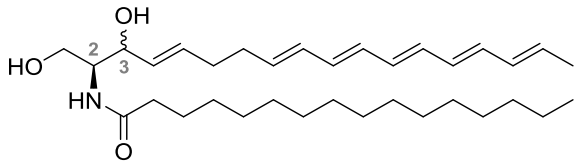

a) **Deprotection:** The (2*S*, 3*R:S* 1:1.5) RBM4-59 (20 mg, 0.03 mmol) was dissolved in anhydrous THF (0.5 mL) under argon atmosphere. Next, 35 µL of TBAF solution was added via syringe (0.04 mmol, 1M in THF). The solution turned orange immediately. After being stirred for 1 h at RT, it was observed by TLC part of the starting material, then to the reaction mixture was added an additional 15 µL of TBAF solution (1M in THF) to fulfil the conversion. After 30 min, a saturated aqueous NH_4Cl (0.5 mL) solution was added, and the mixture was dried with $MgSO_4$ and the resulting amino diol was eluted to another flask with DCM. The solvent was concentrated under reduced pressure and the crude was used in the next reaction without further purification.

b) ***N*-Acylation:** To a solution of EDC (10 mg, 0.05 mmol) and HOBt (5 mg, 0.04 mmol) in anhydrous DCM (200 µL) was added palmitic acid (9 mg, 0.04 mmol) in DCM (300 µL) under argon atmosphere. The resulting mixture was vigorously stirred at RT for 15 min, and next added dropwise to a solution of the amino diol intermediate (0.03 mmol) and Et_3N (9 µL, 0.06 mmol) in anhydrous DCM (500 µL). The reaction mixture was stirred at RT for 1.5 h and then was diluted by addition of DCM (2 mL), and washed successively with water (5 mL) and brine (5 mL). The organic layer was dried over $MgSO_4$, and filtered and concentrated under reduced pressure. The crude was purified by flash column chromatography (hexane:EtOAc; stepwise gradient from 0 to 5% of AcOEt, followed by stepwise gradient from 0 to 4% of MeOH) affording a low yield of RBM4-60 (presumably 2*S*, 3*R:S;* 1:1.5).

Rf: (2*S*, 3*R*:*S*) 0.58 (DCM:MeOH; 9:1)

^{1}H NMR ($CDCl_3$): (2*S*, 3*R*:*S*) δ 6.27 – 5.80 (m, 5H), 5.86 – 5.52 (m, 3H), 5.53 – 5.30 (m,2H), 5.13 – 5.03 (m, 1H), 5.03 - 4.83 (m, 2H), 4.42-4.26 (m, 1H), 4.22 – 3.99 (m, 3H), 2.32 – 2.19 (m, 1H), 2.18 – 2.05 (m, 3H), 2.05 – 1.92 (m, 4H), 1.73 (d, *J* = 7.0 Hz, 3H), 1.60 – 1.46 (m, 2H), 1.20 (s, 22H), 0.83 (t, *J* = 7.0 Hz, 3H).

ESI-MS *m/z* $C_{34}H_{57}NO_3$ $[M+H]^+$ Found**:** 528.4432; Calculated: 528.4417.

_N_-((5_R_,6_S_)-5-((_E_)-hex-1-en-5-yn-1-yl)-2,2,3,3,9,9,10,10-octamethyl-4,8-dioxa-3,9-disilaundecan-6-yl)palmitamide (RBM4-61)

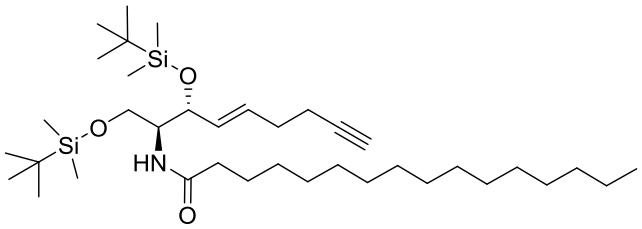

To a solution of (trimethylsilyl)acetylene RBM4-68 (60 mg, 0.1 mmol) in 5 mL of a (1:1:1:0.1) mixture of (THF:H_2O:EtOH:2,6-lutidine) was added in one portion $AgNO_3$ (176 mg, 1.0 mmol). After stirring the white suspension vigorously for 3.5 h was added 3 mL of aqueous KH_2PO_4 (1.0 M) solution. The resulting yellow mixture was stirred for an additional 30 min, filtered through Celite ® pad removing most of the yellow precipitate. The filtrate was extracted with Et_2O (3 x 10 mL), and the combined organic layers were washed once with saturated aqueous NaCl (20 mL) and dried over $MgSO_4$. Evaporation of the solvent under reduced pressure afforded a pale yellow oil, which was used without further purification to next reaction. The intermediate RBM4-69 (50 mg, 0.1 mmol) was redissolved in anhydrous DCM (0.3 mL) and a TBSCl (15 mg, 0.2 mmol) solution in anhydrous DCM (0.5 mL) was added, followed by the addition of imidazole (20 mg, 0.3 mmol) at 0ºC. The reaction mixture was warmed to RT and stirred for 3 h. The reaction was quenched by the addition of saturated aqueous NH_4Cl solution and then was extracted with DCM (3 x 5 mL).The combined organic phases were washed with brine, dried with Mg_2SO_4 and concentrated. The residue was purified by flash column chromatography (hexane:EtOAc; 96:4) to afford RBM4-61 (37 mg, 65%) as a white solid.

Rf: 0.53 (hexane:EtOAc; 9:1); **$[\alpha]_D$:** -1.2 (*c* 1, $CHCl_3$).

^{1}H NMR ($CDCl_3$): δ 5.67 (dt, *J* = 16.0, 6.5 Hz, 1H), 5.57 (t, *J* = 7.5 Hz, 1H), 5.52 (d, *J* = 7.0 Hz, 1H), 4.25 (t, *J* = 6.5 Hz, 1H), 4.01 – 3.89 (m, 1H), 3.83 (dd, *J* = 10.0, 4.0 Hz, 1H), 3.56 (dd, *J* = 10.0, 5.0 Hz, 1H), 2.32 – 2.18 (m, 4H), 2.12 (t, *J* = 7.0 Hz, 2H), 1.94 (t, *J* = 2.5 Hz, 1H), 1.64 – 1.49 (m, 2H), 1.35 – 1.16 (m, 24H), 0.89 (s, 9H), 0.90 – 0.83 (m, 12H), 0.05 (d, *J* = 3.0 Hz, 6H), 0.02 (d, *J* = 8.5 Hz, 6H).

^{13}C NMR ($CDCl_3$): δ 172.7 (C), 132.0 (CH), 130.6 (CH), 84.0 (C), 72.6 (CH), 68.9 (CH), 61.3 (CH_2), 54.9 (CH), 37.3 (CH_2), 32.1 (CH_2), 31.2 (CH_2), 29.9 (CH_2), 29.8 (CH_2), 29.8 (CH_2), 29.8 (CH_2), 29.8 (CH_2), 29.6 (CH_2), 29.6 (CH_2), 29.5 (C), 29.5 (C), 26.0 (CH_3),

26.0 (CH_3), 25.9 (CH_2), 22.8 (CH_2), 18.7 (CH_2), 18.4 (CH_2), 18.3 (CH_2), 14.3 (CH_3), -3.9 (CH_3), -4.8 (CH_3), -5.2 (CH_3), -5.4 (CH_3).

ESI-MS *m/z* $C_{37}H_{73}NO_3Si_2$ $[M+Na]^+$ Found: 658.5031; Calculated: 658.5027; $[M+H]^+$ Found: 636.5265; Calculated: 636.5207.

(9H-fluoren-9-yl)methyl (*S*)-(1-((*tert*-butyldimethylsilyl)oxy)-3-oxopent-4-en-2-yl)-carbamate (RBM4-63)

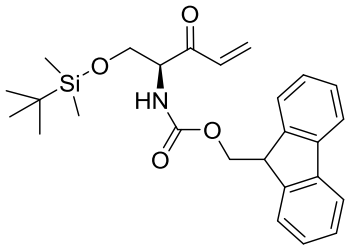

A solution of vinyl magnesium bromide (19.3 mL, 19.3 mmol, 1 M in THF) was added dropwise to a solution of Weinreb amide RBM4-53 (2.6 g, 5.4 mmol) in anhydrous THF (16 mL) at 0ºC. The resulting mixture was slowly warmed and stirred for 30 min at RT. Subsequently, it was transferred via cannula into a cooled (0°C) solution of HCl (83 mL, 1 N). The biphasic mixture was extracted with Et_2O (3 x 20 ml). The combined organic layers were dried over $MgSO_4$, filtered and concentrated under reduced pressure. The residue was purified by flash chromatography (hexane:EtOAc; 91:9) to give vinyl ketone RBM4-63 (2 g, 4.4 mmol, 83%) as a white solid.

Rf: 0.51 (hexane:EtOAc; 8:2); **$[\alpha]_D$** +45.9 (*c* 1, $CHCl_3$).

^{1}H NMR ($CDCl_3$): *δ* 7.77 (d, *J* = 7.5 Hz, 2H), 7.62 (t, *J* = 7.0 Hz, 2H), 7.41 (tt, *J* = 7.5, 1.5 Hz, 2H), 7.32 (td, *J* = 7.5, 1.0 Hz, 2H), 6.58 (dd, *J* = 17.5, 10.5 Hz, 1H), 6.39 (dd, *J* = 17.5, 1.5 Hz, 1H), 5.87 (dd, *J* = 10.5, 1.5 Hz, 1H), 5.84 (s, 1H), 4.69 (ddd, *J* = 8.0, 4.5, 3.5 Hz, 1H), 4.39 (d, *J* = 7.5 Hz, 2H), 4.24 (t, *J* = 7.0 Hz, 1H), 4.06 (dd, *J* = 10.5, 3.5 Hz, 1H), 3.90 (dd, *J* = 10.4, 4.5 Hz, 1H), 0.86 (s, 9H), 0.03 (s, 3H), 0.02 (s, 3H).

^{13}C NMR ($CDCl_3$): *δ* 196.4 (C), 155.9 (C), 144.0 (C), 143.9 (C), 141.4 (C), 133.1 (CH), 129.9 (CH_2), 127.8 (CH), 127.2 (CH), 125.3 (CH), 125.3 (CH), 120.1 (CH), 67.3 (CH_2), 63.5 (CH_2), 60.0 (CH), 47.3 (CH), 25.9 (CH_3), -5.4 (CH_3).

ESI-MS *m/z* $C_{26}H_{33}NO_4Si$ $[M+Na]^+$ Found: 474.2094; Calculated: 474.2077; $[M+H]^+$ Found: 452.2275; Calculated: 452.2257.

(9H-fluoren-9-yl)methyl (S)-(3,10,10,11,11-pentamethyl-6-oxo-2,9-dioxa-3-aza-10-sila-dodecan-7-yl)carbamate (RBM4-64)

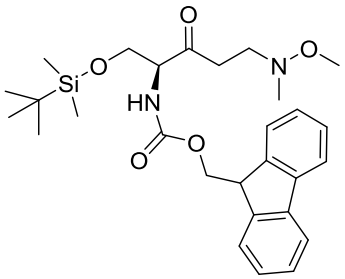

By-product isolated from addition of vinyl magnesium bromide to Weinreb amide RBM4-53 (see section 3.2.4.5).

Rf: 0.32 (hexane:EtOAc; 8:2);

^{1}H NMR ($CDCl_3$): *δ* 7.77 (app. d, *J* = 7.5, 1.0, 0.5 Hz, 2H), 7.63 – 7.57 (m, 2H), 7.40 (app. t, *J* = 7.0 Hz, 2H), 7.31 (td, *J* = 7.5, 1.0 Hz, 2H), 5.81 (d, *J* = 7.0 Hz, 1H), 4.47 – 4.41 (m, 1H), 4.38 (d, *J* = 7.0 Hz, 2H), 4.23 (t, *J* = 7.2 Hz, 1H), 4.11 (dd, *J* = 7.1, 3.6 Hz, 1H), 3.87 (dd, *J* = 10.5, 4.3 Hz, 1H), 3.46 (s, 3H), 3.03 – 2.88 (m, 2H), 2.87 – 2.81 (m, 2H), 2.58 (s, 3H), 0.87 (s, 9H), 0.05 (s, 6H).

^{13}C NMR ($CDCl_3$): *δ* 206.0 (C), 155.8 (C), 143.9 (C), 143.8 (C), 141.3 (C), 127.7 (CH), 127.1 (CH), 125.1 (CH), 120.0 (CH), 67.1 (CH_2), 63.2 (CH_2), 61.6 (CH), 59.9 (CH_3), 54.8 (CH_2), 47.2 (CH), 44.9 (CH_3), 38.0 (CH_2), 25.8 (CH_3), -5.6 (CH_3).

ESI-MS *m/z* $C_{28}H_{40}N_2O_5Si$ $[M+Na]^+$ Found: 535.2606; Calculated: 535.2604; $[M+H]^+$ Found: 513.2775; Calculated: 513.2785.

(9H-fluoren-9-yl)methyl ((2S,3R)-1,3-dihydroxypent-4-en-2-yl)carbamate (RBM4-65)

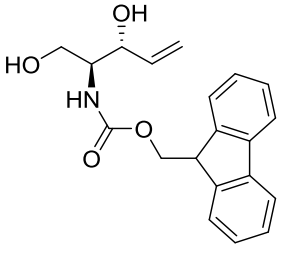

By-product isolated from preparation of RBM4-55, Route II.

Rf: 0.63 (DCM:MeOH; 9:1); **$[\alpha]_D$** +9.4 (*c* 0.8, $CHCl_3$).

^{1}H NMR ($CDCl_3$): *δ* 7.77 (d, *J* = 7.5 Hz, 2H), 7.61 (d, *J* = 7.5 Hz, 2H), 7.41 (app. t, *J* = 7.5 Hz, 1H), 7.33 (td, *J* = 7.5, 1.0 Hz, 2H), 6.01 – 5.88 (m, 1H), 5.59 – 5.53 (m, 1H),

5.41 (app. d, *J* = 16.9 Hz, 1H), 5.29 (app. d, *J* = 10.0 Hz, 1H), 4.49 – 4.37 (m, 3H), 4.23 (t, *J* = 6.6 Hz, 1H), 3.98 (app. d, *J* = 11.8 Hz, 1H), 3.78 – 3.66 (m, 2H).

^{13}C NMR ($CDCl_3$): *δ* 181.7 (C), 144.0 (C), 141.5 (C), 137.4 (CH), 127.9 (CH), 127.2 (CH), 125.2 (CH), 120.2 (CH), 116.9 (CH_2), 75.0 (CH), 67.0 (CH_2), 62.4 (CH_2), 55.2 (CH), 47.5 (CH).

ESI-MS *m/z* $C_{20}H_{21}NO_4$ $[M+Na]^+$ Found: 362.1378; Calculated: 362.1368; $[M+H]^+$ Found: 340.1553; Calculated: 340.1549.

(2*S*,3*R*,*E*)-2-amino-1-((*tert*-butyldimethylsilyl)oxy)-9-(trimethylsilyl)non-4-en-8-yn-3-ol (RBM4-67)

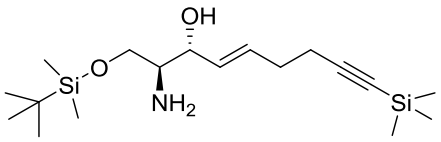

To a solution of RBM4-57 (75 mg, 0.13 mmol) in anhydrous THF (1.7 mL) was added piperidine (405 µL, 4.1 mmol) at RT. After stirring for 2 h, the mixture was diluted with EtOAc. The organic phase was washed with water and brine, dried over $MgSO_4$, and concentrated under reduced pressure. The residue was purified by flash column chromatography on silica gel (DCM:MeOH; 100:0 to 96:4 gradient) to give RBM4-67 as a yellowish oil (40 mg, 89%).

Rf: 0.34 (DCM:MeOH; 95:5); **$[\alpha]_D$:** +2.0 (*c* 0.9, $CHCl_3$).

^{1}H NMR ($CDCl_3$): *δ* 5.78 (dt, *J* = 15.0, 6.0 Hz, 1H), 5.54 (dd, *J* = 15.5, 6.5 Hz, 1H), 4.11 (t, *J* = 6.0 Hz, 1H), 3.72 (dd, *J* = 10.0, 6.0 Hz, 1H), 3.66 (dd, *J* = 10.0, 5.0 Hz, 1H), 2.89 (q, *J* = 5.5 Hz, 1H), 2.37 – 2.21 (m, 4H), 0.90 (s, 9H), 0.14 (s, 9H), 0.07 (s, 6H).

^{13}C NMR ($CDCl_3$): *δ* 131.6 (CH), 130.9 (CH), 106.7 (C), 85.1 (C), 74.9 (CH), 65.5 (CH_2), 56.1 (CH), 31.6 (CH_2), 26.0 (CH_3), 20.1 (CH_2), 0.3 (CH_3), -5.3 (CH_3).

ESI-MS *m/z* $C_{18}H_{37}NO_2Si_2$ $[M+Na]^+$ Found: 378.2273; Calculated: 378.2261; $[M+H]^+$ Found: 356.2445; Calculated: 356.2441.

***N*-((2*S*,3*R*,*E*)-1-((*tert*-butyldimethylsilyl)oxy)-3-hydroxy-9-(trimethylsilyl)non-4-en-8-yn-2-yl)palmitamide (RBM4-68)**

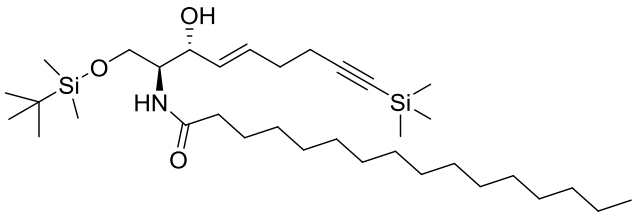

To a solution of EDC (31 mg, 0.16 mmol) and HOBt (16 mg, 0.12 mmol) in anhydrous DCM (1.5 mL) was added palmitic acid (28 mg, 0.11 mmol) in DCM (1.5mL) under argon atmosphere. The resulting mixture was vigorously stirred at RT for 15 min, and next added dropwise to a solution of the amino diol RBM4-67 (35 mg, 0.10 mmol) and Et_3N (29 µL, 0.20 mmol) in anhydrous DCM (1 mL). The reaction mixture was stirred at RT for 3 h and then was diluted with DCM (5mL), and washed successively with water (5 mL) and brine (5 mL). The organic layer was dried over $MgSO_4$, and filtered and concentrated under reduced perssure. The crude was purified by flash column chromatography (hexane:EtOAc; 98:2 to 86:14 gradient) affording 70 % of the colourless oil RBM4-68.

Rf: 0.14 (hexane:EtOAc; 85:15); **$[\alpha]_D$:** +3.7 (*c* 1, $CHCl_3$).

^{1}H NMR ($CDCl_3$): δ 6.24 (d, *J* = 8.0 Hz, 1H), 5.85 – 5.73 (m, 1H), 5.57 (dd, *J* = 15.5, 5.5 Hz, 1H), 4.19 (m, 1H), 4.03 – 3.84 (m, 2H), 3.74 (dd, *J* = 6.5, 4.0 Hz, 1H), 2.28 (m, 4H), 2.23 – 2.17 (t, *J* = 7.5 Hz, 2H), 1.67 – 1.56 (m, 2H), 1.24 (s, 24H), 0.89 (s, 9H), 0.86 (t, *J* = 7.0 Hz, 3H), 0.13 (s, 9H), 0.06 (s, 3H), 0.06 (s, 3H).

^{13}C NMR ($CDCl_3$): δ 173.4 (C), 130.8 (CH), 130.8 (CH), 106.7 (C), 85.1 (C), 74.5 (CH), 63.6 (CH_2), 53.2 (CH), 37.0 (CH_2), 32.1 (CH_2), 31.7 (CH_2), 29.9 (CH_2), 29.8 (CH_2), 29.6 (CH_2), 29.5 (CH_2), 29.4 (CH_2), 25.9 (CH_3), 22.8 (CH_2), 20.1 (CH_2), 18.2 (CH_2), 14.3 (CH_3), 0.3 (CH_3), -5.5 (CH_3), -5.4(CH_3).

ESI-MS *m/z* $C_{34}H_{67}NO_3Si_2$ $[M+Na]^+$ Found: 616.4571; Calculated: 616.4557; $[M+H]^+$ Found: 594.4774; Calculated: 594.4738.

6. REFERENCES

(1) Olsen, I.; Jantzen, E. Sphingolipids in Bacteria and Fungi. *Anaerobe* **2001**, *7*, 103–112.

(2) Shapiro, D.; Flowers, H. M. Studies on Sphingolipids. VII. Synthesis and Configuration of Natural Sphingomyelins. *J. Am. Chem. Soc.* **1962**, *84*, 1047–1050.

(3) Head, B. P.; Patel, H. H.; Insel, P. a. Interaction of Membrane/lipid Rafts with the Cytoskeleton: Impact on Signaling and Function: Membrane/lipid Rafts, Mediators of Cytoskeletal Arrangement and Cell Signaling. *Biochim. Biophys. Acta* **2014**, *1838*, 532–545.

(4) Mao, C.; Obeid, L. M. Ceramidases: Regulators of Cellular Responses Mediated by Ceramide, Sphingosine, and Sphingosine-1-Phosphate. *Biochim. Biophys. Acta* **2008**, *1781*, 424–434.

(5) Futerman, A. H.; Hannun, Y. a. The Complex Life of Simple Sphingolipids. *EMBO Rep.* **2004**, *5*, 777–782.

(6) Hannun, Y. a; Obeid, L. M. Many Ceramides. *J. Biol. Chem.* **2011**, *286*, 27855–27862.

(7) Mandon, E. C.; Ehses, I.; Rother, J.; Echten, G. Van; Sandhoffg, K. Subcellular Localization and Membrane Topology Serine of Palmitoyltransferase , 3-Dehydrosphinganine Reductase , and Sphinganine N-Acyltransferase in Mouse Liver. *J. Biol. Chem.* **1992**, *267*, 11144–11148.

(8) Michel, C.; van Echten-Deckert, G. Conversion of Dihydroceramide to Ceramide Occurs at the Cytosolic Face of the Endoplasmic Reticulum. *FEBS Lett.* **1997**, *416*, 153–155.

(9) Hanada, K. Co-Evolution of Sphingomyelin and the Ceramide Transport Protein CERT. *Biochim. Biophys. Acta* **2014**, *1841*, 704–719.

(10) Tafesse, F. G.; Ternes, P.; Holthuis, J. C. M. The Multigenic Sphingomyelin Synthase Family. *J. Biol. Chem.* **2006**, *281*, 29421–29425.

(11) Maceyka, M.; Spiegel, S. Sphingolipid Metabolites in Inflammatory Disease. *Nature* **2014**, *510*, 58–67.

(12) Hait, N. C.; Oskeritzian, C. a; Paugh, S. W.; Milstien, S.; Spiegel, S. Sphingosine Kinases, Sphingosine 1-Phosphate, Apoptosis and Diseases. *Biochim. Biophys. Acta* **2006**, *1758*, 2016–2026.

(13) Johnson, K. R.; Johnson, K. Y.; Becker, K. P.; Bielawski, J.; Mao, C.; Obeid, L. M. Role of Human Sphingosine-1-Phosphate Phosphatase 1 in the Regulation of Intra- and Extracellular Sphingosine-1-Phosphate Levels and Cell Viability. *J. Biol. Chem.* **2003**, *278*, 34541–34547.

(14) Bourquin, F.; Riezman, H.; Capitani, G.; Grütter, M. G. Structure and Function of Sphingosine-1-Phosphate Lyase, a Key Enzyme of Sphingolipid Metabolism. *Structure* **2010**, *18*, 1054–1065.

(15) Bartke, N.; Hannun, Y. a. Bioactive Sphingolipids: Metabolism and Function. *J. Lipid Res.* **2009**, *50 Suppl*, S91–S96.

(16) Yamaji, T.; Hanada, K. Sphingolipid Metabolism and Interorganellar Transport: Localization of Sphingolipid Enzymes and Lipid Transfer Proteins. *Traffic* **2015**, *16*, 101–122.

(17) Tettamanti, G. Ganglioside / Glycosphingolipid Turnover : New Concepts. *Glycoconj. J.* **2004**, *20*, 301–317.

(18) Borodzicz, S.; Czarzasta, K.; Kuch, M.; Cudnoch-Jedrzejewska, A. Sphingolipids in Cardiovascular Diseases and Metabolic Disorders. *Lipids Health Dis.* **2015**, *14*, 55.

(19) Rajagopalan, V.; Hannun, Y. A. Sphingolipid Metabolism and Signaling as a Target for Cancer Treatment. In *Cell Death in Biology and Diseases. Chapter 8*; 2013; pp 205–229.

(20) Flowers, M.; Fabriás, G.; Delgado, A.; Casas, J.; Abad, J. L.; Cabot, M. C. C6-Ceramide and Targeted Inhibition of Acid Ceramidase Induce Synergistic Decreases in Breast Cancer Cell Growth. *Breast Cancer Res. Treat.* **2012**, *133*, 447–458.

(21) Sänger, N.; Ruckhäberle, E.; Györffy, B.; Engels, K.; Heinrich, T.; Fehm, T.; Graf, A.; Holtrich, U.; Becker, S.; Karn, T. Acid Ceramidase Is Associated with an Improved Prognosis in Both DCIS and Invasive Breast Cancer. *Mol. Oncol.* **2015**, *9*, 58–67.

(22) Farfel-Becker, T.; Vitner, E. B.; Futerman, A. H. Animal Models for Gaucher Disease Research. *Dis. Model. Mech.* **2011**, *4*, 746–752.

(23) Heffernan-Stroud, L. a; Helke, K. L.; Jenkins, R. W.; De Costa, a-M.; Hannun, Y. a; Obeid, L. M. Defining a Role for Sphingosine Kinase 1 in p53-Dependent Tumors. *Oncogene* **2012**, *31*, 1166–1175.

(24) Hannun, Y. a; Obeid, L. M. Principles of Bioactive Lipid Signalling: Lessons from Sphingolipids. *Nat. Rev. Mol. Cell Biol.* **2008**, *9*, 139–150.

(25) Kohno, M.; Momoi, M.; Oo, M. L.; Paik, J.-H.; Lee, Y.-M.; Venkataraman, K.; Ai, Y.; Ristimaki, A. P.; Fyrst, H.; Sano, H.; et al. Intracellular Role for Sphingosine Kinase 1 in Intestinal Adenoma Cell Proliferation. *Mol. Cell. Biol.* **2006**, *26*, 7211–7223.

(26) Borek, C.; Ong, A.; Stevens, V. L.; Wang, E.; Merrill, a H. Long-Chain (sphingoid) Bases Inhibit Multistage Carcinogenesis in Mouse C3H/10T1/2 Cells Treated with Radiation and Phorbol 12-Myristate 13-Acetate. *Proc. Natl. Acad. Sci. U. S. A.* **1991**, *88*, 1953–1957.

(27) Stieber, A.; Mourelatos, Z.; Gonatas, N. K. In Alzheimer ' S Disease the Golgi Apparatus of a Population of Neurons without Neurofibrillary Tangles Is Fragmented and Atrophic. *Am. J. Pathol.* **1996**, *148*, 415–426.

(28) Rivero-Ríos, P.; Gómez-Suaga, P.; Fdez, E.; Hilfiker, S. Upstream Deregulation of Calcium Signaling in Parkinson's Disease. *Front. Mol. Neurosci.* **2014**, *7*, 53.

(29) Zupancic, E.; Carreira, A. C.; Almeida, R. F. M. De; Silva, L. C. Biophysical Implications of Sphingosine Accumulation in Membrane Properties at Neutral and Acidic pH. *J. Phys. Chem. B* **2014**, *118*, 4858–4866.

(30) Sonnino, S.; Prinetti, a. Membrane Domains and the "Lipid Raft" Concept. *Curr. Med. Chem.* **2013**, *20*, 4–21.

(31) Tilcock, C. P.; Cullis, P. R. Lipid Polymorphism. *Ann. N. Y. Acad. Sci.* **1987**, *492*, 88–102.

(32) Marsh, D. Molecular Motion in Phospholipid Bilayers in the Gel Phase: Long Axis Rotation. *Biochemistry* **1980**, *19*, 1632–1637.

(33) Sankaram, M. B.; Thompson, T. E. Interaction of Cholesterol with Various Glycerophospholipids and Sphingomyelin. *Biochemistry* **1990**, *29*, 10670–10675.

(34) Lindblom, G.; Orädd, G. Lipid Lateral Diffusion and Membrane Heterogeneity. *Biochim. Biophys. Acta - Biomembr.* **2009**, *1788*, 234–244.

(35) Devaux, P. F.; Herrmann, A.; Ohlwein, N.; Kozlov, M. M. How Lipid Flippases Can Modulate Membrane Structure. *Biochim. Biophys. Acta - Biomembr.* **2008**, *1778*, 1591–1600.

(36) Binder, W. H.; Barragan, V.; Menger, F. M. Domains and Rafts in Lipid Membranes. *Angew. Chemie - Int. Ed.* **2003**, *42*, 5802–5827.

(37) Singer, S. J.; Nicolson, G. L. The Fluid Mosaic Model of the Structure of Cell Membranes. *Science* **1972**, *175*, 720–731.

(38) Simons, K.; Ikonen, E. Functional Rafts in Cell Membranes. *Nature* **1997**, *387*, 569–572.

(39) Lingwood, D.; Simons, K. Lipid Rafts as a Membrane-Organizing Principle. *Science* **2010**, *327*, 46–50.

(40) Komura, S.; Andelman, D. Physical Aspects of Heterogeneities in Multi-Component Lipid Membranes. *Adv. Colloid Interface Sci.* **2014**, *208*, 34–46.

(41) Leslie, M. Do Lipid Rafts Exist? *Science (80-.).* **2011**, *334*, 1046–1047.

(42) Zhong, J. From Simple to Complex: Investigating the Effects of Lipid Composition and Phase on the Membrane Interactions of Biomolecules Using in Situ Atomic Force Microscopy. *Integr. Biol. (Camb).* **2011**, *3*, 632–644.

(43) Goñi, F. M.; Alonso, A. Biophysics of Sphingolipids I. Membrane Properties of Sphingosine, Ceramides and Other Simple Sphingolipids. *Biochim. Biophys. Acta - Biomembr.* **2006**, *1758*, 1902–1921.

(44) Maula, T.; Kurita, M.; Yamaguchi, S.; Yamamoto, T.; Katsumura, S.; Slotte, J. P. Effects of Sphingosine 2N- and 3O-Methylation on Palmitoyl Ceramide Properties in Bilayer Membranes. *Biophys. J.* **2011**, *101*, 2948–2956.

(45) Phillips, S. C.; Triola, G.; Fabrias, G.; Goñi, F. M.; Dupré, D. B.; Cecilia Yappert, M. Cis-Versus Trans-Ceramides: Effects of the Double Bond on Conformation and H-Bonding Interactions. *J. Phys. Chem. B* **2009**, *113*, 15249–15255.

(46) Jiménez-Rojo, N.; García-Arribas, A. B.; Sot, J.; Alonso, A.; Goñi, F. M. Lipid Bilayers Containing Sphingomyelins and Ceramides of Varying N-Acyl Lengths: A Glimpse into Sphingolipid Complexity. *Biochim. Biophys. Acta - Biomembr.* **2014**, *1838*, 456–464.

(47) Dupuy, F.; Maggio, B. The Hydrophobic Mismatch Determines the Miscibility of Ceramides in Lipid Monolayers. *Chem. Phys. Lipids* **2012**, *165*, 615–629.

(48) Dupuy, F.; Fanani, M. L.; Maggio, B. Ceramide N-Acyl Chain Length: A Determinant of Bidimensional Transitions, Condensed Domain Morphology, and Interfacial Thickness. *Langmuir* **2011**, *27*, 3783–3791.

(49) Sot, J.; Bagatolli, L. a; Goñi, F. M.; Alonso, A. Detergent-Resistant, Ceramide-Enriched Domains in Sphingomyelin/ceramide Bilayers. *Biophys. J.* **2006**, *90*, 903–914.

(50) Holopainen, J. M.; Subramanian, M.; Kinnunen, P. K. J. Sphingomyelinase Induces Lipid Microdomain Formation in a Fluid Phosphatidylcholine/sphingomyelin Membrane. *Biochemistry* **1998**, *37*, 17562–17570.

(51) Huang, H. W.; Goldberg, E. M.; Zidovetzki, R. Ceramide Induces Structural Defects into Phosphatidylcholine Bilayers and Activates Phospholipase A2. *Biochem. Biophys. Res. Commun.* **1996**, *220*, 834–838.

(52) Silva, L.; de Almeida, R. F. M.; Fedorov, A.; Matos, A. P. a; Prieto, M. Ceramide-Platform Formation and -Induced Biophysical Changes in a Fluid Phospholipid Membrane. *Mol. Membr. Biol.* **2006**, *23*, 137–148.

(53) Montes, L. R.; Ruiz-Argüello, M. B.; Goñi, F. M.; Alonso, A. Membrane Restructuring via Ceramide Results in Enhanced Solute Efflux. *J. Biol. Chem.* **2002**, *277*, 11788–11794.

(54) Ruiz-Argüello, M. B.; Basáñez, G.; Goñi, F. M.; Alonso, A. Different Effects of Enzyme-Generated Ceramides and Diacylglycerols in Phospholipid Membrane Fusion and Leakage. *J. Biol. Chem.* **1996**, *271*, 26616–26621.

(55) Colombini, M. Ceramide Channels and Their Role in Mitochondria-Mediated Apoptosis. *Biochim. Biophys. Acta* **2010**, *1797*, 1239–1244.

(56) Samanta, S.; Stiban, J.; Maugel, T. K.; Colombini, M. Visualization of Ceramide Channels by Transmission Electron Microscopy. *Biochim. Biophys. Acta - Biomembr.* **2011**, *1808*, 1196–1201.

(57) Castro, B. M.; Prieto, M.; Silva, L. C. Ceramide: A Simple Sphingolipid with Unique Biophysical Properties. *Prog. Lipid Res.* **2014**, *54*, 53–67.

(58) López-Montero, I.; Rodriguez, N.; Cribier, S.; Pohl, A.; Vélez, M.; Devaux, P. F. Rapid Transbilayer Movement of Ceramides in Phospholipid Vesicles and in Human Erythrocytes. *J. Biol. Chem.* **2005**, *280*, 25811–25819.

(59) Contreras, F. X.; Villar, A. V.; Alonso, A.; Kolesnick, R. N.; Goñi, F. M. Sphingomyelinase Activity Causes Transbilayer Lipid Translocation in Model and Cell Membranes. *J. Biol. Chem.* **2003**, *278*, 37169–37174.

(60) Stancevic, B.; Kolesnick, R. Ceramide-Rich Platforms in Transmembrane Signaling. *FEBS Lett.* **2010**, *584*, 1728–1740.

(61) Goñi, F. M.; Sot, J.; Alonso, A. Biophysical Properties of Sphingosine, Ceramides and Other Simple Sphingolipids. *Biochem. Soc. Trans.* **2014**, *42*, 1401–1408.

(62) Contreras, F.-X.; Sot, J.; Alonso, A.; Goñi, F. M. Sphingosine Increases the Permeability of Model and Cell Membranes. *Biophys. J.* **2006**, *90*, 4085–4092.

(63) Georgieva, R.; Koumanov, K.; Momchilova, A.; Tessier, C.; Staneva, G. Effect of Sphingosine on Domain Morphology in Giant Vesicles. *J. Colloid Interface Sci.* **2010**, *350*, 502–510.

(64) Siskind, L. J.; Fluss, S.; Bui, M.; Colombini, M. Sphingosine Forms Channels in Membranes That Differ Greatly fromThose Formed by Ceramide. *J. Bioenerg. Biomembr.* **2005**, *37*, 227–236.

(65) Jiménez-Rojo, N.; Sot, J.; Viguera, A. R.; Collado, M. I.; Torrecillas, A.; Gómez-Fernández, J. C.; Goñi, F. M.; Alonso, A. Membrane Permeabilization Induced by Sphingosine: Effect of Negatively Charged Lipids. *Biophys. J.* **2014**, *106*, 2577–2584.

(66) Lopez-Garcia, F.; Micol, V.; Villalain, J.; Gomez-Fernandez, J. C. Interaction of Sphingosine and Stearylamine with Phosphatidylserine as Studied by DSC and NMR. *Biochim. Biophys. Acta - Biomembr.* **1993**, *1153*, 1–8.

(67) Sasaki, H.; Arai, H.; Cocco, M. J.; White, S. H. pH Dependence of Sphingosine Aggregation. *Biophys. J.* **2009**, *96*, 2727–2733.

(68) Mivelle, M.; Van Zanten, T. S.; Manzo, C.; Garcia-Parajo, M. F. Nanophotonic Approaches for Nanoscale Imaging and Single-Molecule Detection at Ultrahigh Concentrations. *Microsc. Res. Tech.* **2014**, *77*, 537–545.

(69) Jacobson, K.; Mouritsen, O. G.; Anderson, R. G. W. Lipid Rafts: At a Crossroad between Cell Biology and Physics. *Nat. Cell Biol.* **2007**, *9*, 7–14.

(70) Edidin, M. Lipid Microdomains in Cell Surface Membranes. *Curr. Opin. Struct. Biol.* **1997**, *7*, 528–532.

(71) Wässle, W.; Sandhoff, K. Apparatus for the Loading of Samples on to Thin Layer Chromatography Plates. *J. Chromatogr.* **1968**, *34*, 357–363.

(72) Carrer, D. C.; Maggio, B. Phase Behavior and Molecular Interactions in Mixtures of Ceramide with Dipalmitoylphosphatidylcholine. *J. Lipid Res.* **1999**, *40*, 1978–1989.

(73) Sot, J.; Aranda, F. J.; Collado, M.-I.; Goñi, F. M.; Alonso, A. Different Effects of Long- and Short-Chain Ceramides on the Gel-Fluid and Lamellar-Hexagonal Transitions of Phospholipids: A Calorimetric, NMR, and X-Ray Diffraction Study. *Biophys. J.* **2005**, *88*, 3368–3380.

(74) Perillo, M. a; Polo, a; Guidotti, a; Costa, E.; Maggio, B. Molecular Parameters of Semisynthetic Derivatives of Gangliosides and Sphingosine in Monolayers at the Air-Water Interface. *Chem. Phys. Lipids* **1993**, *65*, 225–238.

(75) Hsueh, Y.-W.; Giles, R.; Kitson, N.; Thewalt, J. The Effect of Ceramide on Phosphatidylcholine Membranes: A Deuterium NMR Study. *Biophys. J.* **2002**, *82*, 3089–3095.

(76) Bonev, B. B. *High-Resolution Solid-State NMR of Lipid Membranes*, 1st ed.; Copyright © 2013 Elsevier Inc. All rights reserved., 2013; Vol. 17.

(77) Boulgaropoulos, B.; Arsov, Z.; Laggner, P.; Pabst, G. Stable and Unstable Lipid Domains in Ceramide-Containing Membranes. *Biophys. J.* **2011**, *100*, 2160–2168.

(78) Chan, K. L. A.; Fale, P. L. V. Label-Free in Situ Quanti Fi Cation of Drug in Living Cells at Micromolar Levels Using Infrared Spectroscopy. **2014**.

(79) Fidorra, M.; Duelund, L.; Leidy, C.; Simonsen, a C.; Bagatolli, L. a. Absence of Fluid-Ordered/fluid-Disordered Phase Coexistence in ceramide/POPC Mixtures Containing Cholesterol. *Biophys. J.* **2006**, *90*, 4437–4451.

(80) Shevchenko, A.; Simons, K. Lipidomics: Coming to Grips with Lipid Diversity. *Nat. Rev. Mol. Cell Biol.* **2010**, *11*, 593–598.

(81) Jones, E. E.; Dworski, S.; Canals, D.; Fabrias, G.; Schoenling, D.; Levade, T.; Denlinger, C.; Hannun, Y. A.; Medin, A.; Drake, R. R. On-Tissue Localization of Ceramides and Other Sphingolipids by MALDI Mass Spectrometry Imaging. **2015**.

(82) Simons, K.; Toomre, D. Lipid Rafts and Signal Transduction. *Nat. Rev. Mol. Cell Biol.* **2000**, *1*, 31–39.

(83) Harder, T.; Scheiffele, P.; Verkade, P.; Simons, K. Lipid Domain Structure of the Plasma Membrane Revealed by Patching of Membrane Components. *J. Cell Biol.* **1998**, *141*, 929–942.

(84) Wilson, B. S.; Pfeiffer, J. R.; Oliver, J. M. Observing FcepsilonRI Signaling from the inside of the Mast Cell Membrane. *J. Cell Biol.* **2000**, *149*, 1131–1142.

(85) Eggeling, C. STED-FCS Nanoscopy of Membrane Dynamics. *Springer Ser. Fluoresc.* **2013**, *13*, 291–310.

(86) Jin, L.; Millard, A. C.; Wuskell, J. P.; Dong, X.; Wu, D.; Clark, H. a; Loew, L. M. Characterization and Application of a New Optical Probe for Membrane Lipid Domains. *Biophys. J.* **2006**, *90*, 2563–2575.

(87) Pinto, S. N.; Fernandes, F.; Fedorov, A.; Futerman, A. H.; Silva, L. C.; Prieto, M. A Combined Fluorescence Spectroscopy, Confocal and 2-Photon Microscopy Approach to Re-Evaluate the Properties of Sphingolipid Domains. *Biochim. Biophys. Acta - Biomembr.* **2013**, *1828*, 2099–2110.

(88) Jovanovic-Talisman, T.; Vukojevic, V. Super-Resolution Fluorescence Imaging and Correlation Spectroscopy: Principles and Examples of Application. *J. Serbian Chem. Soc.* **2013**, *78*, 1671–1688.

(89) Chiantia, S.; Kahya, N.; Ries, J.; Schwille, P. Effects of Ceramide on Liquid-Ordered Domains Investigated by Simultaneous AFM and FCS. *Biophys. J.* **2006**, *90*, 4500–4508.

(90) Larson, D. R.; Gosse, J. a.; Holowka, D. a.; Baird, B. a.; Webb, W. W. Temporally Resolved Interactions between Antigen-Stimulated IgE Receptors and Lyn Kinase on Living Cells. *J. Cell Biol.* **2005**, *171*, 527–536.

(91) Prasad, S.; Zeug, A.; Ponimaskin, E. *Analysis of Receptor-Receptor Interaction by Combined Application of FRET and Microscopy*, 1st ed.; Elsevier Inc., 2013; Vol. 117.

(92) Meyer, B. H.; Segura, J.-M.; Martinez, K. L.; Hovius, R.; George, N.; Johnsson, K.; Vogel, H. FRET Imaging Reveals That Functional Neurokinin-1 Receptors Are Monomeric and Reside in Membrane Microdomains of Live Cells. *Proc. Natl. Acad. Sci. U. S. A.* **2006**, *103*, 2138–2143.

(93) Bhabak, K. P.; Hauser, A.; Redmer, S.; Banhart, S.; Heuer, D.; Arenz, C. Development of a Novel FRET Probe for the Real-Time Determination of Ceramidase Activity. *ChemBioChem* **2013**, *14*, 1049–1052.

(94) Imamura, J.; Suzuki, Y.; Gonda, K.; Roy, C. N.; Gatanaga, H.; Ohuchi, N.; Higuchi, H. Single Particle Tracking Confirms That Multivalent Tat Protein Transduction Domain-Induced Heparan Sulfate Proteoglycan Cross-Linkage Activates Rac1 for Internalization. *J. Biol. Chem.* **2011**, *286*, 10581–10592.

(95) Schütz, G. J.; Kada, G.; Pastushenko, V. P.; Schindler, H. Properties of Lipid Microdomains in a Muscle Cell Membrane Visualized by Single Molecule Microscopy. *EMBO J.* **2000**, *19*, 892–901.

(96) He, H.-T.; Marguet, D. Detecting Nanodomains in Living Cell Membrane by Fluorescence Correlation Spectroscopy. *Annu. Rev. Phys. Chem.* **2011**, *62*, 417–436.

(97) Eggeling, C.; Ringemann, C.; Medda, R.; Schwarzmann, G.; Sandhoff, K.; Polyakova, S.; Belov, V. N.; Hein, B.; von Middendorff, C.; Schönle, A.; et al. Direct Observation of the Nanoscale Dynamics of Membrane Lipids in a Living Cell. *Nature* **2009**, *457*, 1159–1162.

(98) Hein, B.; Willig, K. I.; Hell, S. W. Stimulated Emission Depletion (STED) Nanoscopy of a Fluorescent Protein-Labeled Organelle inside a Living Cell. *Proc. Natl. Acad. Sci. U. S. A.* **2008**, *105*, 14271–14276.

(99) Picas, L.; Milhiet, P. E.; Hernández-Borrell, J. Atomic Force Microscopy: A Versatile Tool to Probe the Physical and Chemical Properties of Supported Membranes at the Nanoscale. *Chem. Phys. Lipids* **2012**, *165*, 845–860.

(100) Loura, L. M. S.; Prieto, M. Lateral Membrane Heterogeneity Probed by FRET Spectroscopy and Microscopy. *Springer Ser. Fluoresc.* **2013**, *13*, 71–114.

(101) Contreras, F.-X.; Basañez, G.; Alonso, A.; Herrmann, A.; Goñi, F. M. Asymmetric Addition of Ceramides but Not Dihydroceramides Promotes Transbilayer (flip-Flop) Lipid Motion in Membranes. *Biophys. J.* **2005**, *88*, 348–359.

(102) Neupane, B.; Ligler, F. S.; Wang, G. Review of Recent Developments in Stimulated Emission Depletion Microscopy: Applications on Cell Imaging. *J. Biomed. Opt.* **2014**, *19*, 80901.

(103) Kuerschner, L.; Thiele, C. Multiple Bonds for the Lipid Interest. *Biochim. Biophys. Acta - Mol. Cell Biol. Lipids* **2014**, *1841*, 1031–1037.

(104) Ecker, J.; Liebisch, G. Application of Stable Isotopes to Investigate the Metabolism of Fatty Acids, Glycerophospholipid and Sphingolipid Species. *Prog. Lipid Res.* **2014**, *54*, 14–31.

(105) Schwarzmann, G.; Arenz, C.; Sandhoff, K. Labeled Chemical Biology Tools for Investigating Sphingolipid Metabolism, Trafficking and Interaction with Lipids and Proteins. *Biochim. Biophys. Acta - Mol. Cell Biol. Lipids* **2014**, *1841*, 1161–1173.

(106) Marsh, D. Electron Spin Resonance in Membrane Research: Protein-Lipid Interactions from Challenging Beginnings to State of the Art. *Eur. Biophys. J.* **2010**, *39*, 513–525.

(107) Pohl, A.; López-Montero, I.; Rouvière, F.; Giusti, F.; Devaux, P. F. Rapid Transmembrane Diffusion of Ceramide and Dihydroceramide Spin-Labelled Analogues in the Liquid Ordered Phase. *Mol. Membr. Biol.* **2009**, *26*, 194–204.

(108) Devaux, P. F.; Fellmann, P.; Hervé, P. Investigation on Lipid Asymmetry Using Lipid Probes: Comparison between Spin-Labeled Lipids and Fluorescent Lipids. *Chem. Phys. Lipids* **2002**, *116*, 115–134.

(109) Kuerschner, L.; Ejsing, C. S.; Ekroos, K.; Shevchenko, A.; Anderson, K. I.; Thiele, C. Polyene-Lipids : A New Tool to Image Lipids. *Nat. Methods* **2005**, *2*, 39–45.

(110) Kyrychenko, A.; Ladokhin, A. S. Molecular Dynamics Simulations of Depth Distribution of Spin- Labeled Phospholipids within Lipid Bilayer. *J. Phys. Chem. B* **2013**, *117*, 5875–5885.

(111) Wildenberg, S. M. J. L. Van Den; Prevo, B.; Peterman, E. J. G.; Ferrand, P. Single Molecule Analysis. *Methods Cell Biol.* **2011**, *783*, 81–99.

(112) Rasmussen, J. M.; Hermetter, A. Chemical Synthesis of Fluorescent Glycero- and Sphingolipids. *Prog. Lipid Res.* **2008**, *47*, 436–460.

(113) Pagano, R. E.; Pagano, R. E.; Sleight, R. G.; Sleight, R. G. Defining Lipid Transport Pathways in Animal Cells. *Science* **1985**, *229*, 1051–1057.

(114) Sharma, D. K.; Choudhury, A.; Singh, R. D.; Wheatley, C. L.; Marks, D. L.; Pagano, R. E. Glycosphingolipids Internalized via Caveolar-Related Endocytosis Rapidly Merge with

the Clathrin Pathway in Early Endosomes and Form Microdomains for Recycling. *J. Biol. Chem.* **2003**, *278*, 7564–7572.

(115) Wang, T. Y.; Silvius, J. R. Different Sphingolipids Show Differential Partitioning into Sphingolipid/cholesterol-Rich Domains in Lipid Bilayers. *Biophys. J.* **2000**, *79*, 1478–1489.

(116) Van Meer, G.; Liskamp, R. M. J. Brilliant Lipids. *Nat. Methods* **2005**, *2*, 14–15.

(117) Kasurinen, J.; Somerharju, P. Metabolism of Pyrenyl Fatty Acids in Baby Hamster Kidney Fibroblasts. Effect of the Acyl Chain Length. *J. Biol. Chem.* **1992**, *267*, 6563–6569.

(118) Hornillos, V.; Tormo, L.; Amat-Guerri, F.; Acuña, a. U. Synthesis and Spectral Properties of Fluorescent Linear Alkylphosphocholines Labeled with All-(E)-1,6-Diphenyl-1,3,5-Hexatriene. *J. Photochem. Photobiol. A Chem.* **2010**, *216*, 79–84.

(119) Antes, P.; Schwarzmann, G.; Sandhoff, K. Distribution and Metabolism of Fluorescent Sphingosines and Corresponding Ceramides Bearing the Diphenylhexatrienyl (DPH) Fluorophore in Cultured Human Fibroblasts. *Eur. J. Cell Biol.* **1992**, *59*, 27–36.

(120) Greenspan, P.; Mayer, E. P.; Fowler, S. D. Nile Red: A Selective Fluorescent Stain for Intracellular Lipid Droplets, J. Cell Biol. 100 (1985) 965–973. *J. Cell Biol.* **1985**, *100*, 965–973.

(121) Wichmann, O.; Wittbrodt, J.; Schultz, C. A Small-Molecule FRET Probe to Monitor Phospholipase A2 Activity in Cells and Organisms. *Angew. Chemie - Int. Ed.* **2006**, *45*, 508–512.

(122) Dagan, A.; Agmon, V.; Gatt, S.; Dinur, T. *Synthesis of Fluorescent Substrates and Their Application to Study of Sphingolipid Metabolism in Vitro and in Intact Cells*; Elsevier Masson SAS, 2000; Vol. 312.

(123) Guo, L.; Zhou, D.; Pryse, K. M.; Okunaded, A. L.; Su, X. Fatty Acid 2-Hydroxylase Mediates Diffusional Mobility of Raft-Associated Lipids, GLUT4 Level, and Lipogenesis in 3T3-L1 Adipocytes. *J. Biol. Chem.* **2010**, *285*, 25438–25447.

(124) Ernst, A. M.; Contreras, F.-X.; Thiele, C.; Wieland, F.; Brügger, B. Mutual Recognition of Sphingolipid Molecular Species in Membranes. *Biochim. Biophys. Acta* **2012**, *1818*, 2616–2622.

(125) Thirsk, C.; Whiting, A. Polyene Natural Products. *J. Chem. Soc. Perkin Trans. 1* **2002**, *1*, 999–1023.

(126) *The Complete Book on Natural Dyes & Pigments*; 2005.

(127) Madden, K.; Whiting, A.; Mosa, F. Non-Isoprenoid Polyene Natural Products - Structures and Synthetic Strategies. *Org. Biomol. Chem.* **2014**, *12*, 7877–7899.

(128) Sklar, L. a; Hudson, B. S.; Simoni, R. D. Conjugated Polyene Fatty Acids as Membrane Probes: Preliminary Characterization. *Proc. Natl. Acad. Sci. U. S. A.* **1975**, *72*, 1649–1653.

(129) Lentz, B. R. Use of Fluorescent Probes to Monitor Molecular Order and Motions within Liposome Bilayers. *Chem. Phys. Lipids* **1993**, *64*, 99–116.

(130) Heyliger, C. E.; Kheshgi, T. J.; Murphy, E. J.; Myers-Payne, S.; Schroeder, F. Fatty Acid Double Bond Orientation Alters Interaction with L-Cell Fibroblasts. *Mol. Cell. Biochem.* **1996**, *155*, 113–119.

(131) Souto, A. A.; Acuña, A. U.; Amat-Guerri, F. A General and Practical Synthesis of Linear Conjugated Pentaenoic Acids. *Tetrahedron Lett.* **1994**, *35*, 5907–5910.

(132) Mateo, C. R.; Souto, a a; Amat-Guerri, F.; Acuña, a U. New Fluorescent Octadecapentaenoic Acids as Probes of Lipid Membranes and Protein-Lipid Interactions. *Biophys. J.* **1996**, *71*, 2177–2191.

(133) Kuerschner, L.; Moessinger, C.; Thiele, C. Imaging of Lipid Biosynthesis: How a Neutral Lipid Enters Lipid Droplets. *Traffic* **2008**, *9*, 338–352.

(134) Kuklev, D. V.; Smith, W. L. Synthesis of Long Chain N-3 and N-6 Fatty Acids Having a Photoactive Conjugated Tetraene Group. *Chem. Phys. Lipids* **2004**, *130*, 145–158.

(135) McIntosh, A. L.; Huang, H.; Atshaves, B. P.; Wellberg, E.; Kuklev, D. V; Smith, W. L.; Kier, A. B.; Schroeder, F. Fluorescent N-3 and N-6 Very Long Chain Polyunsaturated Fatty Acids: Three-Photon Imaging in Living Cells Expressing Liver Fatty Acid-Binding Protein. *J. Biol. Chem.* **2010**, *285*, 18693–18708.

(136) Quesada, E.; Acuña, A. U.; Amat-Guerri, F. New Transmembrane Polyene Bolaamphiphiles as Fluorescent Probes in Lipid Bilayers. *Angew. Chemie - Int. Ed.* **2001**, *40*, 2095–2097.

(137) Acuña, A. U.; Amat-Guerri, F.; Quesada, E.; Vélez, M. Dynamics of Bolaamphiphilic Fluorescent Polyenes in Lipid Bilayers from Polarization Emission Spectroscopy. *Biophys. Chem.* **2006**, *122*, 27–35.

(138) Contreras, F.-X.; Ernst, A. M.; Haberkant, P.; Björkholm, P.; Lindahl, E.; Gönen, B.; Tischer, C.; Elofsson, A.; von Heijne, G.; Thiele, C.; et al. Molecular Recognition of a Single Sphingolipid Species by a Protein's Transmembrane Domain. *Nature* **2012**, *481*, 525–529.

(139) Kuerschner, L.; Richter, D.; Hannibal-Bach, H. K.; Gaebler, A.; Shevchenko, A.; Ejsing, C. S.; Thiele, C. Exogenous Ether Lipids Predominantly Target Mitochondria. *PLoS One* **2012**, *7*, 1–12.

(140) Yan, G.; Peng, L.; Jian, S.; Li, L.; Bottle, S. E. Spin Probes for Electron Paramagnetic Resonance Imaging. *Chinese Sci. Bull.* **2008**, *53*, 3777–3789.

(141) Likhtenshtein, G. I. Nitroxides: 170 Years of History in Biology and Biomedicine. *Int. Res. J. Pure Appl. Chem.* **2015**, *8*, 1–18.

(142) Likhtenstein, G. I.; Ishii, K.; Nakatsuji, S. Dual Chromophore-Nitroxides: Novel Molecular Probes, Photochemical and Photophysical Models and Magnetic Materials. *Photochem. Photobiol.* **2007**, *83*, 871–881.

(143) Blinco, J. P.; Fairfull-Smith, K. E.; Morrow, B. J.; Bottle, S. E. Profluorescent Nitroxides as Sensitive Probes of Oxidative Change and Free Radical Reactions. *Aust. J. Chem.* **2011**, *64*, 373–389.

(144) Liu, Y.; Zhu, M.; Xu, J.; Zhang, H.; Tian, M. Using a TEMPO-Based Fluorescent Probe for Monitoring Oxidative Stress in Living Cells. *Analyst* **2011**, *136*, 4316.

(145) Cao, L.; Wu, Q.; Li, Q.; Shao, S.; Guo, Y. Visualizing the Changes in the Cellular Redox Environment Using a Novel Profluorescent Rhodamine Nitroxide Probe. *New J. Chem.* **2013**, *37*, 2991–2994.

(146) Ahn, H.-Y.; Fairfull-Smith, K. E.; Morrow, B. J.; Lussini, V.; Kim, B.; Bondar, M. V; Bottle, S. E.; Belfield, K. D. Two-Photon Fluorescence Microscopy Imaging of Cellular Oxidative Stress Using Profluorescent Nitroxides. *J. Am. Chem. Soc.* **2012**, *134*, 4721–4730.

(147) Kaiser, R. D.; London, E. Location of Diphenylhexatriene (DPH) and Its Derivatives within Membranes: Comparison of Different Fluorescence Quenching Analyses of Membrane Depth. *Biochemistry* **1998**, *37*, 8180–8190.

(148) Sato, S.; Tsunoda, M.; Suzuki, M.; Kutsuna, M.; Takido-uchi, K.; Shindo, M.; Mizuguchi, H.; Obara, H.; Ohya, H. Synthesis and Spectral Properties of Polymethine-Cyanine Dye-Nitroxide Radical Hybrid Compounds for Use as Fluorescence Probes to Monitor Reducing Species and Radicals. *Spectrochim. Acta - Part A Mol. Biomol. Spectrosc.* **2009**, *71*, 2030–2039.

(149) Mravljak, J.; Ojsteršek, T.; Pajk, S.; Sollner Dolenc, M. Coumarin-Based Dual Fluorescent Spin-Probes. *Tetrahedron Lett.* **2013**, *54*, 5236–5238.

(150) Megha; London, E. Ceramide Selectively Displaces Cholesterol from Ordered Lipid Domains (rafts): Implications for Lipid Raft Structure and Function. *J. Biol. Chem.* **2004**, *279*, 9997–10004.

(151) Fanani, M. L.; Hartel, S.; Maggio, B.; De Tullio, L.; Jara, J.; Olmos, F.; Oliveira, R. G. The Action of Sphingomyelinase in Lipid Monolayers as Revealed by Microscopic Image Analysis. *Biochim. Biophys. Acta - Biomembr.* **2010**, *1798*, 1309–1323.

(152) Green, S. A.; Simpson, D. J.; Zhou, G.; Ho, P. S.; Blough, N. V. Intramolecular Quenching of Excited Singlet States by Stable Nitroxyl Radicals. *J. Am. Chem. Soc.* **1990**, *112*, 7337–7346.

(153) Jiménez-Rojo, N.; Sot, J.; Busto, J. V.; Shaw, W. A.; Duan, J.; Merrill, A. H.; Alonso, A.; Goñi, F. M. Biophysical Properties of Novel 1-Deoxy-(Dihydro)ceramides Occurring in Mammalian Cells. *Biophys. J.* **2014**, *107*, 2850–2859.

(154) Catalán, J.; Ṕrez, P.; Hopf, H.; Klein, D. The Photophysics of All-Trans Polyenes from ttbP5, a Nonphotolabile Pentaene. *J. Chem. Phys.* **2008**, *129*.

(155) Negishi, E. I.; Huang, Z.; Wang, G.; Mohan, S.; Wang, C.; Hattori, H. Recent Advances in Efficient and Selective Synthesis of Di-, Tri-, and Tetrasubstituted Alkenes via Pd-Catalyzed Alkenylation-Carbonyl Olefination Synergy. *Acc. Chem. Res.* **2008**, *41*, 1474–1485.

(156) Cichowicz, N. R.; Nagorny, P. Synthesis of Conjugated Polyenes via Sequential Condensation of Sulfonylphosphonates and Aldehydes. *Org. Lett.* **2012**, *14*, 1058–1061.

(157) Peterson, J. A Carbonyl Olefination Reaction Using Silyl- Substituted Organometallic Compounds. *J. Org. Chem.* **1968**, *33*, 780–784.

(158) Wang, G.; Huang, Z.; Negishi, E. I. Highly Stereoselective and Efficient Synthesis of W-Heterofunctional Di- and Trienoic Esters for Horner-Wadsworth-Emmons Reaction via Alkyne Hydrozirconation and Pd-Catalyzed Alkenylation. *Tetrahedron Lett.* **2009**, *50*, 3220–3223.

(159) Woerly, E. M.; Roy, J.; Burke, M. D. Synthesis of Most Polyene Natural Product Motifs Using Just 12 Building Blocks and One Coupling Reaction. *Nat. Chem.* **2014**, *6*, 484–491.

(160) Wang, G.; Huang, Z.; Negishi, E. Efficient and Selective Syntheses of (all-E)- and (6E , 10Z)-2 ′-O-Methylmyxalamides D via Pd-Catalyzed Alkenylation-Carbonyl Olefination Synergy. *Org. Lett.* **2008**, *10*, 3223–3226.

(161) Maryanoff, B. E. The Wittig Olefination Reaction and Modifications Involving Phosphoryl-Sta Bilized Carbanions. Stereochemistry, Mechanism, and Selected Synthetic Aspects. *Chem. Rev.* **1989**, *89*, 863–927.

(162) Gu, Y.; Tian, S.-K. Olefination Reactions of Phosphorus-Stabilized Carbon Nucleophiles. *Top. Curr. Chem.* **2012**, *327*, 197–238.

(163) Brandt, P.; Norrby, P. A Quantum Chemical Exploration of the Horner-Wadsworth-Emmons Reaction. *J. Org. Chem.* **1998**, *63*, 1280–1289.

(164) Kim, J.; Park, K. S.; Yeo, W. S.; Chong, Y. Quantum Mechanical Investigation of the Horner-Wadsworth-Emmons Reaction of Benzyl Pyridyl Ketone. *Bull. Korean Chem. Soc.* **2008**, *29*, 1269–1272.

(165) Li, W.-R.; Chou, H.-H. A Facile Synthesis of Amides from 9-Fluorenylmethyl Carbamates and Acid Derivatives. *Synthesis (Stuttg).* **2000**, 84–90.

(166) Sun, H.; Kong, R.; Zhu, D.; Lu, M.; Ji, Q.; Liew, C. W.; Lescar, J.; Zhong, G.; Liang, Z.-X. Products of the Iterative Polyketide Synthases in 9- and 10-Membered Enediyne Biosynthesis. *Chem. Commun.* **2009**, 7399–7401.

(167) D'Amico, K. L.; Manos, C.; Christensen, R. L. Electronic Energy Levels in a Homologous Series. *J. Am. Chem. Soc.* **1980**, *102*, 1777–1782.

(168) Pini, E.; Bertacche, V.; Molinari, F.; Romano, D.; Gandolfi, R. Direct Conversion of Polyconjugated Compounds into Their Corresponding Carboxylic Acids by Acetobacter Aceti. *Tetrahedron* **2008**, *64*, 8638–8641.

(169) Snyder, R.; Arvidson, E.; Foote, C.; Harrigan, L.; Christensen, R. L. Electronic Energy Levels in Long Polyenes: S2 -->S0 Emission in All-Trans-1,3,5,7,9,11,13-Tetradecaheptaene. *J. Am. Chem. Soc.* **1985**, *107*, 4117–4122.

(170) Kuhn, R.; Grundmann, C. Synthese von Des-Crocetin (Tetradecaheptaen-(1.3.5.7.9.11.13)-Dicarbonsäure-(1.14). *Chem. Ber.* **1937**, *70*, 1318.

(171) Blout, E. R.; Fields, M. Absorption Spectra. V. The Ultraviolet and Visible Spectra of Certain Polyene Aldehydes and Polyene Azines. *J. Am. Chem. Soc.* **1948**, *70*, 189–193.

(172) Duhamel, L.; Guillemont, J.; Le Gallic, Y.; Plé, G.; Poirier, J.-M.; Ramondenc, Y.; Chabardes, P. Polyunsaturated Aldehydes by Direct Polyvinylogation of Carbonyl Functionalized Phosphonates. *Tetrahedron Lett.* **1990**, *31*, 3129–3132.

(173) Ley, S. V.; Smith, S. C.; Woodward, P. R. Use of T-Butyl 4-Diethylphosphono-3-Oxobutanethioate for Tetramic Acid Synthesis: Total Synthesis of the Plasmodial Pigment Fuligorubin A. *Tetrahedron Lett.* **1988**, *29*, 5829–5832.

(174) Ley, S. V.; Smith, S. C.; Woodward, P. R. Further Reactions of T-Butyl 3-Oxobutanthioate and T-Butyl 4-Diethyl-Phosphono-3-Oxobutanthioate: Carbonyl Coupling Reactions, Amination, Use in the Preparation of 3-Acyltetramic Acids and Application to the Total Synthesis of Fuligorubin A. *Tetrahedron* **1992**, *48*, 1145–1174.

(175) Olson, A. S.; Chen, H.; Du, L.; Dussault, P. H. Synthesis of a 2,4,6,8,10-Dodecapentanoic Acid Thioester as a Substrate for Biosynthesis of Heat Stable Antifungal Factor (HSAF). *RSC Adv.* **2015**, *5*, 11644–11648.

(176) Harding, K. E.; May, L. M.; Dick, K. F. Selective Oxidation of Allylic Alcohols with Chromic Acid. *J. Org. Chem.* **1975**, *40*, 1664–1665.

(177) Fichna, J.; Lewellyn, K.; Yan, F.; Roth, B. L.; Zjawiony, J. K. Synthesis and Biological Evaluation of New Salvinorin A Analogues Incorporating Natural Amino Acids. *Bioorganic Med. Chem. Lett.* **2011**, *21*, 160–163.

(178) Kim, M. H.; Patel, D. V. “BOP” as a Reagent for Mild and Efficient Preparation of Esters. *Tetrahedron Lett.* **1994**, *35*, 5603–5606.

(179) Mckillop, A.; Taylor, R. J. K. .; Watson, R. J. .; Lewis, N. An Improved Procedure for the Preparation of the Garner Aldehyde and Its Use for the Synthesis of N-Protected 1-Halo-2-(R)-Amino-3-Butenes. *Synthesis (Stuttg).* **1994**, 31–33.

(180) Menger, F. M.; Zhang, H. Peptoads, a Group of Amphiphilic Long-Chain Triamides. *Langmuir* **2005**, *21*, 10428–10438.

(181) Neises, B.; Steglich, W. Simple Method for the Esterification of Carboxylic Acids. *Angew. Chemie Int. Ed. English* **1978**, *17*, 522–524.

(182) Sezgin, E.; Schwille, P. Model Membrane Platforms to Study Protein-Membrane Interactions. *Mol. Membr. Biol.* **2012**, *29*, 144–154.

(183) Altaf, M. Bhai, S.; Yadav, V.; Y, M.; V. V., P. Liposomes: An Overview. *J. Pharm. Sci. Innov.* **2012**, *1*, 13–21.

(184) Bangham, A. D.; Standish, M. M.; Watkins, J. C. Diffusion of Univalent Ions across the Lamellae of Swollen Phospholipids. *J. Mol. Biol.* **1965**, *13*, 238–252.

(185) Chen, C.; Zhu, S.; Huang, T.; Wang, S.; Yan, X. Analytical Techniques for Single-Liposome Characterization. *Anal. Methods* **2013**, *5*, 2150–2157.

(186) Puff, N.; Angelova, M. I. Chapter 7 Lipid Vesicles-Development and Applications for Studding Membrane Heterogeneity and Interactions. *Adv. Planar Lipid Bilayers Liposomes* **2006**, *5*, 173–228.

(187) Bagatolli, L. a.; Needham, D. Quantitative Optical Microscopy and Micromanipulation Studies on the Lipid Bilayer Membranes of Giant Unilamellar Vesicles. *Chem. Phys. Lipids* **2014**, *181*, 99–120.

(188) Morales-Penningston, N. F.; Wu, J.; Farkas, E. R.; Goh, S. L.; Konyakhina, T. M.; Zheng, J. Y.; Webb, W. W.; Feigenson, G. W. GUV Preparation and Imaging: Minimizing Artifacts. *Biochim. Biophys. Acta - Biomembr.* **2010**, *1798*, 1324–1332.

(189) Fenz, S. F.; Sengupta, K. Giant Vesicles as Cell Models. *Integr. Biol.* **2012**, *4*, 982.

(190) Kahya, N.; Petra, M. Pushing the Complexity of Model Bilayers : Novel Prospects for Membrane Biophysics. *Fluoresc. Supermolecules, Polym. Nanosyst.* **2008**, *4*, 339–359.

(191) Reeves, J. P.; Dowben, R. M. Formation and Properties of Thin-Walled Phospholipid Vesicles. *J. Cell. Physiol.* **1969**, *73*, 49–60.

(192) Angelova, M. I.; Dimitrov, D. S. Liposome Electroformation. *Faraday Discuss. Chem. Soc.* **1986**, *81*, 303–311.

(193) M. I. Angelova, S.; Soléau, P.; Méléard, F.; Faucon, P. B. Preparation of Giant Vesicles by External AC Electric Fields. Kinetics and Applications. *Prog. Colloid Polym. Sci.* **1992**, *89*, 127–131.

(194) Hudson, B.; Kohler, B. Linear Polyene Electronic Structure and Spectroscopy. *Annu. Rev. Phys. Chem.* **1974**, *25*, 437–460.

(195) Hudson, B. S.; Kohler, B. E.; Schulten, K. *Linear Polyene Electronic Structures and Potential Surfaces*; 1982; Vol. 6.

(196) Quesada, E.; Delgado, J.; Hornillos, V.; Acuña, a. U.; Amat-Guerri, F. Synthesis and Spectral Properties of Amphiphilic Lipids with Linear Conjugated Polyene and Phenylpolyene Fluorescent Groups. *European J. Org. Chem.* **2007**, *2007*, 2285–2295.

(197) Lakowicz, J. R. Quenching of Fluorescence. In *Principles of fluorescence spectroscopy*; 2006; pp 277–330.

(198) Itoh, T. Fluorescence and Phosphorescence from Higher Excited States of Organic Molecules. *Chem. Rev.* **2012**, *112*, 4541–4568.

(199) Patalag, L. J.; Werz, D. B. Fluorescent Penta- and Hexaene Fatty Acids by a Wittig-Horner/elimination Strategy. *J. Org. Chem.* **2012**, *77*, 5297–5304.

(200) Sinkeldam, R. W.; Greco, N. J.; Tor, Y. Fluorescent Analogs of Biomolecular Building Blocks: Design, Properties, and Applications. *Chem. Rev.* **2010**, *110*, 2579–2619.

(201) Morris, J. V; Mahaney, M. a; Huber, J. R. Fluorescence Quantum Yield Determinations. 9,10-Diphenylanthracene as a Reference Standard in Different Solvents. *J. Phys. Chem.* **1976**, *80*, 969–974.

(202) Lide, D. R. *CRC Handbook of Chemistry and Physics*; 1992.

(203) Goñi, F. M.; Alonso, A. Differential Scanning Calorimetry in the Study of Lipid Structures. In *Chemical Biology: Applications and Techniques*; 2006; pp 47–66.

(204) Spink, C. H. Differential Scanning Calorimetry. *Methods Cell Biol.* **2008**, *84*, 115–141.

(205) Huang, C. H.; Li, S. Calorimetric and Molecular Mechanics Studies of the Thermotropic Phase Behavior of Membrane Phospholipids. *Biochim. Biophys. Acta - Rev. Biomembr.* **1999**, *1422*, 273–307.

(206) Davis, P. J.; Coolbear, K. P.; Keough, K. M. Differential Scanning Calorimetric Studies of the Thermotropic Phase Behaviour of Membranes Composed of Dipalmitoyl Lecithin and Mixed-Acid Unsaturated Lecithins. *Can. J. Biochem.* **1980**, *58*, 851–858.

(207) Goñi, F. M.; Alonso, A. Structure and Functional Properties of Diacylglycerols in Membranes. *Prog. Lipid Res.* **1999**, *38*, 1–48.

(208) Aresta-Branco, F.; Cordeiro, A. M.; Marinho, H. S.; Cyrne, L.; Antunes, F.; De Almeida, R. F. M. Gel Domains in the Plasma Membrane of Saccharomyces Cerevisiae: Highly

Ordered, Ergosterol-Free, and Sphingolipid-Enriched Lipid Rafts. *J. Biol. Chem.* **2011**, *286*, 5043–5054.

(209) Rai, V.; Dey, N. The Basics of Confocal Microscopy. In *Laser Scanning, Theory and Applications*; 2011; pp 75–96.

(210) Lakowicz, J. R. Multiphoton Excitation and Microscopy. In *Principles of Fluorescence Spectroscopy*; Springer US: Boston, MA, 1999; pp 606–621.

(211) Denk, W.; Strickler, J. H.; Webb, W. W. Two-Photon Laser Scanning Fluorescence Microscopy. *Science (80-.).* **1990**, *248*, 73–76.

(212) Wesołowska, O.; Michalak, K.; Maniewska, J.; Hendrich, A. B. Giant Unilamellar Vesicles - a Perfect Tool to Visualize Phase Separation and Lipid Rafts in Model Systems. *Acta Biochim. Pol.* **2009**, *56*, 33–39.

(213) Montes, L.-R.; Alonso, A.; Goñi, F. M.; Bagatolli, L. a. Giant Unilamellar Vesicles Electroformed from Native Membranes and Organic Lipid Mixtures under Physiological Conditions. *Biophys. J.* **2007**, *93*, 3548–3554.

(214) Breton, M.; Amirkavei, M.; Mir, L. M. Optimization of the Electroformation of Giant Unilamellar Vesicles (GUVs) with Unsaturated Phospholipids. *J. Membr. Biol.* **2015**, Ahead of Print.

(215) Juhasz, J.; Davis, J. H.; Sharom, F. J. Fluorescent Probe Partitioning in Giant Unilamellar Vesicles of “Lipid Raft” Mixtures. *Biochem. J.* **2010**, *430*, 415–423.

(216) Sot, J.; Ibarguren, M.; Busto, J. V.; Montes, L. R.; Goñi, F. M.; Alonso, A. Cholesterol Displacement by Ceramide in Sphingomyelin-Containing Liquid-Ordered Domains, and Generation of Gel Regions in Giant Lipidic Vesicles. *FEBS Lett.* **2008**, *582*, 3230–3236.

(217) Veiga, M. P.; Arrondo, J. L.; Goñi, F. M.; Alonso, a. Ceramides in Phospholipid Membranes: Effects on Bilayer Stability and Transition to Nonlamellar Phases. *Biophys. J.* **1999**, *76*, 342–350.

(218) Busto, J. V.; García-Arribas, A. B.; Sot, J.; Torrecillas, A.; Gómez-Fernández, J. C.; Goñi, F. M.; Alonso, A. Lamellar Gel (Lβ) Phases of Ternary Lipid Composition Containing Ceramide and Cholesterol. *Biophys. J.* **2014**, *106*, 621–630.

(219) Brynda, M. Introduction to Electron Paramagnetic Resonance Spectroscopy. In *Handbook of Modern Biophysics*; 2010; Vol. 3, pp 59–98.

(220) Klare, J. P. Biomedical Applications of Electron Paramagnetic Resonance (EPR) Spectroscopy. *Biomed. Spectrosc. Imaging* **2012**, *1*, 101–124.

(221) Pentak, D.; Sułkowski, W. W.; Wolinska, A.; Maslanka, S.; Bojko, B.; Maciazek, M.; Równicka, J.; Sulkowska, A. Application of Spin Markers for Study of Liposome Prepared by the Modified Reverse-Phase Evaporation Method. In *Spectroscopy*; 2008; Vol. 22, pp 33–41.

(222) Fajer, P. G. Electron Spin Resonance Spectroscopy Labeling in Peptide and Protein Analysis. In *Encyclopedia of Analytical Chemistry*; 2000; pp 5725–5761.

(223) Berliner, L. *Spin Labeling: Theory and Applications*; 1976.

(224) Tikhonov, A. N.; Subczynski, W. K. Application of Spin Labels To Membrane Bioenergetics. In *Biological Magnetic Resonance*; 2005; pp 147–194.

(225) Brown, L. R.; Bösch, C.; Wüthrich, K. Location and Orientation Relative to the Micelle Surface for Glucagon in Mixed Micelles with Dodecylphosphocholine: EPR and NMR Studies. *Biochim. Biophys. Acta* **1981**, *642*, 296–312.

(226) Freed, J. H. Theory of Slow Tumbling ESR Spectra for Nitroxides. In *Spin Labeling: Theory and Applications*; 1976; pp 53–132.

(227) Goldman, S.; Bruno, G.; Freed, J. H. Estimating Slow-Motional Rotational Correlation Times for Nitroxides by Electron Spin Resonance. *J. Phys. …* **1972**, *76*, 1858–1860.

(228) Gordon, L. M.; Sauerheber, R. D.; Esgate, J. a. Spin Label Studies on Rat Liver and Heart Plasma Membranes: Effects of Membrane Fluidity. *J. Supramol. Struct.* **1978**, *9*, 299–326.

(229) Mizushima, J.; Kawasaki, Y.; Tabohashi, T.; Kitano, T.; Sakamoto, K.; Kawashima, M.; Cooke, R.; Maibach, H. I. Effect of Surfactants on Human Stratum Corneum: Electron Paramagnetic Resonance Study. *Int. J. Pharm.* **2000**, *197*, 193–202.

(230) Nagumo, A.; Sato, Y.; Suzuki, Y. Electron Spin Resonance Studies of Phosphatidylcholine Interacted with Cholesterol and with a Hopanoid in Liposomal Membrane. *Chem. Pharm. Bull. (Tokyo).* **1991**, *39*, 3071–3074.

(231) Sułkowski, W. W.; Pentak, D.; Nowak, K.; Sułkowska, A. The Influence of Temperature and pH on the Structure of Liposomes Formed from DMPC. *J. Mol. Struct.* **2006**, *792-793*, 257–264.

(232) Usta, J.; El Bawab, S.; Roddy, P.; Szulc, Z. M.; Hannun, Y. a.; Bielawska, a. Structural Requirements of Ceramide and Sphingosine Based Inhibitors of Mitochondrial Ceramidase. *Biochemistry* **2001**, *40*, 9657–9668.

(233) Obeid, L. M.; Mao, C.; Xu, R. Human and Mouse Alkaline Ceramidase 1 and Skin Diseases. In *Patent; US 2006/0099681 A1*; 2006; pp 1–15.

(234) Shapiro, D.; Segal, H.; Flowers, H. M. The Total Synthesis of Sphingosine. *J. Am. Chem. Soc.* **1958**, *80*, 1194–1197.

(235) Morales-Serna, J. A.; Llaveria, J.; Díaz, Y.; Matheu, M. I.; Castillón, S. Recent Advances in the Synthesis of Sphingosine and Phytosphingosine, Molecules of Biological Significance. *Curr. Org. Chem.* **2010**, *14*, 2483–2521.

(236) Curfman, C.; Liotta, D. Synthesis of Sphingosine and Sphingoid Bases. *Methods Enzymol.* **2000**, *311*, 391–440.

(237) Liao, J.; Tao, J.; Lin, G.; Liu, D. Chemistry and Biology of Sphingolipids. *Tetrahedron* **2005**, *61*, 4715–4733.

(238) Bera, S.; Mondal, D.; Singh, M.; Kale, R. K. Advances in Serinals for Asymmetric Synthesis. *Tetrahedron* **2013**, *69*, 969–1011.

(239) Garner, P. Stereocontrolled Addition to a Penaldic Acid Equivalent: An Asymmetric Synthesis of Threo-B-Hydroxy-L-Glutamic Acid. *Tetrahedron Lett.* **1984**, *25*, 5855–5858.

(240) Passiniemi, M.; Koskinen, A. M. P. Garner's Aldehyde as a Versatile Intermediate in the Synthesis of Enantiopure Natural Products. *Beilstein J. Org. Chem.* **2013**, *9*, 2641–2659.

(241) Liang, X.; Andersch, J.; Bols, M. Garner's Aldehyde. *J. Chem. Soc. Perkin Trans. 1* **2001**, 2136–2157.

(242) Campbell, A. D.; Raynham, T. M.; Taylor, R. J. K. A Simplified Route to the (R)-Garner Aldehyde and (S)-Vinyl Glycinol. *Synthesis (Stuttg).* **1998**, 1707–1709.

(243) Bose, S.; Ghosh, S. Olefin Metathesis — Application in the Synthesis of Natural Products and Related Organic Compounds. *Proc Indian Natn Sci Acad* **2014**, *80*, 37–54.

(244) Connon, S. J.; Blechert, S. Recent Developments in Olefin Cross-Metathesis. *Angew. Chemie - Int. Ed.* **2003**, *42*, 1900–1923.

(245) Grubbs, R. H.; Chang, S. Recent Advances in Olefin Metathesis and Its Application in Organic Synthesis. *Tetrahedron* **1998**, *54*, 4413–4450.

(246) Hérisson, J.-L.; Chauvin, Y. Catalyse de Transformation Des Oléfines Par Les Complexes Du Tungstène. *Die Makromol. Chemie* **1970**, *141*, 161–176.

(247) Wallace, K. C.; Dewan, J. C.; Schrock, R. R. Isolation and Characterization of the First Simple Tantalacyclobutane Complexes. *Organometallics* **1986**, *5*, 2162–2164.

(248) Chatterjee, A. K.; Choi, T. L.; Sanders, D. P.; Grubbs, R. H. A General Model for Selectivity in Olefin Cross Metathesis. *J. Am. Chem. Soc.* **2003**, *125*, 11360–11370.

(249) Schrock, R. R.; Murdzek, J. S.; Bazan, G. C.; Robbins, J.; DiMare, M.; O'Regan, M. Synthesis of Molybdenum Imido Alkylidene Complexes and Some Reactions Involving Acyclic Olefins. *J. Am. Chem. Soc.* **1990**, *112*, 3875–3886.

(250) Scholl, M.; Ding, S.; Lee, C. W.; Grubbs, R. H. Synthesis and Activity of a New Generation of Ruthenium-Based Olefin Metathesis Catalysts Coordinated with 1,3-Dimesityl-4,5-Dihydroimidazol-2-Ylidene Ligands. *Org. Lett.* **1999**, *1*, 953–956.

(251) Sanford, M. S.; Ulman, M.; Grubbs, R. H. New Insights into the Mechanism of Ruthenium-Catalyzed Olefin Metathesis Reactions. *J. Am. Chem. Soc.* **2001**, *123*, 749–750.

(252) Sanford, M. S.; Love, J. a.; Grubbs, R. H. Mechanism and Activity of Ruthenium Olefin Metathesis Catalysts. *J. Am. Chem. Soc.* **2001**, *123*, 6543–6554.

(253) Ghosal, P.; Shaw, A. K. An Efficient Total Synthesis of the Anticancer Agent (+)-Spisulosine (ES-285) from Garner's Aldehyde. *Tetrahedron Lett.* **2010**, *51*, 4140–4142.

(254) Ullrich, T.; Ghobrial, M.; Peters, C.; Billich, A.; Guerini, D.; Nussbaumer, P. Synthesis and Immobilization of Erythro-C14-Omega-Aminosphingosine-1-Phosphate as a Potential Tool for Affinity Chromatography. *ChemMedChem* **2008**, *3*, 356–360.

(255) Rai, A. N.; Basu, A. Sphingolipid Synthesis via Olefin Cross Metathesis: Preparation of a Differentially Protected Building Block and Application to the Synthesis of D-Erythro-Ceramide. *Org. Lett.* **2004**, *6*, 2861–2863.

(256) Rai, A. N.; Basu, A. Synthesis of the Glycosphingolipid -Galactosyl Ceramide and Analogues via Olefin Cross Metathesis. *J. Org. Chem.* **2005**, *70*, 8228–8230.

(257) Chaudhari, V. D.; Kumar, K. S. A.; Dhavale, D. D. An Efficient Synthesis of D -Erythro- and D -Threo-Sphingosine from D -Glucose : Olefin Cross-Metathesis Approach. *Org. Lett.* **2005**, *7*, 5805–5807.

(258) Yamamoto, T.; Hasegawa, H.; Hakogi, T.; Katsumura, S. Versatile Synthetic Method for Sphingolipids and Functionalized Sphingosine Derivatives via Olefin Cross Metathesis. *Org. Lett.* **2006**, *8*, 5569–5572.

(259) Torssell, S.; Somfai, P. A Practical Synthesis of D - Erythro -Sphingosine Using a Cross-Metathesis Approach. *Org. Biomol. Chem.* **2004**, *2*, 1643–1646.

(260) Nussbaumer, P.; Ettmayer, P.; Peters, C.; Rosenbeiger, D.; Högenauer, K. One-Step Labelling of Sphingolipids via a Scrambling Cross-Metathesis Reaction. *Chem. Commun. (Camb).* **2005**, 5086–5087.

(261) Peters, C.; Billich, A.; Ghobrial, M.; Högenauer, K.; Ullrich, T.; Nussbaumer, P. Synthesis of Borondipyrromethene (BODIPY)-Labeled Sphingosine Derivatives by Cross-Metathesis Reaction. *J. Org. Chem.* **2007**, *72*, 1842–1845.

(262) Bandhuvula, P.; Li, Z.; Bittman, R.; Saba, J. D. Sphingosine 1-Phosphate Lyase Enzyme Assay Using a BODIPY-Labeled Substrate. *Biochem. Biophys. Res. Commun.* **2009**, *380*, 366–370.

(263) Tanaka, H.; Yoshimura, Y.; Dovichi, N. J.; Palcic, M. M.; Hindsgaul, O. A Concise Chemical Synthesis of a Fluorescent betaGal-(1,4)-S-betaGlc-Cer Derivative and Its Enzymatic Elongation by Glycosyltransferases. *Tetrahedron Lett.* **2012**, *53*, 1812–1815.

(264) Wittig, G.; Geissler, G. Zur Reaktionsweise Des Pentaphenyl-Phosphors Und Einiger Derivate. *Justus Liebigs Ann. Chem.* **1953**, *580*, 44–57.

(265) Schlosser, M.; Tuong, H. B.; Schaub, B. The Betaine-Ylid Route to Trans-Alkenols. *Tetrahedron Lett.* **1985**, *26*, 311–314.

(266) Vedejs, E. Georg Wittig and the Betaine: What Controversy? *Phosphorus. Sulfur. Silicon Relat. Elem.* **2015**, *190*, 612–618.

(267) Baccolini, G.; Delpivo, C.; Micheletti, G. Olefin from Nonstabilized Ylides. *Phosphorus. Sulfur. Silicon Relat. Elem.* **2012**, *187*, 1291–1302.

(268) Byrne, P. a; Gilheany, D. G. The Modern Interpretation of the Wittig Reaction Mechanism. *Chem. Soc. Rev.* **2013**, *42*, 6670–6696.

(269) Oh, J. S.; Hyun Kim, B.; Gyu Kim, Y. (E)-Selective Wittig Reactions of Garner's Aldehyde with Nonstabilized Ylides. *Tetrahedron Lett.* **2004**, *45*, 3925–3928.

(270) Coyle, E. E.; Doonan, B. J.; Holohan, A. J.; Walsh, K. a.; Lavigne, F.; Krenske, E. H.; O'Brien, C. J. Catalytic Wittig Reactions of Semi- and Nonstabilized Ylides Enabled by Ylide Tuning. *Angew. Chemie Int. Ed.* **2014**, *53*, 12907–12911.

(271) Ernst, H. Wittig Olefination. In *Carotenoids, Chapter 2, Part III*; 1996; pp 79–102.

(272) Ernst, H. Recent Advances in Industrial Carotenoid Synthesis. *Pure Appl. Chem.* **2002**, *74*, 2213–2226.

(273) Pini, E.; Rossi, E.; Celentano, G.; Stradi, R. A Simple Synthesis of 1-Aryl-Polyenes. *Org. Prep. Proced. Int.* **2002**, *34*, 198–203.

(274) Spangler, C. W.; Mccoy, R. K.; Dembek, A. a; Sapochak, L. S.; Gates, B. D. Preparation of P,p'- Disubstituted-A,w- Diphenyl Polyenes. *J. Chem. Soc. Perkin Trans. 1* **1989**, 151–154.

(275) Ideses, R.; Shani, A. Study of the Radical Mechanism of Iodine-Catalyzed Isomerization of Conjugated Diene Systems. *J. Am. Oil Chem. Soc.* **1989**, *66*, 948–952.

(276) Benson, S. W.; Egger, K. W.; Golden, D. M. Iodine-Catalyzed Isomerization of Olefins. III. Kinetics of the Geometrical Isomerization of Butene-2 and the Rate of Rotation About a Single Bond. *J. Am. Chem. Soc.* **1965**, *87*, 468–476.

(277) Hepperle, S. S.; Li, Q.; East, A. L. L. Mechanism of Cis/trans Equilibration of Alkenes via Iodine Catalysis. *J. Phys. Chem. A* **2005**, *109*, 10975–10981.

(278) Garner, P.; Park, J. M. Asymmetric Synthesis of 5-O-Carbamoylpolyoxamic Acid from D-Serine. *J. Org. Chem.* **1988**, *53*, 2979–2984.

(279) Coleman, R. S.; Carpenter, A. J. Diastereoselective Addition of Vinyl Organometallic Reagents to L-Serinal. *Tetrahedron Lett.* **1992**, *33*, 1697–1700.

(280) Byrne, P. A.; Rajendran, K. V.; Muldoon, J.; Gilheany, D. G. Supporting Information: A Convenient Chromatography-Free Method for the Purification of Alkenes Produced in the Wittig Reaction. *Org. Biomol. Chem.* **2012**, *10*, 3531–3537.

(281) Triola, G.; Fabriàs, G.; Casas, J.; Llebaria, A. Synthesis of Cyclopropene Analogues of Ceramide and Their Effect on Dihydroceramide Desaturase. *J. Org. Chem.* **2003**, *68*, 9924–9932.

(282) Niel, G.; Roux, F.; Maisonnasse, Y.; Maugras, I.; Poncet, J.; Jouin, P. Substrate-Controlled Crotylboration T from N-(tert-Butoxycarbony1)amino Aldehydes. *J. Chem. Soc. Perkin Trans. 1* **1994**, 1275–1280.

(283) Clayden, J.; Greeves, N.; Warren, S.; Wothers, P. *Organic Chemistry. Chapter 34*; 2001.

(284) Karjalainen, O. K.; Koskinen, A. M. P. Diastereoselective Synthesis of Vicinal Amino Alcohols. *Org. Biomol. Chem.* **2012**, *10*, 4311.

(285) Herold, P. Synthesis of D-Erythro- and D-Threo-Sphingosine Derivatives from L-Serine. *Helv. Chim. Acta.* **1988**, *71*, 354–362.

(286) Garner, P.; Park, J. M.; Malecki, E. A Stereodivergent Synthesis of D-Erythro-Sphingosine and D-Threo-Sphingosine from L-Serine. *J. Org. Chem.* **1988**, *53*, 4395–4398.

(287) Nimkar, S.; Menaldino, D.; Merrill, A. H.; Liotta, D. A Stereoselective Synthesis of Sphingosine, a Protein Kinase C Inhibitor. *Tetrahedron Lett.* **1988**, *29*, 3037–3040.

(288) Garner, P.; Park, J. M. Glycosyl Alpha-Amino Acids via Stereocontrolled Buildup of a Penaldic Acid Equivalent. A Novel Synthetic Approach to the Nucleosidic Component of the Polyoxins and Related Substances. *J. Org. Chem.* **1990**, *55*, 3772–3787.

(289) Newman, H. A New Alkenylation Reaction OF Aldehydes and Ketones Using Vinylalanes. *Tetrahedron Lett.* **1971**, *12*, 4571–4572.

(290) Newman, H. A Stereoselective Synthesis of D-Erythro-Sphingosine. *J. Am. Chem. Soc.* **1973**, *95*, 4098–4099.

(291) Gruza, H.; Kiciak, K.; Krasiński, A.; Jurczak, J. The Highly Diastereocontrolled Addition of the Lithium Derivative of Tert Butyldimethylsilyl Propargyl Ether to N-Boc-N,O-Isopropylidene-L-Serinal. *Tetrahedron Asymmetry* **1997**, *8*, 2627–2631.

(292) Wong, L.; Tan, S. S. L.; Lam, Y.; Melendez, A. J. Synthesis and Evaluation of Sphingosine Analogues as Inhibitors of Sphingosine Kinases. *J. Med. Chem.* **2009**, *52*, 3618–3626.

(293) Lu, X.; Cseh, S.; Byun, H. S.; Tigyi, G.; Bittman, R. Total Synthesis of Two Photoactivatable Analogues of the Growth-Factor-like Mediator Sphingosine 1-Phosphate: Differential Interaction with Protein Targets. *J. Org. Chem.* **2003**, *68*, 7046–7050.

(294) Liu, Y.; Bittman, R. Synthesis of Fluorescent Lactosylceramide Stereoisomers. *Chem. Phys. Lipids* **2006**, *142*, 58–69.

(295) Ohshita, K.; Ishiyama, H.; Takahashi, Y.; Ito, J.; Mikami, Y.; Kobayashi, J. Synthesis of Penaresidin Derivatives and Its Biological Activity. *Bioorganic Med. Chem.* **2007**, *15*, 4910–4916.

(296) Mori, K.; Masuda, Y. Synthesis and Stereochemistry of Ceramide B, (2S,3R,4E,6R)-N-(30- Hydroxytriacontanoyl)-6-Hydroxy-4-Sphingenine, a New Ceramide in Human Epidermis. *Tetrahedron Lett.* **2003**, *44*, 129–132.

(297) Dondoni, A.; Perrone, D.; Turturici, E. Synthesis of - D -Galactosyl Ceramide Methylene Isostere. *J. Org. Chem.* **1999**, *64*, 5557–5564.

(298) Anand, N. K.; Carreira, E. M. A Simple , Mild , Catalytic , Enantioselective Addition of Terminal Acetylenes to Aldehdyes. *J. Am. Chem. Soc.* **2001**, *123*, 9687–9688.

(299) Moore, D.; Pu, L. BINOL-Catalyzed Highly Enantioselective Terminal Alkyne Additions to Aromatic Aldehydes. *Org. Lett.* **2002**, *4*, 1855–1857.

(300) Bentoumi, W.; Helhaik, J.; Plé, G.; Ramondenc, Y. Pd-Catalyzed Regio and Stereocontrolled Mono and Bis-Coupling Reactions of 1-Bromo-6-Chlorohexa-1,3,5-Triene: Synthesis of a Naturally Occurring Tetraenynone. *Tetrahedron* **2009**, *65*, 1967–1970.

(301) Yuan, P.; Wu, X. H.; Yu, G. A.; Du, D.; Liu, S. H. Synthesis and Characterization of Bimetallic Ruthenium Complexes Connected through Linear (CH)14 Chain. *J. Organomet. Chem.* **2007**, *692*, 3588–3592.

(302) Lipshutz, B. H.; Lindsley, C. A Streamlined Route to Highly Conjugated, All - E Polyenes Characteristic of Oxo Polyene Macrolide Antibiotics. *J. Am. Chem. Soc.* **1997**, *119*, 4555–4556.

(303) Lipshutz, B. H.; Amorelli, B. Total Synthesis of Piericidin A1. Application of a Modified Negishi Carboalumination-Nickel-Catalyzed Cross-Coupling. *J. Am. Chem. Soc.* **2009**, *131*, 1396–1397.

(304) Chaudhary, V.; Albacker, L. a.; Deng, S.; Chuang, Y. T.; Li, Y.; Umetsu, D. T.; Savage, P. B. Synthesis of Fungal Glycolipid Asperamide B and Investigation of Its Ability to Stimulate Natural Killer T Cells. *Org. Lett.* **2013**, *15*, 5242–5245.

(305) Mori, K.; Uenishi, K. Synthesis of (2S,2'R, 3R,3'E,4E,8E)-1- O-(P-D-Glucopyranosyl)-N-(2'-Hydroxy-3'-Octadecenoyl)-9-Methyl-4,8-Sphingadienine (Pen II), the Major Cerebroside Isolated from Penicillium Funiculosum as the Fruiting-Inducer Against Schizophyllum Commune. *Liebigs Ann.* **1996**, 1–6.

(306) Marshall, J.; Grote, J.; Shearer, B. A Stereoselective Synthesis of the Hydronaphthalene Substructure of Kijanolide. *J. Org. Chem.* **1986**, *51*, 1633–1635.

(307) Lu, X.; Bittman, R. Synthesis of a Photoactivatable (2 S , 3 R) - Sphingosylphosphorylcholine Analogue. *J. Org. Chem.* **2005**, *1597*, 4746–4750.

(308) Grijalvo, S.; Bedia, C.; Triola, G.; Casas, J.; Llebaria, A.; Teixidó, J.; Rabal, O.; Levade, T.; Delgado, A.; Fabriàs, G. Design, Synthesis and Activity as Acid Ceramidase Inhibitors of 2-Oxooctanoyl and N-Oleoylethanolamine Analogues. *Chem. Phys. Lipids* **2006**, *144*, 69–84.

(309) Lee, Y. M.; Lim, C.; Lee, H. S.; Shin, Y. K.; Shin, K. O.; Lee, Y. M.; Kim, S. Synthesis and Biological Evaluation of a Polyyne-Containing Sphingoid Base Probe as a Chemical Tool. *Bioconjug. Chem.* **2013**, *24*, 1324–1331.

(310) Chemin, D.; Linstrumelle, G. A Short Stereocontrolled Synthesis of Leukotriene B4. *Tetrahedron* **1992**, *48*, 1943–1952.

(311) Nicolaou, K. C.; Marron, B. E.; Veale, C. a; Webber, S. E.; Serhan, C. N. Total Synthesis of Novel Geometric Isomers of Lipoxin-A4 and Lipoxin-B4. *J. Org. Chem.* **1989**, *54*, 5527–5535.

(312) Avignon-Tropis, M.; Berjeaud, J. M.; Pougny, J. R.; Frechard-Ortuno, I.; Guillerm, D.; Linstrumelle, G. Stereocontrolled Total Synthesis of Leukotriene B4. *J. Org. Chem.* **1992**, *57*, 651–654.

(313) Mancini, I.; Cavazza, M.; Guella, G.; Pietra, F. Competition among 1,2- and 1,3-Acyl Shifts, and Reduction Reactions, in the UV Irradiation of Cyclopent-2-Enones Bearing a C-3 Terminal-Alkyne Chain. *J. Chem. Soc. Perkin Trans. 1* **1994**, 2181–2185.

(314) Tago, K.; Arai, M.; Kogen, H. A Practical Total Synthesis of Plaunotol via Highly Z-Selective Wittig Olefination of A-Acetal Ketones. *J. Chem. Soc. Perkin Trans. 1* **2000**, 2073–2078.

(315) Ling-Chung, S.; Sales, K. D.; Utley, J. H. P. Measurement of pKa Values for Phosphonium Salts. *J. Chem. Soc. Chem. Commun.* **1990**, 662–664.

(316) Inoue, S.; Honda, K.; Iwase, N.; Sato, K. Cis Selective Wittig Olefination of a-Alkoxy Ketones and Its Application to the Stereoselective Synthesis of Plaunotol. *Bull. Chem. Soc. Jpn.* **1990**, *63*, 1629–1635.

(317) Gaukroger, K.; Hadfield, J. a.; Hepworth, L. a.; Lawrence, N. J.; McGown, A. T. Novel Syntheses of Cis and Trans Isomers of Combretastatin A-4. *J. Org. Chem.* **2001**, *66*, 8135–8138.

(318) Morales-Serna, J. A.; Sauza, A.; Padrón de Jesús, G.; Gaviño, R.; García de la Mora, G.; Cárdenas, J. Facile and Efficient Addition of Terminal Alkynes to Benzotriazole Esters: Synthesis of D-Erythro-Sphingosine Using Ynones as the Key Intermediate. *Tetrahedron Lett.* **2013**, *54*, 7111–7114.

(319) Nudelman, A.; Bechor, Y.; Falb, E.; Fischer, B.; Wexler, B. a.; Nudelman, A. Acetyl Chloride-Methanol as a Convenient Reagent for: A) Quantitative Formation of Amine Hydrochlorides B) Carboxylate Ester Formation C) Mild Removal of N-T-Boc-Protective Group. *Synth. Commun.* **1998**, *28*, 471–474.

(320) Yoshifuji, M.; Loots, M. J.; Schwartz, J. Transmetalation. II. A Convenient Preparation of Vinylic copper(I) Species from Acetylenes Organozirconium Intermediates. *Tetrahedron Lett.* **1977**, *18*, 1303–1306.

(321) Negishi, E.; Horn, D. Van. Selective Carbon-Carbon Bond Formation via Transition Metal Catalysis. 4. A Novel Approach to Cross-Coupling Exemplified by the Nickel-Catalyzed Reaction of Alkenylzirconium Derivatives with Aryl Halides. *J. Am. Chem. Soc.* **1977**, *99*, 3168–3170.

(322) Okukado, N.; Negishi, E. One-Step Conversion of Terminal Acetylenes into Terminally Functionalized (E)-3-Methyl-2-Alkenes via Zirconium-Catalyzed Carboalumination. A Simple and Selective Route to Terpenoids. *Tetrahedron Lett.* **1978**, 2357–2360.

(323) Negishi, E.; Okukado, N.; King, A. O.; Van Horn, D. E.; Spiegel, B. I. Double Metal Catalysis in the Cross-Coupling Reaction and Its Application to the Stereo- and

Regioselective Synthesis of Trisubstituted Olefins. *J. Am. Chem. Soc.* **1978**, *100*, 2254–2256.

(324) Negishi, E.; Valente, L. F.; Kobayashi, M. Palladium-Catalyzed Cross-Coupling Reaction of Homoallylic or Homopropargylic Organozincs with Alkenyl Halides as a New Selective Route to 1,5-Dienes and 1,5-Enynes. *J. Am. Chem. Soc.* **1980**, *9*, 3298–3299.

(325) Panek, J. S.; Hu, T. Stereo- and Regiocontrolled Synthesis of Branched Trisubstituted Conjugated Dienes by Palladium (0) -Catalyzed Cross-Coupling Reaction. *J. Org. Chem.* **1997**, *62*, 4912–4913.

(326) Negishi, E.; Alimardanov, A.; Xu, C. An Efficient and Stereoselective Synthesis of Xerulin via Pd-Catalyzed Cross Coupling and Lactonization Featuring (E)-Lodobromoethylene as a Novel Two-Carbon Synthon. *Org. Lett.* **2000**, *2*, 65–67.

(327) Heravi, M. M.; Hashemi, E.; Nazari, N. Negishi Coupling: An Easy Progress for C-C Bond Construction in Total Synthesis. *Mol. Divers.* **2014**, *18*, 441–472.

(328) Jin, L.; Lei, A. Insights into the Elementary Steps in Negishi Coupling through Kinetic Investigations. *Org. Biomol. Chem.* **2012**, *10*, 6817–6825.

(329) Jana, R.; Pathak, T. P.; Sigman, M. S. Advances in Transition Metal (Pd, Ni, Fe)-Catalyzed Cross-Coupling Reactions Using Alkyl-Organometallics as Reaction Partners. *Chem. Rev.* **2011**, *111*, 1417–1492.

(330) Nicolaou, K. C.; Bulger, P. G.; Sarlah, D. Palladium-Catalyzed Cross-Coupling Reactions in Total Synthesis. *Angew. Chemie - Int. Ed.* **2005**, *44*, 4442–4489.

(331) Schwartz, J.; Labinger, J. A. New Synthetic Methods. 16. Hydrozirconation: Organic Syntheses with a New Transition Metal Reagent. *Angew. Chemie - Int. Ed.* **1976**, *88*, 402–409.

(332) Lessene, G. Advances in the Negishi Coupling. *Aust. J. Chem.* **2004**, *57*, 107–107.

(333) Zeng, F.; Negishi, E. I. A Novel, Selective, and Efficient Route to Carotenoids and Related Natural Products via Zr-Catalyzed Carboalumination and Pd- and Zn-Catalyzed Cross Coupling. *Org. Lett.* **2001**, *3*, 719–722.

(334) Wang, G.; Yin, N.; Negishi, E. Highly Stereoselective Total Synthesis of Fully Hydroxy-Protected Mycolactones A and B and Their Stereoisomerization upon Deprotection. *Chem. - A Eur. J.* **2011**, *17*, 4118–4130.

(335) Zeng, F.; Negishi Ei, E. A Highly Efficient, Selective, and General Method for the Synthesis of Conjugated (all-E)-Oligoenes of the (CH=CH)n Type via Iterative Hydrozirconation-Palladium-Catalyzed Cross-Coupling. *Org. Lett.* **2002**, *4*, 703–706.

(336) Takai, K.; Nitta, K.; Utimoto, K. Simple and Selective Method for RCHO (E)-RCH=CHX Conversion by Means of a CHX3-CrCl2 System. *J. Am. Chem. Soc.* **1986**, *108*, 7408–7410.

(337) Peterson, P. E.; Nelson, D. J.; Risener, R. Preparation of Vinylsilanes and Vinyl Halides Containing Alkene or Epoxide Functional Groups. *J. Org. Chem.* **1986**, *51*, 2382–2382.

(338) Miller, J. A.; Negishi, E.-I. Cyclic Carbolumination of Alkynylsilanes Forming Exocyclic Alkenes. *Isr. J. Chem.* **1984**, *24*, 76–81.

(339) Danilkina, N. A.; Kulyashova, A. E.; Khlebnikov, A. F.; Balova, I. A. Electrophilic Cyclization of Aryldiacetylenes in the Synthesis of Functionalized Enediynes Fused to a Heterocyclic Core. **2014**.

(340) Williams, D. R.; Nishitani, K.; Bennett, W.; Sit, S. Y. A Preparation of Bromoolefins from Carbonyl Compounds. *Tetrahedron Lett.* **1981**, *22*, 3745–3748.

(341) Uenishi, J.; Kawahama, R.; Yonemitsu, O.; Tsuji, J. Palladium-Catalyzed Hydrogenolysis of Conjugated 1 , 1-Dibromo-1-Alkenes to (Z) -1-Bromo-1-Alkenes . An Application to Stepwise and One-Pot Synthesis of Enediynes and Dienynes. *J. Org. Chem.* **1996**, *61*, 5716–5717.

(342) Crousse, B.; Mladenova, M.; Ducept, P. Stereoselective Approaches to (E , E , E) and (Z , E , E)-Alfa-Chloro-Omega -Substituted Hexatrienes : Synthesis of All E Polyenes. *Tetrahedron* **1999**, *55*, 4353–4368.

(343) Lebrun, M. E.; Le Marquand, P.; Berthelette, C. Stereoselective Synthesis of Z Alkenyl Halides via Julia Olefination. *J. Org. Chem.* **2006**, *71*, 2009–2013.

(344) Smithers, R. H. A New Stereoselective Route to Trisubstituted Bromo Olefins Utilizing .alpha.-Bromoalkylides Produced by Halogen-Metal Exchange. *J. Org. Chem.* **1978**, *43*, 2833–2838.

(345) Couladouros, E. a.; Bouzas, E. a.; Magos, A. D. Formal Synthesis of Abyssomicin C. *Tetrahedron* **2006**, *62*, 5272–5279.

(346) Jung, M. E.; Fahr, B. T.; D'Amico, D. C. Total Syntheses of the Cytotoxic Marine Natural Product, Aplysiapyranoid C. *J. Org. Chem.* **1998**, *63*, 2982–2987.

(347) Quesada, E.; Delgado, J.; Gajate, C.; Mollinedo, F.; Acun, A. U. Fluorescent Phenylpolyene Analogues of the Ether Phospholipid Edelfosine for the Selective Labeling of Cancer Cells. *J. Med. Chem.* **2004**, *47*, 5333–5335.

(348) Liu, J.; Abboud, K. A.; Kaifer, A. E. Novel Ferrocenyl Polyene Derivatives and Their Binding to Unmodified Cyclodextrins. **2000**, 6973–6977.

(349) Duhamel, L.; Duhamel, P.; Lecouvé, J.-P. Organolithiens Viniliques À Fonction Carbonylée Masquée Équivalents Synthétiques d'Anions En W Du Méthyl-3 Sorbaldéhyde. *Tetrahedron* **1987**, *43*, 4349–4358.

(350) Amans, D.; Bareille, L.; Bellosta, V.; Cossy, J. Synthesis of the Monomeric Counterpart of Marinomycin A. *J. Org. Chem.* **2009**, *74*, 7665–7674.

(351) Köbrich, G. Bromomethylenation of Carbonyl Compounds by the Wittig Reaction. *Angew. Chemie* **1962**, *74*, 33.

(352) Neumann, H.; Seebach, D. Stereospecific Preparation of Terminal Vinyllithium Derivatives by Br/Li-Exchange with T-Butyllithium. *Tetrahedron Lett.* **1976**, *17*, 4839–4842.

(353) Abad, J.-L.; Villorbina, G.; Fabriàs, G.; Camps, F. Synthesis and Use of Stereospecifically Deuterated Analogues of Palmitic Acid to Investigate the Stereochemical Course of the delta11 Desaturase of the Processionary Moth. *J. Org. Chem.* **2004**, *69*, 7108–7113.

(354) Rosowsky, A.; Wright, J. E. N.epsilon.-[[2-(Trimethylsilyl)ethoxy]carbonyl] Derivatives of Tri-L-Lysine and Tetra-L-Lysine as Potential Intermediates in the Block Polymer Synthesis of Macromolecular Drug Conjugates. *J. Org. Chem.* **1989**, *54*, 5551–5558.

(355) Carpino, L. a; Han, G. Y. The 9-Fluorenylmethoxycarbonyl Amino-Protecting Group. *J. Org. Chem.* **1972**, *37*, 3404–3409.

(356) Villorbina, G.; Canals, D.; Carde, L.; Grijalvo, S.; Pascual, R.; Rabal, O.; Teixidó, J.; Fabriàs, G.; Llebaria, A.; Casas, J.; et al. Solid-Phase Synthesis of a Combinatorial Library of Dihydroceramide Analogues and Its Activity in Human Alveolar Epithelial Cells. *Bioorg. Med. Chem.* **2007**, *15*, 50–62.

(357) Jin, T.; Mu, Y.; Kim, J.-S.; Park, S.-H.; Jin, X.; Kang, J.-C.; Oh, C.-Y.; Ham, W.-H. Formal Synthesis of (+)-A-Conhydrine and Stereoselective Synthesis of Pyrrolidine Analogue via the Diastereoselective Chelation-Controlled Hydride Reduction and Wittig Reaction. *Synth. Commun.* **2014**, *44*, 2401–2408.

(358) Roche, S. P.; Faure, S.; Aitken, D. J. Total Synthesis of Cyclotheonamide C Using a Tandem Backbone-Extension-Coupling Methodology. *Angew. Chem. Int. Ed. Engl.* **2008**, *47*, 6840–6842.

(359) Seco, J. M.; Quiñoá, E.; Riguera, R. A Practical Guide for the Assignment of the Absolute Configuration of Alcohols , Amines and Carboxylic Acids by NMR. *Tetrahedron Asymmetry* **2001**, *12*, 2915–2925.

(360) Gomtsyan, A. Direct Synthesis of Beta-Aminoketones from Amides via Novel Sequential Nucleophilic substitution/Michael Reaction. *Org. Lett.* **2000**, *2*, 11–13.

(361) Koripelly, G. K. Synthetic Studies on Canangone and B-Chamigrene, Carl von Ossietzky–Universität Oldenburg, 2007.

(362) Hoffman, R. V; Maslouh, N.; Cervantes-Lee, F. Highly Stereoselective Syntheses of Syn- and Anti-1,2-Amino Alcohols. *J. Org. Chem.* **2002**, *67*, 1045–1055.

(363) Wu, C.; Berbasov, D. O.; Wulff, W. D. Alkyne Competition in the Benzannulation Reaction with Chromium Carbene Complexes. *J. Org. Chem.* **2010**, *75*, 4441–4452.

(364) Carreira, E. M.; Bois, J. Du. (+)-Zaragozic Acid C: Synthesis and Related Studies. *J. Am. Chem. Soc.* **1995**, *117*, 8106–8125.

(365) Yamamoto, Y. Silver-Catalyzed C(sp)-H and C(sp)-Si Bond Transformations and Related Processes. *Chem. Rev.* **2008**, *108*, 3199–3222.

(366) Tashiro, T.; Hongo, N.; Nakagawa, R.; Seino, K.-I.; Watarai, H.; Ishii, Y.; Taniguchi, M.; Mori, K. RCAI-17, 22, 24-26, 29, 31, 34-36, 38-40, and 88, the Analogs of KRN7000 with a Sulfonamide Linkage: Their Synthesis and Bioactivity for Mouse Natural Killer T Cells to Produce Th2-Biased Cytokines. *Bioorg. Med. Chem.* **2008**, *16*, 8896–8906.

(367) Ueki, M.; Amemiya, M. Removal of 9-Fluorenylmethyloxycarbonyl (Fmoc) Group with Tetrabutylammonium Fluoride. *Tetrahedron Lett.* **1987**, *28*, 6617–6620.

(368) Hu, T.; Panek, J. S. Enantioselective Synthesis of the Protein Phosphatase Inhibitor (-)-Motuporin. *J. Am. Chem. Soc.* **2002**, *124*, 11368–11378.

(369) Kautzner, B.; Wailes, P. C.; Weigold, H. Hydrides of Bis (cyclopentadienyl) Zirconium. *Chem. Commun.* **1969**, 1105.

(370) Wailes, P. C.; Weigold, H. Hydrido Complexes of Zirconium. *J. Organomet. Chem.* **1970**, *24*, 405–411.

(371) Wailes, P. C.; Weigold, H.; Bell, a P. Hydride Complexes of Zirconium IV. Reactions with Olefins. *J. Organomet. Chem.* **1972**, *43*, C32–C34.

(372) Wailes, P. C.; Weigold, H.; Bell, P. Hydrido Complexes III. Reactions with Acetylenes to Give Alkenylzirconium Derivatives. *J. Organomet. Chem.* **1971**, *27*, 373–378.

(373) Hart, D.; Schwartz, J. Hydrozirconation. Organic Synthesis via Organozirconium Intermediates. Synthesis and Rearrangement of Alkylzirconium (IV) Complexes and Their Reaction with. *J. Am. Chem. Soc.* **1974**, *96*, 8115–8116.

(374) Hart, D. W.; Blackburn, T. F.; Schwartz, J. Hydrozirconation. III. Stereospecific and Regioselective Functionalization of Alkylacetylenes via Vinylzirconium (IV) Intermediates. *J. Am. …* **1975**, *97*, 679–680.

(375) Carr, D. B.; Schwartz, J. Preparation of Organoaluminum Compounds by Hydrozirconation-Transmetalation. *J. Am. Chem. Soc.* **1979**, *101*, 3521–3531.

(376) Wipf, P.; Jahn, H. Synthetic Applications of Organochlorozirconocene Complexes. *Tetrahedron* **1996**, *52*, 12853–12910.

(377) Murakami, T.; Furusawa, K. Efficient Stereodivergent Synthesis of Erythro - and Threo - Sphingosines : Unprecedented Reversal of the Stereochemistry in the Addition. *Tetrahedron* **2002**, *58*, 9257–9263.

(378) Wipf, P.; Xu, W. Total Synthesis of the Antimitotic Marine Natural Product (+)-Curacin A. *J. Org. Chem.* **1996**, *61*, 6556–6562.

(379) Wipf, P.; Kendall, C. *Hydrozirconation and Its Applications*; 2004.

(380) Chirik, P. J.; Day, M. W.; Labinger, J. a.; Bercaw, J. E. Alkyl Rearrangement Processes in Organozirconium Complexes. Observation of Internal Alkyl Complexes during Hydrozirconation. *J. Am. Chem. Soc.* **1999**, *121*, 10308–10317.

(381) Annby, U.; Karlsson, S.; Gronowitz, S.; Hallberg, A.; Alvhäll, J. Hydrozirconation-Isomerisation. Reactions of Terminally Functionalised Olefins with Zirconocene Hydrides and General Aspects. *Acta Chem. Scand.* **1993**, *47*, 425–433.

(382) Zhou, B.; Luo, Z.; Lin, S.; Li, Y. A Concise Synthetic Approach to (+)-Valienamine Starting from Garner's Aldehyde. *Synlett* **2012**, *23*, 913–916.

(383) Iwayama, Y.; Ando, H.; Ishida, H.; Kiso, M. A First Total Synthesis of Ganglioside HLG-2. *Chem. a Eur. J.* **2009**, *15*, 4637–4648.

(384) Murakami, T.; Hirono, R.; Furusawa, K. Efficient Stereocontrolled Synthesis of Sphingadienine Derivatives. *Tetrahedron* **2005**, *61*, 9233–9241.

(385) Abad, J. L.; Nieves, I.; Rayo, P.; Casas, J.; Fabriàs, G.; Delgado, A. Straightforward Access to Spisulosine and 4,5-Dehydrospisulosine Stereoisomers: Probes for Pro Fi Ling Ceramide Synthase Activities in Intact Cells. *J. Org. Chem.* **2013**.

(386) Zheng, B.; Srebnik, M. 1,2-Addition of Alkylzirconocene and Alkenylzirconocene Chlorides to Aldehydes Accelerated by Catalytic Amounts of ZnBr2 as a Method of Synthesizing Secondary Alcohols, Secondary Allylic Alcohols, and in-Situ Oppenauer-Type Oxidation of the Alcohols to Ke. *J. Org. Chem.* **1995**, *60*, 3278–3279.

(387) Karjalainen, O. K.; Passiniemi, M.; Koskinen, A. M. P. Short and Straightforward Synthesis of (-)-1-Deoxygalactonojirimycin. *Org. Lett.* **2010**, *12*, 1145–1147.

(388) Suzuki, K.; Hasegawa, T.; Imai, T.; Maeta, I.; Ohba, S. AgAsF6 as Safe Alternative to AgClO4 for Generating Cationic Zirconocene Species : Utilities in Lewis Acid-Promoted Selective C-C Bond Forming Reactions. *Tetrahedron* **1995**, *51*, 4483–4494.

(389) Maeta, H.; Hashimoto, T.; Hasegawa, T.; Suzuki, K. Grignard-Type Addition of Alkenyl- and Alkylzirconocene Chloride to Aldehyde : Remarkable Catalytic Acceleration Effect of AgC104. *Tetrahedron Lett.* **1992**, *33*, 5965–5968.

(390) Maeta, H.; Suzuki, K. Two- and Four-Carbon Homologation of Aldehyde by AgClO4-Catalyzed Addition of Alkoxyalkenylzirconocene Chloride. *Tetrahedron Lett.* **1993**, *34*, 341–344.

(391) Díaz, J. L.; Villacampa, B.; López-Calahorra, F.; Velasco, D. Synthesis of Polyconjugated Carbazolyl – Oxazolones by a Tandem Hydrozirconation – Erlenmeyer Reaction . Study of Their Hyperpolarizability Values. *Tetrahedron Lett.* **2002**, *43*, 4333–4337.

(392) Wipf, P.; Coish, P. D. G. Organozirconocene-Mediated Polyene Synthesis: Preparation of Asukamycin and Manumycin a Side Chains. *Tetrahedron Lett.* **1997**, *38*, 5073–5076.

(393) Wipf, P.; Coish, P. D. G. Total Synthesis of (+-) -Nisamycin. *J. Org. Chem.* **1999**, *64*, 5053–5061.

(394) Huang, Z.; Negishi, E. A Convenient and Genuine Equivalent to HZrCp2Cl Generated in Situ from ZrCp2 Cl2-DIBAL-H. *Org. Lett.* **2006**, *8*, 3675–3678.

(395) Corey, E. J.; Venkateswrlu, A. Protection of Hydroxyl Groups as Tert-Butyldimethylsilyl Derivatives. *J. Am. Chem. Soc.* **1972**, *94*, 6190–6191.

(396) Dilauro, A. M.; Seo, W.; Phillips, S. T. Use of Catalytic Fluoride under Neutral Conditions for Cleaving Silicon-Oxygen Bonds. *J. Org. Chem.* **2011**, *76*, 7352–7358.

(397) Lu, H.; Zhang, F. M.; Pan, J. L.; Chen, T.; Li, Y. F. NH4HF2 as a Selective TBS-Removal Reagent for the Synthesis of Highly Functionalized Spiroketal via Tandem Deprotection/ Spiroketalization Procedure. *J. Org. Chem.* **2014**, *79*, 546–558.

(398) Kaburagi, Y.; Kishi, Y. Operationally Simple and Efficient Workup Procedure for TBAF-Mediated Desilylation: Application to Halichondrin Synthesis. *Org. Lett.* **2007**, *9*, 723–726.

(399) Parlow, J. J.; Vazquez, M. L.; Flynn, D. L. A Mixed Resin Bed for the Quenching and Purification of Tetrabutylammonium Fluoride Mediated Desilylating Reactions. *Bioorganic Med. Chem. Lett.* **1998**, *8*, 2391–2394.

(400) Grijalvo, S.; Matabosch, X.; Llebaria, A.; Delgado, A. A Straightforward Protocol for the Solution-Phase Parallel Synthesis of Ceramide Analogues. *European J. Org. Chem.* **2008**, 150–155.

(401) Bhabak, K. P.; Proksch, D.; Redmer, S.; Arenz, C. Novel Fluorescent Ceramide Derivatives for Probing Ceramidase Substrate Specificity. *Bioorg. Med. Chem.* **2012**, *20*, 6154–6161.

(402) Srivastava, A. K.; Panda, G. Total Synthesis of (-)-Balanol, All Stereoisomers, Their N-Tosyl Analogues, and Fully Protected Ophiocordin: An Easy Route to Hexahydroazepine Cores from Garner Aldehydes. *Chem. a Eur. J.* **2008**, *14*, 4675–4688.

7. SPANISH SUMMARY

Introducción

Los esfingolípidos (SLs) son una amplia familia de lípidos de origen natural que forman parte de las células eucariotas, así como en procariotas del género bacteriano *Sphingomonas*[1]*.* Durante años han sido considerados simples componentes estructurales de las membranas celulares. Sin embargo, en las últimas décadas, se ha establecido su papel como moléculas bioactivas, las cuales intervienen en la señalización y en la regulación de varios procesos celulares[2–4].

Los principales SLs bioactivos son la ceramida (Cer), la esfingosina (Sph), y sus correspondientes análogos fosforilados, la ceramida 1-fosfato (C1P) y la esfingosina 1-fosfato (S1P). Como se indica en la Figura 7.1, estructuralmente los SLs bioactivos comparten la base esfingoide *eritro*-(*E,*2*S,* 3*R*)-2-aminooctadec-4-ene-1,3-diol.

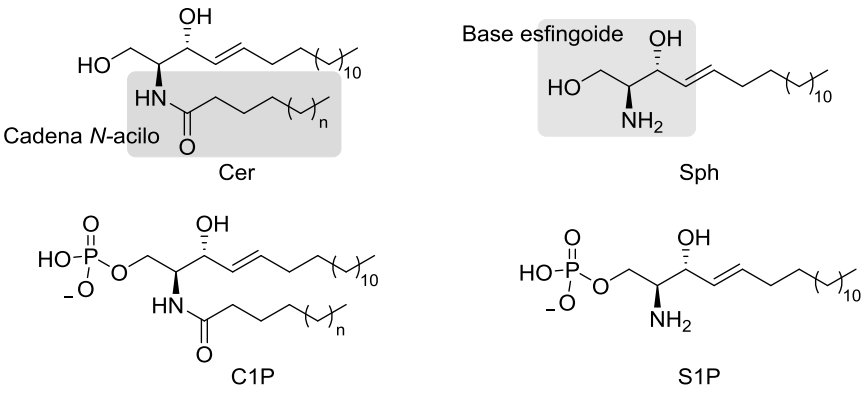

Figura 7.1 Estructura de los principales SLs bioactivos (n representa diferentes longitudes de la cadena acilo).

El metabolismo de los SLs incluye una serie de reacciones biosintéticas y catabólicas, en las que la Cer participa como molécula central. Principalmente, la Cer se puede generar por dos mecanismos[5]: (i) biosíntesis *de novo,* (ii) "la vía de reciclaje", el cual comprende la hidrólisis de glicoesfingolípidos y el ciclo de la esfingomielina. La alteración de este metabolismo puede causar procesos patológicos y contribuir a diversas enfermedades[6]. La presente sección se focalizará en la contribución de la Cer y la Sph en el contexto de las membranas celulares.

Las membranas celulares son bicapas lipídicas, las cuales definen los límites de la célula, así como el perímetro de los orgánulos intracelulares. Una de sus funciones vitales es la de mantener y regular los procesos y las comunicaciones celulares. Dichas bicapas lipídicas están constituidas por fosfolípidos anfipáticos que forman

parte de una gran entidad compleja de componentes donde la presencia de SLs, aunque sea minoritaria, puede estar localmente enriquecida[7].

Los lípidos constituyentes de las membranas biológicas presentan un notable polimorfismo[8], que puede ser responsable de los procesos que tienen lugar en éstas. En condiciones de equilibrio, las bicapas lipídicas adquieren una configuración laminar con diferentes fases: (i) fluida, líquida-desordenada (L_α) o líquida-cristalina (L_d); (ii) Gel o sólida-ordenada (L_β), y (iii) líquida-ordenada (L_o). Generalmente, en condiciones fisiológicas, las bicapas lipídicas existen en fase L_d, caracterizada por conferir la fluidez necesaria para que se produzca el desplazamiento de lípidos y proteínas a lo largo de las membranas.

La heterogeneidad estructural de las membranas se ha intentado definir a través del modelo de balsas lipídicas, "*rafts*", el cual se generalizó como dominios en fase L_o que compartimentan los procesos celulares. Estos dominios son pequeños (10-200 nm), heterogéneos, dinámicos, y enriquecidos en esteroles y esfingolípidos[9]. Además, estos pequeños dominios lipídicos pueden estar estabilizados formando plataformas a través de interacciones proteína-proteína y proteína-lípido (Figura 7.2). Sin embargo, la existencia de los "*rafts*" es controvertida debido a la falta de visualización directa de éstos en biomembranas[10].

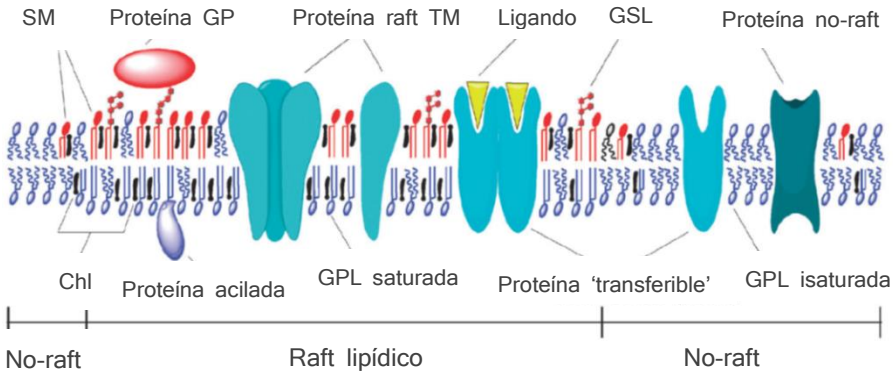

Figura 7.2 Diagrama esquemático de las balsas lipídicas heterogenias "*rafts*"**.** Imagen de Zhong, J.[11]**.**

Los SLs bioactivos pueden ejercer sus efectos fisiológicos a través de cambios en las propiedades de las membranas o bien, a través de enlaces específicos con proteínas diana transitorias[12]. En el caso de la Cer, son varios los estudios que reflejan su capacidad para incrementar el ordenamiento de los fosfolípidos generando una separación lateral de fases, formación de dominios y, consecuentemente, un aumento

de la permeabilidad de la membrana[13–16]. Sin embargo, poco se sabe del efecto que ejerce la Sph en la estructura de las bicapas lipídicas, así como de las interacciones con otros lípidos. Recientemente, se ha puesto de manifiesto su capacidad para permeabilizar y enrigidecer las membranas, efecto que podría estar relacionado con su habilidad para formar intermedios en fase cúbica (no bicapas) cuando se encuentra en membranas cargadas negativamente[17–20].

Actualmente, un problema básico para la relevancia fisiológica de los experimentos con Cer y Sph es el que deriva de la necesidad de emplear concentraciones molares muy altas de estos lípidos, generando un escenario artificial que dista de las condiciones fisiológicas[21]. Por ende, uno de los retos de la biomedicina es profundizar más en el metabolismo, señalización e interacciones de los SLs mediante el empleo de técnicas biofísicas que no alteren las propiedades de las membranas celulares[22].

El estudio y la visualización de los SLs mediante técnicas biofísicas requiere la utilización de análogos de SLs marcados con átomos radioactivos, con radicales, o bien con grupos fluorescentes. Estas modificaciones, idealmente, no deberían alterar notablemente el esfingolípido natural, de manera que serían sondas de elevada aplicabilidad biológica, con alta sensibilidad y versatilidad de detección[23]. No obstante, la mayoría de sondas fluorescentes son estructuras rígidas, de considerable tamaño y volumen (NBD, BODIPY)[24], que se utilizan a concentraciones superiores a las fisiológicas, resultando en una alteración del metabolismo, localización y señalización de los estos análogos en comparación con los lípidos que pretenden mimetizar.

Con objeto de reducir el impacto que produce el volumen de los grupos cromóforos en la estructura y empaquetamiento de los lípidos de membrana, se han utilizado sistemas de dobles enlaces conjugados, fluorescentes, el cual minimiza considerablemente las alteraciones estructurales asociadas a los cromóforos clásicos comentados arriba[25] (Figura 7.3).

El sistema de cinco dobles enlaces conjugados, caracterizados por tener una excitación máxima alrededor de 340 nm y emisión máxima entre 440-475 nm, permite llevar a cabo ensayos de fluorescencia. Además, diferentes estudios han demostrado la capacidad de estos sistemas poliénicos para comportarse *in vivo* de forma comparable a sus análogos naturales[26–28]. Conjuntamente, todas estas características hacen de los lípidos pentaénicos excelentes sondas para el estudio de las interacciones lípido-lípido y lípido-proteína en membranas en condiciones próximas a las fisiológicas. Sin embargo, hasta el momento, no se ha diseñado ninguna sonda de

tipo esfingolípido que contenga el sistema pentaénico incorporado en la estructura de la base esfingoide, el cual permitiría la visualización directa de la distribución de especies derivadas de Sph.

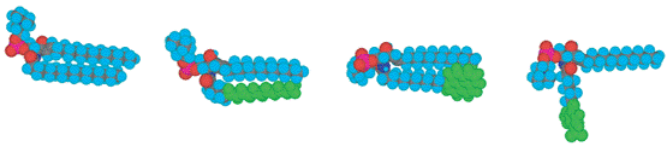

Figura 7.3 Modelos 3D de análogos fluorescentes de SM. De izquierda a derecha: lípido natural, fluorescente pentaénico, fluorescente pirénico, marcado con NBD. Imagen de van Meer *et al.*[29].

Asimismo, en las últimas décadas se han diseñado sondas que combinan sistemas duales de fluoróforos enlazados a radicales nitróxido, de manera que actúan como sondas fluorométricas[30]. Cuando el grupo nitróxido se sitúa próximo al fluoróforo, la fluorescencia se atenúa, mientras que cuando se libera el radical la fluorescencia se recupera. Este tipo de sondas duales permiten obtener información de diversos procesos celulares[31–33].

Objetivos

Con el fin de entender y conocer los mecanismos de acción que ejercen la Cer y la Sph a nivel molecular en el contexto celular, es necesario complementar la información obtenida de estudios con membranas modelos con aquellos obtenidos con herramientas biofísicas en entornos fisiológicos.

Teniendo en cuenta las consideraciones descritas en la sección anterior, se contempló el siguiente objetivo en la presente tesis doctoral:

3. Sintetizar un análogo fluorescente de ceramida, marcado con un sistema conjugado pentaénico, cuya fluorescencia sea modulada por la presencia de un atenuador radicalario, con un control espaciotemporal, el cual pueda ser eliminado por acción de una enzima específica de la membrana celular (ceramidasa neutra, nCDasa). De esta manera, cuando el fluoróforo y el atenuador estén próximos en el espacio, la fluorescencia se atenuará. Pero, una vez el atenuador sea liberado, la Sph pentaénica resultante recuperará la fluorescencia, permitiendo su detección en condiciones fisiológicas. Este tipo de sondas pueden ser de gran utilidad para el estudio de la formación de microdominios a concentraciones cercanas a las presentes en la célula (Figura 7.4).

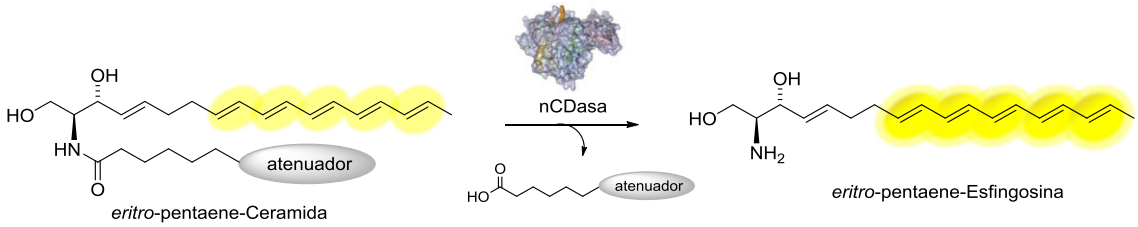

Figura 7.4 Objetivo principal de la presente tesis.

Previamente, en nuestro grupo de investigación, se comprobó que la Cer *N*-acilada con grupos nitróxido (*n*-DOXYL-Cer) se comportaba como sustrato de la nCDasa (resultados no mostrados). Asimismo, estudios realizados mediante calorimetría diferencial de barrido y microscopía confocal/ dos-fotones, confirmaron que las sondas *n*-DOXYL-Cer actuaban como la Cer natural en liposomas, mostrando un perfil cooperativo y distribuyéndose en dominios ordenados. Sin embargo, la introducción de sondas pentaénicas con atenuadores radicalarios en la misma molécula no se había

examinado previamente. En este sentido, y como prueba de concepto, se consideró el siguiente objetivo:

4. Síntesis de un modelo simplificado, basado en un sistema pentaénico con un atenuador radicalario en diferentes posiciones (Figura 7.5), que nos permita:

iv. Evaluar la capacidad del atenuador radicalario para modular la fluorescencia de las sondas en membranas modelo.

v. Verificar si el atenuador, después de hidrolizarse el enlace amida, será capaz de seguir atenuando intermolecularmente el sistema pentaénico.

vi. Confirmar si el sistema pentaénico conjugado es adecuado para ser analizado por microscopia confocal de fluorescencia.

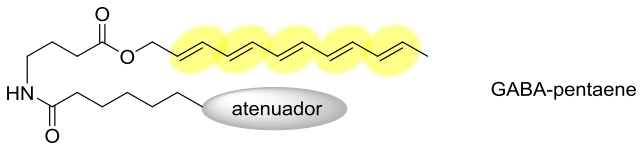

Figure 7.5 Sondas modelo GABA-pentaeno. Estructura simplificada como prueba de concepto.

Resultados y discusión

Análogos GABA-Pentaeno como sondas de membrana

Síntesis de las sondas GABA-pentaeno

En el apartado 3.1 se ha llevado a cabo la síntesis de las sondas GABA-pentaeno, las cuales pretenden ser análogos simplificados de la palmitoil-Cer natural, diferenciándose estructuralmente en la base esfingoide. La eliminación del grupo hidroxilo en C1 y la sustitución del hidroxilo en C3 por un grupo ester, produce globalmente una disminución de la polaridad de la cabeza esfingoide (Figura 7.6).

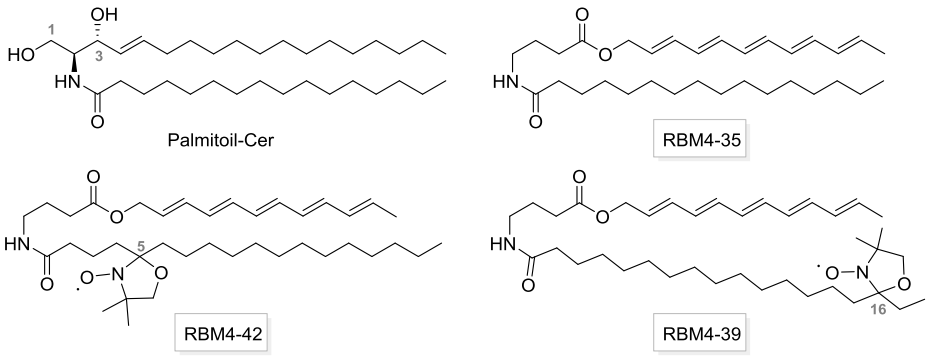

Figura 7.6 Sondas GABA-pentaeno descritas en esta sección.

La síntesis de sistemas poliénicos presenta diversas dificultades debido a la sensibilidad que exhiben a la luz, al oxígeno, a los ácidos próticos y de Lewis, así como en el control de la estereoquímica de los dobles enlaces formados. Los métodos más comunes para la preparación de estos sistemas conjugados están basados en las reacciones de olefinación carbonílica, acoplamientos con metales de transición, alquinilaciones y reacciones de eliminación[34]. Recientemente, la combinación de estas estrategias ha ganado relevancia en el campo de la síntesis de polienos, generando un aumento de selectividad y efectividad del proceso.

Acorde con esta sensibilidad de los sistemas poliénicos, se optó por introducir la estructura pentaénica en la última etapa de la síntesis de las sondas GABA-pentaeno, mediante esterificación del alcohol poliénico RBM4-33 con los respectivos ácidos *N*-acil γ-aminobutírico (GABA) (Figura 7.7). A su vez, el alcohol RBM4-33, descrito en la literatura[35], se obtuvo con un rendimiento global del 25%, por elongación del

aldehído comercial 2,4-hexadienal, aplicando dos ciclos de la olefinación Horner-Wadsworth-Emmons (HWE) y una reducción final con DIBAL-H.

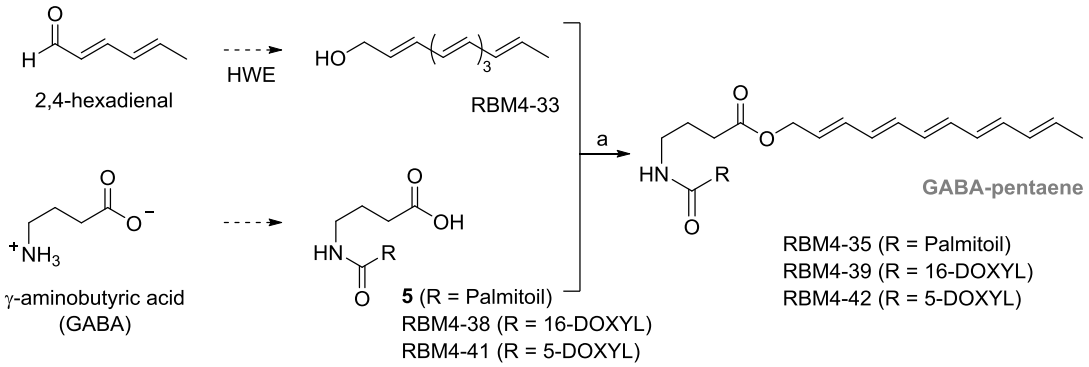

Figura 7.7 Aproximación sintética para la preparación de las sondas GABA-pentaeno. Condiciones de esterificación (a) EDC, DMAP, 0ºC to RT, 5-16h.

Siguiendo esta aproximación sintética, con un total de cuatro etapas desde el alcohol RBM4-33 y el ácido comercial GABA, se obtuvo el derivado *N*-palmitoilado RBM4-35 (Rto: 15%), utilizado como patrón de máxima fluorescencia por no presentar el grupo atenuador. Asimismo, los derivados 16-DOXYL esteárico RBM4-39 (Rto: 30%) y 5-DOXYL esteárico RBM4-42 (Rto: 35%), con un atenuador radicalario, se sintetizaron como sondas para evaluar y modular la atenuación de la fluorescencia originada por el sistema conjugado pentaénico (Figura 7.6).

Estudios biofísicos con las sondas GABA-pentaeno

Una vez sintetizadas las sondas GABA-pentaeno, se procedió a su evaluación mediante ensayos biofísicos. Éstos se llevaron a cabo en colaboración con la Unidad de Biofísica de la Universidad del País Vasco, como parte de una estancia pre-doctoral. Además, los estudios de resonancia paramagnética electrónica (EPR) se realizaron en colaboración con la Unidad de EPR del Instituto de Química Avanzada de Cataluña (IQAC) del Consejo Superior de Investigaciones Científicas (CSIC).

Los estudios biofísicos pretenden analizar los sistemas biológicos a través de sistemas simplificados de membranas modelo. Entre las diversas membranas modelo que existen, los liposomas o vesículas lipídicas, son estructuras microscópicas formadas por una o más bicapas lipídicas concéntricas que limitan compartimentos acuosos. Estas bicapas lipídicas están formadas por fosfolípidos anfipáticos, cuya longitud y número de instauraciones determinan las propiedades estructurales y estados físicos

de las mismas. A su vez, los liposomas se pueden clasificar estructuralmente en vesículas multilamelares (MLVs) y vesículas unilamelares (ULVs), clasificándose estas últimas, en función de su tamaño y método de preparación como vesículas unilamelares grandes (LUVs), vesículas unilamelares pequeñas (SUVs) y vesículas unilamelares gigantes (GUVs).

La caracterización de las sondas GABA-pentaeno se llevó a cabo inicialmente con el registro de sus espectros de excitación y emisión en diferentes disolventes. También se determinaron los coeficientes de extinción molar (ε) y los rendimientos cuánticos (Φ_F) de las nuevas sondas, las cuales presentaron valores consistentes con los descritos en la literatura para sistemas conjugados pentaénicos similares[27,36–38].

A continuación, se prosiguió con la incorporación de las sondas GABA-pentaeno en LUVs de diferentes composiciones. Se emplearon los fosfolípidos DOPC o ePC, para conferir bicapas más fluidas (L_d), y DPPC o DSPC para inducir fases gel (L_β) en las membranas. Las tres sondas exhibieron excitaciones máximas a 353 nm y emisiones máximas alrededor de 478 nm, independientemente del entorno lipídico. Asimismo, se pudo observar que las sondas que contenían el radical nitróxido, cuando fueron incorporadas en membranas en fase-gel, mostraban intensidades de fluorescencia menores respecto a la sonda de referencia RBM4-35. Sin embargo, en bicapas fluidas, todas ellas presentaron intensidades de fluorescencia similares, como se ilustra en la Figura 7.8. Estos resultados son consistentes con el grado de empaquetamiento que presentan las sondas en bicapas rígidas, ya que se reduce la movilidad conformacional de la cadena *N*-DOXYL estearoil, favoreciendo así su proximidad espacial hacia la cadena poliénica.

El ensayo de fluorescencia también nos permitió observar que la atenuación de la fluorescencia por parte de la sonda RBM4-39, con el grupo DOXYL en la posición C16 de la cadena *N*-acilo, exhibía mayor dependencia según la fluidez de la membrana respecto a la sonda RBM4-42, con el grupo DOXYL en la posición C5.

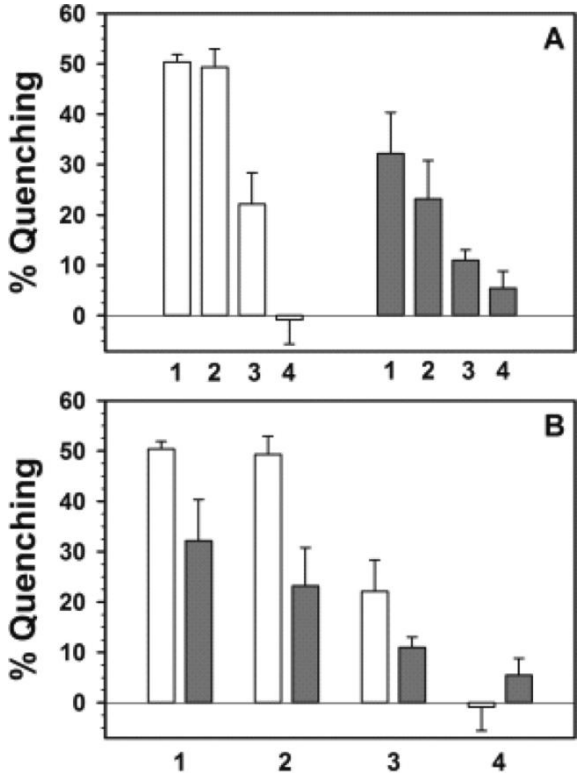

Figura 7.8 (**A**) Efecto de la composición lipídica; (**B**) Efecto de la posición del DOXYL. Atenuación de la emisión de fluorescencia de los pentaenos en liposomas de diferentes composiciones: DSPC (**1**), DPPC (**2**), ePC (**3**), y DOPC (**4**). RBM4-39 (**barras vacías**) y RBM4-42 (**barras rellenas**).

Finalmente, se realizaron estudios de fluorescencia tras la adición de porcentajes variables de las sondas RBM4-39 o RBM4-42 sobre LUVs de diferentes composiciones lipídicas, los cuales contenían la sonda de referencia RBM4-35 (datos no mostrados en el resumen). De este modo, se pudo constatar que era necesaria una relación DOXYL:pentaeno muy elevada para que tuviera lugar una atenuación de la intermolecular de la fluorescencia. En consecuencia, cabe esperar que la liberación de un radical DOXYL a partir de una sonda DOXYL:pentaénica no conduzca a la atenuación intermolecular de la fluorescencia, ya que la relación DOXYL:pentaeno seria 1:1.

Como se ha indicado anteriormente, la base esfingoide de las sondas GABA-pentaeno presentan una polaridad menor a la de la Cer natural, por lo que nos planteamos evaluar la orientación de estas sondas dentro de las membranas modelo. En este sentido, se analizó por calorimetría diferencial de barrido (DSC) el cambio en la temperatura de transición (Tm) entre la fase gel y la laminar fluida de la composición

lipídica bajo estudio, la cual es característica del estado físico de las fases, y nos proporcionaría información de la distribución de las sondas.

Con este fin, se generaron MLVs de DPPC. Cuando la sonda RBM4-35 se incorporó en la vesícula, el termograma (Figura 7.9, rojo) permite observar la desaparición de la temperatura de pre-transición, así como una única temperatura de transición más ensanchada respecto al termograma de DPPC (Figura 7.9, negro). Estos resultados indican que la sonda RBM4-35 se comporta de manera similar a los lípidos anfipáticos insaturados[39,40], orientándose principalmente con la parte polar en la interfase lípido-agua. Asimismo, la disminución de la Tm sugiere que la sonda RBM4-35 se distribuye preferiblemente en las fases fluidas respecto las fases gel. El perfil de RBM4-35 en un tampón acuoso (Figura 7.9, azul), no presentó ninguna señal térmica en el rango de temperaturas bajo estudio, acorde con el perfil esperado para lípidos insaturados.

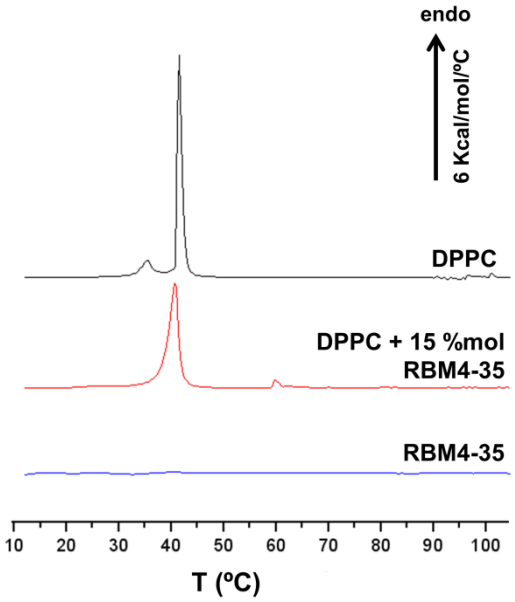

Figura 7.9 Desde arriba a abajo: DSC de dispersiones acuosas de DPPC, DPPC + 15 mol % de RBM4-35, y RBM4-35.

La microscopia confocal de dos fotones representa una técnica adecuada para el estudio de fluoróforos susceptibles al blanqueamiento por longitudes de onda UV, como es el caso de los sistemas pentaénicos. Con objeto de aplicar esta técnica, se generaron GUVs, por electroformación y visualización directa[41], de diferentes composiciones lipídicas con un 2% de sonda poliénica y un 0.3% del marcador comercial de regiones desordenadas DiO.

Cuando se analizaron GUV_S de composición DOPC:eSM:Chl (2:1:1), la mezcla mostró una separación lateral de dominios L_d (regiones iluminadas) y L_o (regiones oscuras)

(Figura 7.10, primera fila). Curiosamente, se observaron los dominios ordenados, L_o, marcados por la sonda RBM4-35, a diferencia de la mayoría de sondas fluorescentes comerciales, que marcan preferiblemente las regiones L_d.

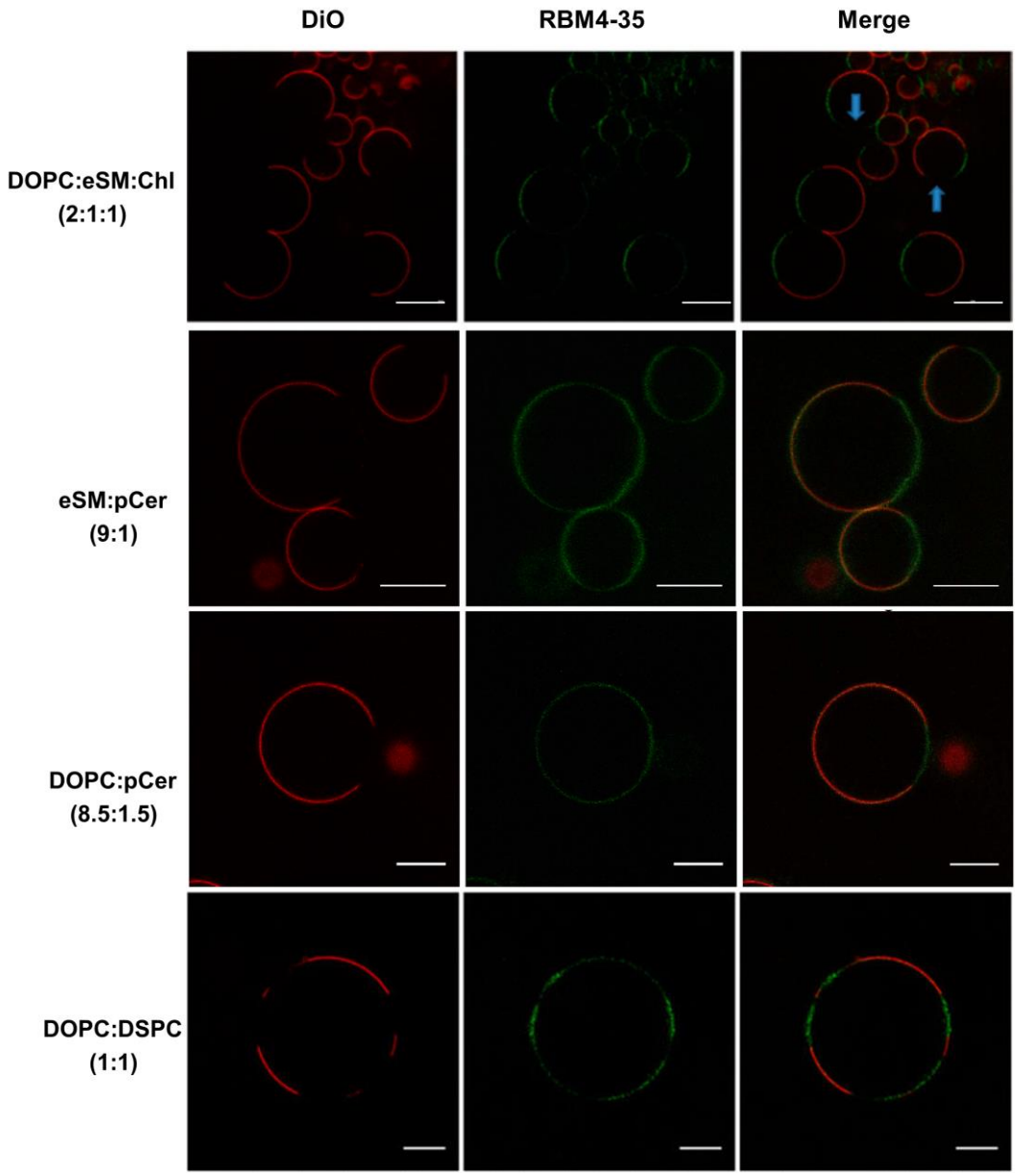

Figura 7.10 Marcaje de dominios lipídicos con RBM4-35. Representación de secciones ecuatoriales de GUVs con diferentes composiciones por confocal/multifotón, conteniendo un 0.3% de DiO y un 2% de RBM4-35. Escala = 10 µm. Flechas azules: proceso de fotoselección.

A continuación se procedió a evaluar vesículas de composición fosfolípido:palmitoil-Cer (Figura 7.10, segunda y tercera fila), las cuales generan una separación de fase lateral por la formación de dominios ricos en Cer y dominios pobres en Cer, los últimos

marcados por el DiO. Sin embargo, en esta mezcla, la sonda RBM4-35 apareció distribuida por toda la bicapa, marcando ambas regiones con intensidades diferentes. Esta capacidad de RBM4-35 para marcar tanto dominios ricos como pobres en Cer, es diferente de la exhibida por fluoróforos voluminosos, como la NBD-Cer[42], que son incapaces de distribuirse en regiones ricas en Cer. En este contexto, la sonda RBM4-35 seria de particular interés para el marcaje de regiones gel en membranas celulares.

Finalmente, cuando la sonda RBM4-35 se examinó en GUVs de composición DSPC:DOPC (1:1), lo que proporciona dominios con diferente fluidez, la sonda pentaénica emitió más intensamente en los dominios en fase gel (Figura 7.10, última fila). Sin embargo, los resultados obtenidos por microscopia confocal/dos fotones, donde RBM4-35 marca preferiblemente en fases gel respecto fluidas, contradicen los datos sugeridos por la DSC.

Tras observar el comportamiento de la sonda de referencia RBM4-35, se evaluaron las sondas marcadas con el grupo nitróxido RBM4-39 y RBM4-42. Para ello se generaron GUVs de composición DOPC:eSM:Chl (2:1:1), mezcla lipídica que muestra la coexistencia de dominios L_o y L_d, como se ha indicado anteriormente. Las imágenes obtenidas por microscopia confocal (no mostradas), muestran como RBM4-39 y RBM4-42 se distribuyen de manera equivalente por los dominios L_o y L_d, a diferencia de lo observado con la sonda RBM4-35 (Figura 7.10, primera fila).

Además, la técnica EPR nos permitió monitorizar el dinamismo molecular de las sondas marcadas con el radical nitróxido, proporcionado información del entorno lipídico en el que fueron incorporadas. De esta manera, LUVs de diferente naturaleza lipídica, con un 15% de las sondas RBM4-39 o RBM4-42, mostraron que, a medida que el ordenamiento de la membrana aumentaba, la movilidad del radical se reducía (Figura 7.11, de izquierda a derecha). Además, el comportamiento anisotrópico de la sonda RBM4-42, con el grupo DOXYL en la posición C5 de la cadena *N*-acilo, exhibió menos dependencia del entorno lipídico debido a su menor movilidad por la proximidad al enlace amida. Los resultados obtenidos por EPR se correlacionan con los valores de atenuación de fluorescencia observados para estas sondas por espectrofluorimetría.

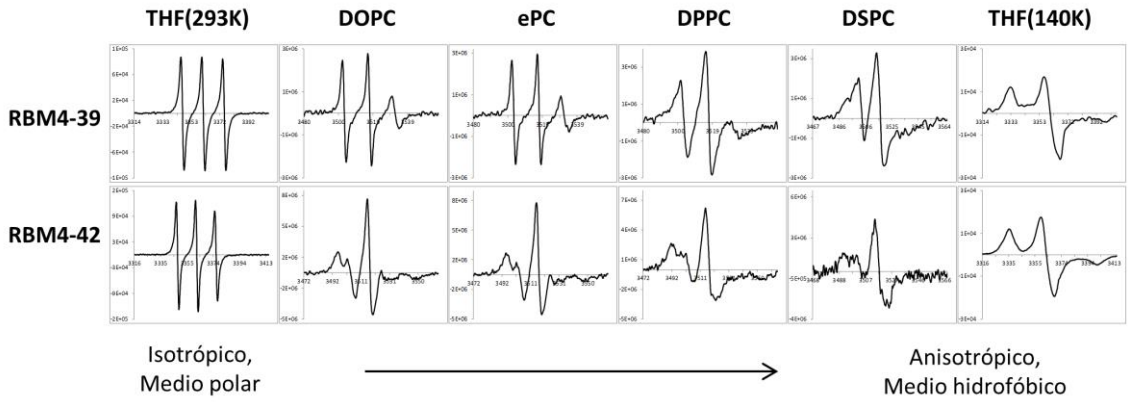

Figura 7.11 Espectros de EPR de las sondas pentaeno-DOXYL en THF o en LUVs de composición indicada. Espectros registrados a 20ºC (293 K) a menos que se indique lo contrario.

En conjunto, las sondas GABA-pentane, aunque inicialmente no fueron diseñadas con este objetivo, han resultado ser sondas interesantes para el estudio de algunas propiedades biofísicas de las membranas. Especialmente, RBM4-35 puede ser de gran utilidad para el marcaje de dominios ordenados, mientras que RBM4-39 puede proporcionar información de transiciones lipídicas gel-fluido.

Estrategias sintéticas para la obtención de análogos de esfingolípidos poliénicos

Uno de los principales objetivos en el campo de los SLs, como se ha comentado en la Introducción, es la visualización directa de interacciones moleculares bajo condiciones fisiológicas. En este sentido, el diseño de análogos de SLs marcados con un sistema fluorescente de cinco dobles enlaces conjugados nos permitiría evaluar su metabolismo, transporte y localización, minimizando la alteración estructural del entorno bajo estudio.

Teniendo en cuenta estas consideraciones, en la segunda parte de esta tesis se presentan las diferentes estrategias sintéticas que se han llevado cabo para la preparación de análogos poliénicos de Cer y Sph. En todas ellas, la introducción de la cabeza esfingoide se ha basado en derivados de la L-serina. Asimismo, se han abordado diferentes estrategias para la elongación del sistema poliénico conjugado.

Aproximación sintética vía metátesis cruzada y olefinación de Wittig

Inicialmente la síntesis de la *eritro*-poliene-Cer se planteó según el análisis retrosintético representado en la Figura 7.12. Con objeto de evaluar la estabilidad de los compuestos poliénicos bajo varias condiciones de desprotección, se llevaron a cabo dos estrategias de protección del sistema 2-amino-1,3-diol. Por un lado, se partió del alcohol alílico **6,** procedente del aldehído de Garner, lo que requeriría condiciones ácidas para su desprotección. Alternativamente, al alcohol **6** se cicló con NaH, en THF, para dar lugar al sistema bicíclico RBM4-12, el cual requeriría condiciones básicas para la desprotección final. La rigidez conformacional de ambos sistemas permitió definir la configuración *eritro* (*anti*) en C2-C3.

Para la obtención de la sal de trifenilfosfonio RBM4-14 fue necesario proteger el grupo hidroxilo secundario con cloruro de metoximetilo, previo a la etapa de metátesis cruzada con el 5-bromopenteno comercial, para evitar la formación de subproductos en posteriores etapas. Una vez unidos, el doble enlace (*E*) en C4-C5 se generó como un único isómero. A continuación, se procedió a la formación de la correspondiente sal RBM4-14, en presencia de un exceso de PPh_3, la cual se obtuvo con un rendimiento global del 40% desde el alcohol alílico **6**.

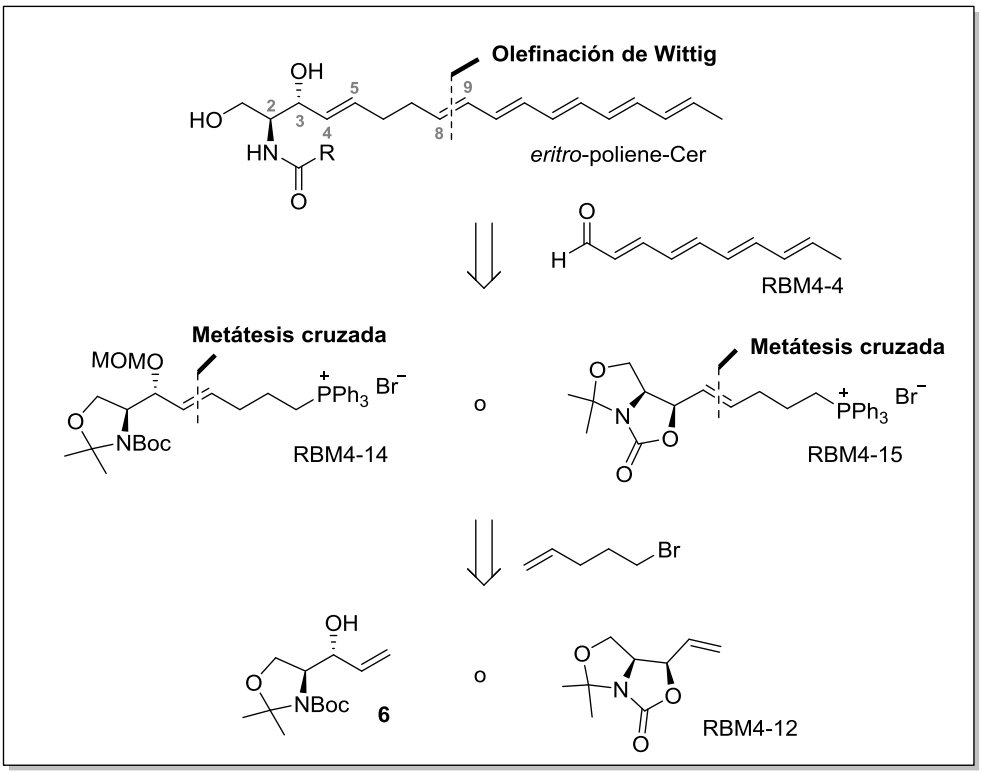

Figura 7.12 Análisis retrosintético para la obtención del compuesto *eritro*-poliene-Cer.

Paralelamente, la sal RBM4-15 se sintetizó mediante una metátesis cruzada[43,44] entre el 5-bromopento y RBM4-12, dando lugar al doble enlace (*E*)-C4-C5. Posteriormente, este intermedio se transformó en la sal RBM4-15, en presencia de PPh_3 y ACN, con un rendimiento global del 40%.

El aldehído poliénico RBM4-4 se preparó siguiendo la metodología descrita por Sun *et al*.[35], basada en la elongación del aldehído comercial 2,4-hexadienal mediante la olefinación HWE, posterior reducción del respectivo éster al alcohol con DIBAL-H, seguida de la oxidación al aldehído con IBX.

Finalmente, la reacción de Wittig entre el aldehído RBM4-4 y la sal RBM4-14, se llevó a cabo según la modificación de Oh *et al.*[45], la cual aumenta la estereoselectividad del proceso, favoreciendo la estereoquímica *E*, por adición de MeOH a -78ºC en el final de reacción. Cuando se utilizó BuLi como base, el compuesto de acoplamiento se obtuvo con 14% de rendimiento y en una relación (*Z:E*) en C8-C9 de (1:2.5). Sin embargo, los diversos intentos para reproducir o mejorar la selectividad de la reacción resultaron infructuosos, recuperándose los productos de partida o subproductos. En el caso de la sal RBM4-15, no tuvo lugar la reacción de Wittig con el aldehído RBM4-4 bajo ninguna

de las condiciones ensayadas. A la vista de estos resultados, se decidió descartar esta ruta sintética para la obtención de la Cer-poliénica.

Aproximación sintética vía alquinilación nucleofílica

Alternativamente, nos planteamos una estrategia sintética basada en el ensamblaje del aldehído de Garner con el alquino poliénico RBM4-17 para dar lugar al enlace C3-C4 de la estructura esfingoide, como se describe en la Figura 7.13. Cabe destacar que la presente aproximación sintética se puso a punto, paralelamente, con un sistema modelo de tres dobles enlaces conjugados.

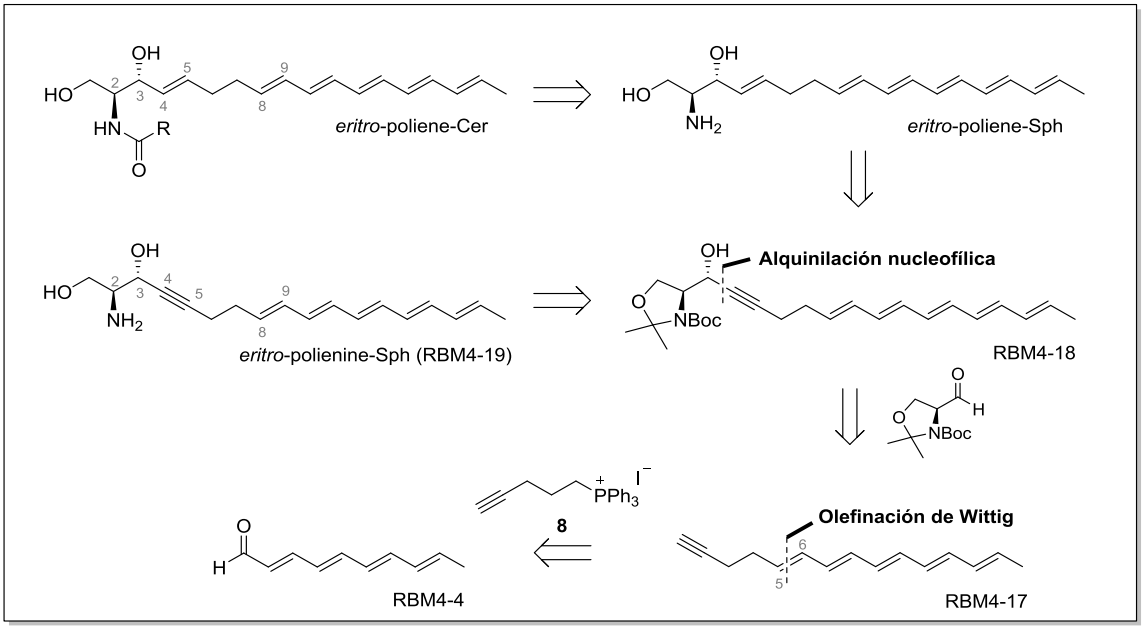

Figura 7.13 Análisis retrosintético para la obtención del compuesto *eritro*-poliene-Cer y *eritro*-polienine-Cer.

Partiendo del aldehído RBM4-4, sintetizado previamente, se diseñó la preparación del alquino poliénico RBM4-17 por olefinación de Wittig con la sal de trifenilfosfonio **8**. Esta sal se obtuvo a partir del 5-yodo-1-pentino, obtenido a partir del 4-pentin-1-ol comercial, seguida de la transformación a la correspondiente sal de trifenilfosfonio (50% dos etapas). A continuación se procedió al acoplamiento con el aldehído RBM4-4, bajo condiciones de Wittig, para favorecer la formación de la olefina (*E*)[45], siendo necesario utilizar BuLi y HMPA para la formación del alquino RBM4-17 con un rendimiento del 55% y selectividad del enlace 5(*Z:E*) (1:2). Con objeto de obtener el sistema todo *trans* (*E*), RBM4-17 se isomerizó[46,47] en presencia de I_2, reduciendo la

proporción del isómero (*Z*) a 5(*Z:E*) (1:6). Finalmente, se consiguió aislar el compuesto todo (*E*), mediante purificación por HPLC-preparativa.

Una vez obtenido RBM4-17, nos basamos en los protocolos de Herold y Garner[48,49] para la adición *anti*-selectiva del correspondiente acetiluro sobre el aldehído de Garner. Sin embargo, la formación del acetiluro de litio con BuLi, en presencia de HMPA, no resultó fructífera. No obstante, la utilización de LDA para generar el correspondiente acetiluro, proporcionó, mediante un estado de transición Felkin-Anh[50], la formación del compuesto *anti*-RBM4-18 (25%) como único diastereómero.

Con objeto de reducir el sistema propargílico C4-C5 del intermedio RBM4-18 al alcohol alílico (*E*), se emplearon diferentes hidruros. Sin embargo, todos los intentos dieron lugar a productos de descomposición. Tras observar la inestabilidad del sistema pentaénico frente a la reducción selectiva del triple enlace, nos planteamos desproteger el intermedio RBM4-18, con el propósito de obtener una estructura fluorescente análoga de Sph. Por ende, los grupos isopropilideno y *N*-Boc se desprotegieron en condiciones ácidas suaves[51] (HCl en MeOH) dando lugar a una nueva sonda fluorescente (*todo E*)-RBM4-19 (40%), marcada por primera vez con un sistema pentaénico en la estructura esfingoide. No obstante, la presente ruta sintética se descartó para la obtención la *eritro*-poliene-Sph o -Cer.

Aproximación sintética vía acoplamiento cruzado de Negishi

Teniendo en consideración la naturaleza lábil de los compuestos pentaénicos, se procedió a diseñar una ruta sintética convergente en la que el sistema poliénico se introdujera en la última etapa de la síntesis. Para ello, se planteó la formación del enlace sp^2-sp^2, en C9-C10, por acoplamiento de Negishi[52,53] entre el haluro poliénico RBM4-50 y la base esfingoide (**A**) (Figura 7.14).

Los primeros intentos para la obtención del haluro poliénico RBM4-50 se basaron en la elongación de un aldehído triénico[35], siguiendo el protocolo de olefinación de Takai[54]. Sin embargo, los compuestos obtenidos por este procedimiento resultaron inestables, lo que atribuimos a la presencia de derivados de cromo. En consecuencia, se procedió a la elongación del aldehído por olefinación de Wittig, por modificación del método descrito en la literatura para este mismo compuesto[37,55]. De esta forma, se obtuvo RBM4-50 con un rendimiento del 70% y una selectividad (*Z:E*)(1:2). A pesar de que no se obtuvo el isómero (*todo-E*), se siguió adelante con la ruta.

Por otro lado, el precursor de la base esfingoide (X) se intentó condensar con el enino **9** mediante una reacción de metátesis cruzada. Aunque **9** está descrito en la literatura[56–58], finalmente se obtuvo por una vía alternativa consistente en la adición del acetiluro de trimetilsililo sobre el 4-bromobuteno comercial, en presencia de HMPA, en una única etapa.

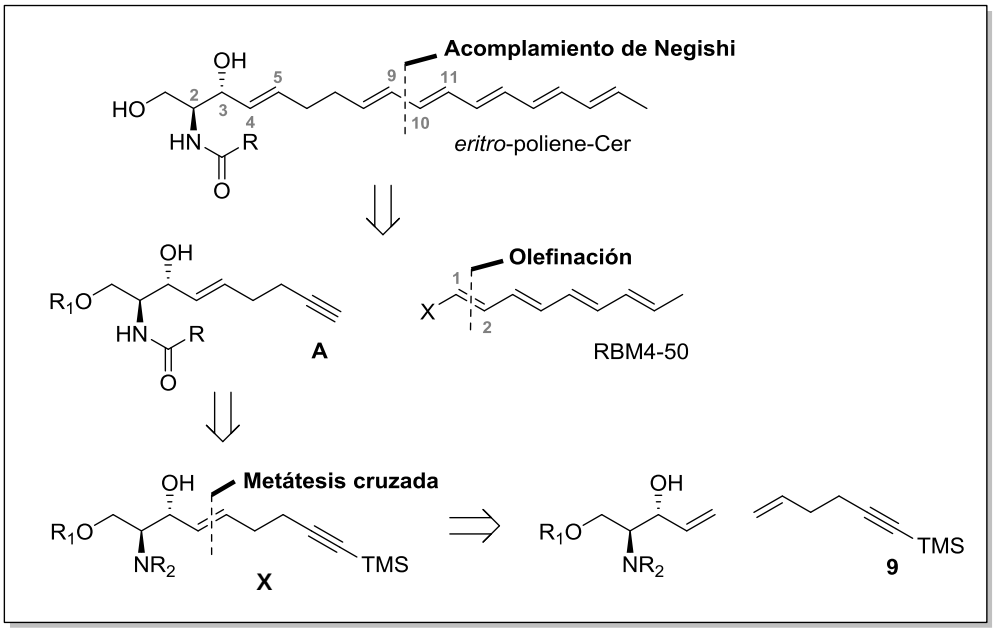

Figura 7.14 Análisis retrosintético para la obtención del compuesto *eritro*-poliene-Cer.

En este punto, se llevó a cabo la metátesis cruzada entre el alqueno **9** y un exceso del alcohol alílico **6**, en presencia del catalizador de Grubbs de 2ª generación, para dar lugar al intermedio RBM4-45. Este intermedio se transformó en los precursores RBM4-46, RBM4-47 y RBM4-48 (Figura 7.15), para su empleo en el acoplamiento de Negishi.

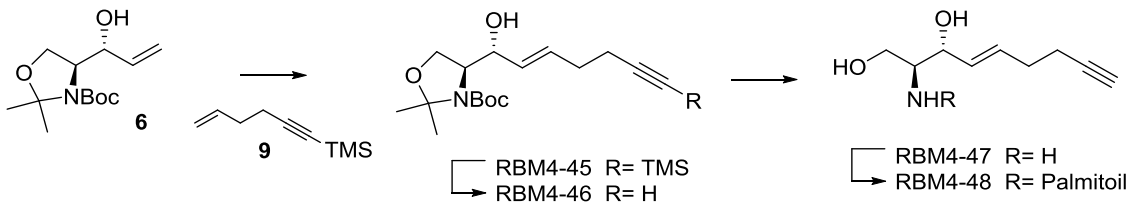

Figura 7.15 Síntesis de precursores para el acoplamiento de Negishi.

Debido a la inestabilidad observada en ciertas ocasiones del sistema poliénico frente a desprotecciones ácidas, se diseñó una base esfingoide alternativa, la cual estuviera protegida con grupos que requiriesen condiciones básicas suaves para su

desprotección. En este sentido, se prepararon, a partir de la L-serina, el aldehído RBM4-54 (Figura 7.17) y el alcohol alílico RBM4-55 (Figura 7.16), usando TBS y Fmoc como grupos protectores, lo que permite tanto su eliminación simultánea como ortogonal.

Con el nuevo alcohol alílico RBM4-55 se llevó a cabo la metátesis cruzada con el alqueno **9**, dando lugar al intermedio RBM4-57, el cual se transformó en los precursores para la reacción de Negishi RBM4-48, RBM4-58 y RBM4-61 (Figura 7.16).

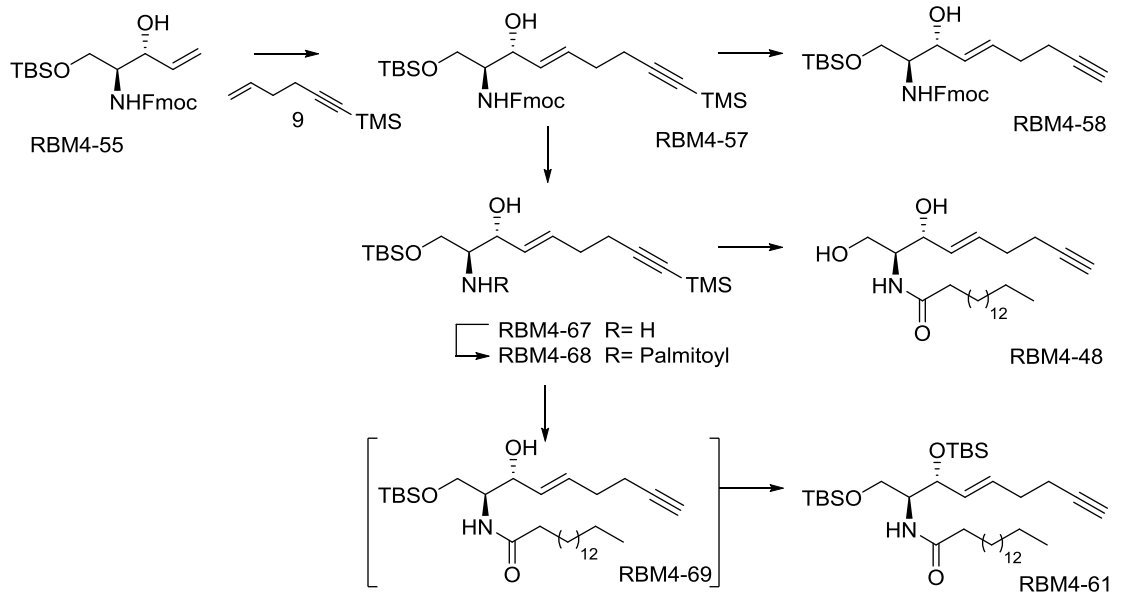

Figura 7.16 Síntesis de precursores para el acoplamiento de Negishi.

Las condiciones de reacción óptimas para el acoplamiento de Negishi con el bromuro poliénico RBM4-50 se pusieron a punto inicialmente con el alquino comercial *N*-(4-pentinil)-ftalimida, usado como modelo. Una vez obtenidas las condiciones óptimas, se procedió al acoplamiento de todos los alquinos esfingoides sintetizados con el bromuro RBM4-50. Sin embargo, ninguna de las reacciones evaluadas proporcionó el producto de acoplamiento deseado, seguramente debido al factor limitante de la escala de reacción. En conjunto, a raíz de la escasa selectividad obtenida en la formación del bromuro RBM4-50 y la necesidad de emplear grandes cantidades del compuesto **6** o RBM4-55 en la metátesis cruzada, se decidió descartar esta ruta sintética para la obtención de la Cer-poliénica.

Aproximación sintética vía hidrozirconación

Finalmente, se planteó abordar una ruta sintética alternativa a partir de los intermedios sintetizados hasta el momento. De este modo, mediante la reacción de hidrozirconación (reacción de Schwartz) entre el alquino poliénico RBM4-17 y el aldehído de Garner o el aldehído RBM4-54, se accedería a la estructura de alcohol (*E*)-alílico de la base esfingoide, en una única etapa (Figura 7.17).

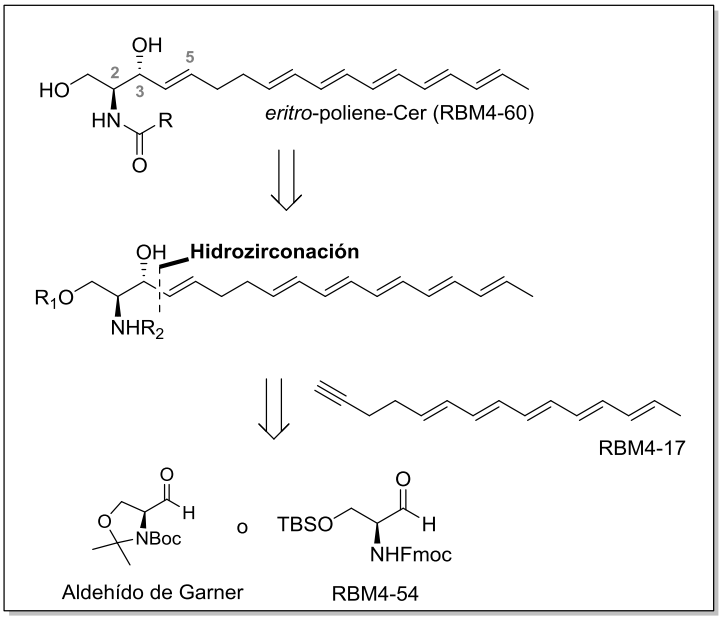

Figura 7.17 Análisis retrosintético para la obtención del compuesto *eritro*-poliene-Cer.

Los primeros intentos se llevaron a cabo con el aldehído de Garner, reproduciendo las condiciones descritas por Murakami *et al*.[59,60], en presencia de $ZnBr_2$ en THF, para favorecer la formación del diastereómero *anti*. Sin embargo, estas condiciones resutaron infructuosas cuando se aplicaron al alquino RBM4-17. Por ello, procedimos a utilizar $AgClO_4$ como catalizador[61,62], a pesar de estar descrito que proporciona menor selectividad estereoquímica. Bajo estas condiciones, se obtuvo el compuesto de acoplamiento correspondiente con un rendimiento del 20% y una diastereoselectividad en C2-C3 *anti/syn* (1:1). No obstante, en la siguiente reacción de desprotección de los grupos isopropilideno y Boc en condiciones ácidas, solamente se observó la formación de diversos compuestos de degradación.

Tras observar estos resultados, se puso a punto la reacción de hidrozirconación entre el aldehído RBM4-54 y el alquino RBM4-17, con varios catalizadores. Cuando se empleó $AgClO_4$ (20% mol) en DCM, se obtuvo el producto de acoplamiento con un 20% de rendimiento y una selectividad en C2-C3 *anti/syn* (1:2.3). Resultados similares

se obtuvieron utilizando Et_2Zn como catalizador. Con el objeto de mejorar la diastereoselectividad observada, se añadió $ZnCl_2$ (50% mol) en DCM, proporcionando con un 20% el producto de acoplamiento en una relación *anti/syn* (1:1.5).

Considerando esta relación *anti/syn* (1:1.5) como aceptable, se procedió a la desprotección simultánea de los grupos TBS y Fmoc con TBAF para acceder a la correspondiente Sph pentaénica. No obstante, no fue posible la purificación de la Sph poliénica a partir de los crudos de reacción, probablemente debido a la presencia de gran cantidad de productos provenientes de reacciones secundarias del TBAF. En vista de ello, se procedió a tratar directamente el crudo de reacción con ácido palmítico en condiciones de acilación. De este modo, se consiguió obtener la primera palmitoil-Cer pentaénica (RBM4-60) con una diastereoselectividad *anti/syn* (1:1.5). Futuros intentos para mejorar la selectividad y el rendimiento serán necesarios para mejorar la eficacia del proceso.

Conclusiones generales

Análogos GABA-Pentaeno como sondas de membrana

- Se han sintetizado tres sondas de tipo GABA-pentaeno como ceramidas fluorescentes. La etapa clave para su preparación ha sido la incorporación del sistema poliénico, mediante una reacción de esterificación, en la última etapa de la síntesis. El compuesto RBM4-35, *N*-acilado con ácido palmítico, ha servido como sonda de referencia de máxima fluorescencia en estudios con membranas artificiales. Por otra parte, las sondas RBM4-39 y RBM4-42, conteniendo los radicales atenuadores 16-DOXYL y 5-DOXYL, respectivamente, han sido diseñadas como moduladoras de la fluorescencia.

- Tras realizar diversos estudios biofísicos con estas sondas en membranas modelo, se puede concluir que todas ellas se orientan en las bicapas lipídicas como moléculas anfipáticas y que un sistema pentaénico es adecuado para los estudios de microscopía propuestos. Asimismo, la sonda RBM4-35 puede ser de gran utilidad para la observación de dominios altamente ordenados por microscopía confocal. Además, la capacidad de la sonda RBM4-39 para detectar lípidos de membrana en estado gel puede ser relevante para detectar microdominios gel en membranas celulares.

Estrategias sintéticas para la obtención de análogos de esfingolípidos poliénicos

- Se han llevado a cabo diferentes estrategias sintéticas para la obtención de análogos de Cer y Sph poliénicos. Entre ellas, cabe destacar la síntesis del alquino pentaénico RBM4-17, el cual nos ha permitido acceder mediante alquinilación nucleofílica a una estructura análoga a la Sph *anti*-polienínica. Asimismo, el alquino RBM4-17 ha sido un intermedio clave para la reacción de hidrozirconación, dando lugar a la primera palmitoil-Cer pentaénica como mezcla *anti/syn* 1:1.5.

- En el transcurso del diseño de aproximaciones sintéticas compatibles con sistemas poliénicos, se han obtenido nuevos sintones derivados de la L-serina (aldehído RBM4-54 y alcohol alílico RBM4-55), los cuales han sido protegidos con *O*-TBS y *N*-Fmoc, requiriendo condiciones suaves para su desprotección.

Referencias

(1) Olsen, I.; Jantzen, E. Sphingolipids in Bacteria and Fungi. *Anaerobe* **2001**, *7*, 103–112.

(2) Head, B. P.; Patel, H. H.; Insel, P. a. Interaction of Membrane/lipid Rafts with the Cytoskeleton: Impact on Signaling and Function: Membrane/lipid Rafts, Mediators of Cytoskeletal Arrangement and Cell Signaling. *Biochim. Biophys. Acta* **2014**, *1838*, 532–545.

(3) Mao, C.; Obeid, L. M. Ceramidases: Regulators of Cellular Responses Mediated by Ceramide, Sphingosine, and Sphingosine-1-Phosphate. *Biochim. Biophys. Acta* **2008**, *1781*, 424–434.

(4) Futerman, A. H.; Hannun, Y. a. The Complex Life of Simple Sphingolipids. *EMBO Rep.* **2004**, *5*, 777–782.

(5) Bartke, N.; Hannun, Y. a. Bioactive Sphingolipids: Metabolism and Function. *J. Lipid Res.* **2009**, *50 Suppl*, S91–S96.

(6) Rajagopalan, V.; Hannun, Y. A. Sphingolipid Metabolism and Signaling as a Target for Cancer Treatment. In *Cell Death in Biology and Diseases. Chapter 8*; 2013; pp 205–229.

(7) Sonnino, S.; Prinetti, a. Membrane Domains and the “Lipid Raft” Concept. *Curr. Med. Chem.* **2013**, *20*, 4–21.

(8) Tilcock, C. P.; Cullis, P. R. Lipid Polymorphism. *Ann. N. Y. Acad. Sci.* **1987**, *492*, 88–102.

(9) Komura, S.; Andelman, D. Physical Aspects of Heterogeneities in Multi-Component Lipid Membranes. *Adv. Colloid Interface Sci.* **2014**, *208*, 34–46.

(10) Leslie, M. Do Lipid Rafts Exist? *Science (80-.).* **2011**, *334*, 1046–1047.

(11) Zhong, J. From Simple to Complex: Investigating the Effects of Lipid Composition and Phase on the Membrane Interactions of Biomolecules Using in Situ Atomic Force Microscopy. *Integr. Biol. (Camb).* **2011**, *3*, 632–644.

(12) Goñi, F. M.; Alonso, A. Biophysics of Sphingolipids I. Membrane Properties of Sphingosine, Ceramides and Other Simple Sphingolipids. *Biochim. Biophys. Acta - Biomembr.* **2006**, *1758*, 1902–1921.

(13) Sot, J.; Bagatolli, L. a; Goñi, F. M.; Alonso, A. Detergent-Resistant, Ceramide-Enriched Domains in Sphingomyelin/ceramide Bilayers. *Biophys. J.* **2006**, *90*, 903–914.

(14) Holopainen, J. M.; Subramanian, M.; Kinnunen, P. K. J. Sphingomyelinase Induces Lipid Microdomain Formation in a Fluid Phosphatidylcholine/sphingomyelin Membrane. *Biochemistry* **1998**, *37*, 17562–17570.

(15) Huang, H. W.; Goldberg, E. M.; Zidovetzki, R. Ceramide Induces Structural Defects into Phosphatidylcholine Bilayers and Activates Phospholipase A2. *Biochem. Biophys. Res. Commun.* **1996**, *220*, 834–838.

(16) Silva, L.; de Almeida, R. F. M.; Fedorov, A.; Matos, A. P. a; Prieto, M. Ceramide-Platform Formation and -Induced Biophysical Changes in a Fluid Phospholipid Membrane. *Mol. Membr. Biol.* **2006**, *23*, 137–148.

(17) Contreras, F.-X.; Sot, J.; Alonso, A.; Goñi, F. M. Sphingosine Increases the Permeability of Model and Cell Membranes. *Biophys. J.* **2006**, *90*, 4085–4092.

(18) Georgieva, R.; Koumanov, K.; Momchilova, A.; Tessier, C.; Staneva, G. Effect of Sphingosine on Domain Morphology in Giant Vesicles. *J. Colloid Interface Sci.* **2010**, *350*, 502–510.

(19) Siskind, L. J.; Fluss, S.; Bui, M.; Colombini, M. Sphingosine Forms Channels in Membranes That Differ Greatly fromThose Formed by Ceramide. *J. Bioenerg. Biomembr.* **2005**, *37*, 227–236.

(20) Jiménez-Rojo, N.; Sot, J.; Viguera, A. R.; Collado, M. I.; Torrecillas, A.; Gómez-Fernández, J. C.; Goñi, F. M.; Alonso, A. Membrane Permeabilization Induced by Sphingosine: Effect of Negatively Charged Lipids. *Biophys. J.* **2014**, *106*, 2577–2584.

(21) Goñi, F. M.; Sot, J.; Alonso, A. Biophysical Properties of Sphingosine, Ceramides and Other Simple Sphingolipids. *Biochem. Soc. Trans.* **2014**, *42*, 1401–1408.

(22) Jacobson, K.; Mouritsen, O. G.; Anderson, R. G. W. Lipid Rafts: At a Crossroad between Cell Biology and Physics. *Nat. Cell Biol.* **2007**, *9*, 7–14.

(23) Wildenberg, S. M. J. L. Van Den; Prevo, B.; Peterman, E. J. G.; Ferrand, P. Single Molecule Analysis. *Methods Cell Biol.* **2011**, *783*, 81–99.

(24) Wang, T. Y.; Silvius, J. R. Different Sphingolipids Show Differential Partitioning into Sphingolipid/cholesterol-Rich Domains in Lipid Bilayers. *Biophys. J.* **2000**, *79*, 1478–1489.

(25) Kuerschner, L.; Thiele, C. Multiple Bonds for the Lipid Interest. *Biochim. Biophys. Acta - Mol. Cell Biol. Lipids* **2014**, *1841*, 1031–1037.

(26) Kuerschner, L.; Ejsing, C. S.; Ekroos, K.; Shevchenko, A.; Anderson, K. I.; Thiele, C. Polyene-Lipids : A New Tool to Image Lipids. *Nat. Methods* **2005**, *2*, 39–45.

(27) Mateo, C. R.; Souto, a a; Amat-Guerri, F.; Acuña, a U. New Fluorescent Octadecapentaenoic Acids as Probes of Lipid Membranes and Protein-Lipid Interactions. *Biophys. J.* **1996**, *71*, 2177–2191.

(28) Kuerschner, L.; Moessinger, C.; Thiele, C. Imaging of Lipid Biosynthesis: How a Neutral Lipid Enters Lipid Droplets. *Traffic* **2008**, *9*, 338–352.

(29) Van Meer, G.; Liskamp, R. M. J. Brilliant Lipids. *Nat. Methods* **2005**, *2*, 14–15.

(30) Blinco, J. P.; Fairfull-Smith, K. E.; Morrow, B. J.; Bottle, S. E. Profluorescent Nitroxides as Sensitive Probes of Oxidative Change and Free Radical Reactions. *Aust. J. Chem.* **2011**, *64*, 373–389.

(31) Cao, L.; Wu, Q.; Li, Q.; Shao, S.; Guo, Y. Visualizing the Changes in the Cellular Redox Environment Using a Novel Profluorescent Rhodamine Nitroxide Probe. *New J. Chem.* **2013**, *37*, 2991–2994.

(32) Ahn, H.-Y.; Fairfull-Smith, K. E.; Morrow, B. J.; Lussini, V.; Kim, B.; Bondar, M. V; Bottle, S. E.; Belfield, K. D. Two-Photon Fluorescence Microscopy Imaging of Cellular Oxidative Stress Using Profluorescent Nitroxides. *J. Am. Chem. Soc.* **2012**, *134*, 4721–4730.

(33) Kaiser, R. D.; London, E. Location of Diphenylhexatriene (DPH) and Its Derivatives within Membranes: Comparison of Different Fluorescence Quenching Analyses of Membrane Depth. *Biochemistry* **1998**, *37*, 8180–8190.

(34) Negishi, E. I.; Huang, Z.; Wang, G.; Mohan, S.; Wang, C.; Hattori, H. Recent Advances in Efficient and Selective Synthesis of Di-, Tri-, and Tetrasubstituted Alkenes via Pd-Catalyzed Alkenylation-Carbonyl Olefination Synergy. *Acc. Chem. Res.* **2008**, *41*, 1474–1485.

(35) Sun, H.; Kong, R.; Zhu, D.; Lu, M.; Ji, Q.; Liew, C. W.; Lescar, J.; Zhong, G.; Liang, Z.-X. Products of the Iterative Polyketide Synthases in 9- and 10-Membered Enediyne Biosynthesis. *Chem. Commun.* **2009**, 7399–7401.

(36) Patalag, L. J.; Werz, D. B. Fluorescent Penta- and Hexaene Fatty Acids by a Wittig-Horner/elimination Strategy. *J. Org. Chem.* **2012**, *77*, 5297–5304.

(37) Quesada, E.; Delgado, J.; Hornillos, V.; Acuña, a. U.; Amat-Guerri, F. Synthesis and Spectral Properties of Amphiphilic Lipids with Linear Conjugated Polyene and Phenylpolyene Fluorescent Groups. *European J. Org. Chem.* **2007**, *2007*, 2285–2295.

(38) Catalán, J.; Ṕrez, P.; Hopf, H.; Klein, D. The Photophysics of All-Trans Polyenes from ttbP5, a Nonphotolabile Pentaene. *J. Chem. Phys.* **2008**, *129*.

(39) Davis, P. J.; Coolbear, K. P.; Keough, K. M. Differential Scanning Calorimetric Studies of the Thermotropic Phase Behaviour of Membranes Composed of Dipalmitoyl Lecithin and Mixed-Acid Unsaturated Lecithins. *Can. J. Biochem.* **1980**, *58*, 851–858.

(40) Goñi, F. M.; Alonso, A. Structure and Functional Properties of Diacylglycerols in Membranes. *Prog. Lipid Res.* **1999**, *38*, 1–48.

(41) Montes, L.-R.; Alonso, A.; Goñi, F. M.; Bagatolli, L. a. Giant Unilamellar Vesicles Electroformed from Native Membranes and Organic Lipid Mixtures under Physiological Conditions. *Biophys. J.* **2007**, *93*, 3548–3554.

(42) Sot, J.; Ibarguren, M.; Busto, J. V.; Montes, L. R.; Goñi, F. M.; Alonso, A. Cholesterol Displacement by Ceramide in Sphingomyelin-Containing Liquid-Ordered Domains, and Generation of Gel Regions in Giant Lipidic Vesicles. *FEBS Lett.* **2008**, *582*, 3230–3236.

(43) Connon, S. J.; Blechert, S. Recent Developments in Olefin Cross-Metathesis. *Angew. Chemie - Int. Ed.* **2003**, *42*, 1900–1923.

(44) Grubbs, R. H.; Chang, S. Recent Advances in Olefin Metathesis and Its Application in Organic Synthesis. *Tetrahedron* **1998**, *54*, 4413–4450.

(45) Oh, J. S.; Hyun Kim, B.; Gyu Kim, Y. (E)-Selective Wittig Reactions of Garner's Aldehyde with Nonstabilized Ylides. *Tetrahedron Lett.* **2004**, *45*, 3925–3928.

(46) Souto, A. A.; Acuña, A. U.; Amat-Guerri, F. A General and Practical Synthesis of Linear Conjugated Pentaenoic Acids. *Tetrahedron Lett.* **1994**, *35*, 5907–5910.

(47) Gaukroger, K.; Hadfield, J. a.; Hepworth, L. a.; Lawrence, N. J.; McGown, A. T. Novel Syntheses of Cis and Trans Isomers of Combretastatin A-4. *J. Org. Chem.* **2001**, *66*, 8135–8138.

(48) Herold, P. Synthesis of D-Erythro- and D-Threo-Sphingosine Derivatives from L-Serine. *Helv. Chim. Acta.* **1988**, *71*, 354–362.

(49) Garner, P.; Park, J. M. Glycosyl Alpha-Amino Acids via Stereocontrolled Buildup of a Penaldic Acid Equivalent. A Novel Synthetic Approach to the Nucleosidic Component of the Polyoxins and Related Substances. *J. Org. Chem.* **1990**, *55*, 3772–3787.

(50) Wong, L.; Tan, S. S. L.; Lam, Y.; Melendez, A. J. Synthesis and Evaluation of Sphingosine Analogues as Inhibitors of Sphingosine Kinases. *J. Med. Chem.* **2009**, *52*, 3618–3626.

(51) Nudelman, A.; Bechor, Y.; Falb, E.; Fischer, B.; Wexler, B. a.; Nudelman, A. Acetyl Chloride-Methanol as a Convenient Reagent for: A) Quantitative Formation of Amine Hydrochlorides B) Carboxylate Ester Formation C) Mild Removal of N-T-Boc-Protective Group. *Synth. Commun.* **1998**, *28*, 471–474.

(52) Panek, J. S.; Hu, T. Stereo- and Regiocontrolled Synthesis of Branched Trisubstituted Conjugated Dienes by Palladium (0) -Catalyzed Cross-Coupling Reaction. *J. Org. Chem.* **1997**, *62*, 4912–4913.

(53) Negishi, E.; Alimardanov, A.; Xu, C. An Efficient and Stereoselective Synthesis of Xerulin via Pd-Catalyzed Cross Coupling and Lactonization Featuring (E)-Lodobromoethylene as a Novel Two-Carbon Synthon. *Org. Lett.* **2000**, *2*, 65–67.

(54) Takai, K.; Nitta, K.; Utimoto, K. Simple and Selective Method for RCHO (E)-RCH=CHX Conversion by Means of a CHX3-CrCI2 System. *J. Am. Chem. Soc.* **1986**, *108*, 7408–7410.

(55) Quesada, E.; Delgado, J.; Gajate, C.; Mollinedo, F.; Acun, A. U. Fluorescent Phenylpolyene Analogues of the Ether Phospholipid Edelfosine for the Selective Labeling of Cancer Cells. *J. Med. Chem.* **2004**, *47*, 5333–5335.

(56) Peterson, P. E.; Nelson, D. J.; Risener, R. Preparation of Vinylsilanes and Vinyl Halides Containing Alkene or Epoxide Functional Groups. *J. Org. Chem.* **1986**, *51*, 2382–2382.

(57) Miller, J. A.; Negishi, E.-I. Cyclic Carbolumination of Alkynylsilanes Forming Exocyclic Alkenes. *Isr. J. Chem.* **1984**, *24*, 76–81.

(58) Danilkina, N. A.; Kulyashova, A. E.; Khlebnikov, A. F.; Balova, I. A. Electrophilic Cyclization of Aryldiacetylenes in the Synthesis of Functionalized Enediynes Fused to a Heterocyclic Core. **2014**.

(59) Murakami, T.; Furusawa, K. Efficient Stereodivergent Synthesis of Erythro - and Threo -Sphingosines : Unprecedented Reversal of the Stereochemistry in the Addition. *Tetrahedron* **2002**, *58*, 9257–9263.

(60) Murakami, T.; Hirono, R.; Furusawa, K. Efficient Stereocontrolled Synthesis of Sphingadienine Derivatives. *Tetrahedron* **2005**, *61*, 9233–9241.

(61) Maeta, H.; Hashimoto, T.; Hasegawa, T.; Suzuki, K. Grignard-Type Addition of Alkenyl- and Alkylzirconocene Chloride to Aldehyde : Remarkable Catalytic Acceleration Effect of AgC104. *Tetrahedron Lett.* **1992**, *33*, 5965–5968.

(62) Maeta, H.; Suzuki, K. Two- and Four-Carbon Homologation of Aldehyde by AgClO4- Catalyzed Addition of Alkoxyalkenylzirconocene Chloride. *Tetrahedron Lett.* **1993**, *34*, 341–344.

8. ANNEX

The present doctoral thesis contains attached a CD. The following material is included:

- Annex:
  - NMR spectral data of compounds **2** to **15**.
  - NMR spectral data of compounds **RBM4-2** to **RBM4-60**

- PDF file of the Doctoral thesis.